

AUS DEM INSTITUT FÜR MEDIZINISCHE MIKROBIOLOGIE,
VIROLOGIE UND HYGIENE
der Universitätsmedizin Rostock

Antisense-Regulation der Genexpression von *Streptococcus pyogenes* in
Virulenz und Therapie

Kumulative Habilitationsschrift
zur
Erlangung des akademischen Grades
doctor philosophiae naturalis habilitata (Dr. phil. nat. habil.)
der Mathematisch-Naturwissenschaftlichen Fakultät
der Universität Rostock

Vorgelegt von

Nadja Patenge, geb. am 04.10.1966 in Berlin

aus Rostock

Rostock, 10.12.2019



Dieses Werk ist lizenziert unter einer
Creative Commons Namensnennung-Nicht kommerziell 4.0
International Lizenz.

Gutachter:

Bernd Kreikemeyer

Institut für Medizinische Mikrobiologie, Virologie und Hygiene

Universität Rostock

Hubert Bahl

Institut für Biowissenschaften

Universität Rostock

Jörg Vogel

Institut für Molekulare Infektionsbiologie

Universität Würzburg

Jahr der Probevorlesung:

2020

Jahr des wissenschaftlichen Kolloquiums

2021

Komm göttliches Licht,
erleuchte die Erde,
erfüll unsre Herzen,
nimm Wohnung in uns.

Lied aus Taizé

Inhaltsverzeichnis

1. Verwendete Originalarbeiten2

2. Einleitung5

2.1 Bedeutung und Therapie des Krankheitserregers *Streptococcus pyogenes*5

2.2 Regulatorische RNAs beeinflussen die Virulenz von *Streptococcus pyogenes*6

2.3 Antisense-Peptidnukleinsäuren („peptide nucleic acids“, PNA) als Therapeutika8

3. Ergebnisse und Diskussion.....10

3.1 Identifikation von sRNAs in *S. pyogenes*.....10

3.1.1 Identifikation von sRNA-Genen in *S. pyogenes* mit Hilfe von DNA Arrays.....10

3.1.2 Computerbasiertes sRNA-Screening im Genom von *S. pyogenes*12

3.2 Funktionelle Analyse von sRNA-Kandidaten aus *S. pyogenes*.....13

3.2.1 Die sRNA MarS beeinflusst die Virulenz von *S. pyogenes*14

3.2.2 Ein Glyzin-Riboswitch in *S. pyogenes* reguliert die Expression eines putativen Aminosäure-Symportergens18

3.3 Peptid Nukleinsäuren (PNAs) als Antisense-Therapeutika in *S. pyogenes*.....21

3.3.1 CPP-konjugierte anti-*gyrA* PNAs wirken antimikrobiell in *S. pyogenes*22

3.3.2 Einfluss verschiedener CPPs auf die antimikrobielle Wirkung von Antisense-PNAs23

4. Zusammenfassung und Ausblick27

5. Quellenverzeichnis29

6. Anlagen38

6.1 Originalarbeiten.....38

6.2 Vollständiges Publikationsverzeichnis.....109

7. Danksagung.....114

8. Selbstständigkeitserklärung.....115

1. Verwendete Originalarbeiten

1. Barkowsky, G., Lemster, A.-L., Pappesch, R., Jacob, A., Krüger, S., Schröder, A., Kreikemeyer, B., & **Patenge, N.** 2019. Influence of different Cell-Penetrating Peptides on the antimicrobial efficiency of antisense-PNAs in *Streptococcus pyogenes*. *Mol. Ther. Nucleic Acids*, 18, 444-454 available from: PM:31655262

Eigener Anteil:

- Konzeption der Studie
- Planung der Experimente, Anleitung bei der Durchführung der Experimente
- Design der PNA-Konstrukte (gemeinsam mit AJ)
- Auswertung der Daten zu den Experimenten der Studie
- Interpretation der Daten
- Schreiben des Manuskripts (gemeinsam mit GB)

2. Khani, A., Popp, N., Kreikemeyer, B., & **Patenge, N.** 2018. A Glycine Riboswitch in *Streptococcus pyogenes* Controls Expression of a Sodium:Alanine Symporter Family Protein Gene. *Front Microbiol.*, 9, 200 available from: PM:29527194

Eigener Anteil:

- Konzeption der Studie
- Planung der Experimente (gemeinsam mit AK)
- Anleitung bei der Durchführung der Experimente
- Auswertung der Daten zu den Experimenten der Studie
- Interpretation der Daten
- Schreiben des Manuskripts (gemeinsam mit AK)

3. Pappesch, R., Warnke, P., Mikkat, S., Normann, J., Wisniewska-Kucper, A., Huschka, F., Wittmann, M., Khani, A., Schwengers, O., Oehmcke-Hecht, S., Hain, T., Kreikemeyer, B., & **Patenge, N.** 2017. The Regulatory Small RNA MarS Supports Virulence of *Streptococcus pyogenes*. *Sci. Rep.*, 7, (1) 12241 available from: PM:28947755

Eigener Anteil:

- Konzeption der Studie
- Planung der Experimente (gemeinsam mit RP, PW, SM)

- Auswertung der Daten zu den Experimenten der Studie (gemeinsam mit RP, PW, SM, SO-H, TH)
- Interpretation der Daten (gemeinsam mit RP)
- Schreiben des Manuskripts (gemeinsam mit RP)

4. Patenge, N., Pappesch, R., Krawack, F., Walda, C., Mraheil, M.A., Jacob, A., Hain, T., & Kreikemeyer, B. 2013. Inhibition of Growth and Gene Expression by PNA-peptide Conjugates in *Streptococcus pyogenes*. Mol.Ther.Nucleic Acids, 2, e132 available from: PM:24193033

Eigener Anteil:

- Konzeption der Studie (gemeinsam mit BK)
- Planung der Experimente
- Design der PNA-Konstrukte (gemeinsam mit AJ und TH)
- Durchführung der initialen Wachstumsexperimente (gemeinsam mit RP, FK, CW)
- Auswertung der Daten zu den Experimenten der Studie
- Interpretation der Daten
- Schreiben des Manuskripts

5. Patenge, N., Billion, A., Raasch, P., Normann, J., Wisniewska-Kucper, A., Retej, J., Boisguerin, V., Hartsch, T., Hain, T., & Kreikemeyer, B. 2012. Identification of novel growth phase- and media-dependent small non-coding RNAs in *Streptococcus pyogenes* M49 using intergenic tiling arrays. BMC.Genomics, 13, (1) 550 available from: PM:23062031

Eigener Anteil:

- Konzeption der Studie (gemeinsam mit BK)
- Planung der Experimente
- Durchführung der Expressionsexperimente (gemeinsam mit JN, AW-K)
- Auswertung der Mikroarray Daten, Datenvergleich verschiedener Screening Methoden
- Bioinformatische Identifikation von Sequenzmotiven
- Auswertung der Daten zu den Experimenten der Studie
- Interpretation der Daten
- Schreiben des Manuskripts

6. Raasch, P., Schmitz, U., **Patenge, N.**, Vera, J., Kreikemeyer, B., & Wolkenhauer, O. 2010. Non-coding RNA detection methods combined to improve usability, reproducibility and precision. BMC.Bioinformatics., 11, (1) 491 available from: PM:20920260

Eigener Anteil:

- Planung und Durchführung der RT-PCR Experimente
- Interpretation der Daten zu den RT-PCR Experimenten
- Beteiligung am Schreiben des Manuskripts (10 %)

2. Einleitung

2.1 Bedeutung und Therapie des Krankheitserregers *Streptococcus pyogenes*

Streptococcus pyogenes (Group A Streptokokkus, GAS) ist ein Gram-positives humanpathogenes Bakterium, das sich durch eine große Diversität der klinischen Manifestation auszeichnet. Zum einen ruft *S. pyogenes* milde, oberflächliche Erkrankungen hervor, die ohne Behandlung wieder abklingen. Dazu gehören Pharyngitis, Tonsillitis und Impetigo. *S. pyogenes* ist beispielsweise die häufigste bakterielle Ursache für Pharyngitis im Kindesalter. Infektionen mit *S. pyogenes* werden bei 20-40 % der Fälle diagnostiziert (Shaikh *et al.*, 2010). Da es bei unbehandelten GAS Infektionen zu schweren invasiven Verläufen oder zum Auftreten von Autoimmunfolgeerkrankungen kommen kann, ist eine Behandlung mit Antibiotika streng indiziert (Cunningham, 2008).

Bekannte Beispiele für invasive Infektionen sind das streptokokkale toxische Schocksyndrom (STSS) und die nekrotisierende Faszitis (Bisno *et al.*, 2000, Francis and Warren, 1988, Meleney and Zau, 1924, Stevens *et al.*, 1989). Die Zahl der Todesfälle, die jährlich weltweit durch invasive Streptokokken Infektionen verursacht wird, beträgt ungefähr 163.000 (Carapetis *et al.*, 2005). Damit zählt GAS global zu den bedeutendsten Krankheitserregern. Insbesondere in Ländern mit limitierten Ressourcen kommt es im zunehmenden Maße zu invasiven Verläufen (Sims *et al.*, 2016).

Häufige Poststreptokokken-Autoimmunfolgeerkrankungen sind das Akute Rheumatische Fieber (ARF) und die Rheumatische Endokarditis (RHD). Diese Folgeerkrankungen treten weltweit auf, typischer Weise in Kindheit und Jugend im Alter zwischen 5 und 15 Jahren (Bisno *et al.*, 2003, McDonald *et al.*, 2004). Zudem wurden gegen das Zentralnervensystem gerichtete Autoimmunreaktionen mit Streptokokkeninfektionen in Zusammenhang gebracht. Dazu zählen unter anderem die Sydenham Chorea und die „Pediatric Autoimmune Neuropsychiatric Disorder Associated with Streptococci“ (PANDAS) (Murphy *et al.*, 2015). Akute Poststreptokokkale Glomerulonephritis (APSGN) ist eine weitere Autoimmunreaktion, die nach Streptokokkeninfektionen auftritt. Die Inzidenz von APSGN ist weltweit zurückgegangen und in den Industrienationen handelt es sich aufgrund der guten medizinischen Versorgung um eine seltene Erkrankung, die hauptsächlich bei älteren Patienten mit Vorerkrankungen auftritt (Rodriguez-Iturbe and Haas, 2016).

Penicillin ist heute die Standardtherapie bei Infektionen mit GAS, da Penicillin in der Regel effizient wirkt, ein enges Wirkspektrum hat und gewöhnlich gut vertragen wird (Shulman *et al.*, 2012). Zudem wird β -Lactam-Antibiotika ein neuroprotektiver Effekt zugeschrieben, der über ihre antibakterielle Wirkung hinausgeht (Murphy *et al.*, 2015). Obgleich bei *S. pyogenes* bislang universell eine Empfindlichkeit gegen β -Lactam-Antibiotika besteht, kommt es im zunehmenden Maße zu einem Behandlungsversagen bei der Gabe von Penicillin in Fällen von Pharyngitis (Brook, 2013, Markowitz *et al.*, 1993). Als mögliche Ursachen werden die gleichzeitige Kolonisierung von beta-Laktamase-produzierenden Bakterien (Brook, 2009), die Bildung von Biofilmen (Baldassarri *et al.*, 2006) oder die Internalisierung von GAS in Epithelzellen (Kaplan *et al.*, 2006) diskutiert.

Macrolide, Lincosamide und Streptogramine (MLS) werden als alternative Antibiotika bei Penicillin-Allergien oder Behandlungsversagen empfohlen (Shulman *et al.*, 2012). In den USA sind die Resistenzraten gegenüber Makrolidantibiotika gleichbleibend gering (Richter *et al.*, 2005). In Europa wurde zunächst eine Zunahme Makrolid-resistenter GAS-Stämme beobachtet, die von einer Abnahme von Erythromycin-Resistenzen in einigen europäischen Ländern abgelöst wurde (Cattoir, 2016). Es konnte für mehrere geographische Regionen gezeigt werden, dass das Auftreten von Erythromycin-Resistenzen bei *S. pyogenes* mit dem Makrolidantibiotika-Verbrauch korrelierte (Albrich *et al.*, 2004, Granizo *et al.*, 2000, Seppala *et al.*, 1997).

Unter diesen Voraussetzungen sollte die Anwendung und Verbreitung von Antibiotika bei der Behandlung von Streptokokken-Infektionen limitiert werden. In der Folge ist die Suche nach neuen effizienten Therapien eine zentrale Aufgabe der wissenschaftlichen und klinischen Forschung. Dazu muss zunächst die molekulare Pathogenese von *S. pyogenes* untersucht werden, um spezifische Therapieziele identifizieren zu können.

2.2 Regulatorische RNAs beeinflussen die Virulenz von *Streptococcus pyogenes*

Der Erfolg einer Streptokokkeninfektion hängt von einer großen Anzahl verschiedener Virulenzfaktoren ab, die im Infektionsverlauf strikt reguliert werden. Die Kontrolle der Expression von Virulenzfaktorgenen durch einzelständige Transkriptionsfaktoren oder Zweikomponentensysteme in GAS beeinflusst die Virulenz und ist bereits gut untersucht (Kreikemeyer *et al.*, 2003, Patenge *et al.*, 2013a). Eine weitere Ebene der Regulation bakterieller Genexpression wird durch kleine regulatorische RNAs („small non-coding RNAs“, sRNAs) vermittelt (Storz *et al.*, 2011). Bakterielle sRNAs können die Genexpression

reprimieren, indem sie die Translation inhibieren oder die mRNA Stabilität herabsetzen (Podkaminski and Vogel, 2010). Sie können jedoch auch als Aktivator dienen, indem sie Transkripte stabilisieren oder die Initiation der Translation unterstützen (Waters and Storz, 2009). Einige Beispiele für typische Regulationsmechanismen bakterieller sRNAs sind in Abbildung 1 dargestellt. Diverse Prozesse, von Stressantwort über Kohlehydratmetabolismus bis hin zur Zusammensetzung der bakteriellen Zelloberfläche, werden von sRNAs kontrolliert (Gorke and Vogel, 2008, Gottesman *et al.*, 2006). Es ist daher nicht überraschend, dass sRNAs auch in der Regulation von Virulenzfaktorgenen pathogener Bakterien eine Rolle spielen (Papenfort and Vogel, 2010). Allerdings sind Informationen zu RNA-abhängigen regulatorischen Netzwerken in Streptokokken noch limitiert (Patenge *et al.*, 2015).

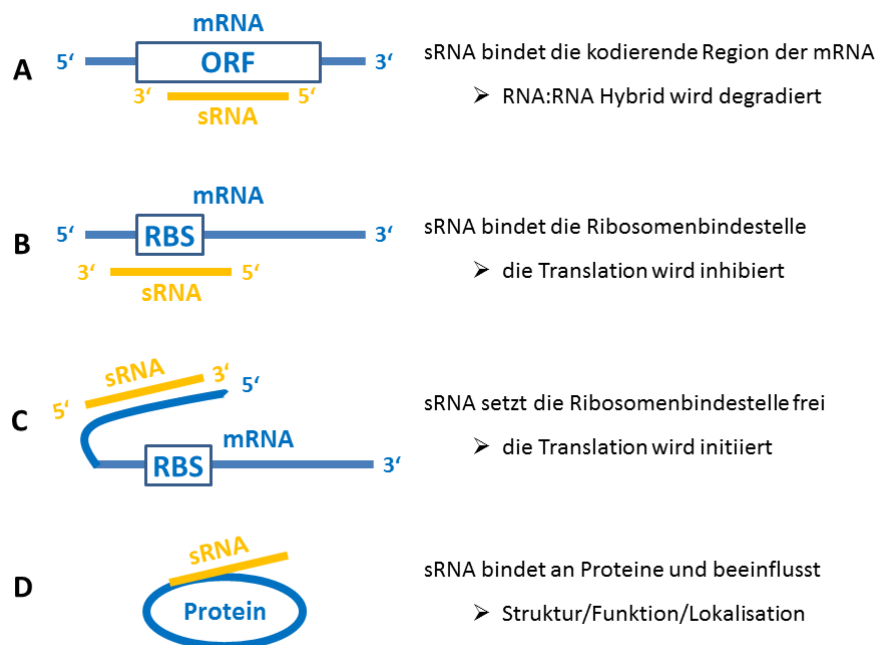


Abbildung 1. Schematische Darstellung von vier typischen Regulationsmechanismen bakterieller sRNAs. A, B, C: sRNA:mRNA Interaktion. D: Interaktion einer sRNA mit einem Target Protein. Abbildung modifiziert nach R. L. Zapf (CC BY-SA 4.0).

Die bisher am gründlichsten untersuchte sRNA in *S. pyogenes* ist FasX. Die Transkription von *fasX* wird vom *fasBCA* Operon kontrolliert (Kreikemeyer *et al.*, 2001). Unter den Targetgenen von FasX befinden sich einige bedeutende *S. pyogenes* Virulenzfaktorgen. FasX bindet an das 5'-Ende des Streptokinasegen-Transkripts, stabilisiert auf diesem Weg die mRNA und stimuliert die Streptokinase Synthese (Ramirez-Pena *et al.*, 2010). Die Translation der Pilusgen-Transkripte wird hingegen gehemmt, indem die Ribosomenbindestelle (RBS) blockiert wird (Danger *et al.*, 2015a, Liu *et al.*, 2012). Mithilfe

desgleichen Mechanismus wird die Synthese der Fibronektin bindenden Proteine PrtF1/2 durch FasX inhibiert (Danger *et al.*, 2015b). Es wird angenommen, dass FasX als Schalter zwischen Kolonisation und Dissemination der Bakterien dient, indem es die Synthese der Pili- und Fibronektin bindenden Proteine negativ reguliert, während die Produktion der Streptokinase erhöht wird.

FasX gehört zu den sRNAs, die *in trans* auf die Expression unterschiedlicher Gene im Genom wirken. Im Gegensatz dazu gehören Riboswitches zu den *cis*-regulatorischen Elementen, die auf derselben RNA lokalisiert sind wie ihre Zielgene. Riboswitches bestehen aus zwei Modulen: i) einem Aptamer, das in der Lage ist einen Liganden zu binden und ii) einer Expressionsplattform, die die Expression der stromabwärts gelegenen Gene kontrolliert. Nachdem ein spezifisches Effektormolekül gebunden hat, nimmt die Expressionsplattform eine definierte stabile Konformation an. Diese Sekundärstruktur kann dabei zu einer Induktion oder einer Repression der Expression der stromabwärts gelegenen kodierenden Sequenz führen.

Riboswitches stellen ein interessantes therapeutisches antimikrobielles Target dar, da die Modifikation ihrer Funktion durch kleine Ligandenanaloga erfolgt, die in der Regel einfach synthetisiert und verabreicht werden können (Machtel *et al.*, 2016). In Streptokokken wurden bislang Riboswitches beschrieben, die spezifisch sind für S-Adenosylmethionin (SAM), die Queuosin Vorstufe preQ1 und Fluorid (Fuchs *et al.*, 2006, Fuchs *et al.*, 2007, Kang *et al.*, 2014, Meyer *et al.*, 2008, Nelson *et al.*, 2015).

Da anzunehmen ist, dass weitere sRNAs und Riboswitches im Infektionsverlauf an der Kontrolle relevanter Gene in *S. pyogenes* beteiligt sind, sollten in der vorliegenden Arbeit putative sRNA-Gene und *cis*-regulatorische Elemente identifiziert und deren Funktion im Anschluss charakterisiert werden.

2.3 Antisense-Peptidnukleinsäuren („peptide nucleic acids“, PNA) als Therapeutika

Um die Anwendung und Verbreitung von Antibiotika bei der Behandlung von Streptokokkeninfektionen begrenzen zu können, müssen innovative Therapiestrategien entwickelt werden. Eine Möglichkeit stellen Antisense-basierte Wirkstoffe dar, die in der Regel sensitiv und spezifisch sind. Die Wirkung beruht darauf, dass essentielle bakterielle Gene mithilfe der Antisense-Technik ausgeschaltet werden. Peptid-Nukleinsäuren (PNAs) sind Moleküle, die aufgrund ihrer chemischen Eigenschaften für die Verwendung als Antisense-Wirkstoff

interessant sind. Es handelt sich um synthetische organische Polymere, die Ähnlichkeiten mit DNA und RNA aufweisen. Dabei ist das Zucker-Phosphat Rückgrat der Nucleinsäuren durch ein Peptidgerüst ersetzt, an das die vier Basen Adenin, Cytosin, Thymin und Guanin kovalent gebunden sind (Abbildung 2).

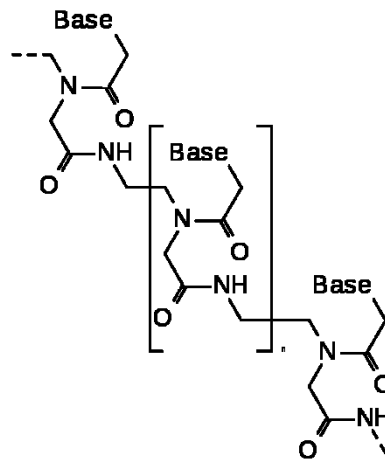


Abbildung 2. Schematische Darstellung der PNA Struktur.
<https://commons.wikimedia.org/w/index.php?curid=1737834>

PNAs können Basenpaarungen eingehen und zeigen eine hohe Affinität zu komplementären DNA- und RNA-Molekülen (Nielsen and Egholm, 1999). Aufgrund ihrer Struktur sind PNAs außerordentlich stabil. Sie sind über einen weiten Bereich Temperatur- und pH-resistent und sind zudem unempfindlich gegenüber vielen Chemikalien. Bislang sind weder zelluläre Proteasen noch Nucleasen bekannt, die in der Lage sind, PNAs abzubauen. Daher weisen PNAs eine hohe Stabilität in Humanserum und Zellextrakten auf (Demidov *et al.*, 1994). In der Diagnostik nutzt man PNAs bereits bei der *in-situ*-Hybridisierung zur Identifikation bakterieller Spezies und für die Bestimmung der Telomerlänge in eukaryotischen Zellen (Blanco and Artero, 2010, Carbonari *et al.*, 2011). Weitere potentielle Anwendungen von PNAs sind Funktionsanalysen mittels sequenzspezifischer Hemmung der Genexpression sowie die Antisense-basierte antimikrobielle Wachstumshemmung durch Ausschaltung essentieller Gene (Hatamoto *et al.*, 2010, Nielsen and Egholm, 1999).

Die mögliche praktische Anwendung als antibakterieller Wirkstoff wurde bislang am intensivsten in *Escherichia coli* untersucht. PNAs, die gegen ein essentielles Gen gerichtet waren, konnten das Bakterienwachstum in mikromolarer Konzentration hemmen (Good and Nielsen, 1998). Die Aufnahme der PNAs in Gram-negative Bakterien wird allerdings durch die LPS-Schicht der äußeren Membran limitiert und war in mutierten Stämmen deutlich erhöht (Good *et al.*, 2000). Kationische, antimikrobielle Peptide permeabilisieren die Zellen

und wirken synergistisch mit Substanzen, die eine niedrige Aufnahme aufweisen (Hancock, 1997). Das synthetische Peptid KFFKFFKFFK ($[(KFF)_3K]$) wurde zuerst von Vaara und Porro beschrieben (Vaara and Porro, 1996). Durch die Kopplung von $(KFF)_3K$ an PNAs konnte deren Aufnahme durch *E. coli* verbessert werden (Eriksson *et al.*, 2002). In neueren Studien zeigte sich, dass der Einsatz von $(KFF)_3K$ als Carrier Peptid die Effizienz der PNA-Wirkung auch in anderen Gram-negativen und in Gram-positiven Bakterienspezies steigern konnte (Hatamoto *et al.*, 2010). So gelang beispielsweise die Hemmung der Expression von Reportergenen sowie eine Wachstumshemmung durch das Ausschalten essentieller Gene im Gram-positiven Bakterium *Staphylococcus aureus* (Dryselius *et al.*, 2005, Nekhotiaeva *et al.*, 2004). Für *S. pyogenes* hingegen wurde dieser Ansatz bislang nicht verfolgt.

In dieser Arbeit sollte die Anwendung von Antisense-PNAs zur Wachstumshemmung und Inhibierung der Genexpression in *S. pyogenes* etabliert werden. Dazu wurden als *Proof of Principle* PNAs eingesetzt, die spezifisch für das essentielle Gen *gyrA* waren. Darüber hinaus sollte untersucht werden, welche Carrier-Peptide für den Einsatz von Antisense-PNAs in *S. pyogenes* geeignet sind.

3. Ergebnisse und Diskussion

3.1 Identifikation von sRNAs in *S. pyogenes*

Bakterielle sRNAs sind an der Regulation diverser metabolischer Prozesse beteiligt. Darüber hinaus kontrollieren sie die Expression verschiedener Pathogenese-relevanter Gene. Um den Mechanismus der sRNA-Funktion in *S. pyogenes* zu untersuchen und ihre Eignung als therapeutische Ziele zu evaluieren, müssen zunächst die sRNA kodierenden Gene im Bakteriengenom identifiziert werden. Ein Übersichtsartikel über Publikationen zur genomweiten Detektion von sRNAs in Streptokokken wurde kürzlich von unserer Arbeitsgruppe veröffentlicht (Patenge *et al.*, 2015). Grundsätzlich gibt es zwei unterschiedliche Herangehensweisen für ein genomweites sRNA-Screening: i) Transkriptionsanalysen und ii) Bioinformatische Vorhersagen.

3.1.1 Identifikation von sRNA-Genen in *S. pyogenes* mit Hilfe von DNA Arrays

Für genomweite sRNA-Screens können Expressionsuntersuchungen durchgeführt werden. Hierbei werden mit Hilfe von Transkript-Analyseverfahren, z.B. DNA-Arrays oder NGS-

Sequenzierung, kleine Transkripte identifiziert. In dieser Arbeit wurden DNA Mikroarrays zur Detektion von intergenischen sRNAs in *S. pyogenes* eingesetzt. Dazu wurden 17.823 Sonden synthetisiert, die die intergenischen Regionen des Referenzgenoms von *S. pyogenes* NZ131 (NCBI Accession Number: NC_011375) repräsentierten. Als Positivkontrolle dienen 174 Sonden, die spezifisch waren für tRNA-Gene oder für bereits in anderen Arbeiten identifizierte sRNA-Gene. Drei Beispiele sind die sRNAs FasX (Kreikemeyer *et al.*, 2001), SR914400 und SR1754950 (Perez *et al.*, 2009).

S. pyogenes M49 Stamm 591 wurde in chemisch definiertem Medium (CDM) kultiviert. Den Bakterienkulturen wurden während verschiedener Wachstumsphasen Proben entnommen. Es wurde Gesamt RNA isoliert und cDNA synthetisiert, die für die Arrayanalyse eingesetzt werden konnte. In der Analyse wurden 55 putative sRNA-Gene identifiziert. Bei 42 Signalen handelte es sich um neue sRNA-Kandidaten. Es wurden außerdem 12 sRNAs detektiert, die zuvor in einer Studie mit *S. pyogenes* MIT1 Stamm 5005 identifiziert worden waren (Perez *et al.*, 2009). Die Rfam Datenbank („RNA families database“) wurde für eine Computer gestützte Vorhersage der Funktion der putativen sRNAs eingesetzt (Gardner *et al.*, 2009). 14 sRNA Kandidaten konnten funktionelle Kategorien zugeordnet werden. Unter anderem wurden drei T-box Elemente, drei Mitglieder der CRISPR-Familie, eine tmRNA, und eine Endoribonuklease vorhergesagt. Ein putatives *cis*-regulatorisches Element zeigte Ähnlichkeiten zur Familie der Glyzin-Riboswitches (Patenge *et al.*, 2012).

Mit der DNA-Mikroarray Technik konnte die Position des jeweiligen Transkriptionsstarts (englisch: „transcriptional start site“, TSS) nicht ermittelt werden. Daher wurde für sechs putative sRNAs der TSS experimentell mit Hilfe der RACE-PCR (englisch: “rapid amplification of cDNA-ends with polymerase chain reaction”) bestimmt. Die TSS, die in dieser Analyse identifiziert wurden, lagen stromabwärts von bioinformatisch vorhergesagten bakteriellen Promotorsequenzen (Patenge *et al.*, 2012). Darüber hinaus wurde die Expression, Orientierung und Größe von sieben sRNA-Kandidaten mittels Northern Blot und genspezifischer RT-PCR validiert (Patenge *et al.*, 2012).

Zu Beginn dieser Arbeit war bereits in genomweiten Screens in verschiedenen Gram-positiven pathogenen Bakterienspezies eine hohe Anzahl an putativen sRNA-Genen identifiziert worden (Beaume *et al.*, 2011, Chen *et al.*, 2011, Kumar *et al.*, 2010, Mraheil *et al.*, 2011, Tsui *et al.*, 2010). Daher war es wahrscheinlich, dass sRNAs auch in *S. pyogenes* eine Rolle in der Regulation der Genexpression spielen. In *S. pyogenes* MIT1 Stamm MGAS2221 waren 40 sRNAs in der exponentiellen Wachstums Phase in Komplexmedium

exprimiert (Perez *et al.*, 2009). Das sRNAome von *S. pyogenes* M49 Stamm 591, das in dieser Arbeit analysiert wurde, war nach Wachstum in chemisch definiertem Medium aufgenommen worden. Von 55 sRNAs, die in dieser Arbeit detektiert wurden, waren nur 12 in der vorhergegangenen Studie nachgewiesen worden. Diese Ergebnisse unterstützen die Annahme, dass die sRNA Expression Serotyp spezifisch ist und darüber hinaus von Umweltfaktoren abhängt.

3.1.2 Computerbasiertes sRNA-Screening im Genom von *S. pyogenes*

Die Vorhersage bakterieller sRNA-Gene mit Hilfe von bioinformatischen Methoden beruht auf der Analyse typischer Parameter. Dazu gehören unter anderem die DNA Zusammensetzung, die Sekundärstruktur der putativen RNA, das Vorkommen von Promotor- und Terminator-Sequenzen und eine Struktur- oder Sequenz-basierte Konservierung. Da es bislang keinen zuverlässigen Algorithmus für die Detektion von sRNA-Genen gibt, behilft man sich mit der Kombination verschiedener Techniken (Machado-Lima *et al.*, 2008, Meyer, 2007). Mangelnde Standardisierung der Input und Output Formate erschwert jedoch die Vergleichbarkeit verschiedener Vorhersagemethoden.

Um diesen Prozess zu erleichtern, wurde am Lehrstuhl Systembiologie und Bioinformatik an der Universität Rostock ein Java-basiertes Programmiergerüst (engl. „framework“) entwickelt, das den Vergleich der Daten aus verschiedenen Anwendungen und Vorhersagemethoden ermöglicht, indem transparente Arbeitsabläufe (engl. „workflows“), konstruiert werden. Die Software *moses* (modular sequence suite) prozessiert und kombiniert die Ergebnisse verschiedener Methoden, mit deren Hilfe Regionen im Genom identifiziert werden können, die Kandidaten für sRNA-Gene enthalten. Dazu erstellt der Nutzer Workflows aus Modulen (Raasch *et al.*, 2010). Schlüsselmodule, die von *moses* bereitgestellt werden, sind unter anderem BLAST (Altschul *et al.*, 1990), RNAfold (Lorenz *et al.*, 2016), RNAz (Washietl *et al.*, 2005), ClustalW (Larkin *et al.*, 2007), and Dynalign (Mathews and Turner, 2006).

Die Effizienz der modularen Methodenkombination durch *moses* wurde überprüft, indem eine Kombination der vier Methoden RNAz-, RNAfold- und Dynalign und TranstermHP (Kingsford *et al.*, 2007) an einem Set von bekannten sRNAs aus *Escherichia coli*, *Listeria monocytogenes* and *S. pyogenes* angewendet wurde. Die Sensitivität („signal precision“) der kombinierten Methode war im Vergleich zu den einzelnen Methoden um 15 % erhöht bei einer gleichzeitig verringerten falsch positiv Rate (Raasch *et al.*, 2010).

Die Software wurde schließlich verwendet, um neue sRNA-Gene in *S. pyogenes* zu identifizieren. Aus einer Kandidatenliste von 20 Genen wurden vier Gene im Rahmen dieser Arbeit weiter untersucht. Die Expression der vier Kandidatengene konnte durch Reverse Transkription mit anschließender PCR (RT-PCR) verifiziert werden (Raasch *et al.*, 2010). Zudem wurde der Transkriptionsstart von *moses4* mittels 5' RACE-PCR bestimmt (Patenge *et al.*, 2012).

Ein weiteres Computer basiertes Screening wurde mit der Software sRNAScanner (Sridhar *et al.*, 2010) durchgeführt. Diese Analyse führte zur Identifikation von 137 sRNA Kandidatengen im Genom von *S. pyogenes* NZ131 (NCBI Accession Number: NC_011375) (Patenge *et al.*, 2012). Die Expression des Kandidatengens sRNAScan7 wurde mittels Northern Blot Analyse und RT-PCR bestätigt (Patenge *et al.*, 2012).

Die Ergebnisse der bioinformatischen sRNA-Screening Methoden wurden mit den Daten aus dem oben beschriebenen DNA Mikroarray Experiment verglichen. Dabei zeigte sich, dass der Überlapp der verschiedenen Datensätze gering war (Patenge *et al.*, 2012). Von den 20 putativen sRNAs, die mithilfe von *moses* identifiziert wurden, konnten nur fünf in den Arrays nachgewiesen werden. Von den 137 sRNAScanner Vorhersagen zeigten 11 sRNAs ein Signal in der Array Analyse. Acht Kandidaten wurden durch beide Softwares identifiziert. Die bereits zuvor identifizierte sRNA FasX wurde in allen drei Screens nachgewiesen (Patenge *et al.*, 2012). Die Unterschiede in den Ergebnislisten ergeben sich zum einen daraus, dass in den bioinformatischen Screens auch Kandidaten vorhergesagt wurden, die unter den Bedingungen der DNA Mikroarray Experimente nicht nachweisbar waren, da ihre Expression beispielsweise nur unter Stress induziert wird. Zum anderen sind die Sensitivität und die Spezifität der bioinformatischen sRNA-Detektion im Rahmen der eingesetzten Algorithmen begrenzt.

3.2 Funktionelle Analyse von sRNA-Kandidaten aus *S. pyogenes*

In den folgenden Kapiteln werden zwei Beispiele für sRNAs in *S. pyogenes* ausführlich beschrieben. Zum einen die *trans*-aktivierende sRNA MarS, die einen zentralen Transkriptionsregulator in *S. pyogenes* M49 Stamm 591 beeinflusst. Zum anderen ein *cis*-regulatorisches Element, das Eigenschaften eines Glyzin-Riboswitches aufweist.

3.2.1 Die sRNA MarS beeinflusst die Virulenz von *S. pyogenes*

In der DNA Array Expressionsanalyse wurde das sRNA-Kandidatengen sRNASpy490957c identifiziert, das in Milchsäurebakterien konserviert ist (Patenge *et al.*, 2012). sRNASpy490957c gehörte zu den putativen sRNA-Genen, die im Wachstumsverlauf von *S. pyogenes* M49 Stamm 591 differenziert exprimiert wurden. Der Genlokus ist in Abbildung 3 schematisch dargestellt.



Abbildung 3. Genregion des sRNA Kandidatengens sRNASpy490957c (*marS*). Die Gene sind durch Pfeile dargestellt, die in Transkriptionsrichtung orientiert sind. P: das erste (5') *marS* Nukleotid, tt: das letzte (3') *marS* Nukleotid (Pappesch *et al.*, 2017). *Spy_490957c* codiert eine putative Ribonukleotidreduktase. *Spy_490958c* codiert die Cardiolipin Synthase.

In dieser Arbeit wurde eine Deletionsmutante untersucht, in der das sRNA-Kandidatengen durch eine Spectinomycin-Resistenzkassette ersetzt worden war. Da in Abwesenheit der putativen sRNA die Expression des Transkriptionsaktivators Mga im Vergleich zum Wildtyp reduziert war und darüber hinaus gezeigt werden konnte, dass die sRNA mit dem 5' Ende der *mga* mRNA interagieren konnte, wurde die kleine RNA MarS („*mga*-activating regulatory sRNA“) genannt. Im Folgenden wird das sRNA-Gen mit *marS* und die kleine RNA mit MarS bezeichnet.

Die Größe (161 bp) und der Transkriptionsstart der kleinen RNA wurden in 5'RACE („rapid amplification of cDNA ends“) und Northern Blot Analysen bestimmt (Pappesch *et al.*, 2017, Patenge *et al.*, 2012). Die Stabilität der kleinen RNA wurde nach Rifampicinbehandlung mittels RT-qPCR gemessen. Das Transkript wies in *S. pyogenes* M49 Stamm 591 eine hohe Stabilität auf. Nach 15 min lagen noch $\geq 80\%$ des Transkripts vor (Pappesch *et al.*, 2017). Diese Beobachtung deckt sich mit Ergebnissen aus Experimenten mit *S. pyogenes* MIT1 Stamm MGAS2221 (Perez *et al.*, 2009).

Um Hinweise auf die Funktion von MarS zu erhalten, wurde zunächst in *S. pyogenes* M49 Stamm 591 eine isogene *marS* Deletionsmutante konstruiert ($\Delta marS$). Die Gendeletion wurde durch ektopische *marS* Expression von einem Shuttle Vektor unter der Kontrolle des

endogenen Promotors komplementiert ($\Delta marS::marS$) (Pappesch *et al.*, 2017). Das Verhalten der Deletionsmutante wurde *in vitro* unter infektiionsrelevanten Bedingungen untersucht. In Abwesenheit von *marS* war das Wachstum in humanem Vollblut reduziert. In humanem Plasma wuchs $\Delta marS$ hingegen unvermindert. Um zu überprüfen, ob zelluläre Blutbestandteile das Wachstum von $\Delta marS$ in humanem Vollblut beeinträchtigten, wurde das Überleben von $\Delta marS$ in Gegenwart von humanen neutrophilen Granulozyten untersucht. Unter diesen Bedingungen war die Überlebensrate von $\Delta marS$ im Vergleich zum WT signifikant reduziert. Dieser Effekt war in $\Delta marS::marS$ aufgehoben.

Die Adhärenz von $\Delta marS$ an humane Keratinozyten war signifikant verringert gegenüber dem WT, während die Adhärenz von $\Delta marS::marS$ sich nicht vom WT unterschied (Pappesch *et al.*, 2017). Diese Beobachtungen führten zu der Hypothese, dass MarS an der Regulation der Phagozytose Abwehr und der Adhärenz an Wirtszellen beteiligt ist.

Kleine regulatorische RNAs wirken häufig durch direkte molekulare Interaktion mit Ziel mRNAs. Der IntaRNA Algorithmus (Wright *et al.*, 2014) wurde verwendet, um putative MarS-Target Interaktionen vorherzusagen. Unter den 28 Genen, die durch das Programm als potentielle Bindungspartner identifiziert wurden, befanden sich *mga* und *hasB*.

Dabei kodiert *mga* den zentralen Transkriptionsaktivator Mga („multiple virulence gene regulator“). Die putative MarS Bindestelle ist in der 5' untranslatierten Region (5'UTR) von *mga* lokalisiert. Eine BLAST Analyse (Altschul *et al.*, 1990) ergab, dass diese Sequenz in den Serotypen M2, M4, M18, M28, M44, M49, M53, M59, M66, M71, M82, M83, M87, M89, und M101 konserviert ist.

Bei *hasB* handelt es sich um ein Kapselsynthesegen, das die UDP-glucose 6-dehydrogenase kodiert. Die vorhergesagte MarS Bindestelle ist im *hasABC* polycistronischen Transkript am 3' Ende des ORF von *hasA* lokalisiert. In MarS gibt es eine gemeinsame Bindestelle für beide putative Targetgene. Die Sekundärstruktur von MarS wurde mit RNAfold (The ViennaRNA Web Services, <http://rna.tbi.univie.ac.at/>) vorhergesagt und mit Hilfe von VARNA GUI (Darty *et al.*, 2009) dargestellt (Abbildung 4). Die Basen der Bindestelle sind in der schematischen Darstellung farblich hervorgehoben.

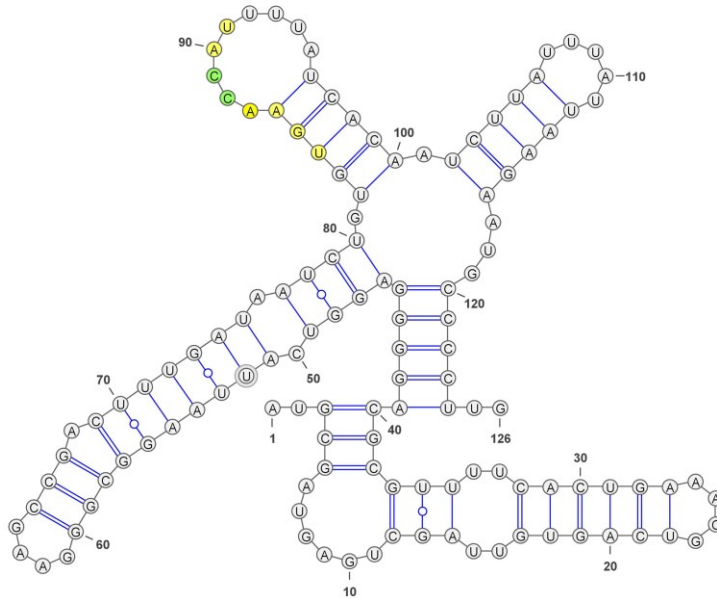


Abbildung 4. Sekundärstruktur von MarS. Dargestellt sind die Nucleotide 1-126. Der Terminator wurde der Übersichtlichkeit halber nicht berücksichtigt. Die Basen der putativen Bindestelle sind farblich hervorgehoben. In grün sind die Basen markiert, die für die Interaktionsstudien mutiert wurden (mmMarS, „mismatch“ MarS, (88-CC-89/88-GG-89) (Pappesch *et al.*, 2017).

Die Interaktion von MarS mit der 5'UTR von *mga* wurde *in vitro* mit Hilfe von RNA-RNA Gel Shift Experimenten („electrophoretic mobility shift assays“, EMSAs) untersucht. Biotin-markierte 5'UTR *mga* RNA wurde mit ansteigenden Mengen MarS inkubiert. Es wurde ein Komplex mit höherem Molekulargewicht detektiert, dessen Konzentration nach Zugabe von unmarkierter *mga* RNA-Sonde abnahm. Bei Inkubation der Biotin-markierten *mga* RNA-Sonde mit mmMarS („mismatch“ MarS, 88-CC-89/88-GG-89, Abbildung 4), bei der zwei Basen in der Bindestelle ausgetauscht waren, wurde kein Komplex gebildet (Pappesch *et al.*, 2017).

Der Einfluss von MarS auf die Expression des putativen Zielgens *mga* wurde mit Hilfe der Deletionsmutante $\Delta marS$ und dem Komplementationsstamm $\Delta marS::marS$ in *S. pyogenes* M49 Stamm 591 untersucht. Es wurde Gesamt-RNA aus den verschiedenen Stämmen isoliert, cDNA synthetisiert und im Anschluss eine quantitative PCR (qPCR) durchgeführt. Dazu wurden genspezifische Primer für *mga* und für die Virulenzfaktorgene *emm* (M Protein), *sclA* („streptococcal collagen-like protein“) und *sof* („serum opacity factor“) verwendet. Von *emm*, *sclA* und *sof* ist bekannt, dass sie direkt von Mga positiv reguliert werden (Hondorp and McIver, 2007). Die Transkriptmenge aller getesteten Gene war in der Mutante signifikant reduziert im Vergleich zum WT. Der WT Phänotyp war in $\Delta marS::marS$ wieder hergestellt.

Aus diesen Ergebnissen lässt sich schließen, dass MarS einen positiven regulatorischen Einfluss auf die Expression von *mga* hat und damit indirekt auch die Expression von Virulenzfaktorgenen beeinflusst, die von Mga reguliert werden. Da das M Protein eine anti-phagozytische Wirkung hat, lässt sich die reduzierte Überlebensrate von $\Delta marS$ im Vergleich zum WT nach Inkubation mit neutrophilen Granulozyten durch eine verringerte *emm* Expression erklären.

Die Kapselsynthese wurde in *S. pyogenes* M18 Stamm MGAS8232 untersucht, der eine stärkere Hyaluronsäureproduktion als *S. pyogenes* M49 Stamm 591 aufweist (Barkowsky, 2019). In *S. pyogenes* M18 Stamm MGAS8232 $\Delta marS$ war der Hyaluronsäuregehalt der Bakterien signifikant reduziert im Vergleich zum WT. Die Kapselmenge war im Komplementationsstamm $\Delta marS::marS$ auf WT-Niveau (Pappesch *et al.*, 2017).

Um den Einfluss von MarS auf die Virulenz von *S. pyogenes in vivo* zu untersuchen, wurde ein murines Infektionsmodell verwendet. BALB/c Mäuse wurden intraperitoneal mit 8×10^7 Kolonie bildenden Einheiten (KbE) *S. pyogenes* M49 Stamm 591 WT, $\Delta marS$ oder $\Delta marS::marS$ infiziert. Alle Tiere zeigten schwere Zeichen der Infektion und wurden nach 24 h erlöst. In Niere, Leber und Milz der infizierten Tiere konnte nach Infektion mit $\Delta marS$ eine signifikant erhöhte Bakterienlast nachgewiesen werden im Vergleich zum WT. Die Abwesenheit von MarS hat in diesem Experiment zu einer erhöhten bakteriellen Dissemination geführt.

Es wird angenommen, dass FasX als Schalter zwischen Kolonisation und Dissemination von *S. pyogenes* dient, indem es die Synthese der Pili- und Fibronektin bindenden Proteine negativ reguliert, während die Produktion der Streptokinase erhöht wird (Danger *et al.*, 2015a, Danger *et al.*, 2015b). MarS hingegen unterstützt die Adhärenz der Bakterien an Wirtszellen durch positive Regulation der Produktion von extrazellulären Matrixbindeproteinen und durch Stimulation der Kapselsynthese. Gleichzeitig wird die bakterielle Dissemination durch MarS vermindert. Diese Beobachtungen deuten darauf hin, dass MarS im frühen Stadium der Infektion an der Kontrolle der Kolonisation des Wirts durch *S. pyogenes* beteiligt ist.

In zukünftigen Projekten soll die Funktion von MarS detailliert charakterisiert werden, indem mehr Zielgene identifiziert werden und der jeweilige Regulationsmechanismus aufgeklärt wird. Darüber hinaus sollen die Expressionsprofile von *marS* in drei epidemiologisch relevanten *S. pyogenes* Isolaten aufgenommen werden und der Einfluss von

marS auf die Pathogenität dieser Stämme untersucht werden. Dabei können Erkenntnisse über allgemeine und *emm*-Typ-spezifische Targetspektren gewonnen werden, die Hinweise über Stoffwechselwege und Virulenzfaktoren liefern, die durch MarS beeinflusst werden.

3.2.2 Ein Glyzin-Riboswitch in *S. pyogenes* reguliert die Expression eines putativen Aminosäure-Symportergens

Unter den putativen sRNAs, die in der Array Analyse im Genom von *S. pyogenes* identifiziert wurden, befanden sich 18 Motive für *cis*-regulatorische Elemente, die mit Hilfe der rfam Datenbank („RNA family data base“) (Gardner *et al.*, 2009) zugeordnet wurden (Patenge *et al.*, 2012). In der 5'UTR eines putativen Aminosäure-Symportergens („sodium:alanine symporter family protein“ (SAF)) wurde ein Glyzin-bindendes Aptamer vorhergesagt. Glyzin wird für optimales Wachstum in *S. pyogenes* benötigt (Levering *et al.*, 2016). Ein Glyzin-Riboswitch wäre daher ein interessantes therapeutisches Target für die gezielte Inhibition des Glyzinmetabolismus oder -transports.

Nachdem die Expression der Riboswitch Region in *S. pyogenes* M49 Stamm 591 bereits in der Array Analyse gezeigt worden war (Patenge *et al.*, 2012) und zudem im klinischen Isolat *S. pyogenes* SF370 durch Northern Blot Analyse detektiert werden konnte (Le Rhun *et al.*, 2015), sollte in dieser Arbeit untersucht werden, ob das putative *cis*-regulatorische Element tatsächlich eine Glyzin abhängige Genregulation vermitteln kann. Dazu wurde ein 889 bp Fragment (*gly*), das den vorhergesagten Glyzin-Riboswitch enthielt, mit dem Luciferase Reportergen (*luc2*) fusioniert (Podbielski *et al.*, 1999). *S. pyogenes* M49 Stamm 591 wurde mit dem Plasmid pW11_*glyluc2* transformiert. Luciferase (LUC) Aktivität wurde nach Wachstum in der Gegenwart unterschiedlicher Glyzinkonzentrationen gemessen.

Die Experimente wurden in chemisch definiertem Medium (CDM) durchgeführt und die LUC-Aktivität auf die Zelldichte normalisiert, so dass Wachstumsunterschiede in Abhängigkeit von der Glyzinkonzentration berücksichtigt wurden. In Abwesenheit von Glyzin und in der Gegenwart niedriger Glyzinkonzentrationen (0.01–0.1 mM) war die LUC Aktivität am höchsten. Die LUC-Aktivität war bei Konzentrationen von 1-10 mM Glyzin signifikant verringert. Die Konzentration von Serin oder Alanin im Medium hatte keinen Einfluss auf die LUC-Aktivität (Khani *et al.*, 2018).

Da niedrige Konzentrationen von Glyzin im *glyluc2* Konstrukt die Reportergen Expression induzieren konnten, sollte durch RT-qPCR überprüft werden, ob die Glyzin-

konzentration im Medium die Expression der stromabwärts des putativen Glyzin-Riboswitches (*ribogly*) gelegenen Gene beeinflusst. Das SAF-Gen (*Na⁺/Ala symp*) und das putative „cation efflux system“ Gen (*cation efflux*) waren in Gegenwart hoher Glyzinkonzentrationen (2,6 mM und 10 mM) reprimiert im Vergleich zu 1 mM Glyzin.

In der Northern Blot Analyse konnte gezeigt werden, dass ein 3 kb Volllängen Transkript der *ribogly_Na⁺/Ala symp_cation efflux* Genregion nur in Gegenwart niedriger Glyzinkonzentration vorlag, während bei höheren Glyzinkonzentrationen ein kurzes 600 bp *ribogly* Fragment nachgewiesen wurde (Khani *et al.*, 2018). Die Genregion und die Transkripte, die im Northern Blot detektiert wurden, sind in Abbildung 5 schematisch dargestellt.

Die Transkripte von Genen, die durch Riboswitches reguliert werden, zeigen häufig auch eine differentielle Stabilität, die durch Ribonuklease Aktivität kontrolliert wird (Mellin and Cossart, 2015). Um die Stabilität der *ribogly*-regulierten Transkripte zu untersuchen, wurde *S. pyogenes* M49 Stamm 591 unter reprimierenden (10 mM Glyzin) und nicht-reprimierenden (0,1 mM Glyzin) Bedingungen kultiviert.

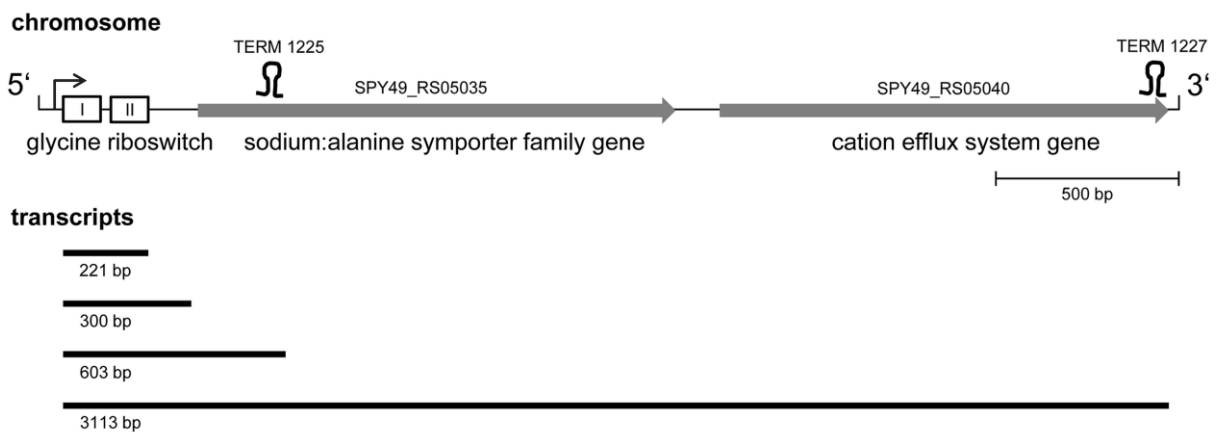


Abbildung 5. Schematische Darstellung der *ribogly* Genregion. Glyzin-Riboswitch Aptamere 1 und 2: Kästchen I und II; Gene sind als graue Pfeile dargestellt, die in Transkriptionsrichtung orientiert sind; die Terminatoren 1225 und 1227 (TransTermHP Vorhersage (Kingsford *et al.*, 2007)) sind als Haarnadel Strukturen eingezeichnet; Transkripte, die in der Northern Blot Analyse identifiziert wurden, sind als schwarze Linien dargestellt (Khani *et al.*, 2018).

Die Transkription wurde durch Zugabe von Rifampicin gestoppt und Proben zur RNA Isolierung wurden zu unterschiedlichen Zeitpunkten nach Zugabe (1, 2, 5, und 10 min) genommen. Die Stabilität wurde mittels RT-qPCR ermittelt. Während die Stabilität des *ribogly* Transkripts unter beiden Bedingungen gering war (Halbwertszeit: 0,5 min), hing die

Stabilität des *Na⁺/Ala sym^p* Transkripts von der Glyzinkonzentration im Medium ab. Bei einer niedrigen Glyzinkonzentration (0,1 mM) betrug die Halbwertszeit 5 min, während sie bei einer hohen Glyzinkonzentration (10 mM) bei 0,5 min lag. Diese Ergebnisse deuten auf eine weitere, Ribonuklease-abhängige Regulationsebene hin.

Die Rfam Analyse des Referenzgenoms NZ131 identifizierte einen 90 bp Sequenzbereich mit Homologie zu einem singulären Glyzin-Riboswitch Aptamer. Da die Northern Blot Analyse eine 200 bp Bande detektierte, wurde mit Hilfe von RNAfold (The Vienna RNA Web Services, <http://rna.tbi.univie.ac.at/>) die Sekundärstruktur der Riboswitch Sequenz vorhergesagt und mit VARNA GUI (Darty *et al.*, 2009) dargestellt (Abbildung 6). Die Analyse ergab eine typische Konsensus-Struktur für einen Tandem Aptamer Riboswitch, der zwei Glyzin Bindestellen enthält (Esquiaqui *et al.*, 2014, Ruff *et al.*, 2016). Die konservierten Basen sind in Abbildung 6 grün markiert.

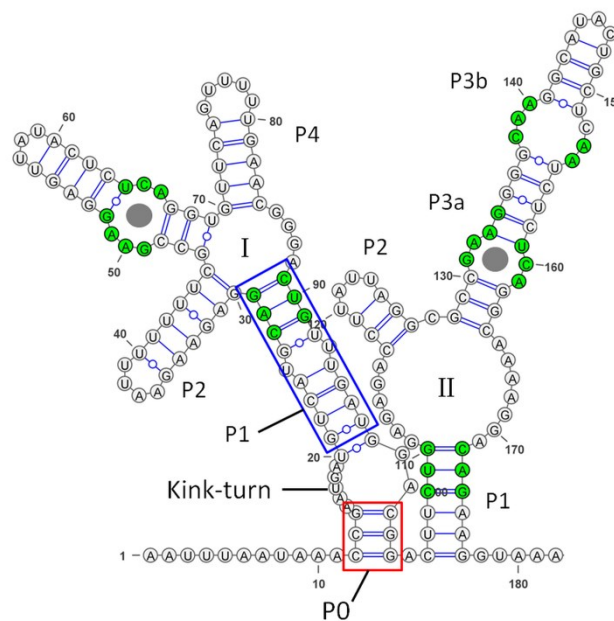


Abbildung 6. Sekundärstruktur des putativen Glyzin-Riboswitches in *S. pyogenes*. Die konservierten Basen sind grün markiert (Ruff *et al.*, 2016). Die putativen Glyzin Bindestellen werden durch graue Kreise symbolisiert. P1, das „Kink-turn“ Motif und P0 sind in Anlehnung an die Charakterisierung des Glyzin-Riboswitch aus *Vibrio cholerae* hervorgehoben (Esquiaqui *et al.*, 2014).

Typischer Weise stimulieren Glyzin-Riboswitches die Expression von Genen, deren Genprodukte an der Spaltung oder dem Export von Glyzin beteiligt sind (Serganov and Nudler, 2013, Serganov and Patel, 2009). In *Streptomyces griseum* wird ein Detoxifikations

System durch einen Glyzin-Riboswitch aktiviert (Tezuka and Ohnishi, 2014). Das SAF-Gen in *S. pyogenes* kodiert ein Mitglied der „Alanine or Glycine:Cation Symporter“ (AGCS) Familie [„Transporter Classification Database“ (TCDB)] (Saier *et al.*, 2016). Proteine, die zur AGCS Familie gehören, transportieren (symportieren) Alanin und/oder Glyzin mit Na⁺ und/oder H⁺. Ein Beispiel ist *dagA* aus dem marinen Bakterium *Alteromonas haloplanktis*, das einen Natrium abhängigen Transporter kodiert, der die Aufnahme von Glyzin und Glutamin vermittelt (MacLeod and MacLeod, 1992). In diesem Kontext lässt sich spekulieren, dass die Bindung von Glyzin an den Riboswitch in *S. pyogenes* mit der Repression der SAF-Genexpression zur Abschaltung eines bisher unbekanntes Glyzin Aufnahmesystems führt.

3.3 Peptid Nukleinsäuren (PNAs) als Antisense-Therapeutika in *S. pyogenes*

Um der Entwicklung und Ausbreitung von resistenten Erregern entgegenzuwirken, muss der Einsatz von Antibiotika optimiert werden. Darüber hinaus sollten neue Medikamente entwickelt werden, die als alternative Therapie eingesetzt werden können. Eine Möglichkeit wären Antisense-Therapeutika, die spezifisch auf essentielle Gene oder Antibiotikaresistenz Gene wirken. Folgende Eigenschaften wären wünschenswert für antimikrobielle Antisense-Wirkstoffe, die bei der Therapie von *S. pyogenes* Infektionen eingesetzt werden: (1) hohe Spezifität für das Targetgen, (2) effiziente Aufnahme in die Bakterienzelle, (3) geringe unspezifische Toxizität, (4) hohe Stabilität und, um die Eradikation intrazellulärer Erreger zu ermöglichen, (5) Import in die eukaryotischen Wirtszellen. PNAs können diese Eigenschaften potentiell vereinen und wurden bereits bei verschiedenen humanpathogenen Erregern getestet.

Dabei stellt die Translokation der PNAs in die Bakterien bisher die größte Hürde dar. PNAs werden nicht spontan von den Bakterienzellen aufgenommen. Die Konjugation von PNAs mit CPPs begünstigt den Transport in die Zellen. Da bakterielle Oberflächen unterschiedliche Barrieren aufweisen, u. a. Zellwand, Kapsel und Membrankomponenten, ist die Effizienz der CPPs Spezies-abhängig. In dieser Arbeit wurde daher in einem *Proof of Principle* zunächst nachgewiesen, dass CPP-konjugierte Antisense-PNAs grundsätzlich antimikrobiell auf *S. pyogenes* wirken können. Darauf aufbauend sollten im Anschluss effiziente CPPs für die Translokation identifiziert werden.

3.3.1 CPP-konjugierte anti-*gyrA* PNAs wirken antimikrobiell in *S. pyogenes*

Zu Beginn dieser Arbeit gab es nur eine geringe Anzahl von Publikationen, in denen die antimikrobielle Wirkung von Antisense-PNAs auf Gram-positive Bakterien beschrieben wurde. In diesen Studien wurde beobachtet, dass der Effekt auf Gram-positive Spezies geringer war im Vergleich zu *E. coli* und dass höhere Konzentrationen für eine Wachstumsinhibition benötigt wurden (Hatamoto *et al.*, 2009, Nekhotiaeva *et al.*, 2004). Das Ziel dieser Arbeit war zunächst, den Einfluss von Peptid-gekoppelten Antisense-PNAs auf das Wachstum von *S. pyogenes* zu überprüfen. Als Zielgen wurde *gyrA* ausgewählt. Das Genprodukt von *gyrA* ist die Untereinheit A der bakteriellen Gyrase. Dabei handelt es sich um eine DNA Topoisomerase, die für die Replikation des Bakteriengenoms benötigt wird und damit essentiell für das Wachstum ist. Die Antisense-PNAs wurden komplementär zur Startkodon Region der *gyrA* mRNA konstruiert (Nukleotide -5 bis 5) (Abbildung 7a). Als Kontrolle dienten PNAs gleicher Basenzusammensetzung mit randomisierter Sequenz („scrambled PNAs“, scPNAs) (Abbildung 7b).

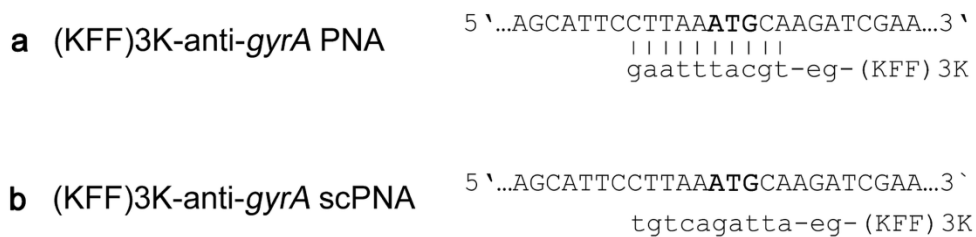


Abbildung 7. Design der anti-*gyrA* PNAs in *S. pyogenes*. Dargestellt sind (KFF)3K-konjugierte PNAs. Die obere Zeile repräsentiert jeweils die Sequenz der Startkodon Region von *gyrA*; das Startkodon ist fett gedruckt. In der unteren Zeile ist die PNA-Sequenz angegeben. eg: 8-amino-3,6-dioxaoctansäure. a: (KFF)3K-konjugierte anti-*gyrA* PNA. b: (KFF)3K-konjugierte scPNA (Patenge *et al.*, 2013b).

Zwei verschiedene CPPs wurden mit den anti-*gyrA* PNAs gekoppelt. Zum einen wurde das synthetische (KFF)3K Peptid konjugiert (Vaara and Porro, 1996), das häufig für Untersuchungen in Gram-negativen Bakterien eingesetzt wird. Zum anderen wurde das vom HIV-1 Transkriptionsaktivator abgeleitete Peptid HIV-1 TAT konjugiert (AS 48-57: GRKKRRQRRRYK), das bisher sowohl in eukaryotischen Zellen als auch in verschiedenen Bakterienspezies als Transportpeptid verwendet wurde (Vives *et al.*, 1997a).

S. pyogenes M49 Stamm 591 wurde mit verschiedenen PNA-Konstrukten inkubiert. Die konzentrationsabhängige Wachstumsinhibition wurde durch Trübungsmessung ermittelt. Anti-*gyrA* PNA, die nicht an CPPs gekoppelt waren, hemmten das Wachstum von *S. pyogenes* nicht. CPP-konjugierte anti-*gyrA* PNAs bewirkten eine konzentrationsabhängige Wachstumsinhibition im Bereich von 1,6-4,0 μM ((KFF)3K) bzw. 0,4-1,4 μM (HIV-1 TAT). Sowohl die scPNA-Kontrollen als auch die (KFF)3K und HIV-1 TAT Peptide allein wiesen nur eine geringe unspezifische Toxizität auf ($\geq 5.6 \mu\text{M}$ bzw. $\geq 20 \mu\text{M}$). HIV-1 TAT-gekoppelte anti-*gyrA* PNAs zeigten demnach eine höhere und spezifischere antimikrobielle Wirkung auf *S. pyogenes* als (KFF)3K-gekoppelte anti-*gyrA* PNAs. Der sequenzspezifische Einfluss der Antisense-PNAs auf die Transkriptmenge des Targetgens wurde exemplarisch an (KFF)3K-gekoppelten anti-*gyrA* PNAs untersucht. Um Stress-bedingte Schwankungen der *gyrA* Expression zu vermeiden, wurden die Bakterien mit einer geringen Antisense-PNA Konzentration (1,6 μM) inkubiert. Die relative *gyrA* Transkriptmenge wurde mit Hilfe der RT-qPCR Analyse ermittelt (Patenge *et al.*, 2013b). Dabei zeigte sich eine Reduktion der *gyrA* mRNA Abundanz nach Antisense-Behandlung auf 60 % im Vergleich zur unbehandelten Kontrolle.

3.3.2 Einfluss verschiedener CPPs auf die antimikrobielle Wirkung von Antisense-PNAs

Nachdem gezeigt werden konnte, dass HIV-1 TAT-gekoppelte anti-*gyrA* PNAs das Wachstum von *S. pyogenes* inhibieren, sollten weitere effiziente CPPs identifiziert werden. Es wurden anti-*gyrA* PNAs (Abbildung 7) mit 18 verschiedenen CPPs konjugiert. Es wurden CPPs ausgewählt, die sich zuvor als Carrier Moleküle in eukaryotischen Zellen bewährt hatten und eine geringe Toxizität aufwiesen (Tabelle 1).

S. pyogenes M49 Stamm 591 wurde mit 10 μM CPP-anti-*gyrA* PNA Konjugaten inkubiert. Die Reduktion der Kolonie bildenden Einheiten (KbE) wurde im Vergleich zu einer unbehandelten Kontrolle ermittelt. Von 18 CPP Antisense-Konstrukten zeigten nur drei einen antimikrobiellen Effekt: HIV-1 TAT-anti-*gyrA* PNA, K8-anti-*gyrA* PNA und (RXR)4XB-anti-*gyrA* PNA. Für eine genauere Analyse der CPP Antisense-Konstrukte wurde die konzentrationsabhängige bakterizide Wirkung der CPP-anti-*gyrA* PNA Konjugate bestimmt. Eine signifikante Reduktion der KbE/ml um mindestens eine Log_{10} -Stufe im Vergleich zur unbehandelten Kontrolle wurde nach Inkubation mit 4-10 μM HIV-1 TAT-anti-*gyrA* PNA, K8-anti-*gyrA* PNA und (RXR)4XB-anti-*gyrA* PNA nachgewiesen (Barkowsky, 2019).

Table 1: CPPs für die Translokation von anti-*gyrA* PNAs in *S. pyogenes*

CPP	CPP Sequence	Reference
Antennapedia homeodomain (Penetratin)	RQIKIWFQNRRMKWKK	(Derossi <i>et al.</i> , 1994)
ELA	Dansyl-G-C-ELALELALALEAALELA	(Turner <i>et al.</i> , 2010)
HIV-1 TAT (48–57)	GRKKRRQRRRYK	(Vives <i>et al.</i> , 1997b)
Human Calcitonin	LGTYQDFNKFHTFPQTAIGVGAP	(Trehin <i>et al.</i> , 2004)
(KFF) ₃ K	KFFKFFKFFK	(Vaara and Porro, 1996)
MAP	KLALKLALKALKAAALKLA	(Mueller <i>et al.</i> , 2008, Palm <i>et al.</i> , 2006)
mVE-cadherin (pVEC)	LLIILRRRIRKQAHAAHSK	
M918	MVTVLFRRRLRIRACGPPRVRV	(El-Andaloussi <i>et al.</i> , 2007b)
Oligoarginin (R6)	RRRRRR	(Maiolo <i>et al.</i> , 2005, Mueller <i>et al.</i> , 2008, Tunnemann <i>et al.</i> , 2008)
Oligoarginin (R10)	RRRRRRRRRR	
Oligoleucine (L6)	LLLLLL	Diese Arbeit
Oligolysin (K8)	KKKKKKKK	(Mitchell <i>et al.</i> , 2000)
PDESTK	PDESTK	(Roth <i>et al.</i> , 1998)
TLM	PLSSIFSRIGDP	(Manceur <i>et al.</i> , 2007)
TP10	AGYLLGKINLKALAALAKKIL	(El-Andaloussi <i>et al.</i> , 2007a)
Transportan	GWTLNSAGYLLGKINLKALAALAKKIL	(Lindgren <i>et al.</i> , 2000)
VT5	DPKGDPKGVTVTVTVTGKGDPKPD	(Oehlke <i>et al.</i> , 1997)
(RXR) ₄ XB	RXRRXRRXRRXRXB	(Abes <i>et al.</i> , 2008)

Die Toxizität der CPPs wurde mit Hilfe einer CPP-scPNA-Kontrolle bestimmt (Abbildung 7). HIV-1 TAT-anti-*gyrA* scPNA führte zu einer signifikanten Keimzahlreduktion nach Inkubation mit 5 und 10 µM scPNA. K8-anti-*gyrA* scPNA and (RXR)₄XB-anti-*gyrA* scPNA zeigten erst bei einer Konzentration von 10 µM einen bakteriziden Effekt.

Die minimale Hemmkonzentration (MHK) der CPP- anti-*gyrA* PNA Konstrukte wurde im Bouillon Mikrodilutionsverfahren bestimmt. Die MHK der HIV-1 TAT- und K8-anti-*gyrA* PNAs betrug 15,6 µM. (RXR)₄XB-anti-*gyrA* PNA war weniger effizient bei einer MHK von 62,5 µM. Alle korrespondierenden scPNA Kontrollen zeigten eine niedrigere antimikrobielle Aktivität (MHK 62,5 bzw. 125 µM) (Barkowsky, 2019).

Im nächsten Schritt wurde untersucht, ob die CPP-PNA Konjugate einen bakteriziden Effekt auf *S. pyogenes* Stämme zeigen, die unterschiedliche M-Serotypen mit epidemiologischer Relevanz repräsentieren. Dazu wurden sechs klinische Isolate jeweils mit 5 µM der CPP-PNA Konstrukte inkubiert. Nach sechs Stunden wurden Proben genommen und die Keimzahlreduktion analysiert. HIV-1 TAT-anti-*gyrA* PNA zeigte eine KbE/ml Reduktion von mindestens zwei Log₁₀-Stufen bei allen Stämmen mit Ausnahme von MGAS8232 (M18). K8-anti-*gyrA* PNA bewirkte eine signifikante Keimzahlreduktion bei allen Stämmen mit Ausnahme von AP1 (M1). Im Gegensatz dazu bewirkte (RXR)4XB-anti-*gyrA* PNA eine Reduktion der KbE/ml von mindestens zwei Log₁₀-Stufen bei allen Stämmen, die in diesem Experiment untersucht wurden (Barkowsky, 2019).

Um zu überprüfen, ob die Antisense-Konstrukte einen Einfluss auf die Transkriptmenge des Zielgens *gyrA* hatten, wurde *S. pyogenes* M49 Stamm 591 mit einer subletalen Dosis (2 µM) CPP-anti-*gyrA* PNA behandelt. Im Anschluss wurde Gesamt-RNA aus den Bakterien isoliert. Die *gyrA* mRNA wurde mit Hilfe von RT-qPCR relativ quantifiziert. Im Vergleich zur unbehandelten Kontrolle war das *gyrA* Transkript nach Behandlung mit CPP-anti-*gyrA* PNAs signifikant reduziert. Die Behandlung mit HIV-1 TAT-anti-*gyrA* PNA, (RXR)4XB-anti-*gyrA* PNA und K8-anti-*gyrA* PNA führte zu einer *gyrA* mRNA Reduktion auf 70 %, 60 % bzw. 56 % (Barkowsky, 2019).

Die antimikrobielle Wirkung der CPP-anti-*gyrA* PNAs sollte *in vivo* evaluiert werden. In dieser Arbeit wurde ein *Galleria mellonella* Infektionsmodell eingesetzt. Die Larven der großen Wachsmotte eignen sich als Modell zur Untersuchung von bakteriellen Infektionen und werden seit einigen Jahren für Arbeiten mit *S. pyogenes* eingesetzt (Tsai *et al.*, 2016). Invertebratenmodelle haben einige Vorteile gegenüber Säugetiermodellen, z. B. geringe ethische Bedenken und kostengünstige Anschaffung und Haltung der Tiere, die einen hohen Durchsatz begünstigen. *G. mellonella* kann bei 37 °C kultiviert werden, so dass die Experimente mit humanpathogenen Erregern bei Wirtstemperatur durchgeführt werden können. Den Insekten fehlt ein adaptives Immunsystem, die Komponenten des angeborenen Immunsystems sind jedoch vorhanden (Pereira *et al.*, 2018). Daher wird man langfristig nicht auf Säugetier Infektionsmodelle verzichten können, initiale Screening Experimente können jedoch in der Larve durchgeführt werden.

Die Larven wurden mit *S. pyogenes* M49 Stamm 591 infiziert und anschließend mit 4 nmol CPP-PNAs behandelt. Die Tiere wurden über einen Zeitraum von sieben Tagen

beobachtet. Das Überleben der CPP-PNA behandelten Larven wurde mit dem von Kontrolltieren verglichen, die eine 0.9 % Kochsalzlösung erhalten hatten. Die Larven, denen HIV-1 TAT-anti-*gyrA* PNA, K8-anti-*gyrA* PNA oder (RXR)4XB-anti-*gyrA* PNA injiziert worden war, zeigten signifikant erhöhte Überlebensraten im Vergleich zur Kontrolle. Ant-anti-*gyrA* PNA, mVE-cadherin-anti-*gyrA* PNA und ELA-anti-*gyrA* PNA, die *in vitro* keinen antimikrobiellen Effekt zeigten, beeinflussten die Überlebensrate der infizierten Larven hingegen nicht.

Die Kombination von Antisense-Präparaten mit konventionellen Antibiotika ist ein denkbarer Therapieansatz. Diese Strategie könnte die Antibiotikakonzentration senken, die für eine effiziente Behandlung benötigt wird. Daher sollte in dieser Arbeit untersucht werden, ob die Behandlung mit HIV-1 TAT-anti-*gyrA* PNA, die antibakterielle Effizienz von Antibiotika *in vivo* erhöhen kann. Zunächst wurden die Larven mit 1 µg Levofloxacin behandelt, das die bakterielle Gyrase hemmt. Die Überlebensrate der behandelten Larven erhöhte sich von 20 % auf 46 %. Nach einer Behandlung mit 1 µg Levofloxacin in Kombination mit 4 nmol HIV-1 TAT-anti-*gyrA* PNA überlebten 63 % der Larven. Für eine vergleichbare Überlebensrate mit Levofloxacin allein wurde eine Dosis von 15 µg benötigt.

In dieser Arbeit sollten CPPs identifiziert werden, die den Import von Antisense-PNAs in *S. pyogenes* unterstützen. Dazu wurden 18 CPPs untersucht, die unterschiedlichen Klassen angehören. Drei CPPs konnten identifiziert werden, die die Aufnahme in *S. pyogenes* vermitteln: die kationischen CPPs K8 and HIV1 TAT und das Arginin-reiche, amphipathische Peptid (RXR)4XB. Grundsätzlich unterstützen basische Reste die Aufnahme der CPPs in die Zelle, da die positive Ladung eine Interaktion mit der negativ geladenen Oberfläche ermöglicht. Es wurde in vorangegangenen Studien gezeigt, dass Arginin effektiver wirkt als Lysin, so dass CPPs besser importiert werden, wenn Lysin Reste durch Arginin ersetzt werden (Mitchell *et al.*, 2000, Wender *et al.*, 2000). Im Gegensatz zu K8 konjugierten anti-*gyrA* PNA zeigten Oligoarginin-gekoppelte Antisense-PNAs jedoch keine antimikrobielle Wirkung auf *S. pyogenes*. In eukaryotischen Zellen wurde gezeigt, dass die Insertion von 6-Aminohexansäure (X) oder β-Alanin (B) in Oligoarginin die Aufnahme in die Zelle verminderte, wobei es die Aufnahme in den Kern verbesserte (Wu *et al.*, 2007). In *S. pyogenes* konnte hingegen (RXR)4XB, im Gegensatz zu R8, die PNA Aufnahme vermitteln. Diese Beispiele unterstützen die Annahme, dass CPPs Organismen-spezifisch in die Zelle transportiert werden, da sich die Oberflächenbeschaffenheit der Zielzellen unterscheidet.

4. Zusammenfassung und Ausblick

Streptococcus pyogenes ist ein strikt humanpathogenes Bakterium, das weltweit eine hohe Belastung der menschlichen Gesundheit und der Gesundheitssysteme darstellt. Bisher steht kein Impfstoff zur Verfügung. Hohe Erkrankungsraten bei teilweise schweren Verläufen oder das Auftreten von Folgeerkrankungen sind eine große Herausforderung. Das Verständnis der Pathogenese und die Entwicklung innovativer Therapiestrategien sind daher erstrebenswert. In dieser Arbeit lag der Fokus auf der Antisense-Regulation der Genexpression.

Diese spielt bei der Kontrolle lebenswichtiger bakterieller Prozesse eine Rolle, bei pathogenen Organismen jedoch auch bei der Regulation von Virulenz-relevanten Genen. Kleine regulatorische RNAs (sRNAs) wirken häufig über eine Antisense-Interaktion. In dieser Arbeit konnten zunächst durch Expressionsanalysen und bioinformatische Vorhersagen potentielle sRNAs identifiziert werden. Dabei wurden in den Expressionsanalysen 37 *trans*-regulatorische und 18 *cis*-regulatorische sRNAs detektiert.

Bei sRNAs, die *in trans* wirken, bindet die sRNA in der Regel an die mRNA ihrer Targetgene. In dieser Arbeit wurde gezeigt, dass die sRNA MarS in der Lage ist, an das 5'-Ende des *mga* Transkripts zu binden. Bei Mga handelt es sich um einen zentralen Transkriptionsaktivator in *S. pyogenes*. In Abwesenheit von MarS war die Expression von *mga* und *mga*-kontrollierten Virulenzfaktorengen reduziert. Es konnte unter anderem ein Einfluss von MarS auf die Kapselsynthese, das Überleben im Blut und auf die Dissemination der Bakterien im murinen Infektionsmodell gezeigt werden.

In nachfolgenden Studien soll das MarS Regulon umfassend aufgeklärt werden. Dazu werden unter Zuhilfenahme von bioinformatischen Algorithmen weitere putative Zielgene von MarS vorhergesagt. Unter Bedingungen, die die *marS* Expression im Wildtyp unterstützen, wird eine Transkriptom-Analyse in *marS* Deletionsmutanten verschiedener Serotypen durchgeführt, um differentiell exprimierte Gene zu identifizieren. Die Ergebnisse der bioinformatischen Vorhersagen und der Transkriptom-Daten sollen verglichen und experimentell validiert werden. Diese Arbeiten dienen sowohl der Serotyp-übergreifenden Analyse der *S. pyogenes* Pathogenese als auch der Identifikation neuer potentieller Therapieziele.

Der Mechanismus von *cis*-regulatorischen Riboswitches beruht auf einer Konformationsänderung der regulatorischen RNA nach Bindung eines Liganden, die die

Expression der nachfolgenden Gene beeinflusst. Dabei erfolgt eine stabile Basenpaarung zwischen intramolekularen RNA Strängen. Diese Studie konnte zeigen, dass eine Sequenz in *S. pyogenes*, die Ähnlichkeiten zu bekannten Glyzin-Riboswitches aufweist, tatsächlich die differentielle Expression der stromabwärtsgelegenen Gene in Abhängigkeit der Glyzinkonzentration kontrolliert.

Mit dem in dieser Arbeit etablierten Reporter-gen-basierten Workflow zur Untersuchung von Riboswitches in *S. pyogenes* können in Zukunft weitere *cis*-regulatorische Elemente, deren Liganden bisher unbekannt sind, analysiert werden. Die Ergebnisse dieser Studien können zum einen molekularbiologische Tools für die induzierbare Genexpression liefern als auch die therapeutische, gezielte Abschaltung essentieller Prozesse durch Ligandenanaloga ermöglichen. Des Weiteren ist eine Charakterisierung der Ligandenbindung und des molekularen Mechanismus des Glyzin-Riboswitches im Vergleich zu anderen Bakterien interessant, um die Rolle der Aptamere genauer zu definieren.

Genexpressions-Kontrolle durch Antisense-Bindung kann auch therapeutisch genutzt werden. In dieser Arbeit wurden Peptid Nukleinsäuren (PNAs) als Antisense-Agens eingesetzt. Um die Aufnahme in *S. pyogenes* zu ermöglichen, wurden die PNAs kovalent an Carrierpeptide gekoppelt. Die PNA vermittelte Repression des essentiellen Gens *gyrA* führte zu einer Wachstumshemmung von *S. pyogenes*. Im *Galleria mellonella* Infektionsmodell erhöhte die Antisense-PNA Behandlung die Überlebensrate der Larven. Dabei konnte der Effekt durch Kombinationsgabe mit Antibiotika verstärkt werden.

In zukünftigen Arbeiten sollen weitere Carrier Moleküle geprüft werden, um die PNA Aufnahme in *S. pyogenes* zu optimieren. Alternativ zu Peptiden können Moleküle eingesetzt werden, die über einen Transporter aufgenommen werden, wie beispielsweise Vitamin B12. Effektive Carrier-PNA Konjugate, die im Insekten Infektionsmodell validiert worden sind, sollen im nächsten Schritt im murinen Infektionsmodell evaluiert werden. Eine wichtige klinische Herausforderung stellen Antibiotikaresistenzen in pathogenen Bakterien dar. Um dieser Problematik zu begegnen, sollen PNA Antisense-Konstrukte eingesetzt werden, die spezifisch sind für Resistenzgene. Dieser Ansatz ist für mehrere Spezies neben *S. pyogenes* geplant. Unter anderem sollen *S. pneumoniae* und verschiedene Arten der Gattung *Klebsiella* mit entsprechenden Konstrukten behandelt werden.

5. Quellenverzeichnis

- ABES, R., MOULTON, H. M., CLAIR, P., YANG, S. T., ABES, S., MELIKOV, K., PREVOT, P., YOUNGBLOOD, D. S., IVERSEN, P. L., CHERNOMORDIK, L. V. & LEBLEU, B. 2008. Delivery of steric block morpholino oligomers by (R-X-R)₄ peptides: structure-activity studies. *Nucleic Acids Res*, 36, 6343-54.
- ALBRICH, W. C., MONNET, D. L. & HARBARTH, S. 2004. Antibiotic selection pressure and resistance in *Streptococcus pneumoniae* and *Streptococcus pyogenes*. *Emerg Infect Dis*, 10, 514-7.
- ALTSCHUL, S. F., GISH, W., MILLER, W., MYERS, E. W. & LIPMAN, D. J. 1990. Basic local alignment search tool. *J. Mol. Biol*, 215, 403-410.
- BALDASSARRI, L., CRETI, R., RECCHIA, S., IMPERI, M., FACINELLI, B., GIOVANETTI, E., PATARACCHIA, M., ALFARONE, G. & OREFICI, G. 2006. Therapeutic failures of antibiotics used to treat macrolide-susceptible *Streptococcus pyogenes* infections may be due to biofilm formation. *J Clin Microbiol*, 44, 2721-7.
- BARKOWSKY, G., LEMSTER, A.-L., PAPPESCH, R., JACOB, A., KRÜGER, S., SCHRÖDER, A., KREIKEMEYER, B., & PATENGE, N. 2019. Influence of different Cell-Penetrating Peptides on the antimicrobial efficiency of antisense Peptide Nucleic Acids in *Streptococcus pyogenes*. *Mol. Ther. Nucleic Acids*, In press.
- BEAUME, M., HERNANDEZ, D., DOCQUIER, M., DELUCINGE-VIVIER, C., DESCOMBES, P. & FRANCOIS, P. 2011. Orientation and expression of methicillin-resistant *Staphylococcus aureus* small RNAs by direct multiplexed measurements using the nCounter of NanoString technology. *J. Microbiol. Methods*, 84, 327-334.
- BISNO, A. L., BRITO, M. O. & COLLINS, C. M. 2003. Molecular basis of group A streptococcal virulence. *Lancet Infect Dis*, 3, 191-200.
- BISNO, A. L., COCKERILL, F. R., 3RD & BERMUDEZ, C. T. 2000. The initial outpatient-physician encounter in group A streptococcal necrotizing fasciitis. *Clin Infect Dis*, 31, 607-8.
- BLANCO, A. M. & ARTERO, R. 2010. A practical approach to FRET-based PNA fluorescence in situ hybridization. *Methods*, 52, 343-351.
- BROOK, I. 2009. The role of beta-lactamase-producing-bacteria in mixed infections. *BMC Infect Dis*, 9, 202.
- BROOK, I. 2013. Penicillin failure in the treatment of streptococcal pharyngo-tonsillitis. *Curr Infect Dis Rep*, 15, 232-5.
- CARAPETIS, J. R., STEER, A. C., MULHOLLAND, E. K. & WEBER, M. 2005. The global burden of group A streptococcal diseases. *Lancet Infect. Dis*, 5, 685-694.

- CARBONARI, M., CIBATI, M., SETTE, N., CATIZONE, A. & FIORILLI, M. 2011. Measurement of telomere length using PNA probe by cytometry. *Methods Cell Biol*, 103, 189-202.
- CHEN, Y., INDURTHI, D. C., JONES, S. W. & PAPOUTSAKIS, E. T. 2011. Small RNAs in the genus *Clostridium*. *MBio*, 2, e00340-10.
- CUNNINGHAM, M. W. 2008. Pathogenesis of group A streptococcal infections and their sequelae. *Adv. Exp. Med. Biol*, 609, 29-42.
- DANGER, J. L., CAO, T. N., CAO, T. H., SARKAR, P., TREVINO, J., PFLUGHOEFT, K. J. & SUMBY, P. 2015a. The small regulatory RNA FasX enhances group A *Streptococcus* virulence and inhibits pilus expression via serotype-specific targets. *Mol. Microbiol*, 96, 249-262.
- DANGER, J. L., MAKTHAL, N., KUMARASWAMI, M. & SUMBY, P. 2015b. The FasX Small Regulatory RNA Negatively Regulates the Expression of Two Fibronectin-Binding Proteins in Group A *Streptococcus*. *J. Bacteriol*, 197, 3720-3730.
- DARTY, K., DENISE, A. & PONTY, Y. 2009. VARNA: Interactive drawing and editing of the RNA secondary structure. *Bioinformatics*, 25, 1974-1975.
- DEMIDOV, V. V., POTAMAN, V. N., FRANK-KAMENETSKII, M. D., EGHOLM, M., BUCHARD, O., SONNICHSEN, S. H. & NIELSEN, P. E. 1994. Stability of peptide nucleic acids in human serum and cellular extracts. *Biochem. Pharmacol*, 48, 1310-1313.
- DEROSSI, D., JOLIOT, A. H., CHASSAING, G. & PROCHIANTZ, A. 1994. The third helix of the Antennapedia homeodomain translocates through biological membranes. *J Biol Chem*, 269, 10444-50.
- DRYSELIUS, R., NEKHOTIAEVA, N. & GOOD, L. 2005. Antimicrobial synergy between mRNA- and protein-level inhibitors. *J. Antimicrob. Chemother*, 56, 97-103.
- EL-ANDALOUSSI, S., JARVER, P., JOHANSSON, H. J. & LANGEL, U. 2007a. Cargo-dependent cytotoxicity and delivery efficacy of cell-penetrating peptides: a comparative study. *Biochemical Journal*, 407, 285-292.
- EL-ANDALOUSSI, S., JOHANSSON, H. J., HOLM, T. & LANGEL, U. 2007b. A novel cell-penetrating peptide, M918, for efficient delivery of proteins and peptide nucleic acids. *Molecular Therapy*, 15, 1820-1826.
- ERIKSSON, M., NIELSEN, P. E. & GOOD, L. 2002. Cell permeabilization and uptake of antisense peptide-peptide nucleic acid (PNA) into *Escherichia coli*. *J. Biol. Chem*, 277, 7144-7147.
- ESQUIAQUI, J. M., SHERMAN, E. M., IONESCU, S. A., YE, J. D. & FANUCCI, G. E. 2014. Characterizing the dynamics of the leader-linker interaction in the glycine riboswitch with site-directed spin labeling. *Biochemistry*, 53, 3526-3528.

- FRANCIS, J. & WARREN, R. E. 1988. Streptococcus pyogenes bacteraemia in Cambridge--a review of 67 episodes. *Q J Med*, 68, 603-13.
- FUCHS, R. T., GRUNDY, F. J. & HENKIN, T. M. 2006. The S(MK) box is a new SAM-binding RNA for translational regulation of SAM synthetase. *Nat. Struct. Mol. Biol*, 13, 226-233.
- FUCHS, R. T., GRUNDY, F. J. & HENKIN, T. M. 2007. S-adenosylmethionine directly inhibits binding of 30S ribosomal subunits to the SMK box translational riboswitch RNA. *Proc. Natl. Acad. Sci. U. S. A*, 104, 4876-4880.
- GARDNER, P. P., DAUB, J., TATE, J. G., NAWROCKI, E. P., KOLBE, D. L., LINDGREEN, S., WILKINSON, A. C., FINN, R. D., GRIFFITHS-JONES, S., EDDY, S. R. & BATEMAN, A. 2009. Rfam: updates to the RNA families database. *Nucleic Acids Res*, 37, D136-D140.
- GOOD, L. & NIELSEN, P. E. 1998. Antisense inhibition of gene expression in bacteria by PNA targeted to mRNA. *Nat. Biotechnol*, 16, 355-358.
- GOOD, L., SANDBERG, R., LARSSON, O., NIELSEN, P. E. & WAHLESTEDT, C. 2000. Antisense PNA effects in *Escherichia coli* are limited by the outer-membrane LPS layer. *Microbiology*, 146 (Pt 10), 2665-2670.
- GORKE, B. & VOGEL, J. 2008. Noncoding RNA control of the making and breaking of sugars. *Genes Dev*, 22, 2914-2925.
- GOTTESMAN, S., MCCULLEN, C. A., GUILLIER, M., VANDERPOOL, C. K., MAJDALANI, N., BENHAMMOU, J., THOMPSON, K. M., FITZGERALD, P. C., SOWA, N. A. & FITZGERALD, D. J. 2006. Small RNA regulators and the bacterial response to stress. *Cold Spring Harb. Symp. Quant. Biol*, 71, 1-11.
- GRANIZO, J. J., AGUILAR, L., CASAL, J., DAL-RE, R. & BAQUERO, F. 2000. Streptococcus pyogenes resistance to erythromycin in relation to macrolide consumption in Spain (1986-1997). *J Antimicrob Chemother*, 46, 959-64.
- HANCOCK, R. E. 1997. Antibacterial peptides and the outer membranes of gram-negative bacilli. *J. Med. Microbiol*, 46, 1-3.
- HATAMOTO, M., NAKAI, K., OHASHI, A. & IMACHI, H. 2009. Sequence-specific bacterial growth inhibition by peptide nucleic acid targeted to the mRNA binding site of 16S rRNA. *Appl. Microbiol. Biotechnol*, 84, 1161-1168.
- HATAMOTO, M., OHASHI, A. & IMACHI, H. 2010. Peptide nucleic acids (PNAs) antisense effect to bacterial growth and their application potentiality in biotechnology. *Appl. Microbiol. Biotechnol*, 86, 397-402.

HONDORP, E. R. & MCIVER, K. S. 2007. The Mga virulence regulon: infection where the grass is greener. *Mol. Microbiol*, 66, 1056-1065.

KANG, M., EICHHORN, C. D. & FEIGON, J. 2014. Structural determinants for ligand capture by a class II preQ1 riboswitch. *Proc. Natl. Acad. Sci. U. S. A.*, 111, E663-E671.

KAPLAN, E. L., CHHATWAL, G. S. & ROHDE, M. 2006. Reduced ability of penicillin to eradicate ingested group A streptococci from epithelial cells: clinical and pathogenetic implications. *Clin Infect Dis*, 43, 1398-406.

KHANI, A., POPP, N., KREIKEMEYER, B. & PATENGE, N. 2018. A Glycine Riboswitch in *Streptococcus pyogenes* Controls Expression of a Sodium:Alanine Symporter Family Protein Gene. *Front Microbiol*, 9, 200.

KINGSFORD, C. L., AYANBULE, K. & SALZBERG, S. L. 2007. Rapid, accurate, computational discovery of Rho-independent transcription terminators illuminates their relationship to DNA uptake. *Genome Biol*, 8, R22.

KREIKEMEYER, B., BOYLE, M. D., BUTTARO, B. A., HEINEMANN, M. & PODBIELSKI, A. 2001. Group A streptococcal growth phase-associated virulence factor regulation by a novel operon (Fas) with homologies to two-component-type regulators requires a small RNA molecule. *Mol. Microbiol*, 39, 392-406.

KREIKEMEYER, B., MCIVER, K. S. & PODBIELSKI, A. 2003. Virulence factor regulation and regulatory networks in *Streptococcus pyogenes* and their impact on pathogen-host interactions. *Trends Microbiol*, 11, 224-232.

KUMAR, R., SHAH, P., SWIATLO, E., BURGESS, S. C., LAWRENCE, M. L. & NANDURI, B. 2010. Identification of novel non-coding small RNAs from *Streptococcus pneumoniae* TIGR4 using high-resolution genome tiling arrays. *BMC. Genomics*, 11, 350.

LARKIN, M. A., BLACKSHIELDS, G., BROWN, N. P., CHENNA, R., MCGETTIGAN, P. A., MCWILLIAM, H., VALENTIN, F., WALLACE, I. M., WILM, A., LOPEZ, R., THOMPSON, J. D., GIBSON, T. J. & HIGGINS, D. G. 2007. Clustal W and Clustal X version 2.0. *Bioinformatics*, 23, 2947-8.

LE RHUN, A., BEER, Y. Y., REIMEGARD, J., CHYLINSKI, K. & CHARPENTIER, E. 2015. RNA sequencing uncovers antisense RNAs and novel small RNAs in *Streptococcus pyogenes*. *RNA. Biol*, 0.

LEVERING, J., FIEDLER, T., SIEG, A., VAN GRINSVEN, K. W., HERING, S., VEITH, N., OLIVIER, B. G., KLETT, L., HUGENHOLTZ, J., TEUSINK, B., KREIKEMEYER, B. & KUMMER, U. 2016. Genome-scale reconstruction of the *Streptococcus pyogenes* M49 metabolic network reveals growth requirements and indicates potential drug targets. *J. Biotechnol*, 232, 25-37.

LINDGREN, M., GALLET, X., SOOMETS, U., HALLBRINK, M., BRAKENHIELM, E., POOGA, M., BRASSEUR, R. & LANGEL, U. 2000. Translocation properties of novel cell penetrating transportan and penetratin analogues. *Bioconjug Chem*, 11, 619-26.

- LIU, Z., TREVINO, J., RAMIREZ-PENA, E. & SUMBY, P. 2012. The small regulatory RNA FasX controls pilus expression and adherence in the human bacterial pathogen group A Streptococcus. *Mol. Microbiol.*
- LORENZ, R., HOFACKER, I. L. & STADLER, P. F. 2016. RNA folding with hard and soft constraints. *Algorithms Mol Biol*, 11, 8.
- MACHADO-LIMA, A., DEL PORTILLO, H. A. & DURHAM, A. M. 2008. Computational methods in noncoding RNA research. *J Math Biol*, 56, 15-49.
- MACHTEL, P., BAKOWSKA-ZYWICKA, K. & ZYWICKI, M. 2016. Emerging applications of riboswitches - from antibacterial targets to molecular tools. *J. Appl. Genet*, 57, 531-541.
- MACLEOD, P. R. & MACLEOD, R. A. 1992. Identification and sequence of a Na⁽⁺⁾-linked gene from the marine bacterium *Alteromonas haloplanktis* which functionally complements the *dagA* gene of *Escherichia coli*. *Mol. Microbiol*, 6, 2673-2681.
- MAIOLO, J. R., FERRER, M. & OTTINGER, E. A. 2005. Effects of cargo molecules on the cellular uptake of arginine-rich cell-penetrating peptides. *Biochim Biophys Acta*, 1712, 161-72.
- MANCEUR, A., WU, A. & AUDET, J. 2007. Flow cytometric screening of cell-penetrating peptides for their uptake into embryonic and adult stem cells. *Anal Biochem*, 364, 51-9.
- MARKOWITZ, M., GERBER, M. A. & KAPLAN, E. L. 1993. Treatment of streptococcal pharyngotonsillitis: reports of penicillin's demise are premature. *J Pediatr*, 123, 679-85.
- MATHEWS, D. H. & TURNER, D. H. 2006. Prediction of RNA secondary structure by free energy minimization. *Curr Opin Struct Biol*, 16, 270-8.
- MCDONALD, M., CURRIE, B. J. & CARAPETIS, J. R. 2004. Acute rheumatic fever: a chink in the chain that links the heart to the throat? *Lancet Infect Dis*, 4, 240-5.
- MELENEY, F. L. & ZAU, Z. D. 1924. The Viability of Hemolytic Streptococcus in Certain Solutions Containing Gelatin. *J Exp Med*, 39, 811-25.
- MELLIN, J. R. & COSSART, P. 2015. Unexpected versatility in bacterial riboswitches. *Trends Genet*, 31, 150-6.
- MEYER, I. M. 2007. A practical guide to the art of RNA gene prediction. *Brief Bioinform*, 8, 396-414.
- MEYER, M. M., ROTH, A., CHERVIN, S. M., GARCIA, G. A. & BREAKER, R. R. 2008. Confirmation of a second natural preQ1 aptamer class in Streptococcaceae bacteria. *RNA*, 14, 685-695.

- MITCHELL, D. J., KIM, D. T., STEINMAN, L., FATHMAN, C. G. & ROTHBARD, J. B. 2000. Polyarginine enters cells more efficiently than other polycationic homopolymers. *J Pept Res*, 56, 318-25.
- MRAHEIL, M. A., BILLION, A., MOHAMED, W., MUKHERJEE, K., KUENNE, C., PISCHIMAROV, J., KRAWITZ, C., RETEY, J., HARTSCH, T., CHAKRABORTY, T. & HAIN, T. 2011. The intracellular sRNA transcriptome of *Listeria monocytogenes* during growth in macrophages. *Nucleic Acids Res*, 39, 4235-4248.
- MUELLER, J., KRETZSCHMAR, I., VOLKMER, R. & BOISGUERIN, P. 2008. Comparison of cellular uptake using 22 CPPs in 4 different cell lines. *Bioconjug Chem*, 19, 2363-74.
- MURPHY, T. K., PATEL, P. D., MCGUIRE, J. F., KENNEL, A., MUTCH, P. J., PARKER-ATHILL, E. C., HANKS, C. E., LEWIN, A. B., STORCH, E. A., TOUFEXIS, M. D., DADLANI, G. H. & RODRIGUEZ, C. A. 2015. Characterization of the pediatric acute-onset neuropsychiatric syndrome phenotype. *J Child Adolesc Psychopharmacol*, 25, 14-25.
- NEKHOTIAEVA, N., AWASTHI, S. K., NIELSEN, P. E. & GOOD, L. 2004. Inhibition of *Staphylococcus aureus* gene expression and growth using antisense peptide nucleic acids. *Mol. Ther*, 10, 652-659.
- NELSON, J. W., PLUMMER, M. S., BLOUNT, K. F., AMES, T. D. & BREAKER, R. R. 2015. Small molecule fluoride toxicity agonists. *Chem. Biol*, 22, 527-534.
- NIELSEN, P. E. & EGHOLM, M. 1999. An introduction to peptide nucleic acid. *Curr. Issues Mol. Biol*, 1, 89-104.
- OEHLKE, J., KRAUSE, E., WIESNER, B., BEYERMANN, M. & BIENERT, M. 1997. Extensive cellular uptake into endothelial cells of an amphipathic beta-sheet forming peptide. *FEBS Lett*, 415, 196-9.
- PALM, C., NETZEREAB, S. & HALLBRINK, M. 2006. Quantitatively determined uptake of cell-penetrating peptides in non-mammalian cells with an evaluation of degradation and antimicrobial effects. *Peptides*, 27, 1710-6.
- PAPENFORT, K. & VOGEL, J. 2010. Regulatory RNA in bacterial pathogens. *Cell Host. Microbe*, 8, 116-127.
- PAPPESCH, R., WARNKE, P., MIKKAT, S., NORMANN, J., WISNIEWSKA-KUCPER, A., HUSCHKA, F., WITTMANN, M., KHANI, A., SCHWENGER, O., OEHMCKE-HECHT, S., HAIN, T., KREIKEMEYER, B. & PATENGE, N. 2017. The Regulatory Small RNA MarS Supports Virulence of *Streptococcus pyogenes*. *Sci. Rep*, 7, 12241.
- PATENGE, N., BILLION, A., RAASCH, P., NORMANN, J., WISNIEWSKA-KUCPER, A., RETEY, J., BOISGUERIN, V., HARTSCH, T., HAIN, T. & KREIKEMEYER, B. 2012. Identification of novel growth phase- and media-dependent small non-coding RNAs in *Streptococcus pyogenes* M49 using intergenic tiling arrays. *BMC. Genomics*, 13, 550.

- PATENGE, N., FIEDLER, T. & KREIKEMEYER, B. 2013a. Common regulators of virulence in streptococci. *Curr. Top. Microbiol. Immunol*, 368, 111-153.
- PATENGE, N., PAPPESCH, R., KHANI, A. & KREIKEMEYER, B. 2015. Genome-wide analyses of small non-coding RNAs in streptococci. *Front Genet*, 6, 189.
- PATENGE, N., PAPPESCH, R., KRAWACK, F., WALDA, C., MRAHEIL, M. A., JACOB, A., HAIN, T. & KREIKEMEYER, B. 2013b. Inhibition of Growth and Gene Expression by PNA-peptide Conjugates in *Streptococcus pyogenes*. *Mol. Ther. Nucleic Acids*, 2, e132.
- PEREIRA, T. C., DE BARROS, P. P., FUGISAKI, L. R. O., ROSSONI, R. D., RIBEIRO, F. C., DE MENEZES, R. T., JUNQUEIRA, J. C. & SCORZONI, L. 2018. Recent Advances in the Use of *Galleria mellonella* Model to Study Immune Responses against Human Pathogens. *J Fungi (Basel)*, 4.
- PEREZ, N., TREVINO, J., LIU, Z., HO, S. C., BABITZKE, P. & SUMBY, P. 2009. A genome-wide analysis of small regulatory RNAs in the human pathogen group A *Streptococcus*. *PLoS. One*, 4, e7668.
- PODBIELSKI, A., WOISCHNIK, M., LEONARD, B. A. & SCHMIDT, K. H. 1999. Characterization of *nra*, a global negative regulator gene in group A streptococci. *Mol. Microbiol*, 31, 1051-1064.
- PODKAMINSKI, D. & VOGEL, J. 2010. Small RNAs promote mRNA stability to activate the synthesis of virulence factors. *Mol. Microbiol*, 78, 1327-1331.
- RAASCH, P., SCHMITZ, U., PATENGE, N., VERA, J., KREIKEMEYER, B. & WOLKENHAUER, O. 2010. Non-coding RNA detection methods combined to improve usability, reproducibility and precision. *BMC. Bioinformatics*, 11, 491.
- RAMIREZ-PENA, E., TREVINO, J., LIU, Z., PEREZ, N. & SUMBY, P. 2010. The group A *Streptococcus* small regulatory RNA FasX enhances streptokinase activity by increasing the stability of the *ska* mRNA transcript. *Mol. Microbiol*, 78, 1332-1347.
- RODRIGUEZ-ITURBE, B. & HAAS, M. 2016. Post-*Streptococcal* Glomerulonephritis. In: FERRETTI, J. J., STEVENS, D. L. & FISCHETTI, V. A. (eds.) *Streptococcus pyogenes : Basic Biology to Clinical Manifestations*. Oklahoma City (OK).
- ROTH, A. F., SULLIVAN, D. M. & DAVIS, N. G. 1998. A large PEST-like sequence directs the ubiquitination, endocytosis, and vacuolar degradation of the yeast α -factor receptor. *J Cell Biol*, 142, 949-61.
- RUFF, K. M., MUHAMMAD, A., MCCOWN, P. J., BREAKER, R. R. & STROBEL, S. A. 2016. Singlet glycine riboswitches bind ligand as well as tandem riboswitches. *RNA*, 22, 1728-1738.

SAIER, M. H., JR., REDDY, V. S., TSU, B. V., AHMED, M. S., LI, C. & MORENO-HAGELSIEB, G. 2016. The Transporter Classification Database (TCDB): recent advances. *Nucleic Acids Res*, 44, D372-D379.

SEPPALA, H., KLAUKKA, T., VUOPIO-VARKILA, J., MUOTIALA, A., HELENIUS, H., LAGER, K. & HUOVINEN, P. 1997. The effect of changes in the consumption of macrolide antibiotics on erythromycin resistance in group A streptococci in Finland. Finnish Study Group for Antimicrobial Resistance. *N Engl J Med*, 337, 441-6.

SERGANOV, A. & NUDLER, E. 2013. A decade of riboswitches. *Cell*, 152, 17-24.

SERGANOV, A. & PATEL, D. J. 2009. Amino acid recognition and gene regulation by riboswitches. *Biochim. Biophys. Acta*, 1789, 592-611.

SHAIKH, N., LEONARD, E. & MARTIN, J. M. 2010. Prevalence of streptococcal pharyngitis and streptococcal carriage in children: a meta-analysis. *Pediatrics*, 126, e557-64.

SHULMAN, S. T., BISNO, A. L., CLEGG, H. W., GERBER, M. A., KAPLAN, E. L., LEE, G., MARTIN, J. M. & VAN BENEDEN, C. 2012. Clinical practice guideline for the diagnosis and management of group A streptococcal pharyngitis: 2012 update by the Infectious Diseases Society of America. *Clin Infect Dis*, 55, 1279-82.

SIMS, S. A., COLQUHOUN, S., WYBER, R. & CARAPETIS, J. R. 2016. Global Disease Burden of Group A Streptococcus.

SRIDHAR, J., SAMBATURU, N., SABARINATHAN, R., OU, H. Y., DENG, Z., SEKAR, K., RAFI, Z. A. & RAJAKUMAR, K. 2010. sRNAsScanner: a computational tool for intergenic small RNA detection in bacterial genomes. *PLoS. One*, 5, e11970.

STEVENS, D. L., TANNER, M. H., WINSHIP, J., SWARTS, R., RIES, K. M., SCHLIEVERT, P. M. & KAPLAN, E. 1989. Severe group A streptococcal infections associated with a toxic shock-like syndrome and scarlet fever toxin A. *N Engl J Med*, 321, 1-7.

STORZ, G., VOGEL, J. & WASSARMAN, K. M. 2011. Regulation by small RNAs in bacteria: expanding frontiers. *Mol. Cell*, 43, 880-891.

TEZUKA, T. & OHNISHI, Y. 2014. Two glycine riboswitches activate the glycine cleavage system essential for glycine detoxification in *Streptomyces griseus*. *J. Bacteriol*, 196, 1369-1376.

TREHIN, R., KRAUSS, U., BECK-SICKINGER, A. G., MERKLE, H. P. & NIELSEN, H. M. 2004. Cellular uptake but low permeation of human calcitonin-derived cell penetrating peptides and Tat(47-57) through well-differentiated epithelial models. *Pharm Res*, 21, 1248-56.

TSAI, C. J., LOH, J. M. & PROFT, T. 2016. *Galleria mellonella* infection models for the study of bacterial diseases and for antimicrobial drug testing. *Virulence*, 7, 214-29.

- TSUI, H. C., MUKHERJEE, D., RAY, V. A., SHAM, L. T., FEIG, A. L. & WINKLER, M. E. 2010. Identification and characterization of noncoding small RNAs in *Streptococcus pneumoniae* serotype 2 strain D39. *J. Bacteriol*, 192, 264-279.
- TUNNEMANN, G., TER-AVETISYAN, G., MARTIN, R. M., STOCKL, M., HERRMANN, A. & CARDOSO, M. C. 2008. Live-cell analysis of cell penetration ability and toxicity of oligo-arginines. *J. Pept. Sci*, 14, 469-476.
- TURNER, Y., WALLUKAT, G., SAALIK, P., WIESNER, B., PRITZ, S. & OEHLKE, J. 2010. Cellular uptake and biological activity of peptide nucleic acids conjugated with peptides with and without cell-penetrating ability. *J. Pept. Sci*, 16, 71-80.
- VAARA, M. & PORRO, M. 1996. Group of peptides that act synergistically with hydrophobic antibiotics against gram-negative enteric bacteria. *Antimicrob. Agents Chemother*, 40, 1801-1805.
- VIVES, E., BRODIN, P. & LEBLEU, B. 1997a. A truncated HIV-1 Tat protein basic domain rapidly translocates through the plasma membrane and accumulates in the cell nucleus. *J Biol Chem*, 272, 16010-7.
- VIVES, E., BRODIN, P. & LEBLEU, B. 1997b. A truncated HIV-1 Tat protein basic domain rapidly translocates through the plasma membrane and accumulates in the cell nucleus. *J. Biol. Chem*, 272, 16010-16017.
- WASHIETL, S., HOFACKER, I. L. & STADLER, P. F. 2005. Fast and reliable prediction of noncoding RNAs. *Proc. Natl. Acad. Sci. U. S. A*, 102, 2454-2459.
- WATERS, L. S. & STORZ, G. 2009. Regulatory RNAs in bacteria. *Cell*, 136, 615-628.
- WENDER, P. A., MITCHELL, D. J., PATTABIRAMAN, K., PELKEY, E. T., STEINMAN, L. & ROTHBARD, J. B. 2000. The design, synthesis, and evaluation of molecules that enable or enhance cellular uptake: peptoid molecular transporters. *Proc Natl Acad Sci U S A*, 97, 13003-8.
- WRIGHT, P. R., GEORG, J., MANN, M., SORESCU, D. A., RICHTER, A. S., LOTT, S., KLEINKAUF, R., HESS, W. R. & BACKOFEN, R. 2014. CopraRNA and IntaRNA: predicting small RNA targets, networks and interaction domains. *Nucleic Acids Res*, 42, W119-W123.
- WU, R. P., YOUNGBLOOD, D. S., HASSINGER, J. N., LOVEJOY, C. E., NELSON, M. H., IVERSEN, P. L. & MOULTON, H. M. 2007. Cell-penetrating peptides as transporters for morpholino oligomers: effects of amino acid composition on intracellular delivery and cytotoxicity. *Nucleic Acids Res*, 35, 5182-91.

6. Anlagen

6.1 Originalarbeiten

Molecular Therapy
Nucleic Acids
Original Article



Influence of Different Cell-Penetrating Peptides on the Antimicrobial Efficiency of PNAs in *Streptococcus pyogenes*

Gina Barkowsky,¹ Anna-Lena Lemster,¹ Roberto Pappesch,¹ Anette Jacob,^{2,3} Selina Krüger,¹ Anne Schröder,¹ Bernd Kreikemeyer,¹ and Nadja Patenge¹

¹Institute of Medical Microbiology, Virology and Hygiene, University Medicine Rostock, 18057 Rostock, Germany; ²Peps4LS GmbH, INF 583, 69120 Heidelberg, Germany;

³Functional Genome Analysis, Deutsches Krebsforschungszentrum, 69120 Heidelberg, Germany

Streptococcus pyogenes is an exclusively human pathogen causing a wide range of clinical manifestations from mild superficial infections to severe, life-threatening, invasive diseases. *S. pyogenes* is consistently susceptible toward penicillin, but therapeutic failure of penicillin treatment has been reported frequently. At the same time, streptococcal resistance to alternative antibiotics, e.g., macrolides, is common. To reduce the application of antibiotics for treatment of *S. pyogenes* infections, it is mandatory to develop novel therapeutic strategies. Antisense peptide nucleic acids (PNAs) are synthetic DNA derivatives widely applied for hybridization-based microbial diagnostics. They have a high potential as therapeutic agents, because PNA antisense targeting of essential genes was shown to reduce growth of several pathogenic bacterial species. Spontaneous cellular uptake of PNAs is restricted in eukaryotes and in bacteria. To overcome this problem, PNAs can be coupled to cell-penetrating peptides (CPPs) that support PNA translocation over the cell membrane. In bacteria, the efficiency of CPP-mediated PNA uptake is species specific. Previously, HIV-1 transactivator of transcription (HIV-1 TAT) peptide-coupled anti-*gyrA* PNA was shown to inhibit growth of *S. pyogenes*. Here, we investigate the effect of 18 CPP-coupled anti-*gyrA* PNAs on *S. pyogenes* growth and virulence. HIV-1 TAT, oligolysine (K8), and (RXR)₄XB peptide-coupled anti-*gyrA* PNAs efficiently abolished bacterial growth *in vitro*. Consistently, treatment with these three CPP-PNAs increased survival of larvae in a *Galleria mellonella* infection model.

INTRODUCTION

Streptococcus pyogenes (group A streptococcus [GAS]) is a Gram-positive, exclusively human pathogen responsible for a variety of diseases ranging from mild self-limiting superficial infections of the throat or skin to life-threatening invasive diseases, including bacteremia and necrotizing fasciitis. The global burden of streptococcal infections is high, with 18 million invasive infections per year and 500,000 deaths.¹ The impact of GAS diseases is especially high in resource-limited settings, and a rise of

global invasive disease burden caused by GAS has been reported recently.² Untreated superficial infections often lead to the development of severe invasive infections or autoimmune sequelae.^{1,3}

To date, penicillin is the standard treatment of streptococcal pharyngitis, because GAS is invariably susceptible toward penicillin. Macrolides are recommended as alternate antibiotics for the treatment of *S. pyogenes* infections in patients who are allergic to β -lactams or in cases of penicillin failure.⁴ Resistance rates to macrolides in the United States have remained relatively low.⁵ In contrast, a rise of macrolide resistance in *S. pyogenes* has been observed in Europe, followed by a decrease in erythromycin resistance in several European countries.⁶ Today, a major goal of public health is to limit the application and distribution of antibiotics. One possible strategy is the application of antisense therapeutics targeting essential genes or antibiotic-resistance genes. Desired features of *S. pyogenes*-specific antimicrobials are a high specificity for the target gene, effective uptake into the bacterial cell, low unspecific toxicity, high stability, and—for the eradication of intracellular bacteria—import into eukaryotic cells. Antisense peptide nucleic acids (PNAs) potentially combine these properties and have been tested as antimicrobial agents in many bacterial species. PNAs are synthetic DNA derivatives, which bind sequence specific to DNA and RNA and are able to form stable duplexes and triplexes.⁷ The nucleic acid sugar-phosphate backbone is replaced by a pseudo-peptide backbone, resulting in a high chemical stability and resistance to nucleases and proteases.^{7,8} Cellular uptake of PNAs is limited by bacterial membranes and cell walls. Coupling of PNAs to cell-penetrating peptides (CPPs) may facilitate PNA translocation into bacteria and thereby enhance antimicrobial efficiency. CPPs are naturally occurring or designed peptides that are able to penetrate cell membranes and have been used for the

Received 2 July 2019; accepted 8 September 2019;
<https://doi.org/10.1016/j.omtn.2019.09.010>

Correspondence: Nadja Patenge, Institute of Medical Microbiology, Virology and Hygiene, University Medicine Rostock, Schillingallee 70, 18057 Rostock, Germany. E-mail: nadja.patenge@med.uni-rostock.de



Table 1. CPP-PNA Anti-*gyrA* Conjugates for Antisense Studies in *S. pyogenes*

CPP	CPP Sequence	CPP-PNA Designation	Reference
Antennapedia homeodomain (Penetratin)	RQIKIWFQNRRMKWKK	Ant-anti- <i>gyrA</i> PNA	16
		Ant-anti- <i>gyrA</i> scPNA	
ELA	Dansyl-G-C-ELALE LALEALEAALELA	ELA-anti- <i>gyrA</i> PNA	17
		ELA-anti- <i>gyrA</i> scPNA	
HIV-1 TAT (48–57)	GRKKRRQRRRYK	TAT-anti- <i>gyrA</i> PNA	18
		TAT-anti- <i>gyrA</i> scPNA	
Human calcitonin	LGTYQDFNKFHTFPQTAIGVGAP	hCalcitonin-anti- <i>gyrA</i> PNA	19
		hCalcitonin-anti- <i>gyrA</i> scPNA	
(KFF) ₃ K	KFFKFFKFFK	(KFF) ₃ K-anti- <i>gyrA</i> PNA	20
		(KFF) ₃ K-anti- <i>gyrA</i> scPNA	
MAP	KLALKLALKALKAAKLA	MAP-anti- <i>gyrA</i> PNA	21,22
		MAP-anti- <i>gyrA</i> scPNA	
mVE-cadherin (pVEC)	LLHLRRRIRKQAHASK	mVE-cadherin-anti- <i>gyrA</i> PNA	21,22
		mVE-cadherin-anti- <i>gyrA</i> scPNA	
M918	MVTVLFRRLRIRACGPPRVV	M918-anti- <i>gyrA</i> PNA	23
		M918-anti- <i>gyrA</i> scPNA	
Oligoarginin (R6)	RRRRRR	R6-anti- <i>gyrA</i> PNA	21,24,25
		R6-anti- <i>gyrA</i> scPNA	
Oligoarginin (R10)	RRRRRRRRRR	R10-anti- <i>gyrA</i> PNA	
		R10-anti- <i>gyrA</i> scPNA	
Oligoleucine (L6)	LLLLLL	L6-anti- <i>gyrA</i> PNA	this work
		L6-anti- <i>gyrA</i> scPNA	
Oligolysin (K8)	KKKKKKKK	K8-anti- <i>gyrA</i> PNA	26
		K8-anti- <i>gyrA</i> scPNA	
PDESTK	PDESTK	PDESTK-anti- <i>gyrA</i> PNA	27
		PDESTK-anti- <i>gyrA</i> scPNA	
TLM	PLSSFSRIGDP	TLM-anti- <i>gyrA</i> PNA	28
		TLM-anti- <i>gyrA</i> scPNA	
TP10	AGYLLGKINLKALAALAKKIL	TP10-anti- <i>gyrA</i> PNA	29
		TP10-anti- <i>gyrA</i> scPNA	
Transportan	GWTLSAGYLLGKINLKALAALAKKIL	Transportan-anti- <i>gyrA</i> PNA	30
		Transportan-anti- <i>gyrA</i> scPNA	
VT5	DPKGDPKGVTVTVTVTVTKGDKPKPD	VT5-anti- <i>gyrA</i> PNA	31
		VT5-anti- <i>gyrA</i> scPNA	
(RXR) ₄ XB	RXRRXRXRXRXB	(RXR) ₄ XB-anti- <i>gyrA</i> PNA	32
		(RXR) ₄ XB-anti- <i>gyrA</i> scPNA	

introduction of different kinds of cargo into eukaryotic cells and bacteria.^{9,10} Typical examples of CPPs used in bacteria are the synthetic (KFF)₃K and the HIV-1 transactivator of transcription (HIV-1 TAT)-derived peptides. (KFF)₃K facilitated uptake of PNAs, among others, in *Escherichia coli* and *Staphylococcus aureus*.^{11,12} HIV-1 TAT was able to penetrate *Listeria monocytogenes*, *S. aureus*, and *S. epidermidis*.^{13,14} We observed previously that HIV-1 TAT-coupled anti-*gyrA* PNAs were able to inhibit

growth in *S. pyogenes*.¹⁵ In this study, we tested anti-*gyrA* PNAs coupled to 18 different CPPs. We selected CPPs, which have been tested before as carrier molecules in eukaryotic cells and were known to exhibit low toxicity (Table 1). We found that HIV-1 TAT, oligolysine (K8), and (RXR)₄XB-coupled anti-*gyrA* PNAs efficiently abolished growth of *S. pyogenes in vitro*. In a *Galleria mellonella* infection model, treatment of infected larvae with these CPP-PNAs increased survival.

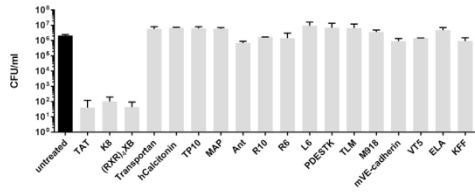


Figure 1. Reduction of the Bacterial Count following Treatment of *S. pyogenes* 591 (M49) with 10 μM CPP-Anti-*gyrA* PNAs for 6 h
PNA conjugates are indicated by the name of the respective CPP. Data are presented as mean values and SD. The experiment was performed twice.

RESULTS

Design of CPP-Coupled Anti-*gyrA* PNAs Specific for *S. pyogenes*

In a previous study, we observed antimicrobial effects of peptide-coupled anti-*gyrA* antisense PNAs specific for *S. pyogenes*.¹⁵ Growth inhibition by this construct was caused by antisense targeting of the

essential gene *gyrA*. Its gene product represents the subunit A of the DNA topoisomerase gyrase, which is involved in replication and is thus required for bacterial growth. Since carrier molecules show a species-specific influence on cargo uptake, we wanted to explore the effect of a variety of CPPs coupled to anti-*gyrA* antisense PNAs on *S. pyogenes* (Table 1). Peptides were coupled to PNAs via a flexible ethyleneglycol linker (8-amino-3, 6-dioxaoctanoic acid). The sequence of anti-*gyrA* antisense PNAs was tgacattaag-NH₂, covering *gyrA* -5 to 5. The sequence of the corresponding control PNAs (scrambled PNAs [scPNAs]) was attagactgt-NH₂. scPNAs were composed of the same base pairs as the antisense PNAs in a randomized order.

Antimicrobial Effect of CPP-Coupled Anti-*gyrA* PNAs on *S. pyogenes*

To determine the impact of different CPPs on the efficacy of antisense PNAs targeting *S. pyogenes*, a prescreening approach was performed. *S. pyogenes* M49 strain 591 was incubated for 6 h with

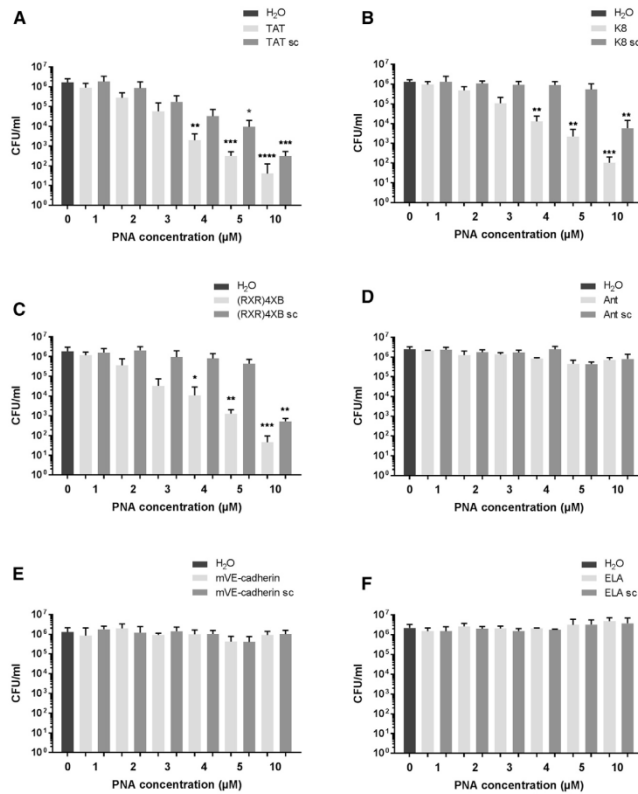


Figure 2. Concentration-Dependent Reduction of the Bacterial Counts following Treatment of *S. pyogenes* 591 (M49) with CPP-Anti-*gyrA* PNAs for 6 h

PNA conjugates are indicated by the name of the respective CPP: TAT (A), K8 (B), (RXR)4XB (C), Ant (D), mVE-cadherin (E), and ELA (F). Scrambled PNA controls are indicated by sc. Data are presented as mean values and SD. Statistical significance was determined using the Kruskal-Wallis test. Differences between PNA conjugate samples and the mock control (H₂O) were expressed as **p* ≤ 0.05; ***p* ≤ 0.01; ****p* ≤ 0.001; *****p* ≤ 0.0001. Sample size: *n* = 5 (A-C); *n* = 3 (D-F).

Table 2. MIC of CPP-PNA Anti-*gyrA* Conjugates

CPP-PNA	MIC (μM)
K8-anti- <i>gyrA</i> PNA	15.6
K8-anti- <i>gyrA</i> scPNA	62.5
TAT-anti- <i>gyrA</i> PNA	15.6
TAT-anti- <i>gyrA</i> scPNA	62.5
(RXR) ₄ XB-anti- <i>gyrA</i> PNA	62.5
(RXR) ₄ XB-anti- <i>gyrA</i> scPNA	125

10 μM CPP-anti-*gyrA* PNA conjugates. Reduction of bacterial counts caused by different CPP-coupled antisense PNAs compared with an untreated control was determined. From 18 CPP-antisense PNA conjugates, three showed an antimicrobial effect in this assay: TAT-anti-*gyrA* PNA, K8-anti-*gyrA* PNA, and (RXR)₄XB-anti-*gyrA* PNA (Figure 1). Similar results were obtained with *S. pyogenes* M1 strain AP1, with the exception of K8-anti-*gyrA* PNAs, which did not show any antimicrobial effect in AP1 (data not shown; Figure 3B).

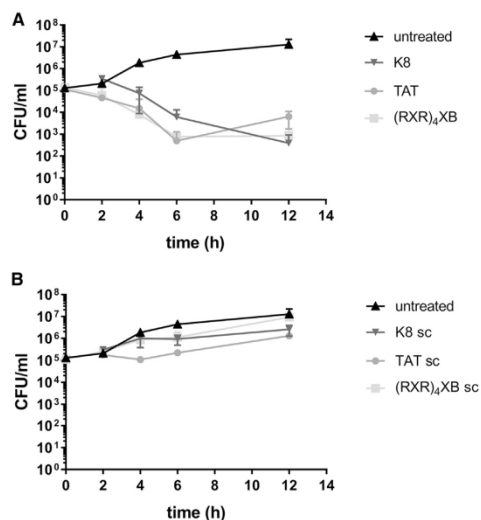
Six CPP-anti-*gyrA* PNA conjugates were selected for further analyses: three constructs that showed antimicrobial activity in the pilot experiment and three constructs that did not show any effect. Concentration-dependent bactericidal activity was investigated by treatment of *S. pyogenes* in a CPP-anti-*gyrA* PNA conjugate concentration range from 1 to 10 μM (Figure 2). Reduction of bacterial counts was observed following incubation of *S. pyogenes* with TAT-anti-*gyrA* PNA (Figure 2A), K8-anti-*gyrA* PNA (Figure 2B), and (RXR)₄XB-anti-*gyrA* PNA (Figure 2C), respectively. Colony-forming units (CFU) per milliliter in treated samples were significantly reduced compared with the untreated control sample in a concentration range from 4 to 10 μM PNA. TAT-anti-*gyrA* scPNA caused a significant reduction of CFU per milliliter following treatment with 5 and 10 μM scPNA, hinting toward a toxic effect of TAT CPP at higher concentrations (Figure 2A). K8-anti-*gyrA* scPNA and (RXR)₄XB-anti-*gyrA* scPNA showed a significant reduction of bacterial counts following treatment with 10 μM scPNA (Figures 2B and 2C). In contrast, no reduction of CFU per milliliter was observed following incubation with an Antennapedia homeodomain-derived CPP (Ant)-anti-*gyrA* PNA, ELA-anti-*gyrA* PNA, mVE-cadherin-anti-*gyrA* PNA, and the corresponding scrambled control CPP-PNAs (Figures 2D–2F).

Minimum Inhibitory Concentration

We determined the minimum inhibitory concentration (MIC) of the CPP-antisense PNAs that showed antimicrobial activity in the kill assay (Table 2). K8-anti-*gyrA* PNA and TAT-anti-*gyrA* PNA showed the lowest MIC at 15.6 μM . (RXR)₄XB-anti-*gyrA* PNA was less effective with a MIC of 62.5 μM . All scPNA controls showed a lower antimicrobial activity than the corresponding antisense constructs.

Bactericidal Kinetics of CPP-Coupled Anti-*gyrA* PNAs

To monitor reduction of bacterial counts over the course of the experiment, *S. pyogenes* was treated with 5 μM CPP-antisense

**Figure 3. Killing Kinetics of CPP-Anti-*gyrA* PNA Treatment**

(A) Bacterial counts following treatment of *S. pyogenes* 591 (M49) with CPP-anti-*gyrA* PNAs. (B) Bacterial counts following treatment of *S. pyogenes* 591 (M49) with CPP-anti-*gyrA* scPNAs. PNA conjugates are indicated by the name of the respective CPP. Scrambled PNA controls are indicated by sc. Data are presented as mean values and SD. Sample size: $n \geq 3$.

PNAs (Figure 3A) or scrambled control PNAs (Figure 3B). Samples were taken at time points 2, 4, 6, and 12 h following antisense treatment. CFUs per milliliter were determined by plating of serial dilutions. During the course of the experiment, no complete clearance was achieved.

Susceptibility of Different *S. pyogenes* Isolates to CPP-Anti-*gyrA* PNAs

We determined the antimicrobial effect of CPP-PNA conjugates on different *S. pyogenes* isolates representing distinct M serotypes of epidemiological relevance. Bacterial strains were treated with 5 μM CPP-PNA constructs.

Samples were collected after 6 h, and bacterial counts were analyzed (Figure 4). TAT-anti-*gyrA* PNA exhibited antimicrobial activity against all strains except MGAS8232 (M18). K8-anti-*gyrA* PNA was effective toward all strains with the exception of AP1 (M1). In contrast, (RXR)₄XB-anti-*gyrA* PNA was able to reduce bacterial counts of all strains tested in this experiment.

Hyaluronic Acid Content in Different *S. pyogenes* Isolates

To determine whether differential capsule production was correlated to sensitivity toward CPP-PNA conjugates, hyaluronic acid (HA) was

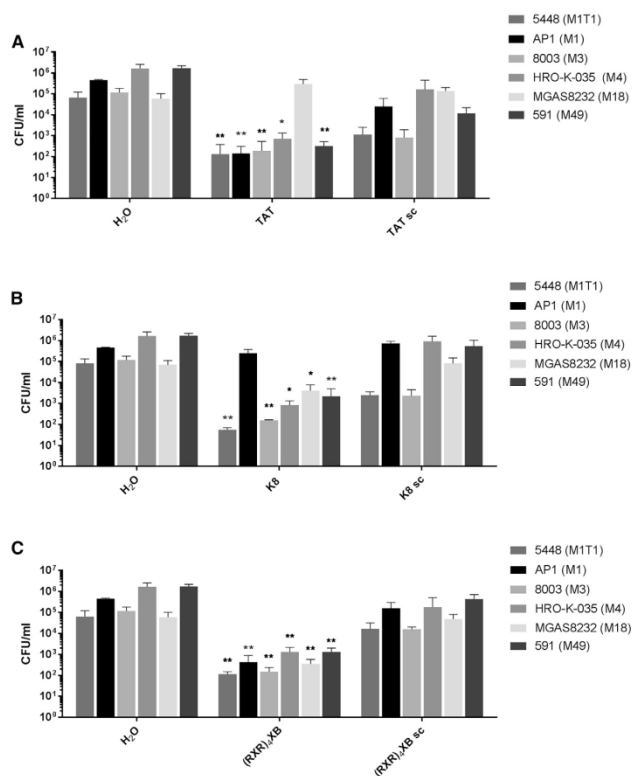


Figure 4. Susceptibility of Different *S. pyogenes* Isolates to CPP-Anti-*gyrA* PNA Treatment

Reduction of the bacterial count following treatment of different *S. pyogenes* strains with 5 μ M CPP-anti-*gyrA* PNAs. PNA conjugates are indicated by the name of the respective CPP. Scrambled PNA controls are indicated by sc. (A) TAT-anti-*gyrA* PNA and TAT-anti-*gyrA* scPNA. (B) K8-anti-*gyrA* PNA and K8-anti-*gyrA* scPNA. (C) (RXR)₄XB-anti-*gyrA* PNA and (RXR)₄XB-anti-*gyrA* scPNA. Data are presented as mean values and SD. Statistical significance was determined using the Kruskal-Wallis test. Differences between PNA conjugate samples and the corresponding mock control (H₂O) were expressed as * $p \leq 0.05$; ** $p \leq 0.01$. Sample size: $n = 5$.

(RXR)₄XB-anti-*gyrA* PNA led to a significant reduction of *gyrA* transcript compared with the untreated control sample (Figure 6). The *gyrA* mRNA level decreased to 70%, 60%, and 56%, respectively, of the amount detected in the mock-treated bacteria.

Evaluation of CPP-Antisense PNA Conjugates in a *G. mellonella* Infection Model

Antimicrobial efficiency of CPP-antisense PNA conjugates was evaluated *in vivo*, using a *G. mellonella* infection model. Larvae were infected with *S. pyogenes* strain 591 (M49) and treated with 4 nmol CPP-PNAs. Survival of larvae was observed over 7 days. We compared survival of larvae treated with CPP-anti-*gyrA* PNAs with mock-treated larvae. Larvae treated with TAT-anti-*gyrA* PNA, K8-anti-*gyrA* PNA, or (RXR)₄XB-anti-*gyrA* PNA showed increased survival compared with mock-treated larvae (Figures 7A–7C). Ant-, mVE-cadherin-, and ELA-anti-*gyrA* PNAs that did not show antimicrobial effects *in vitro* did not affect survival of infected larvae (Figures 7D–7F).

One promising therapeutic strategy is a combination of antisense agents with conventional antibiotics to reduce the concentration needed for efficient antibiotics treatment.

Previously, we observed that a combination of TAT-anti-*gyrA* PNA with antibiotics targeting gyrase subunits resulted in synergistic or additive antimicrobial effects on *S. pyogenes* *in vitro*.¹⁵ To test whether TAT-anti-*gyrA* PNA treatment could enhance antibiotics efficiency *in vivo*, we first treated infected *G. mellonella* larvae with 1 μ g levofloxacin, which increased survival of infected larvae from 20% to 46% (Figure 8A). In combination with 4 nmol TAT-anti-*gyrA* PNA, survival was increased to 63% (Figure 8B). A comparable survival of infected larvae was achieved by application of 15 μ g levofloxacin (Figure 8A). Combination of PNA and levofloxacin also increased survival of the

extracted from *S. pyogenes* strains. HA content of MGAS8232 (M18) was significantly higher than in all other isolates tested (Figure 5). Since TAT-anti-*gyrA* PNAs were not effective in MGAS8232 (M18) (Figure 4A), this result indicates that HA represents a barrier for TAT-antisense PNAs but neither for K8-antisense PNAs nor for (RXR)₄XB-antisense PNAs.

CPP-Anti-*gyrA* PNAs Affect the Abundance of Target Gene Transcripts in *S. pyogenes*

The influence of *S. pyogenes* treatment with CPP-anti-*gyrA* PNAs on the amount of *gyrA* mRNA was investigated by reverse transcription, followed by quantitative real-time PCR (Figure 6). Bacteria were treated with a sublethal dose of CPP-PNA conjugates.

Following incubation, total RNA was extracted, and qRT-PCR was performed. Transcript abundance of the 5S RNA gene was used for normalization. The *gyrA* mRNA level in mock-treated *S. pyogenes* samples served as control. Treatment with 2 μ M TAT-anti-*gyrA* PNA, K8-anti-*gyrA* PNA, and

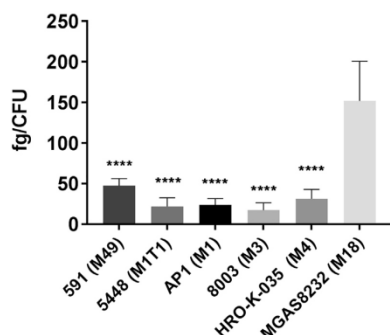


Figure 5. Hyaluronic Acid Content of Different *S. pyogenes* Serotypes
Statistical significance was determined using one-way ANOVA/Tukey's multiple comparisons test. Data are presented as mean values and SD. Differences between *S. pyogenes* serotypes and *S. pyogenes* MGAS8232 were expressed as **** $p \leq 0.0001$. Sample size: $n = 5$.

infected larvae compared with TAT-anti-*gyrA* PNA treatment alone (33%) (Figure 8B).

DISCUSSION

PNAs are nucleic acid derivatives with a variety of properties rendering them suitable as antisense molecules, including chemical and thermal stability, strong binding to DNA and RNA, reasonable solubility, a lack of immunogenicity, and low intracellular toxicity.³³

However, poor delivery into target cells hampers application of PNAs as antisense therapeutics. In bacteria, the cell membrane, the bacterial cell wall, and extracellular surface structures, such as the lipopolysaccharide layer or the capsule, represent barriers limiting cellular uptake of PNAs. Treatment of intracellular pathogens poses an additional challenge, because PNAs have to be delivered into the host cell, escape the endosomal pathway, and finally penetrate the bacteria. One possible strategy to improve cellular uptake is PNA coupling to CPPs. The efficiency of a given CPP to enhance delivery is species specific. In Gram-negative bacteria, among others, (KFF)₃K and HIV-1-TAT have been identified as useful carriers.^{34,35} Growth of intracellular *Salmonella enterica* Serovar Typhimurium could be inhibited by (RXR)₄XB-conjugated antisense peptide-phosphorodiamidate morpholino oligomers.³⁶ In Gram-positive bacteria, (KFF)₃K was efficient in *S. aureus*.¹² Intracellular *L. monocytogenes* could be targeted with HIV-1-TAT- and (RXR)₄XB-conjugated PNAs.¹⁴ In our previous study, we found that HIV-1-TAT-coupled anti-*gyrA* PNAs showed antimicrobial activity in *S. pyogenes*.¹⁵

The aim of this study was to compare the efficiency of potential carrier molecules delivering antisense PNAs in *S. pyogenes*. We tested 18 CPPs belonging to different classes. Three CPPs were shown to support uptake of anti-*gyrA* PNAs: the cationic CPPs

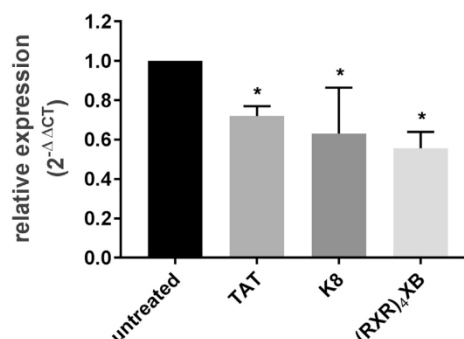


Figure 6. Relative Expression of *gyrA* following Treatment with CPP-Antisense PNAs

Reduction of the transcript level was observed following treatment of *S. pyogenes* strains with 2 μ M CPP-anti-*gyrA* PNAs. PNA conjugates are indicated by the name of the respective CPP. Data are presented as mean values and SD. Statistical significance was determined using the Mann-Whitney U-test. Differences between PNA conjugate samples and the untreated control were expressed as * $p \leq 0.05$. Sample size: $n = 3$.

K8 and HIV-1-TAT and the arginine-rich, amphipathic peptide (RXR)₄XB. In general, basic residues support internalization of CPPs into cells, because their positive charge initiates interaction with the negatively charged surface. Specifically, it has been shown that arginine residues were more effective than lysines and that the replacement of lysine residues with arginine improved cellular uptake.^{26,37} Here, we show that oligoarginine-coupled antisense PNAs were not able to inhibit *S. pyogenes* growth, whereas K8-conjugated anti-*gyrA* PNA showed an antimicrobial effect. In eukaryotic cells, insertion of 6-aminohexanoic acid (X) or β -alanine (B) residues into oligoarginine R8 decreased the cellular uptake but increased the splice-correction activity of the resulting compound.³⁸ We observed that in contrast to R8, which did not function as a carrier in *S. pyogenes*, (RXR)₄XB was able to mediate uptake of antisense PNAs. Penetratin (Ant) did not support antisense PNA uptake into *S. pyogenes*. This result is in accordance with an observation in *L. monocytogenes*. PNA uptake into *L. monocytogenes* was mediated by HIV-1-TAT and (RXR)₄XB but not by Ant.¹⁴ PDSTK, a peptide derived from a PEST-like sequence from yeast, was able to support PNA antisense effects in *S. aureus*.¹² We did not detect antimicrobial activity of PDSTK-conjugated antisense PNA in *S. pyogenes*.

We further analyzed the bactericidal effect of TAT-, K8-, and (RXR)₄XB-anti-*gyrA* PNAs. All three CPP-anti-*gyrA* PNAs showed a dose-dependent antimicrobial effect in kill assays. Incubation of *S. pyogenes* with up to 5 μ M K8- and (RXR)₄XB-conjugated scPNAs did not lead to the reduction of bacterial counts. In contrast, TAT-anti-*gyrA* scPNA showed a sequence-independent

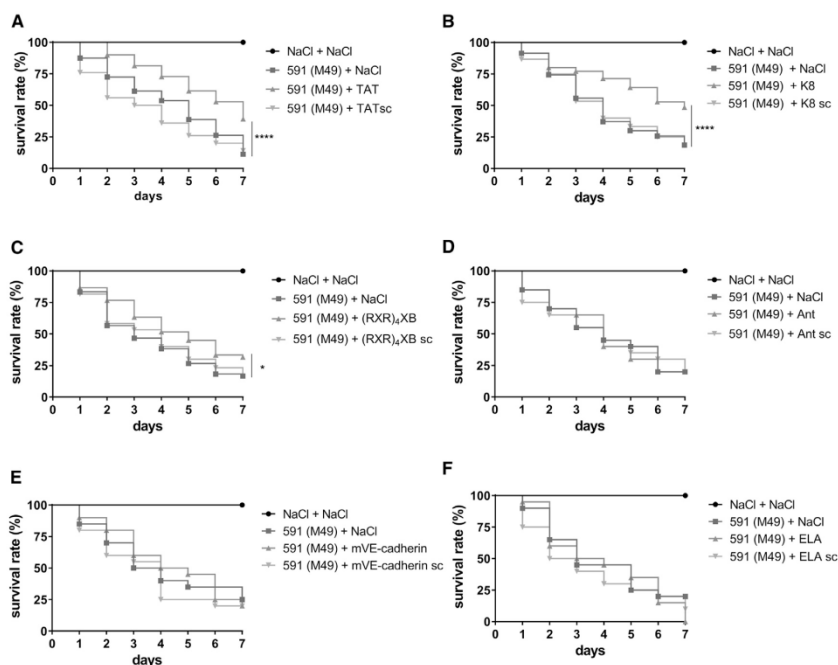


Figure 7. Survival of *Galleria mellonella* Larvae Treated with 4 nmol CPP-PNAs following Infection with *S. pyogenes*

PNA conjugates are indicated by the name of the respective CPP: TAT (A), K8 (B), (RXR)₄XB (C), Ant (D), mVE-cadherin (E), and ELA (F). Scrambled PNA controls are indicated by sc. Statistical significance was determined using the log-rank test. Differences between curves were expressed as * $p \leq 0.05$; **** $p \leq 0.0001$. Sample size: $n = 60$ larvae per group (A–C); $n = 20$ larvae per group (D–F).

antimicrobial effect in this assay, indicating a toxic influence of the TAT peptide on *S. pyogenes* under these conditions. In a previous study, we tested the effect of the TAT peptide alone on *S. pyogenes* and did not observe any antibacterial activity up to 20 μM .¹⁵ Six hours following treatment with 5 μM or 10 μM TAT-, K8-, and (RXR)₄XB-anti-*gyrA* PNAs, a log CFU reduction of three or four, respectively, was observed, but no clearance was achieved. In contrast, *L. monocytogenes* could be cleared after 20 min incubation with 8 μM TAT- and (RXR)₄XB-antisense PNAs specific for the gene of RNA polymerase α subunit (*rpoA*).¹⁴

MIC determination revealed that TAT-anti-*gyrA* PNA and K8-anti-*gyrA* PNA were effective at the same MIC of 15.6 μM , whereas the respective scrambled controls showed a MIC of 62.5 μM . Here, no toxic effect of the TAT peptide was observed. The MICs of (RXR)₄XB-anti-*gyrA* PNA and its corresponding scrambled control were 62.5 μM and 125 μM , respectively. Compared with *L. monocytogenes*, these MIC values are rather high. TAT- and

(RXR)₄XB-anti-*rpoA* PNAs exhibited a MIC of 1–4 μM , depending on the *L. monocytogenes* isolate tested.¹⁴

To assess whether the bactericidal effect of the CPP-antisense PNAs is sufficient for treatment of a *S. pyogenes* infection *in vivo*, a *G. mellonella* infection model was used.³⁹ TAT-, K8-, and (RXR)₄XB-anti-*gyrA* PNAs increased survival of infected *G. mellonella* larvae. In contrast, treatment of infected larvae with Ant-, mVE-cadherin-, and ELA-anti-*gyrA* PNAs, which did not show bactericidal activity *in vitro*, did not affect survival. A combination of anti-*gyrA* PNAs with antibiotics targeting gyrase subunit A was shown to result in synergistic or additive antimicrobial effects on *S. aureus* and *S. pyogenes* *in vitro*.^{15,40} Here, we demonstrate that combination therapy of infected larvae with TAT-anti-*gyrA* PNAs and levofloxacin led to increased survival rates compared with each treatment alone, supporting the idea that a combination of antisense PNAs with conventional antibiotics is a potent strategy to decrease the concentration of antibiotics during treatment of *S. pyogenes* infections.

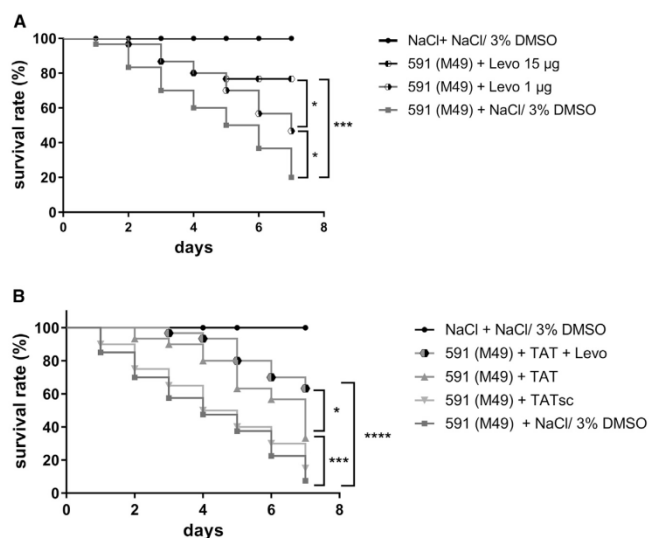


Figure 8. Survival of *Galleria mellonella* Larvae Treated with Levofloxacin Alone or in Combination with TAT-Anti-*gyrA* PNA following Infection with *S. pyogenes*

(A) Levo, levofloxacin. (B) TAT, 4 nmol TAT-anti-*gyrA* PNA. Scrambled PNA controls are indicated by sc. Statistical significance was determined using the log-rank test. Differences between curves were expressed as * $p \leq 0.05$; *** $p \leq 0.001$; **** $p \leq 0.0001$. Sample size: $n = 30$ larvae per group.

anti-*gyrA* PNA on larvae survival in the *G. mellonella* infection model was lower compared with the other conjugates. Overall, our results underline the importance of suitable vectors for PNA delivery to achieve optimal antimicrobial function and identified efficient CPPs for testing of additional *S. pyogenes* target genes.

MATERIALS AND METHODS

PNA Synthesis

CPP-PNAs were synthesized and purified by high-performance liquid chromatography (HPLC) (Peps4LS, Heidelberg, Germany). Sequences of all CPP-PNAs used in this work are listed in Table 1.

Bacterial Strains and Culture Conditions

S. pyogenes strains were cultured in Todd-Hewitt broth, supplemented with 0.5% yeast extract (THY; Oxoid, Thermo Fisher Scientific, Darmstadt, Germany), at 37°C under a 5% CO₂/20% O₂ atmosphere. All strains used in this study are listed in Table 3.

Bacterial Kill Assay

Overnight cultures of the respective *S. pyogenes* strain were diluted in PBS/brain heart infusion (BHI) (7/2) to approximately 2×10^5 CFU/mL. 450 µL bacterial suspension, containing $\sim 10^5$ CFU, was transferred to a 2-mL reaction tube. 50 µL PNA was added to a final PNA concentration of 1–10 µM or as indicated. 50 µL H₂O served as mock control. The reaction tubes were incubated for 6 h at 37°C and 7 rpm (Rotor SB3; Stuart, Staffordshire, UK). Viable cell counts were determined by plating appropriate dilutions on THY agar plates. CFUs were determined by visual inspection following overnight incubation at 37°C under a 5% CO₂/20% O₂ atmosphere. At time point 0, the viable cell count corresponded to $1-3 \times 10^5$ CFU/mL. The initial CPP screen has been performed in two biological replicates. Each subsequent experiment has been performed in at least three independent biological replicates, as indicated in the figure legends.

Extraction of Total RNA

For RNA isolation, 450 µL bacterial suspension (10^7 CFU/mL in THY) was prepared for each experimental condition, treated with 2 µM CPP-PNA conjugates, and incubated in a 2-mL

We were surprised that from 18 CPP-PNA conjugates tested in this study, only three showed an efficient antimicrobial effect. For future experiments, different types of carriers should be investigated. One possible alternative to peptide carriers is vitamin B12, which has been successfully used in *E. coli* and *Salmonella Typhimurium*.⁴¹ The authors showed that vitamin B12 worked more efficiently in *E. coli* than (KFF)₃K, which is widely used in this organism.

Furthermore, we will aim at the identification of additional antisense target genes specific for *S. pyogenes*. Beside other essential genes, antisense targeting of virulence factor genes is a promising strategy. For instance, antisense PNAs directed against *ska*, the gene coding for streptokinase, could potentially diminish *S. pyogenes* virulence. Streptokinase is involved in the lysis of fibrin clots and thereby supports bacterial spreading. It has been shown that a small compound inhibiting *ska* expression was able to improve survival in a murine infection model.⁴²

In this study, we were able to confirm that *gyrA* is a suitable target for PNA-mediated antisense inhibition of gene expression in *S. pyogenes*. We found that TAT-, K8-, and (RXR)₄XB-anti-*gyrA* PNAs showed antibacterial activity *in vitro* and *in vivo* with comparable characteristics. TAT-conjugated scPNAs showed *in vitro* an unspecific effect, probably caused by TAT toxicity, which was not apparent *in vivo*. K8-coupled anti-*gyrA* PNA showed high antimicrobial efficiency *in vitro* and was effective on all *S. pyogenes* serotypes tested except AP1. In contrast, (RXR)₄XB-coupled anti-*gyrA* PNA showed high bactericidal efficiency in the kill assay but exhibited higher MICs than TAT and K8-PNA conjugates. Additionally, the effect of (RXR)₄XB-coupled

Table 3. *S. pyogenes* Strains

Strain	M Type	Isolation	Reference
5448	MIT1	STSS	Dr. Nikolai Siemens, Karolinska Institut, Lund, Sweden
API	M1	sepsis	Centre for Reference and Research on Streptococci, Prague, Czech Republic
M3 8003	M3	necrotizing fasciitis	Dr. Nikolai Siemens, Karolinska Institut, Lund, Sweden
HRO-K-035	M4	throat infection	clinical isolate, University Medicine Rostock, Germany
MGAS8232	M18	ARF	⁴³
591	M49	skin	R. Lütticken, Aachen, Germany

ARF, acute rheumatic fever; STSS, streptococcal toxic-shock syndrome.

reaction tube for 6 h at 37°C and 7 rpm (Rotor SB3; Stuart, Staffordshire, UK). Subsequently, five samples per condition were pooled. Bacteria were pelleted immediately, shock frozen in liquid nitrogen, and stored at -80°C until use. Bacterial cells were disrupted in a homogenizer (Peqlab Biotechnologie, Erlangen, Germany). Total RNA was extracted, according to the protocol, supplied with the Direct-zol RNA MiniPrep Kit (Zymo Research, Irvine, CA). After extraction, RNA was treated with acid phenol:chloroform:isoamyl alcohol (125:24:1; pH 4.5; Thermo Fisher Scientific), and TURBO DNase (Thermo Fisher Scientific), according to the manufacturer's instructions. RNA was stored at -80°C until further use.

Reverse Transcription Followed by quantitative real-time PCR

cDNA synthesis was performed using the SuperScript First-Strand Synthesis System for RT-PCR (Invitrogen, Thermo Fisher Scientific). Quantitative real-time PCR amplification was conducted with SYBR Green (Thermo Fisher Scientific) using the ViiA 7 Real-Time PCR System (Applied Biosystems, Darmstadt, Germany). The 5S rRNA gene served as internal control. Relative expression was calculated using the 2^{-ΔΔCt} method.⁴⁴ Primers were designed based on the full genome sequence of *S. pyogenes* M49 strain NZ131 (NCBI: NC011375): *gyrA*-specific primers: 5'-TGAGTGTTCATTGTGGCAAGAGC-3' and 5'-AGAGAATACGACGATGCACAGG-3'; 5S-specific primers: 5'-AGCGACTACCTTATCTCACAG-3' and 5'-GAGATACACCTGTACCCATG-3'.

Determination of the MIC

MIC determination was performed following the protocol of the Clinical and Laboratory Standards Institute (CLSI).⁴⁵ In MIC assays containing CPP-PNAs, lysed horse blood (LHB)/cation-adjusted Mueller-Hinton broth (CAMHB) medium was supplemented with 0.02% acetic acid and 0.4% BSA. MICs were recorded as the lowest concentration where no turbidity was observed in the wells.

G. mellonella Infection Model

Larvae of the greater wax moth *G. mellonella* were obtained from Reptilienkosmos (Niederkrüchten, Germany). For infection experiments, *S. pyogenes* strains were grown overnight in THY, washed twice in a 0.9% NaCl solution, and suspended in 0.9% NaCl to a

final concentration of 1–3 × 10⁸ CFU/mL. Larvae with a weight of 150–200 mg were infected with 1–3 × 10⁶ CFU/larva. Bacteria were injected into the hemocoel of the larvae between the last two pairs of pro-legs using a microapplicator (World Precision Instruments, Sarasota, FL) and a fine dosage syringe (Omnican F; B. Braun, Melsungen, Germany; 0.01–1 mL, 0.30 × 12 mm). As mock control, 0.9% NaCl was injected. For CPP-PNA treatment, larvae were injected 30 min postinfection with 4 nmol CPP-PNA/larva. Larvae were incubated for 7 days, and survival was monitored daily.⁴⁶

Statistical Analyses

All experiments were performed at least three times or as indicated by sample size (n). Statistical significance was determined using the tests indicated in the respective figure legends. Statistical analyses were performed using GraphPad Prism 7 software.

AUTHOR CONTRIBUTIONS

N.P. designed this study. G.B., A.-L.L., R.P., S.K., and A.S. conducted the experiments. N.P., G.B., A.J., and B.K. contributed to the interpretation of data and manuscript writing.

CONFLICTS OF INTEREST

The authors declare no competing interests.

ACKNOWLEDGMENTS

Support for the work of G.B. and B.K. was provided by a grant from the Ministerium für Bildung, Wissenschaft und Kultur, Mecklenburg-Vorpommern (ESF/14-BM-A55-0010/16). Support for the work of N.P. was provided by the University Medicine Rostock (Forun 889008).

REFERENCES

- Carapetis, J.R., Steer, A.C., Mulholland, E.K., and Weber, M. (2005). The global burden of group A streptococcal diseases. *Lancet Infect. Dis.* 5, 685–694.
- Sims Sanyahumbi, A., Colquhoun, S., Wyber, R., and Carapetis, J.R. (2016). Global disease burden of group A streptococcus. In *Streptococcus pyogenes: Basic Biology to Clinical Manifestations*, J.J. Ferretti, D.L. Stevens, and V.A. Fischetti, eds. (University of Oklahoma Health Sciences Center).
- Cunningham, M.W. (2008). Pathogenesis of group A streptococcal infections and their sequelae. *Adv. Exp. Med. Biol.* 609, 29–42.

4. Bisno, A.L., Gerber, M.A., Gwaltney, J.M., Jr., Kaplan, E.L., and Schwartz, R.H.; Infectious Diseases Society of America (2002). Practice guidelines for the diagnosis and management of group A streptococcal pharyngitis. *Clin. Infect. Dis.* 35, 113–125.
5. Richter, S.S., Heilmann, K.P., Beekmann, S.E., Miller, N.J., Miller, A.L., Rice, C.L., Doern, C.D., Reid, S.D., and Doern, G.V. (2005). Macrolide-resistant *Streptococcus pyogenes* in the United States, 2002–2003. *Clin. Infect. Dis.* 41, 599–608.
6. Cattoir, V. (2016). Mechanisms of antibiotic resistance. In *Streptococcus pyogenes: Basic Biology to Clinical Manifestations*, J.J. Ferretti, D.L. Stevens, and V.A. Fischetti, eds. (University of Oklahoma Health Sciences Center).
7. Nielsen, P.E., and Egholm, M. (1999). An introduction to peptide nucleic acid. *Curr. Issues Mol. Biol.* 1, 89–104.
8. Demidov, V.V., Potaman, V.N., Frank-Kamenetskii, M.D., Egholm, M., Buchard, O., Sönnichsen, S.H., and Nielsen, P.E. (1994). Stability of peptide nucleic acids in human serum and cellular extracts. *Biochem. Pharmacol.* 48, 1310–1313.
9. Gupta, B., Levchenko, T.S., and Torchilin, V.P. (2005). Intracellular delivery of large molecules and small particles by cell-penetrating proteins and peptides. *Adv. Drug Deliv. Rev.* 57, 637–651.
10. Lehto, T., Ezzat, K., Wood, M.J.A., and El Andaloussi, S. (2016). Peptides for nucleic acid delivery. *Adv. Drug Deliv. Rev.* 106 (Pt A), 172–182.
11. Eriksson, M., Nielsen, P.E., and Good, L. (2002). Cell permeabilization and uptake of antisense peptide-peptide nucleic acid (PNA) into *Escherichia coli*. *J. Biol. Chem.* 277, 7144–7147.
12. Nekhotiaeva, N., Awasthi, S.K., Nielsen, P.E., and Good, L. (2004). Inhibition of *Staphylococcus aureus* gene expression and growth using antisense peptide nucleic acids. *Mol. Ther.* 10, 652–659.
13. Abushahba, M.F., Mohammad, H., and Seleem, M.N. (2016). Targeting multidrug-resistant *Staphylococci* with an anti-*rpoA* peptide nucleic acid conjugated to the HIV-1 Tat cell penetrating peptide. *Mol. Ther. Nucleic Acids* 5, e339.
14. Abushahba, M.F., Mohammad, H., Thangamani, S., Hussein, A.A., and Seleem, M.N. (2016). Impact of different cell penetrating peptides on the efficacy of antisense therapeutics for targeting intracellular pathogens. *Sci. Rep.* 6, 20832.
15. Patenge, N., Pappesch, R., Krawack, F., Walda, C., Mraheil, M.A., Jacob, A., Hain, T., and Kreikemeyer, B. (2013). Inhibition of growth and gene expression by PNA-peptide conjugates in *Streptococcus pyogenes*. *Mol. Ther. Nucleic Acids* 2, e132.
16. Derossi, D., Joliet, A.H., Chassaing, G., and Prochiantz, A. (1994). The third helix of the Antennapedia homeodomain translocates through biological membranes. *J. Biol. Chem.* 269, 10444–10450.
17. Turner, Y., Wallukat, G., Säilik, P., Wiesner, B., Pritz, S., and Oehlke, J. (2010). Cellular uptake and biological activity of peptide nucleic acids conjugated with peptides with and without cell-penetrating ability. *J. Pept. Sci.* 16, 71–80.
18. Vivès, E., Brodin, P., and Lebleu, B. (1997). A truncated HIV-1 Tat protein basic domain rapidly translocates through the plasma membrane and accumulates in the cell nucleus. *J. Biol. Chem.* 272, 16010–16017.
19. Tréhin, R., Krauss, U., Beck-Sickingler, A.G., Merkle, H.P., and Nielsen, H.M. (2004). Cellular uptake but low permeation of human calcitonin-derived cell penetrating peptides and Tat(47–57) through well-differentiated epithelial models. *Pharm. Res.* 21, 1248–1256.
20. Vaara, M., and Porro, M. (1996). Group of peptides that act synergistically with hydrophobic antibiotics against gram-negative enteric bacteria. *Antimicrob. Agents Chemother.* 40, 1801–1805.
21. Mueller, J., Kretzschmar, I., Volkmer, R., and Boisguerin, P. (2008). Comparison of cellular uptake using 22 CPPs in 4 different cell lines. *Bioconjug. Chem.* 19, 2363–2374.
22. Palm, C., Netzereb, S., and Hällbrink, M. (2006). Quantitatively determined uptake of cell-penetrating peptides in non-mammalian cells with an evaluation of degradation and antimicrobial effects. *Peptides* 27, 1710–1716.
23. El-Andaloussi, S., Johansson, H.J., Holm, T., and Langel, U. (2007). A novel cell-penetrating peptide, M918, for efficient delivery of proteins and peptide nucleic acids. *Mol. Ther.* 15, 1820–1826.
24. Maiolo, J.R., Ferrer, M., and Ottinger, E.A. (2005). Effects of cargo molecules on the cellular uptake of arginine-rich cell-penetrating peptides. *Biochim. Biophys. Acta* 1712, 161–172.
25. Tünnemann, G., Ter-Avetisyan, G., Martin, R.M., Stöckl, M., Herrmann, A., and Cardoso, M.C. (2008). Live-cell analysis of cell penetration ability and toxicity of oligo-arginines. *J. Pept. Sci.* 14, 469–476.
26. Mitchell, D.J., Kim, D.T., Steinman, L., Fathman, C.G., and Rothbard, J.B. (2000). Polyarginine enters cells more efficiently than other polycationic homopolymers. *J. Pept. Res.* 56, 318–325.
27. Roth, A.F., Sullivan, D.M., and Davis, N.G. (1998). A large PEST-like sequence directs the ubiquitination, endocytosis, and vacuolar degradation of the yeast a-factor receptor. *J. Cell Biol.* 142, 949–961.
28. Manceur, A., Wu, A., and Audet, J. (2007). Flow cytometric screening of cell-penetrating peptides for their uptake into embryonic and adult stem cells. *Anal. Biochem.* 364, 51–59.
29. El-Andaloussi, S., Järver, P., Johansson, H.J., and Langel, U. (2007). Cargo-dependent cytotoxicity and delivery efficacy of cell-penetrating peptides: a comparative study. *Biochem. J.* 407, 285–292.
30. Lindgren, M., Gallet, X., Soomets, U., Hällbrink, M., Bråkenhielm, E., Pooga, M., Brasseur, R., and Langel, U. (2000). Translocation properties of novel cell penetrating transportan and penetratin analogues. *Bioconjug. Chem.* 11, 619–626.
31. Oehlke, J., Krause, E., Wiesner, B., Beyersmann, M., and Bienert, M. (1997). Extensive cellular uptake into endothelial cells of an amphipathic beta-sheet forming peptide. *FEBS Lett.* 415, 196–199.
32. Abes, R., Moulton, H.M., Clair, P., Yang, S.T., Abes, S., Melikov, K., Prevot, P., Youngblood, D.S., Iversen, P.L., Chernomordik, L.V., and Lebleu, B. (2008). Delivery of steric block morpholino oligomers by (R-X-R)4 peptides: structure-activity studies. *Nucleic Acids Res.* 36, 6343–6354.
33. Sharma, C., and Awasthi, S.K. (2017). Versatility of peptide nucleic acids (PNAs): role in chemical biology, drug discovery, and origins of life. *Chem. Biol. Drug Des.* 89, 16–37.
34. Bai, H., You, Y., Yan, H., Meng, J., Xue, X., Hou, Z., Zhou, Y., Ma, X., Sang, G., and Luo, X. (2012). Antisense inhibition of gene expression and growth in gram-negative bacteria by cell-penetrating peptide conjugates of peptide nucleic acids targeted to *rpoD* gene. *Biomaterials* 33, 659–667.
35. Ghosal, A., and Nielsen, P.E. (2012). Potent antibacterial antisense peptide-peptide nucleic acid conjugates against *Pseudomonas aeruginosa*. *Nucleic Acid Ther.* 22, 323–334.
36. Mitev, G.M., Mellbye, B.L., Iversen, P.L., and Geller, B.L. (2009). Inhibition of intracellular growth of *Salmonella enterica* serovar Typhimurium in tissue culture by antisense peptide-phosphorodiamidate morpholino oligomer. *Antimicrob. Agents Chemother.* 53, 3700–3704.
37. Wender, P.A., Mitchell, D.J., Pattabiraman, K., Peikey, E.T., Steinman, L., and Rothbard, J.B. (2000). The design, synthesis, and evaluation of molecules that enable or enhance cellular uptake: peptoid molecular transporters. *Proc. Natl. Acad. Sci. USA* 97, 13003–13008.
38. Wu, R.P., Youngblood, D.S., Hassinger, J.N., Lovejoy, C.E., Nelson, M.H., Iversen, P.L., and Moulton, H.M. (2007). Cell-penetrating peptides as transporters for morpholino oligomers: effects of amino acid composition on intracellular delivery and cytotoxicity. *Nucleic Acids Res.* 35, 5182–5191.
39. Tsai, C.J., Loh, J.M., and Prof, T. (2016). *Galleria mellonella* infection models for the study of bacterial diseases and for antimicrobial drug testing. *Virulence* 7, 214–229.
40. Dryselius, R., Nekhotiaeva, N., and Good, L. (2005). Antimicrobial synergy between mRNA- and protein-level inhibitors. *J. Antimicrob. Chemother.* 56, 97–103.
41. Równicki, M., Wojciechowska, M., Wierzb, A.J., Czarniecki, J., Bartosiak, D., Gryko, D., and Trylska, J. (2017). Vitamin B₁₂ as a carrier of peptide nucleic acid (PNA) into bacterial cells. *Sci. Rep.* 7, 7644.
42. Sun, H., Xu, Y., Sitkiewicz, I., Ma, Y., Wang, X., Yestrepky, B.D., Huang, Y., Lapadatescu, M.C., Larsen, M.J., Larsen, S.D., et al. (2012). Inhibitor of streptokinase gene expression improves survival after group A streptococcus infection in mice. *Proc. Natl. Acad. Sci. USA* 109, 3469–3474.

43. Smoot, J.C., Barbian, K.D., Van Gompel, J.J., Smoot, L.M., Chaussee, M.S., Sylva, G.L., Sturdevant, D.E., Ricklefs, S.M., Porcella, S.F., Parkins, L.D., et al. (2002). Genome sequence and comparative microarray analysis of serotype M18 group A streptococcus strains associated with acute rheumatic fever outbreaks. *Proc. Natl. Acad. Sci. USA* 99, 4668–4673.
44. Livak, K.J., and Schmittgen, T.D. (2001). Analysis of relative gene expression data using real-time quantitative PCR and the $2^{-\Delta\Delta C(T)}$ method. *Methods* 25, 402–408.
45. Weinstein, M.P., Patel, J.B., Burnham, C.-A., Campeau, S., Conville, P.S., Doern, C., Eliopoulos, G.M., Galas, M.F., Humphries, R.M., Jenkins, S.G., et al. (2018). *Methods for Dilution Antimicrobial Susceptibility Tests for Bacteria That Grow Aerobically*, 11th Edition (Clinical and Laboratory Standards Institute).
46. Mukherjee, K., Altincicek, B., Hain, T., Domann, E., Vilcinskas, A., and Chakraborty, T. (2010). *Galleria mellonella* as a model system for studying *Listeria* pathogenesis. *Appl. Environ. Microbiol.* 76, 310–317.



A Glycine Riboswitch in *Streptococcus pyogenes* Controls Expression of a Sodium:Alanine Symporter Family Protein Gene

Afsaneh Khani, Nicole Popp[†], Bernd Kreikemeyer and Nadja Patenge*

Institute of Medical Microbiology, Virology and Hygiene, University Medicine Rostock, Rostock, Germany

OPEN ACCESS

Edited by:

Awdhesh Kalia,
University of Texas MD Anderson
Cancer Center, United States

Reviewed by:

Victor Antonio García-Angulo,
Universidad de Chile, Chile
Anthony Flores,
McGovern Medical School,
United States

*Correspondence:

Nadja Patenge
nadja.patenge@med.uni-rostock.de

[†]Present address:

Nicole Popp,
BD Life Sciences, Heidelberg,
Germany

Specialty section:

This article was submitted to
Infectious Diseases,
a section of the journal
Frontiers in Microbiology

Received: 14 November 2017

Accepted: 29 January 2018

Published: 20 February 2018

Citation:

Khani A, Popp N, Kreikemeyer B and
Patenge N (2018) A Glycine
Riboswitch in *Streptococcus*
pyogenes Controls Expression of a
Sodium:Alanine Symporter Family
Protein Gene. *Front. Microbiol.* 9:200.
doi: 10.3389/fmicb.2018.00200

Regulatory RNAs play important roles in the control of bacterial gene expression. In this study, we investigated gene expression regulation by a putative glycine riboswitch located in the 5'-untranslated region of a sodium:alanine symporter family (SAF) protein gene in the group A *Streptococcus pyogenes* serotype M49 strain 591. Glycine-dependent gene expression mediated by riboswitch activity was studied using a luciferase reporter gene system. Maximal reporter gene expression was observed in the absence of glycine and in the presence of low glycine concentrations. Differences in glycine-dependent gene expression were not based on differential promoter activity. Expression of the SAF protein gene and the downstream putative cation efflux protein gene was investigated in wild-type bacteria by RT-qPCR transcript analyses. During growth in the presence of glycine (≥ 1 mM), expression of the genes were downregulated. Northern blot analyses revealed premature transcription termination in the presence of high glycine concentrations. Growth in the presence of 0.1 mM glycine led to the production of a full-length transcript. Furthermore, stability of the SAF protein gene transcript was drastically reduced in the presence of glycine. We conclude that the putative glycine riboswitch in *S. pyogenes* serotype M49 strain 591 represses expression of the SAF protein gene and the downstream putative cation efflux protein gene in the presence of high glycine concentrations. Sequence and secondary structure comparisons indicated that the streptococcal riboswitch belongs to the class of tandem aptamer glycine riboswitches.

Keywords: glycine, riboswitch, *Streptococcus pyogenes*, cis-regulatory element, amino acid riboswitch, regulatory RNAs, transcription genetic

INTRODUCTION

Bacterial riboswitches are cis-regulatory elements found in the 5'-untranslated regions (UTRs) of mRNAs. Regulation of gene expression by riboswitches is widespread in bacteria. In general, aptamer structures within the riboswitch recognize small molecule ligands and interact with an expression platform. Ligand binding promotes formation of an exclusive conformation and leads to the regulation of downstream genes. Repression of gene expression is achieved by transcription termination, inhibition of translation via sequestration of the ribosome binding site, or mRNA processing. Binding of ligands which induce gene expression, allows transcription elongation

or translation initiation. Riboswitches from different classes recognize a large range of cellular compounds, including coenzymes (Winkler W. et al., 2002; Winkler W.C. et al., 2002; Winkler et al., 2003), magnesium cations (Dann et al., 2007), purines and their derivatives (Batey, 2012), second-messenger molecules (Sudarsan et al., 2008), and amino acids (Serganov and Patel, 2009). In many cases, riboswitches control the expression of genes that are involved in the biosynthesis, degradation, or transport of the respective metabolite.

Bacteria depend on the availability of amino acids for continuous protein biosynthesis. Therefore, expression of genes required for amino acid transport, synthesis, and degradation is tightly regulated. Typical sensors for amino acid levels are T-box elements and attenuators located in the mRNA. T-box RNA binds tRNAs and modulates transcription or translation of the gene under control (Grundy and Henkin, 1993). Attenuators contain codons for an effector amino acid. At a low concentration of the effector, translation stalls and formation of an anti-terminator structure is favored (Yanofsky, 1981). In addition, two riboswitches are able to bind amino acids directly. Lysine riboswitches control genes involved in lysine biosynthesis and lysine transport (Grundy et al., 2003; Rodionov et al., 2003; Sudarsan et al., 2003). Glycine riboswitches most often regulate the expression of glycine cleavage system genes, but were also found upstream of various other genes involved in the synthesis, conversion, or transport of glycine (Barrick et al., 2004). Glycine riboswitches are widely distributed and have been identified in Gram-positive and Gram-negative bacteria (Barrick and Breaker, 2007).

Streptococcus pyogenes [Group A streptococcus (GAS)] is a Gram-positive human pathogen responsible for a variety of diseases ranging from mild self-limiting superficial infections of the throat or skin to life-threatening invasive diseases including bacteremia and necrotizing fasciitis. Common post-streptococcal autoimmune complications are acute rheumatic fever and acute post-streptococcal glomerulonephritis. The impact of GAS diseases is especially high in resource-limited settings and in a recent publication a rise of global invasive disease burden caused by GAS was reported (Sims et al., 2016).

To limit the application and distribution of antibiotics and to identify GAS specific therapeutic targets, investigation of metabolic regulation processes can be very fruitful. Riboswitches have been already studied as promising antibacterial targets in a variety of bacteria. Modification of riboswitch function is achieved by the administration of ligand analogs, usually small compounds which are easy to manufacture and to deliver (Machtel et al., 2016). Glycine supplementation is required for optimal growth of GAS (Levering et al., 2016). The presence of a putative glycine riboswitch in GAS opens the possibility to specifically inhibit glycine metabolism or transport. Therefore, we investigated in this study gene expression regulation by a *cis*-regulatory element with sequence similarities to known glycine riboswitches. One glycine binding aptamer was predicted in the 5'-UTR of a sodium:alanine symporter family protein (SAF) gene in GAS M49 strain 591. We found that the genetic element indeed regulates glycine-dependent gene expression of the SAF gene by transcription termination/anti-termination. On a second

level of regulation, SAF gene transcript stability is reduced in the presence of glycine.

MATERIALS AND METHODS

Bacterial Strains and Culture Conditions

Group A streptococcus serotype M49 strain 591 was kindly provided by R. Lütticken (Aachen, Germany). All GAS strains were cultured in chemically defined medium (CDM) (van de Rijn and Kessler, 1980) or Todd-Hewitt broth (Thermo Fisher Scientific, Darmstadt, Germany) supplemented with 0.5% yeast extract (Thermo Fisher Scientific, Darmstadt, Germany) (THY), as indicated, at 37°C with a 5% CO₂/20% O₂ atmosphere. *Escherichia coli* strain DH5 α (Gibco BRL, Eggenstein, Germany) was used as host for the construction, proliferation, and storage of recombinant plasmids. All *E. coli* strains were cultured in Lennox L Broth Base (Thermo Fisher Scientific, Darmstadt, Germany). For selection, antibiotics were added at the appropriate concentrations.

Construction of Recombinant GAS Strains

Riboswitch controlled LUC reporter gene constructs were generated by cloning an 875 bp genomic fragment into the MCS of pFW11-*luc2* (Podbielski et al., 1999). Promoter controlled LUC reporter gene constructs were generated by fusing a 588 bp fragment carrying the promoter region 5' of *ribogly* to *luc2*. Inserts were amplified by PCR using chromosomal DNA from GAS M49 strain 591 as template. All primers used for the generation of the respective fragments are listed in Supplementary Table 1. The resulting plasmids were verified by classical Sanger sequencing (GATC Biotech AG, Konstanz, Germany). GAS M49 strain 591 was transformed with the respective plasmids. Insertion of the recombinant fusion genes into the genome was verified by PCR analyses and classical Sanger sequencing (GATC Biotech AG, Konstanz, Germany) of a genomic PCR fragment.

Quantitative Assay for Luciferase Activity

For assessment of luciferase activity from riboswitch-*luc* fusions, GAS *luc* reporter strains were grown in CDM, supplemented with 0–10 mM of the amino acids glycine, alanine, or serine as indicated. For measurement of luminescence, 1 ml aliquots of the cell suspensions were withdrawn at hourly intervals, OD₆₀₀ was measured, and samples were processed as described by Podbielski et al. (1999). Luminescence was measured for 15 s in a Luminometer Lumimat LB 9501 (Berthold Technologies GmbH, Bad Wildbad, Germany). RLU values at each time point were calculated by subtracting luminescence at time 0 from luminescence at time x. RLU/OD₆₀₀ were calculated to normalize for growth differences.

Extraction of Total RNA

Group A streptococcus strains were grown for 3 h in CDM complemented with glycine as indicated. Bacteria were pelleted

immediately, quickly frozen in liquid nitrogen, and stored at -80°C until use. Bacterial cells were disrupted in a homogenizer (Peqlab Biotechnologie GmbH, Erlangen, Germany). Total RNA from GAS strains was extracted according to the protocol supplied with the Direct-zolTM RNA MiniPrep Kit (Zymo Research, Irvine). After extraction, RNA was treated with acid phenol:chloroform:isoamyl alcohol (125:24:1), pH 4.5 (Thermo Fisher Scientific, Darmstadt, Germany), and TURBOTM DNase (Thermo Fisher Scientific, Darmstadt, Germany) according to the manufacturer's instructions. RNA was stored at -80°C until further use.

Reverse Transcription Followed by Quantitative PCR (RT-qPCR)

Following DNase treatment, cDNA synthesis was performed using the Superscript first-strand synthesis system for RT-PCR (Invitrogen, Thermo Fisher Scientific, Darmstadt, Germany). Quantitative PCR amplification was conducted with SYBR green (Thermo Fisher Scientific, Darmstadt, Germany) using the ViiATM 7 Real-Time PCR System (Applied Biosystems, Darmstadt, Germany). The 5S rRNA gene served as internal control. Relative expression was calculated employing the $2^{-\Delta\Delta\text{ct}}$ method (Schmittgen and Livak, 2008). All primers used for RT-qPCR are listed in Supplementary Table 1.

Northern Blot Analyses

RNA samples (6 μg) were loaded onto a denaturing 1.5% formaldehyde agarose gel and separated by electrophoresis. Size standards (MillenniumTM RNA Marker; Thermo Fisher Scientific, Darmstadt, Germany) were loaded on the same gel. RNA was blotted onto neutral nylon membranes (Roti[®]-Nylon 0.2, Carl Roth GmbH & co KG, Karlsruhe, Germany) and UV cross-linked (UV150 mJoule/cm²). Templates for the probes were generated by PCR with the primers listed in Supplementary Table 1. The 5' end of the reverse primers contained the T7 promoter sequence (CTTAATACGACTCACTATAGGG) for *in vitro* transcription using the MEGAscript[®] T7 Kit (Thermo Fisher Scientific, Darmstadt, Germany). Probes were labeled with biotin using the Pierce[™] RNA 3' End Biotinylation Kit (Thermo Fisher Scientific, Darmstadt, Germany). Biotin labeled RNA probes were purified using the RNA Clean & Concentrator[™]-5 kit (Zymo Research, Freiburg, Germany). Membranes were hybridized overnight with RNA probes complementary to the respective transcripts as indicated. IRDye 800CW Streptavidin (LI-COR Biotechnology GmbH, Bad Homburg, Germany) was used for detection, and the blot was scanned on an Odyssey[®] Imager CLX 1283 (LI-COR Biotechnology GmbH, Bad Homburg, Germany).

Transcript Stability Determination

Group A streptococcus strains were grown for 3 h in CDM complemented with glycine as indicated. RNA synthesis was inhibited by addition of rifampicin (1 mg/ml) to the cultures. Following the addition of rifampicin, 5 ml samples were recovered after 0, 1, 2, 5, and 10 min. Samples were added

to two volumes of RNAprotect Cell Reagent (Qiagen GmbH, Hilden, Germany), incubated at room temperature for 5 min, pelleted by centrifugation and quick frozen in liquid nitrogen. RNA was isolated from the samples as described above and transcript abundance was determined by RT-qPCR. The half-life of the transcripts was calculated by non-linear regression analyses (Least squares fit, GraphPad Prism).

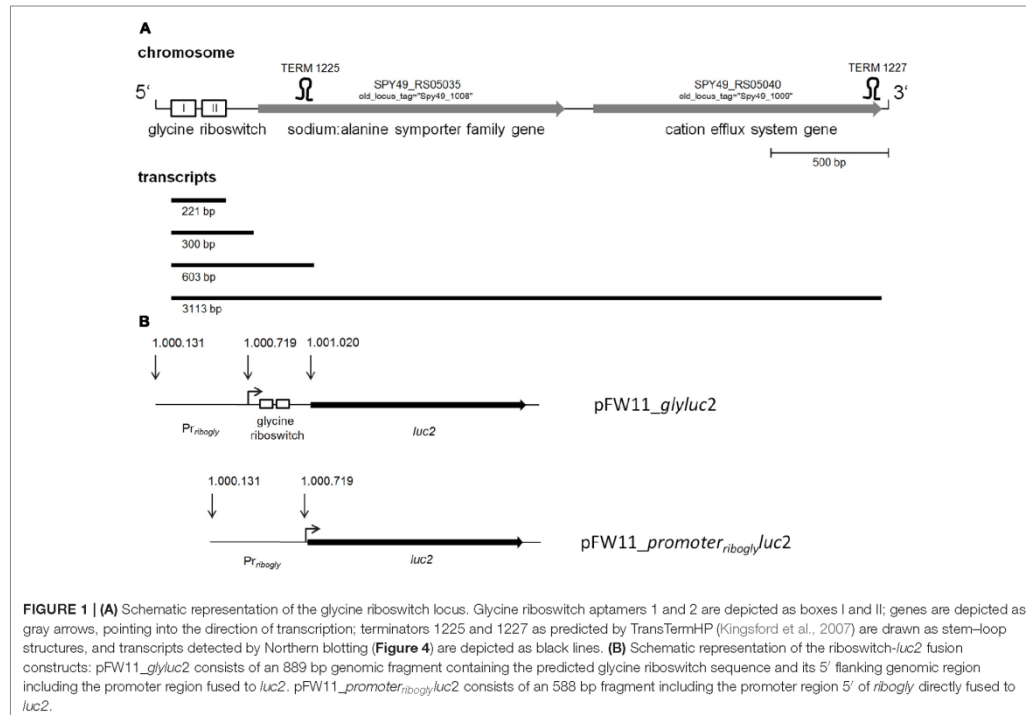
Statistical Analyses

All experiments were performed at least three times or as indicated by the sample size (n). Statistical significance was determined using the tests indicated in the respective figure legends.

RESULTS

The Putative Glycine Riboswitch Mediates Glycine-Dependent Expression of a Luciferase Reporter Gene

In a previous study, we detected expression of 18 putative riboswitches using intergenic DNA tiling arrays (Patenge et al., 2012). One riboswitch candidate was identified downstream of *pcrA* (Spy49_1007c) and was designated sRNASpy491007c. It belongs to the Rfam family RF00504 of glycine riboswitches (Nawrocki et al., 2015) and is located in the 5-prime region of the sodium:alanine symporter family protein (SAF) gene (Reizer et al., 1994) (Figure 1). A luciferase (LUC) reporter gene system was employed to determine a potential response to glycine. An 889 bp genomic fragment containing the predicted glycine riboswitch sequence and, to allow for homologous recombination, its 5' flanking genomic region was amplified by PCR and fused to the *luc* reporter gene carried by pFW11_ *luc2* (Podbielski et al., 1999) (Figure 1B). GAS M49 strain 591/pFW11_ *glyluc2* was grown in CDM containing varying concentrations of glycine. Glycine is required for optimal growth of GAS (Levering et al., 2016). Consistently, growth was poor in medium without glycine and in medium containing a low glycine concentration (0.01 mM glycine) compared to growth in medium containing 0.1 to 10 mM glycine (Figure 2A). LUC activity was measured over time and normalized to cell density to compensate for differences in growth (Figure 2B). Maximal reporter gene expression was observed following 3 h of growth in the absence of glycine and in the presence of low glycine concentrations (0.01–0.1 mM). In the presence of 10 mM glycine, reporter gene expression was always repressed. During growth in 1 mM glycine, moderate LUC activity could be detected in the exponential growth phase. Since the gene downstream of the putative glycine riboswitch encodes a putative sodium:alanine symporter and since alanine and serine are structurally similar to glycine, we tested the effect of these two amino acids on reporter gene expression. Growth of GAS M49 strain 591/pFW11_ *glyluc2* in the absence of serine and in CDM containing 0.01 mM serine was slow compared to growth in the presence of 0.1–10 mM serine (Figure 2C). GAS M49 strain 591/pFW11_ *glyluc2* grew similar in CDM with and without alanine (Figure 2E). Neither



the presence of serine nor alanine did influence reporter gene expression (Figures 2D,F).

The Putative Glycine Riboswitch Controls Expression the SAF Gene and a Putative Cation Efflux System Gene

To address the question, whether the putative glycine riboswitch controls expression of its downstream genes, RT-qPCR experiments were conducted. WT bacteria were grown in CDM containing 0.1, 2.6, and 10 mM glycine. Total RNA was isolated, reverse transcribed, and amplified using primers specific for the putative glycine riboswitch (*ribogly*), the SAF gene (*Na⁺/Ala sym*), and the putative cation efflux system gene (*cation efflux*), respectively (Figure 3A). Transcript abundance at 0.1 mM glycine served as calibrator for all three reactions. Abundance of the riboswitch RNA was unaltered at all glycine concentrations tested. In contrast, the SAF and the cation efflux system gene mRNA were dramatically decreased at 2.6 and 10 mM glycine in comparison to 0.1 mM glycine.

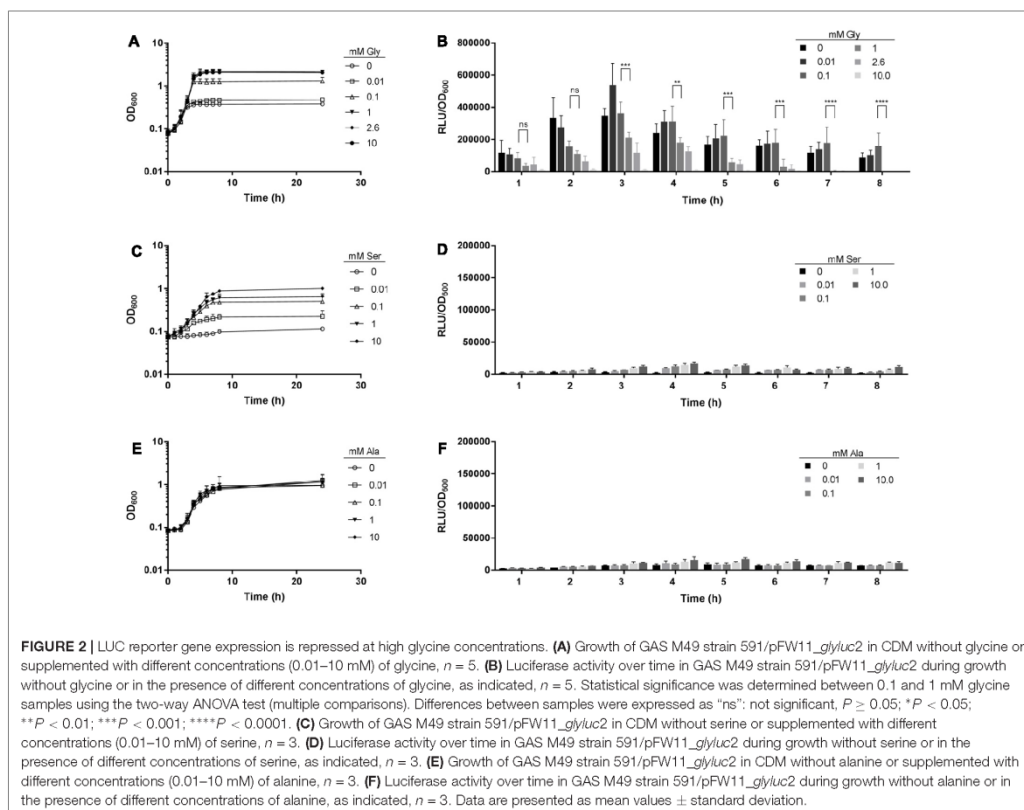
Glycine-Dependent Gene Control Is Not Based on Changes of Promoter Activity

To investigate the regulatory influence of the promoter region, a 588 bp fragment carrying the promoter region 5' of *ribogly* was

fused to *luc* (Figure 1B). GAS M49 strain 591 was transformed with pFW11_promoter_ribogly/luc2. Transcript abundance of *luc2* was determined by RT-qPCR following growth in the presence of 0.1, 2.6, and 10 mM glycine. Transcript level at 0.1 mM glycine served as calibrator. Expression of *luc2* was not influenced by the glycine concentration in the medium (Figure 3B).

Transcript Sizes Are Dependent on the Glycine Concentration in the Medium

Expression of both, the SAF gene and the cation efflux system gene, was repressed in the presence of high glycine concentrations (Figure 3). Primers to amplify gene junctions were designed and used in reverse-transcriptase experiments followed by PCR. The detection of a PCR product suggested co-transcription of the two genes. To verify this result, Northern blot analyses were performed. WT bacteria were grown in CDM containing 0.1, 2.6, or 10 mM glycine, respectively. Total RNA was isolated from the cultures and separated by agarose gel electrophoresis. Blots were sequentially hybridized with RNA probes specific for *ribogly* and the SAF gene transcript (*Na⁺/Ala sym*). In the presence of high glycine concentrations (2.6 and 10 mM), the *ribogly* probe detected a highly abundant 200 bp band, which might represent a transcription termination or a RNA cleavage product (Figure 4). No SAF gene transcript could be detected (Figure 4). Consistent



with the *luc* reporter gene assay and RT-qPCR results, expression of the gene was repressed under these conditions. In the presence of 0.1 mM glycine, a 3 kb band could be detected with the *ribogly* and the *Na⁺/Ala symp* probes. The apparent size of the band corresponds to the calculated size of a co-transcript of the SAF gene and the cation efflux system gene (3113 bp, **Figure 1**). A second band with the apparent size of 600 bp could be detected with both probes. This corresponds to the product of termination within the SAF gene at the putative terminator TERM 125 (TransTermHP v2.07) (Kingsford et al., 2007). A 300 bp band was detected using the *ribogly* probe but not following hybridization with the *Na⁺/Ala symp* probe. The transcripts detected by Northern blotting are depicted schematically in relation to the corresponding genes (**Figure 1**).

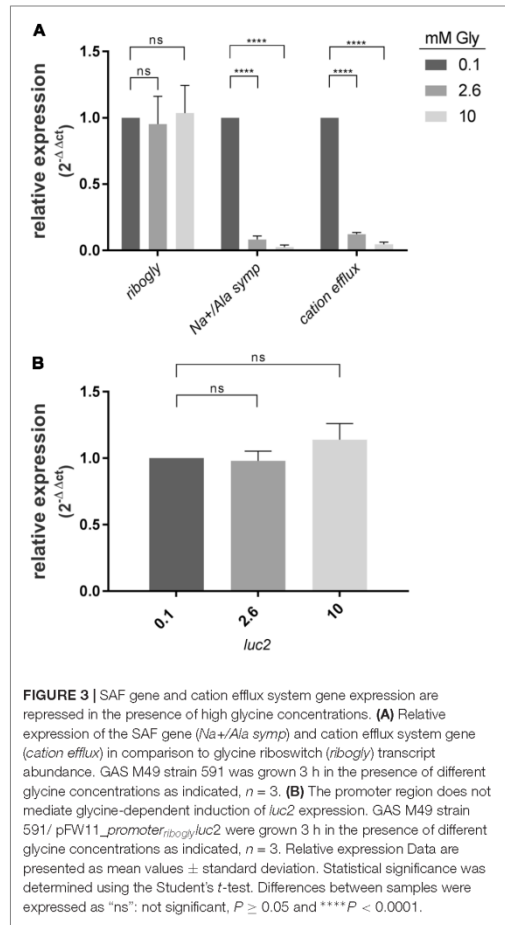
SAF Gene Transcript Stability Is Reduced at High Glycine Concentrations in the Medium

Transcripts of genes controlled by riboswitches are often processed or exhibit differential stability (Mellin and Cossart,

2015). We aimed to investigate *ribogly* and SAF gene transcript stability under repressing and non-repressing conditions. WT GAS M49 strain 591 was grown in the presence of 0.1 or 10 mM glycine, respectively. Transcription was stopped by addition of rifampicin and samples were collected for RT-qPCR analyses at 1, 2, 5, and 10 min following rifampicin treatment (**Figure 5**). 5S rRNA and *groES* mRNA served as controls. 5S rRNA was stable over the observation period. The half-life of *groES* mRNA was similar during growth in 0.1 mM glycine (1.8 min) and 10 mM glycine (1.9 min). Stability of *ribogly* was low under both conditions. Its half-life was 0.4 min in 0.1 and 10 mM glycine. In contrast, the stability of *Na⁺/Ala symp* was low during growth in 10 mM glycine (0.5 min) but much higher in 0.1 mM glycine (5 min), suggesting an additional ribonuclease-dependent regulation level.

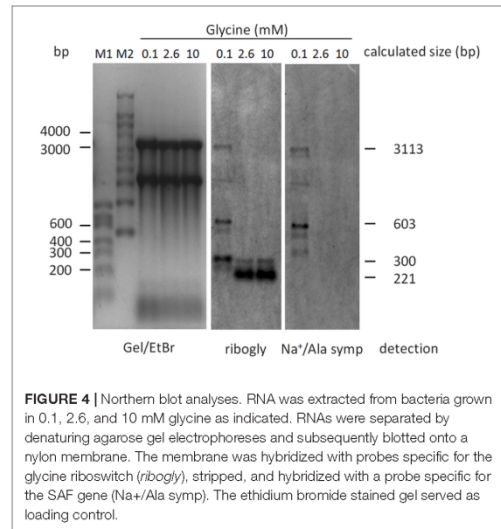
ribogly Belongs to the Tandem Aptamer Glycine Riboswitches

In the reference genome of *S. pyogenes* NZ131 (accession number: NC_011375.1), a 90 bp putative glycine riboswitch



was annotated. A search using the rfam database (Nawrocki et al., 2015) predicted the presence of one glycine-binding aptamer. Since we observed a band of approximate 200 bp in Northern blot analyses of total RNA from GAS M49 strain 591 (Figure 4), we performed secondary structure prediction using RNAfold (The ViennaRNA Web Services¹). Secondary structure modeling was based on 182 bp of the reference genome of *S. pyogenes* NZ131. The result is illustrated in Figure 6 using VARNA GUI (Darty et al., 2009). The analysis revealed the typical consensus structure of a tandem aptamer riboswitch containing two glycine binding sites (Esquiaqui et al., 2014; Ruff et al., 2016). The conserved residues are labeled in green.

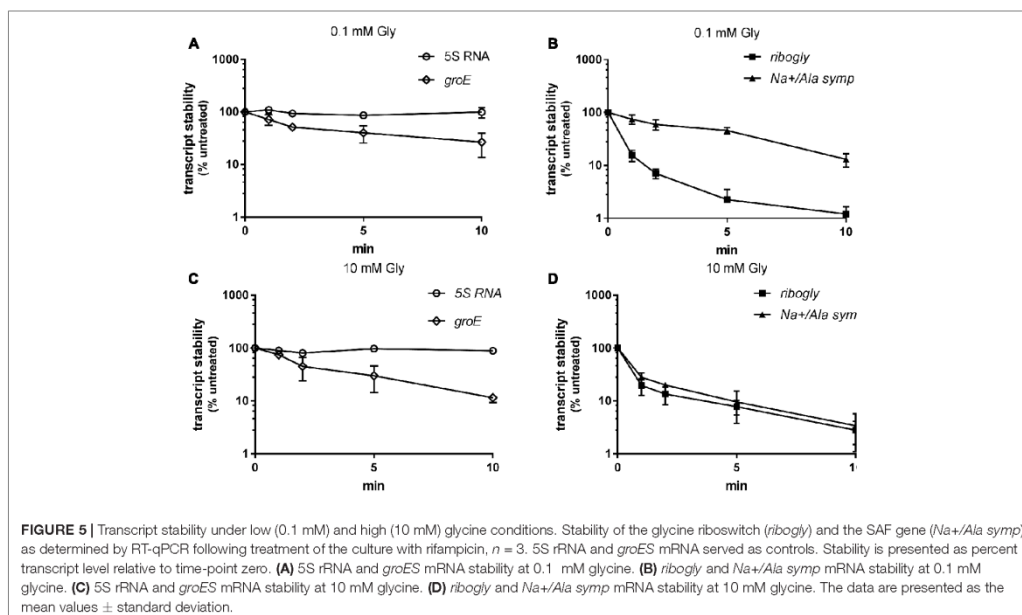
¹<http://rna.tbi.univie.ac.at/>



DISCUSSION

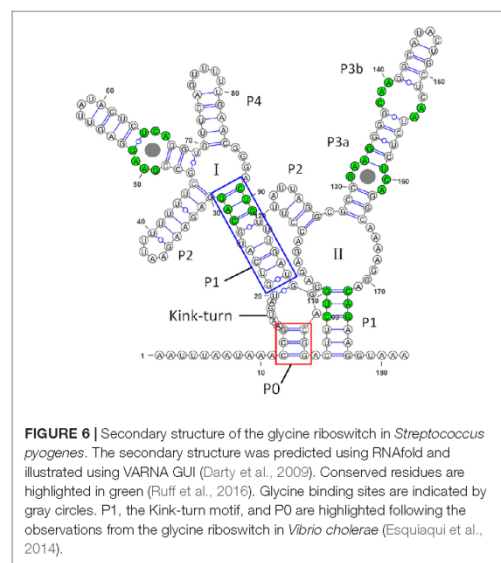
Riboswitches often regulate expression of genes involved in the metabolism or transport of their ligands. Typically, glycine riboswitches induce the expression of genes responsible for glycine cleavage or export following glycine binding (Barrick et al., 2004). In *Bacillus subtilis*, the glycine riboswitch is composed of two similar aptamers followed by a single expression platform (Mandal et al., 2004). In *S. pyogenes*, one aptamer, similar to the *B. subtilis* aptamers, was predicted upstream of a putative SAF gene. Previously, we observed expression of the riboswitch region in GAS M49 strain 591 by intergenic tiling arrays (Patenge et al., 2012). In the SF370 clinical isolate, expression of the putative streptococcal riboswitch was detected by Northern blot analyses (Le Rhun et al., 2015). In this work, we investigated whether the putative glycine riboswitch mediates glycine-dependent gene regulation.

LUC reporter gene assays and Northern blot analyses revealed that expression of the SAF gene was repressed in the presence of glycine. The corresponding promoter region did not mediate glycine-dependent downregulation of *luc* in a promoter-reporter gene fusion construct. As a general rule, amino acid riboswitches increase the expression of glycine cleavage system genes or glycine export protein genes upon binding to glycine (Serganov and Patel, 2009; Serganov and Nudler, 2013). In *Streptomyces griseus* a detoxification system is activated by a glycine riboswitch (Tezuka and Ohnishi, 2014). In contrast, *lysC* in *B. subtilis* is repressed by a lysine-responsive riboswitch due to transcription termination in the presence of a high L-lysine concentration (Phan and Schumann, 2009). The *lysC* gene of *B. subtilis* consists of two overlapping reading frames coding for the α - and β -subunits of a lysine-responsive aspartokinase II, which



catalyzes the first step in the biosynthesis of methionine, lysine, and threonine (Chen et al., 1987). The SAF gene in *S. pyogenes* encodes a member of the Alanine or Glycine:Cation Symporter (AGCS) Family [Transporter Classification Database (TCDB)] (Saier et al., 2016). Proteins belonging to the AGCS family have been reported to transport alanine and/or glycine in symport with Na^+ and/or H^+ . The *dagA* gene from the marine bacterium *Alteromonas haloplanktis* is a sodium-dependent transporter and is involved in the uptake of glycine and glutamine (MacLeod and MacLeod, 1992). We hypothesize that binding of glycine by the riboswitch in *S. pyogenes* leads to the downregulation of a so far unidentified glycine uptake system.

The truncated form of the *B. subtilis* riboswitch RNA controlling *lysC* is predominantly produced, even under conditions promoting anti-termination (Phan and Schumann, 2009). In contrast, we did only detect small amounts of the truncated 200 bp riboswitch RNA under inducing conditions. Stability of the riboswitch RNA was low at all glycine concentrations tested. The half-life of the full-length transcript decreased at high glycine concentrations. A combination of classical riboswitch function and mRNA stability control has been reported recently. In *E. coli*, *lysC* expression is controlled on the level of translation initiation by a lysine riboswitch. Upon lysine binding, the riboswitch adopts a conformation that sequesters the ribosomal binding site and at the same time exposes RNaseE cleavage sites (Caron et al., 2012). RNase E is a component of the RNA degradosome in Gram negative bacteria (Callaghan et al., 2004). In most Gram positive organisms, RNase E is replaced by other ribonucleases, e.g., RNaseY and



RNases J1 and J2 (Cho, 2017). In *S. pyogenes*, RNase Y is involved in mRNA turnover (Chen et al., 2013). Structural investigation of the GlmS ribozyme from *B. anthracis* revealed

autocatalytic cleavage of GlmS mRNA at a single site 5' of the riboswitch sequence following binding of glucosamine-6-phosphate (GlcN6P). Specific cleavage renders GlmS mRNA susceptible to degradation by RNase J (Cochrane et al., 2007). It is tempting to speculate that processing of the glycine riboswitch controlled transcript in *S. pyogenes* leads to the exposure of RNase cleavage sites and thereby to decreasing SAF gene transcript stability.

The glycine riboswitch is the only riboswitch that exhibits tandem architecture, with two adjacent, homologous aptamers followed by a single expression platform. In *B. subtilis*, glycine binding by the riboswitch aptamers has been initially reported to function in a cooperative manner (Mandal et al., 2004). However, a full-length derivative of the riboswitch containing its extended 5' leader, did not show cooperative binding (Sherman et al., 2012). The tandem glycine riboswitch from *Vibrio cholerae*, including the leader sequence, was studied using an equilibrium dialysis-based assay. The results showed that ligand binding by aptamer-1 is linked to aptamer dimerization and stabilizes the P1 stem of aptamer-2, which controls the expression platform (Ruff and Strobel, 2014). In a recent study, analysis of sequenced genomes revealed a significant number of singlet glycine riboswitches. Several singlet riboswitches were characterized biochemically and it could be demonstrated that singlet riboswitches were able to bind glycine with affinities comparable to those of previously published tandem glycine riboswitches. Conserved stem-loop structures (ghost aptamers), situated up- or down-stream of the singlet aptamer, respectively, form interactions with the aptamer domain that are necessary for ligand-binding activity (Ruff et al., 2016). In *S. pyogenes*, one aptamer was annotated upstream of the SAF gene. A second aptamer containing a P4 stem was revealed by *in silico* secondary structure predictions. The sequence directly upstream of the first aptamer is similar to the conserved leader region, which interacts with the recently discovered K-turn linker of tandem glycine riboswitches and modulates ligand binding (Kladwang et al., 2012; Sherman et al., 2012; Baird and Ferre-D'Amare, 2013; Esquiaqui et al., 2016). This indicates that the *S. pyogenes* glycine riboswitch belongs to the class of tandem riboswitches, featuring the recently identified K-turn linker.

Inducible expression systems are useful tools in molecular biology. Characterization of essential genes and production of potential toxic gene products are only two of many examples for the requirement of conditional gene expression control. Riboswitch based systems for precise gene regulation have the advantage, that expression can be controlled by the addition of small compounds that easily enter the cell and that are in many cases comparably inexpensive (Machtel et al., 2016). A glycine-inducible expression system has been developed using the riboswitch from *B. subtilis*. The authors could demonstrate glycine-dependent production

of recombinant proteins (Phan and Schumann, 2007). With a comparable strategy, a gene knock-down or knock-out system could be engineered, employing the *S. pyogenes* glycine riboswitch.

Riboswitches are potential targets for antimicrobial therapies (Machtel et al., 2016). Extensively studied targets include purine riboswitches. Purines are essential for bacterial survival and purine riboswitches control purine metabolism and transport (Lunse et al., 2014). There is an ongoing search for suitable purine analogs that bind the riboswitch with comparable affinity as guanosine (Kim et al., 2009; Mulhbachter et al., 2010). Beside essential pathways, riboswitch control of biofilm formation is a promising target for antimicrobial drugs (Reyes-Darias and Krell, 2017). Lysine riboswitches have also been explored as potential targets and several lysine analogs with high affinity binding have been identified, but there were difficulties arising from toxicity of the compounds and bacterial resistance (Blount et al., 2007). Glycine is required for optimal *S. pyogenes* growth. The *S. pyogenes* glycine riboswitch is highly conserved among different serotypes. Sequence identity of the riboswitch within the completed *S. pyogenes* genomic sequences is 99–100%. Downregulation of streptococcal glycine transport by targeting the glycine riboswitch with a glycine analog could serve as a novel therapeutic strategy. Alternatively, ligands for the not yet characterized riboswitches in *S. pyogenes* should be identified and investigated for their drug target potential.

AUTHOR CONTRIBUTIONS

AK and NIP performed the experiments presented in the manuscript. AK, NIP, BK, and NAP contributed to the design of this study, analyses, and interpretation of the data, drafting the manuscript, and approved it for publication.

FUNDING

Our work was supported by grants from the Bundesministerium für Bildung und Forschung (FKZ 0315437B) and from the Ministerium für Bildung, Wissenschaft und Kultur, Mecklenburg-Vorpommern (ESF/14-BM-A55-0010/16), and the University Medicine Rostock (Forun 889008).

SUPPLEMENTARY MATERIAL

The Supplementary Material for this article can be found online at: <https://www.frontiersin.org/articles/10.3389/fmicb.2018.00200/full#supplementary-material>

REFERENCES

Baird, N. J., and Ferre-D'Amare, A. R. (2013). Modulation of quaternary structure and enhancement of ligand binding by the K-turn of tandem glycine riboswitches. *RNA* 19, 167–176. doi: 10.1261/rna.036269.112

Barrick, J. E., and Breaker, R. R. (2007). The distributions, mechanisms, and structures of metabolite-binding riboswitches. *Genome Biol.* 8:R239. doi: 10.1186/gb-2007-8-11-r239

Barrick, J. E., Corbino, K. A., Winkler, W. C., Nahvi, A., Mandal, M., Collins, J., et al. (2004). New RNA motifs suggest an expanded scope for riboswitches

- in bacterial genetic control. *Proc. Natl. Acad. Sci. U.S.A.* 101, 6421–6426. doi: 10.1073/pnas.0308014101
- Batey, R. T. (2012). Structure and mechanism of purine-binding riboswitches. *Q. Rev. Biophys.* 45, 345–381. doi: 10.1017/S0033583512000078
- Blount, K. F., Wang, J. X., Lim, J., Sudarsan, N., and Breaker, R. R. (2007). Antibacterial lysine analogs that target lysine riboswitches. *Nat. Chem. Biol.* 3, 44–49. doi: 10.1038/nchembio842
- Callaghan, A. J., Aurikko, J. P., Ilag, L. L., Gunter, G. J., Chandran, V., Kuhnelt, K., et al. (2004). Studies of the RNA degradosome-organizing domain of the *Escherichia coli* ribonuclease RNase E. *J. Mol. Biol.* 340, 965–979. doi: 10.1016/j.jmb.2004.05.046
- Caron, M. P., Bastet, L., Lussier, A., Simoneau-Roy, M., Masse, E., and Lafontaine, D. A. (2012). Dual-acting riboswitch control of translation initiation and mRNA decay. *Proc. Natl. Acad. Sci. U.S.A.* 109, E3444–E3453. doi: 10.1073/pnas.1214024109
- Chen, N. Y., Hu, F. M., and Paulus, H. (1987). Nucleotide sequence of the overlapping genes for the subunits of *Bacillus subtilis* aspartokinase II and their control regions. *J. Biol. Chem.* 262, 8787–8798.
- Chen, Z., Itzek, A., Malke, H., Ferretti, J. J., and Kreth, J. (2013). Multiple roles of RNase Y in *Streptococcus pyogenes* mRNA processing and degradation. *J. Bacteriol.* 195, 2585–2594. doi: 10.1128/JB.00997-13
- Cho, K. H. (2017). The structure and function of the gram-positive bacterial RNA degradosome. *Front. Microbiol.* 8:154. doi: 10.3389/fmicb.2017.00154
- Cochrane, J. C., Lipchok, S. V., and Strobel, S. A. (2007). Structural investigation of the GlnS ribozyme bound to its catalytic cofactor. *Chem. Biol.* 14, 97–105. doi: 10.1016/j.chembiol.2006.12.005
- Damm, C. E. III, Wakeman, C. A., Sieling, C. L., Baker, S. C., Irnov, I., and Winkler, W. C. (2007). Structure and mechanism of a metal-sensing regulatory RNA. *Cell* 130, 878–892. doi: 10.1016/j.cell.2007.06.051
- Darty, K., Denise, A., and Ponty, Y. (2009). VARNA: Interactive drawing and editing of the RNA secondary structure. *Bioinformatics* 25, 1974–1975. doi: 10.1093/bioinformatics/btp250
- Esquiaqui, J. M., Sherman, E. M., Ionescu, S. A., Ye, J. D., and Fanucci, G. E. (2014). Characterizing the dynamics of the leader-linker interaction in the glycine riboswitch with site-directed spin labeling. *Biochemistry* 53, 3526–3528. doi: 10.1021/bi500404b
- Esquiaqui, J. M., Sherman, E. M., Ye, J. D., and Fanucci, G. E. (2016). Conformational flexibility and dynamics of the internal loop and helical regions of the kink-turn motif in the glycine riboswitch by site-directed spin-labeling. *Biochemistry* 55, 4295–4305. doi: 10.1021/acs.biochem.6b00287
- Grundy, F. J., and Henkin, T. M. (1993). tRNA as a positive regulator of transcription antitermination in *B. subtilis*. *Cell* 74, 475–482. doi: 10.1016/0092-8674(93)80049-K
- Grundy, F. J., Lehman, S. C., and Henkin, T. M. (2003). The L box regulon: lysine sensing by leader RNAs of bacterial lysine biosynthesis genes. *Proc. Natl. Acad. Sci. U.S.A.* 100, 12057–12062. doi: 10.1073/pnas.2133705100
- Kim, J. N., Blount, K. F., Puskasz, I., Lim, J., Link, K. H., and Breaker, R. R. (2009). Design and antimicrobial action of purine analogues that bind Guanine riboswitches. *ACS Chem. Biol.* 4, 915–927. doi: 10.1021/cb900146k
- Kingsford, C. L., Ayanbule, K., and Salzberg, S. L. (2007). Rapid, accurate, computational discovery of Rho-independent transcription terminators illuminates their relationship to DNA uptake. *Genome Biol.* 8:R22. doi: 10.1186/gb-2007-8-2-r22
- Kladwang, W., Chou, F. C., and Das, R. (2012). Automated RNA structure prediction uncovers a kink-turn linker in double glycine riboswitches. *J. Am. Chem. Soc.* 134, 1404–1407. doi: 10.1021/ja2093508
- Le Rhun, A., Beer, Y. Y., Reimegard, J., Chylinski, K., and Charpentier, E. (2015). RNA sequencing uncovers antisense RNAs and novel small RNAs in *Streptococcus pyogenes*. *RNA Biol.* 13, 177–195. doi: 10.1080/15476286.2015.1110674
- Levering, J., Fiedler, T., Sieg, A., van Grinsven, K. W., Hering, S., Veith, N., et al. (2016). Genome-scale reconstruction of the *Streptococcus pyogenes* M49 metabolic network reveals growth requirements and indicates potential drug targets. *J. Biotechnol.* 232, 25–37. doi: 10.1016/j.jbiotec.2016.01.035
- Lunse, C. E., Schuller, A., and Mayer, G. (2014). The promise of riboswitches as potential antibacterial drug targets. *Int. J. Med. Microbiol.* 304, 79–92. doi: 10.1016/j.jimm.2013.09.002
- Machtel, P., Bakowska-Zywicka, K., and Zywicki, M. (2016). Emerging applications of riboswitches - from antibacterial targets to molecular tools. *J. Appl. Genet.* 57, 531–541. doi: 10.1007/s13353-016-0341-x
- MacLeod, P. R., and MacLeod, R. A. (1992). Identification and sequence of a Na⁺-linked gene from the marine bacterium *Alteromonas haloplanktis* which functionally complements the *dagA* gene of *Escherichia coli*. *Mol. Microbiol.* 6, 2673–2681. doi: 10.1111/j.1365-2958.1992.tb01444.x
- Mandal, M., Lee, M., Barrick, J. E., Weinberg, Z., Emilsson, G. M., Ruzzo, W. L., et al. (2004). A glycine-dependent riboswitch that uses cooperative binding to control gene expression. *Science* 306, 275–279. doi: 10.1126/science.1100829
- Mellin, J. R., and Cossart, P. (2015). Unexpected versatility in bacterial riboswitches. *Trends Genet.* 31, 150–156. doi: 10.1016/j.tig.2015.01.005
- Mulhbachter, J., Brouillette, E., Allard, M., Fortier, L. C., Malouin, F., and Lafontaine, D. A. (2010). Novel riboswitch ligand analogs as selective inhibitors of guanine-related metabolic pathways. *PLoS Pathog.* 6:e1000865. doi: 10.1371/journal.ppat.1000865
- Navrocki, E. P., Burge, S. W., Bateman, A., Daub, J., Eberhardt, R. Y., Eddy, S. R., et al. (2015). Rfam 12.0: updates to the RNA families database. *Nucleic Acids Res.* 43, D130–D137. doi: 10.1093/nar/gku1063
- Patenge, N., Billion, A., Raasch, P., Normann, J., Wisniewska-Kucper, A., Retej, J., et al. (2012). Identification of novel growth phase- and media-dependent small non-coding RNAs in *Streptococcus pyogenes* M49 using intergenic tiling arrays. *BMC Genomics* 13:550. doi: 10.1186/1471-2164-13-550
- Phan, T. T., and Schumann, W. (2007). Development of a glycine-inducible expression system for *Bacillus subtilis*. *J. Biotechnol.* 128, 486–499. doi: 10.1016/j.jbiotec.2006.12.007
- Phan, T. T., and Schumann, W. (2009). Transcriptional analysis of the lysine-responsive and riboswitch-regulated *lysC* gene of *Bacillus subtilis*. *Curr. Microbiol.* 59, 463–468. doi: 10.1007/s00284-009-9461-4
- Podbielski, A., Woischnik, M., Leonard, B. A., and Schmidt, K. H. (1999). Characterization of *nra*, a global negative regulator gene in group A streptococci. *Mol. Microbiol.* 31, 1051–1064. doi: 10.1046/j.1365-2958.1999.01241.x
- Reizer, J., Reizer, A., and Saier, M. H. Jr. (1994). A functional superfamily of sodium/solute symporters. *Biochim. Biophys. Acta* 1197, 133–166. doi: 10.1016/0304-4157(94)90003-5
- Reyes-Darias, J. A., and Krell, T. (2017). Riboswitches as potential targets for the development of anti-biofilm drugs. *Curr. Top. Med. Chem.* doi: 10.2174/1568026617666170407163517 [Epub ahead of print].
- Rodionov, D. A., Vitreschak, A. G., Mironov, A. A., and Gelfand, M. S. (2003). Regulation of lysine biosynthesis and transport genes in bacteria: yet another RNA riboswitch? *Nucleic Acids Res.* 31, 6748–6757.
- Ruff, K. M., Muhammad, A., McCown, P. J., Breaker, R. R., and Strobel, S. A. (2016). Single glycine riboswitches bind ligand as well as tandem riboswitches. *RNA* 22, 1728–1738. doi: 10.1261/rna.057935.116
- Ruff, K. M., and Strobel, S. A. (2014). Ligand binding by the tandem glycine riboswitch depends on aptamer dimerization but not double ligand occupancy. *RNA* 20, 1775–1788. doi: 10.1261/rna.047266.114
- Saier, M. H. Jr., Reddy, V. S., Tsu, B. V., Ahmed, M. S., Li, C., and Moreno-Hagelsieb, G. (2016). The transporter classification database (TCDB): recent advances. *Nucleic Acids Res.* 44, D372–D379. doi: 10.1093/nar/gkv1103
- Schmittgen, T. D., and Livak, K. J. (2008). Analyzing real-time PCR data by the comparative C(T) method. *Nat. Protoc.* 3, 1101–1108. doi: 10.1038/nprot.2008.73
- Serganov, A., and Nudler, E. (2013). A decade of riboswitches. *Cell* 152, 17–24. doi: 10.1016/j.cell.2012.12.024
- Serganov, A., and Patel, D. J. (2009). Amino acid recognition and gene regulation by riboswitches. *Biochim. Biophys. Acta* 1789, 592–611. doi: 10.1016/j.bbaggm.2009.07.002
- Sherman, E. M., Esquiaqui, J., Elsayed, G., and Ye, J. D. (2012). An energetically beneficial leader-linker interaction abolishes ligand-binding cooperativity in glycine riboswitches. *RNA* 18, 496–507. doi: 10.1261/rna.031286.111
- Sims, S. A., Colquhoun, S., Wyber, R., and Carapetis, J. R. (2016). “Global disease burden of group A *Streptococcus*,” in *Streptococcus Pyogenes: Basic Biology to Clinical Manifestations*, eds J. J. Ferretti, D. L. Stevens, and V. A. Fischetti (Oklahoma City, OK: University of Oklahoma Health Sciences Center).

- Sudarsan, N., Lee, E. R., Weinberg, Z., Moy, R. H., Kim, J. N., Link, K. H., et al. (2008). Riboswitches in eubacteria sense the second messenger cyclic di-GMP. *Science* 321, 411–413. doi: 10.1126/science.1159519
- Sudarsan, N., Wickiser, J. K., Nakamura, S., Ebert, M. S., and Breaker, R. R. (2003). An mRNA structure in bacteria that controls gene expression by binding lysine. *Genes Dev.* 17, 2688–2697. doi: 10.1101/gad.1140003
- Tezuka, T., and Ohnishi, Y. (2014). Two glycine riboswitches activate the glycine cleavage system essential for glycine detoxification in *Streptomyces griseus*. *J. Bacteriol.* 196, 1369–1376. doi: 10.1128/JB.01480-13
- van de Rijn, L., and Kessler, R. E. (1980). Growth characteristics of group A streptococci in a new chemically defined medium. *Infect. Immun.* 27, 444–448.
- Winkler, W., Nahvi, A., and Breaker, R. R. (2002). Thiamine derivatives bind messenger RNAs directly to regulate bacterial gene expression. *Nature* 419, 952–956. doi: 10.1038/nature01145
- Winkler, W. C., Cohen-Chalamish, S., and Breaker, R. R. (2002). An mRNA structure that controls gene expression by binding FMN. *Proc. Natl. Acad. Sci. U.S.A.* 99, 15908–15913. doi: 10.1073/pnas.212628899
- Winkler, W. C., Nahvi, A., Sudarsan, N., Barrick, J. E., and Breaker, R. R. (2003). An mRNA structure that controls gene expression by binding S-adenosylmethionine. *Nat. Struct. Biol.* 10, 701–707. doi: 10.1038/nsb967
- Yanofsky, C. (1981). Attenuation in the control of expression of bacterial operons. *Nature* 289, 751–758. doi: 10.1038/289751a0

Conflict of Interest Statement: The authors declare that the research was conducted in the absence of any commercial or financial relationships that could be construed as a potential conflict of interest.

Copyright © 2018 Khani, Popp, Kretekemeyer and Patenge. This is an open-access article distributed under the terms of the Creative Commons Attribution License (CC BY). The use, distribution or reproduction in other forums is permitted, provided the original author(s) and the copyright owner are credited and that the original publication in this journal is cited, in accordance with accepted academic practice. No use, distribution or reproduction is permitted which does not comply with these terms.

SCIENTIFIC REPORTS

OPEN The Regulatory Small RNA MarS Supports Virulence of *Streptococcus pyogenes*

Received: 19 April 2016

Accepted: 12 September 2017

Published online: 25 September 2017

Roberto Pappesch¹, Philipp Warnke¹, Stefan Mikkat², Jana Normann¹, Aleksandra Wisniewska-Kucper¹, Franziska Huschka^{1,5}, Maja Wittmann¹, Afsaneh Khani¹, Oliver Schwengers^{3,4}, Sonja Oehmcke-Hecht¹, Torsten Hain³, Bernd Kreikemeyer¹ & Nadja Patenge¹

Small regulatory RNAs (sRNAs) play a role in the control of bacterial virulence gene expression. In this study, we investigated an sRNA that was identified in *Streptococcus pyogenes* (group A *Streptococcus*, GAS) but is conserved throughout various streptococci. In a deletion strain, expression of *mga*, the gene encoding the multiple virulence gene regulator, was reduced. Accordingly, transcript and proteome analyses revealed decreased expression of several Mga-activated genes. Therefore, and because the sRNA was shown to interact with the 5' UTR of the *mga* transcript in a gel-shift assay, we designated it MarS for *mga*-activating regulatory sRNA. Down-regulation of important virulence factors, including the antiphagocytic M-protein, led to increased susceptibility of the deletion strain to phagocytosis and reduced adherence to human keratinocytes. In a mouse infection model, the *marS* deletion mutant showed reduced dissemination to the liver, kidney, and spleen. Additionally, deletion of *marS* led to increased tolerance towards oxidative stress. Our *in vitro* and *in vivo* results indicate a modulating effect of MarS on virulence gene expression and on the pathogenic potential of GAS.

Streptococcus pyogenes (group A *Streptococcus*, GAS) is a strictly human pathogen that is responsible for a variety of infections of distinct severity¹. While superficial infections of the upper respiratory tract and the skin can be treated effectively with antibiotics, invasive streptococcal diseases remain life-threatening. The development of invasive infections and immune sequelae involves at least one or more of the following parameters: insufficient treatment of a primary infection, persistence of streptococci in the host tissue, and the expression of specific virulence factor genes by the bacteria². Control of virulence gene expression by stand-alone transcription factors and two-component systems are known to play a role in virulence determination in GAS³. An additional level of bacterial gene expression control is provided by small regulatory RNAs (sRNAs)⁴. Bacterial sRNAs can serve as negative regulators by inhibiting translation or by decreasing mRNA stability and can also function as positive regulators by stabilizing mRNA transcripts or initiating the translation of mRNAs^{5,6}. Although several global sRNA screens have recently been performed in streptococci, the RNA-dependent regulatory network in GAS is not yet well understood⁷.

Several *trans*-acting sRNAs, targeting mRNA sequences by direct base pairing, have been discovered in GAS. The pleiotropic effect locus (Pel) was described to have an effect on virulence and to influence the production of several virulence factors, including the M-protein, the cysteine protease SpeB, fibronectin-binding protein, and streptokinase⁸. The untranslated mRNA of *pel*, which also contains the gene for the streptolysin S peptide (*sagA*), was shown to be an effector of virulence factor expression in GAS⁹. However, in the GAS MIT1 lineage, no regulatory function of PEL could be observed^{10,11}.

The sRNA gene *rivX* is located downstream of the transcriptional regulator gene *rivR*. While RivR was shown to affect transcriptional activation by Mga, possibly by interacting with Mga protein, RivX was hypothesized to act through a separate but as yet unknown pathway to increase the expression of multiple genes that are regulated directly or indirectly by Mga¹². In a conflicting report, RivR was shown to be a negative regulator of capsule

¹Institute of Medical Microbiology, Virology and Hygiene, University Medicine Rostock, Rostock, Germany. ²Core Facility Proteome Analysis, University Medicine Rostock, Rostock, Germany. ³Institute for Medical Microbiology, Justus-Liebig University of Giessen, Giessen, Germany. ⁴Institute for Medical Microbiology, Justus-Liebig University of Giessen, Giessen, Germany. ⁵Present address: Franziska Huschka, Institute for Medical Microbiology, Virology and Hygiene, University Medical Center Hamburg-Eppendorf, Hamburg, Germany. Correspondence and requests for materials should be addressed to N.P. (email: nadja.patenge@med.uni-rostock.de)

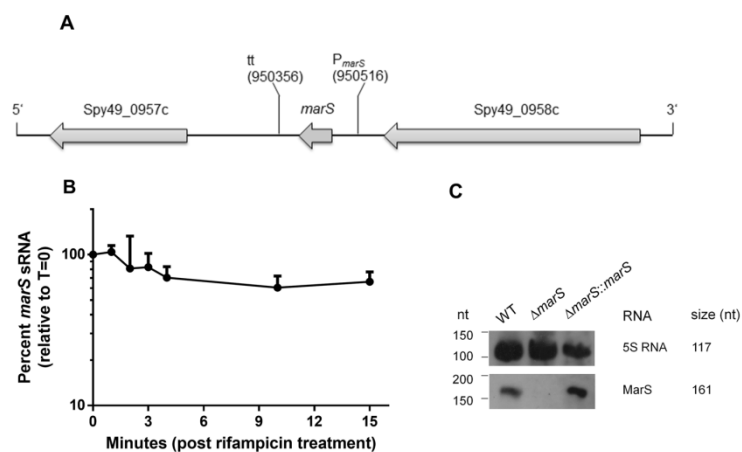


Figure 1. Genomic localization and transcript stability of *marS*. (A) Schematic diagram of the genomic locus of *marS*. Genes are represented by arrows pointing in the direction of transcription. P: first nucleotide of *marS*, tt: last nucleotide of *marS*. (B) Stability of MarS in GAS M49 591, determined by RT-qPCR following treatment of the culture with rifampicin. The data are presented as the percent *marS* transcript levels relative to time-point zero. The mean value of three experiments \pm standard deviation is shown. (C) Northern blot analyses of *marS* expression during growth in THY medium (OD₆₀₀ of 0.8). The probes were specific for the RNAs indicated on the right of each blot. For comparison, the approximate sizes of the RNA, as determined by 5' RACE analysis, are indicated on the far right. The full-length blot is presented in Supplementary Figure 3.

production in GAS while no regulatory function could be assigned to RivX. No influence of the *rivX* locus on the expression of *mga* or *mga*-associated genes was detected in this study¹³.

Until now, the only extensively characterized and functionally validated sRNA in GAS was FasX. FasX acts as positive regulator of the *fasBCA* operon, coding for the fibronectin/fibrinogen binding/haemolytic activity/streptokinase regulator¹⁴. FasX was shown to positively affect streptokinase production by stabilizing *sku* mRNA¹⁵. FasX also acts as a negative regulator of pilus expression by destabilizing the pilus operon mRNA and inhibiting the translation of the *cpa* transcript, which encodes a minor pilus protein¹⁶. By binding to and inhibiting the translation of different mRNAs of the fibronectin, collagen, T-antigen (FCT) region, control over the pilus gene region by FasX varies in a serotype-specific fashion¹⁷. In a subsequent report, FasX was shown to negatively control the production of two fibronectin-binding proteins, PrtF1 and PrtF2, encoded by the FCT region¹⁸.

In this study, we phenotypically characterize the GAS wild-type strain 591 (referred to as GAS M49 591 throughout the text) lacking the *mga*-activating regulatory sRNA (MarS). Employing transcript analyses, proteomics, and a mouse infection model, we show that MarS modulates Mga-dependent virulence factor gene expression, affects capsule production, and influences the fate of GAS in the host. We also show a direct interaction of MarS with the 5' UTR of the *mga* transcript using an electrophoretic mobility shift assay (EMSA).

Results

Deletion of *marS* in GAS 591. Genome-wide screening of the GAS wild-type strain 591 (referred to as GAS M49 591 throughout the text) resulted in an extensive list of candidate sRNA genes¹⁹. To identify sRNAs that were potentially involved in pathogenicity of GAS, we focused on sRNA genes that were differentially expressed in different media or throughout growth. Among those, *marS* (formerly designated sRNASpy490957c) is conserved throughout lactic acid bacteria, and a *cis*-regulatory function was predicted by a comparative genomics-based study using CMfinder²⁰. However, the sRNA is transcribed independently from adjacent genes in several GAS serotypes^{10,19,21}. Furthermore, in *Streptococcus mutans* and *S. pyogenes*, the presence of a terminator sequence and a strong promoter downstream of *marS* indicates that transcription is terminated prior to the downstream gene, *Spy49_0957c*, which is transcribed from an independent promoter^{19,22}. A schematic representation of the genomic locus is presented in Fig. 1A. The sRNA gene does not encode a peptide. However, on the antisense sequence of the *marS* gene, a 108-bp ORF is located, which could lead to the expression of a 35 AA peptide for which no homologues were found by BLAST²³ analysis. The stability of the *marS* transcript, MarS, was determined following rifampicin treatment by RT-qPCR. Transcript stability was high in GAS M49 591 (Fig. 1B), consistent with prior findings obtained in the GAS MIT1 strain MGAS2221¹⁰. To study the role of MarS, an isogenic deletion strain was constructed and designated Δ *marS*. Complementation of the gene deletion was achieved by ectopic expression of the sRNA gene from a shuttle vector under the control of its own promoter (Δ *marS*::*marS*). This strategy helps exclude an influence of spurious mutations introduced during mutagenesis and was recently suggested by Cho²⁴. Furthermore, whole genome sequencing was performed to rule out the

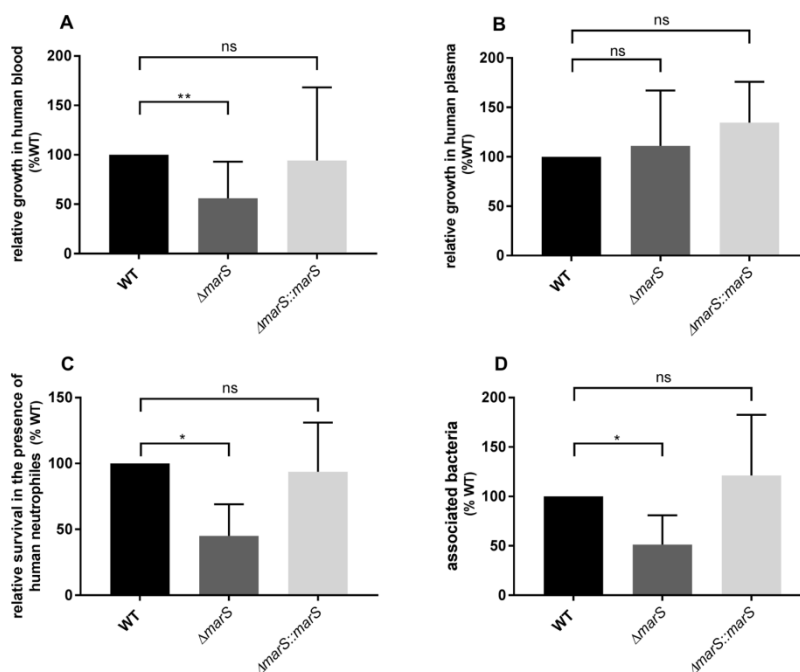


Figure 2. Deletion of *marS* leads to a decreased survival of GAS M49 591 in human blood and greater susceptibility to phagocytosis. (A) Relative growth of $\Delta marS$ (dark grey) and $\Delta marS::marS$ (light grey) in comparison to WT (black) in human blood, $n = 12$, and (B) in human plasma, $n = 4$. (C) Relative survival of $\Delta marS$ (dark grey) and $\Delta marS::marS$ (light grey) in comparison to WT (black) after incubation for 30 min with human neutrophils, $n = 5$. (D) Relative abundance of associated $\Delta marS$ (dark grey) and $\Delta marS::marS$ (light grey) bacteria in comparison to WT (black) after incubation with neutrophils $n = 5$. The Data are presented relative to WT (% WT, mean values \pm standard deviation). Statistical significance was determined using the Wilcoxon signed-rank test. Differences between samples were expressed as “ns = not significant” ($P \geq 0.05$), marginally significant ($P < 0.05$)*, and significant ($P < 0.01$)**.

occurrence of spontaneous mutations in the recombinant strains. Expression of *marS* in the respective strains was determined by Northern blot analyses of total RNA isolated from bacteria grown to the exponential phase (Fig. 1C). There was no detectable expression of *marS* in the deletion strain. By contrast, $\Delta marS::marS$ showed increased expression in comparison to the parental strain, likely due to a higher copy number of the expression vector. These results were verified by RT-qPCR. No PCR product was detected in the RNA sample from $\Delta marS$, whereas the transcript level in $\Delta marS::marS$ was increased 2-fold in comparison to WT. GAS M49 591 and the recombinant derivatives had similar growth characteristics in THY medium (WT: $\mu = 1.11 \pm 0.09$; $\Delta marS$: $\mu = 1.09 \pm 0.09$; $\Delta marS::marS$: $\mu = 0.89 \pm 0.12$). The differences between the strains were not significant (t-test). These data were generated from three independent experiments.

Lack of MarS results in decreased survival of GAS M49 591 in human blood. To investigate the role of MarS in a more pathogenically relevant environment, we assessed the ability of GAS M49 591 WT, the *marS* deletion mutant, and the *marS* complementation strain to grow *ex-vivo* in human blood. $\Delta marS$ showed decreased growth in human blood in comparison to WT (Fig. 2A, Fig. S1). In the complementation strain, growth was restored to the WT level. To distinguish whether cellular or non-cellular components of human blood were responsible for the reduced growth of $\Delta marS$, growth in human plasma was assessed. As shown in Fig. 2B and Fig. S2A, growth of $\Delta marS$ was not inhibited in human plasma. Consistently, the deletion of *marS* resulted in a higher susceptibility towards phagocytosis by human neutrophils (Fig. 2C, Fig. S2B). The number of extracellular bacteria was slightly reduced in the *marS* deletion strain relative to WT (Fig. 2D). Statistical analyses of non-normalized data showed that the decrease of associated bacteria was not significant (Fig. S2C).

MarS positively influences capsule production. The hyaluronic acid capsule of GAS supports evasion of the host immune system through molecular mimicry and confers resistance to phagocytosis^{25–27}. Since $\Delta marS$ showed decreased growth in human blood and a higher susceptibility towards human neutrophils, we tested

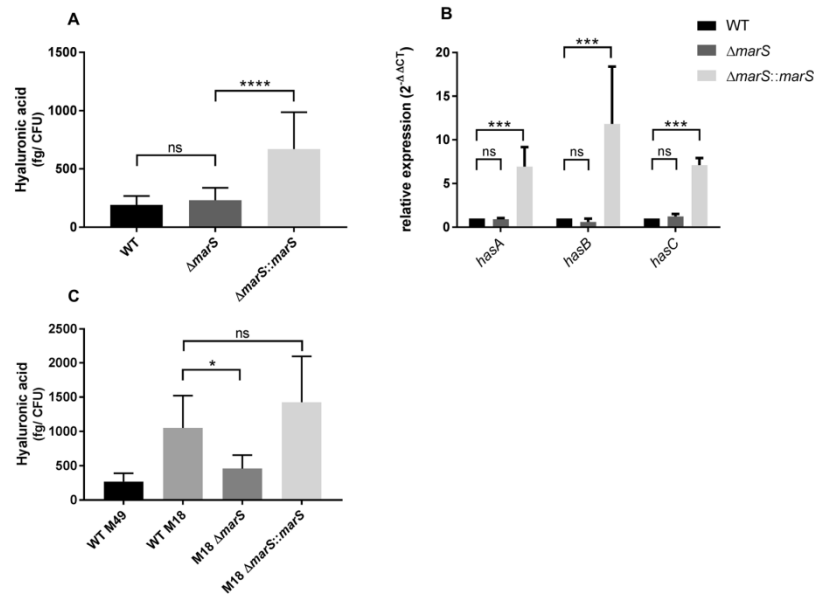


Figure 3. MarS positively influences capsule production by GAS. **(A)** Amount of capsule in $\Delta marS$ (dark grey) and $\Delta marS::marS$ (light grey) in comparison to WT (black), $n = 16$. **(B)** Relative expression of *hasABC*, encoding hyaluronic acid synthesis proteins, in GAS M49 591, $n = 8$. Statistical significance for **(B)** was determined using the two-way ANOVA, multiple comparisons. Differences between samples were expressed as “ns = not significant” ($P \geq 0.05$) and highly significant ($P < 0.0001$ ***). **(C)** Amount of capsule in GAS M49 591 (WT M49, black), GAS M18 MGAS8232 $\Delta marS$ (dark grey) and GAS M18 MGAS8232 $\Delta marS::marS$ (light grey) in comparison to GAS M18 MGAS8232 WT (WT M18, grey), $n = 5$. The data are presented as the mean values \pm standard deviation. Statistical significance for **(A)** and **(C)** was determined using the two-tailed Mann-Whitney U test. Differences between samples were expressed as “ns = not significant” ($P \geq 0.05$), marginally significant ($P < 0.05$)*, significant ($P < 0.01$ **), and highly significant ($P < 0.0001$ ***).

whether capsule production is impaired in this strain. No significant difference in hyaluronic acid abundance was detected between $\Delta marS$ and the parental strain (Fig. 3A). Interestingly, the complementation strain showed increased hyaluronic acid content in comparison to WT. This observation is in accordance with the higher *marS* transcript abundance in $\Delta marS::marS$ (Fig. 1C) and suggests a positive effect of MarS on capsule production. To analyse a potential influence of MarS on *hasABC* mRNA abundance, we measured *hasABC* transcript abundance by RT-qPCR (Fig. 3B). The gene products of the *hasABC* operon are responsible for hyaluronic acid synthesis in GAS^{28,29}. $\Delta marS$ showed no significant differences in *hasABC* transcript level in comparison to the parental strain, whereas the complementation strain showed a significantly increased abundance of the *hasABC* transcripts in comparison to both WT and $\Delta marS$. GAS M49 591 is characterized by a low endogenous level of capsule production²⁸. Thus, the effect of MarS on hyaluronic acid synthesis was investigated in MGAS8232 (serotype M18) (referred to as GAS M18 MGAS8232 throughout the text). The hyaluronic acid production of GAS M18 MGAS8232 was considerably higher than that of M49 (Fig. 3C). The GAS M18 MGAS8232 *marS* deletion strain showed a reduced capsule production in comparison to both the GAS M18 MGAS8232 WT and the complementation strain GAS M18 MGAS8232 $\Delta marS::marS$ (Fig. 3C). This result indicates a positive regulatory effect of MarS on capsule production in GAS.

MarS influences adherence to human keratinocytes. To test whether MarS influences adherence and invasion, bacteria were incubated with a human keratinocyte cell line (HaCaT). Deletion of *marS* led to a reduced ability to adhere to HaCaT cells, which was restored in the complementation strain (Fig. 4).

Putative target mRNAs of MarS include *mga* and *hasB*. One of the major mechanisms of sRNA-mediated regulation in bacteria is direct binding of the sRNA via base pairing to a target mRNA. Complex formation depends on complementary regions within the RNA sequences and on the respective secondary structures. The IntaRNA^{30,31} algorithm was employed to predict MarS-mRNA interactions in GAS M49 591. The sequence of *S. pyogenes* NZ131 (NC_011375.1) served as a reference genome. Among the 28 predicted targets, *mga*, the gene encoding the multiple virulence gene regulator, was identified with a high probability (Table 1).

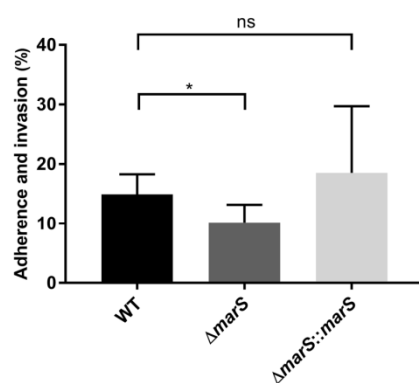


Figure 4. MarS influences adherence and internalization. Adherence to and internalization into human keratinocytes of *ΔmarS* (dark grey) and *ΔmarS::marS* (light grey) in comparison to WT (black), $n = 6$. The Data are presented as the mean values \pm standard deviation. Statistical significance was determined using the two-tailed Mann-Whitney U test. Differences between samples were expressed as “ns = not significant” ($P \geq 0.05$) and marginally significant ($P < 0.05$)*.

Rank	p-value	fdr value	Target	Locus_tag	Gene	Energy
1	0.0003	0.46126	Spy49_1814	SPY49_RS08930		-12.06
2	0.0007	0.55764	Spy49_0125	SPY49_RS00815		-11.40
3	0.0013	0.70451	Spy49_1673c	SPY49_RS08270	mga	-10.89
4	0.0036	0.81466	Spy49_0999	SPY49_RS04990		-9.96
5	0.0040	0.81466	Spy49_0695c	SPY49_RS03545	mvaS2	-9.87
6	0.0043	0.81466	Spy49_0036	SPY49_RS00340		-9.80
7	0.0054	0.81466	Spy49_1678c	SPY49_RS08295		-9.59
8	0.0055	0.81466	Spy49_1719c	SPY49_RS08470	csp	-9.57
9	0.0063	0.81466	Spy49_1426c	SPY49_RS07050	rpsR	-9.45
10	0.0064	0.81466	Spy49_1639c	SPY49_RS08100	nudC	-9.42
11	0.0068	0.81466	Spy49_0502c	SPY49_RS02625		-9.37
12	0.0069	0.81466	Spy49_0898	SPY49_RS04510	glyA	-9.35
13	0.0071	0.81466	Spy49_1173c	SPY49_RS05800	ftsZ	-9.33
14	0.0072	0.81466	Spy49_1714c	SPY49_RS08445		-9.31
15	0.0075	0.81466	Spy49_0207	SPY49_RS01190	rnpA	-9.28
16	0.0077	0.81466	Spy49_0169	SPY49_RS01025		-9.24
17	0.0099	0.8874	Spy49_1320c	SPY49_RS06540		-8.99
18	0.0103	0.8874	Spy49_1674c	SPY49_RS08275		-8.96
19	0.0104	0.8874	Spy49_1443c	SPY49_RS07135		-8.94
20	0.0111	0.8874	Spy49_1578c	SPY49_RS07805	salY	-8.88
21	0.0113	0.8874	Spy49_1806	SPY49_RS08895	hasB	-8.86
22	0.0119	0.8874	Spy49_1655	SPY49_RS08175		-8.80
23	0.0121	0.8874	Spy49_0144	SPY49_RS00905	nga	-8.79
24	0.0128	0.90121	Spy49_1533c	SPY49_RS07550		-8.73
25	0.0142	0.90121	Spy49_1480c	SPY49_RS07300		-8.62
26	0.0152	0.90121	Spy49_1159c	SPY49_RS05730		-8.55
27	0.0171	0.90121	Spy49_0916c	SPY49_RS04600		-8.43
28	0.0193	0.90121	Spy49_1700c	SPY49_RS08390		-8.29

Table 1. IntaRNA predictions.

The putative binding site lies within the 5' untranslated region (5' UTR) of *mga* (Fig. 5A) and is conserved in serotypes M2, M4, M18, M28, M44, M49, M53, M59, M66, M71, M82, M83, M87, M89, and M101 as determined by BLAST²³ analysis. *In silico* prediction also identified *hasB*, encoding the UDP-glucose 6-dehydrogenase, which

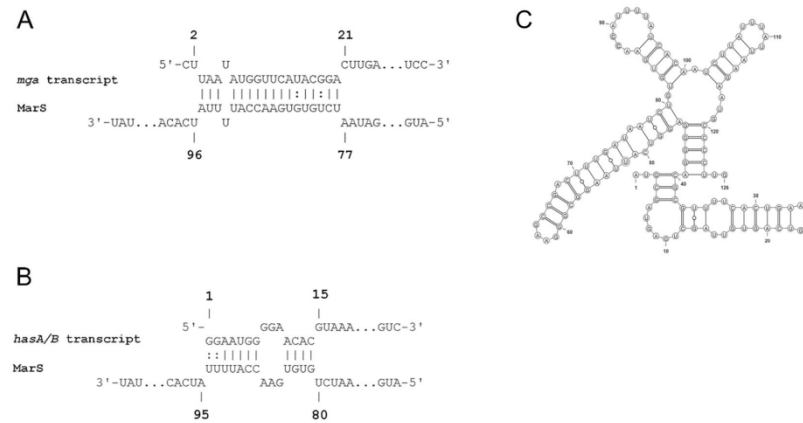


Figure 5. Putative interaction of MarS and its target transcripts. **(A)** Schematic of the putative binding of MarS to the *mga* transcript as predicted by IntaRNA. **(B)** Schematic of the putative binding of MarS to the *hasA/B*-transcript as predicted by IntaRNA. **(C)** Secondary structure predicted by RNAfold. Nucleotides 1–126 are depicted; the terminator stem loop is omitted for clarity.

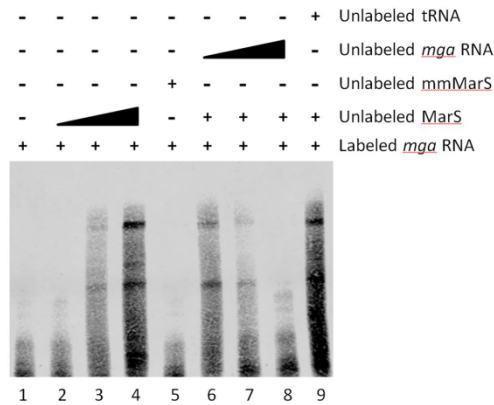


Figure 6. MarS binds to the 5' UTR of *mga*. RNA-RNA EMSA verifying base pairing between MarS and the 5' UTR of *mga*. A biotin-labeled *mga* 5' UTR RNA probe was incubated with wild-type MarS (lanes 2 to 4) or a MarS mutant (mmMarS), in which two bases situated in the putative binding site were exchanged (88-CC-89/88-GG-89) (lane 5). An unlabelled *mga* RNA probe was employed for cold competition (lanes 6–8), and unlabelled yeast tRNA was used as a specificity control (lane 9).

is part of the capsule synthesis operon in GAS (Table 1). The predicted binding site is located on the *hasABC* polycistronic transcript at the 3' end of the *hasA* coding region (Fig. 5B). For both targets, a common binding site is situated in MarS. The secondary structure of MarS was predicted by RNAfold (The ViennaRNA Web Services, <http://rna.tbi.univie.ac.at/>) and illustrated using VARNA GUI³² (Fig. 5C).

MarS binds to the 5' untranslated region of *mga*. To determine whether MarS binds directly to the 5' untranslated region of the *mga* mRNA, we performed RNA-RNA electrophoretic mobility shift assays (EMSAs). A biotin-labeled RNA corresponding to the 5' end of the *mga* RNA was incubated with increasing amounts of MarS, which resulted in a shift of the probe to a higher molecular weight complex (Fig. 6, lanes 2–4). To verify the role of the predicted mRNA binding site in MarS (Fig. 5C), we used a mutated form of MarS (mmMarS), in which two residues of the putative binding site were replaced (88-CC-89/88-GG-89). In reactions containing mmMarS,

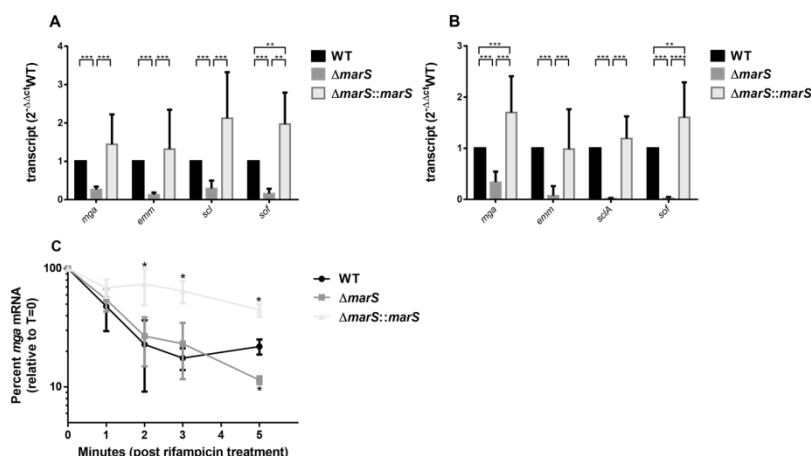


Figure 7. MarS influences *mga* and Mga-dependent transcript abundance. **(A)** Relative expression of *mga* and Mga-dependent transcripts in $\Delta marS$ (dark grey) and $\Delta marS::marS$ (light grey) in comparison to WT (black). Bacteria were grown in THY to the transitional growth phase, $n = 8$. **(B)** Relative expression of *mga* and Mga-dependent transcripts in $\Delta marS$ (dark grey) and $\Delta marS::marS$ (light grey) in comparison to WT (black). Bacteria were exposed to human blood for 1 h, $n = 8$. The data are presented in comparison to WT as the mean values \pm standard deviation. **(C)** Stability of *mga* transcript in $\Delta marS$ (dark grey) and $\Delta marS::marS$ (light grey) and WT (black) as determined by RT-qPCR following treatment of the culture with rifampicin; $n = 3$. Stability is presented as percent *mga* transcript level relative to time-point zero. The data are presented as the mean values \pm standard deviation. The Student's t-test was used to calculate statistical significance. Differences between samples are expressed as “not significant” ($P \geq 0.05$) and marginally significant ($P < 0.05$)*.

the *mga* RNA probe was not shifted (Fig. 6, lane 5). The specificity of the binding was confirmed by incubation with increasing concentrations of unlabeled *mga* RNA, which reduced the shifting (Fig. 6, lanes 6–8).

Deletion of *marS* results in lower *mga* and *mga*-controlled transcript levels. The influence of MarS on the transcript abundance of the putative target *mga* and virulence factor genes directly regulated by Mga³³ was investigated. Total RNA from GAS M49 591 and the recombinant derivatives either grown in THY (Fig. 7A) or following exposure to human blood (Fig. 7B) was analysed by RT-qPCR with primers specific for *mga*, *emm*, *scdA* (streptococcal collagen-like protein), and *sof* (serum opacity factor). In all cases tested, the abundance of the transcripts was significantly decreased in the deletion mutant compared to that in WT (Fig. 7A/B). In $\Delta marS::marS$, the phenotype could be restored. Together, these results indicate a positive regulatory influence of MarS on *mga* and thereby on the expression of genes regulated by Mga. To examine the impact of *mga* mRNA stability on this effect, the transcript abundance was determined following rifampicin treatment (Fig. 7C). The lack of MarS did not influence *mga* transcript stability within the first three min. In $\Delta marS::marS$, *mga* mRNA stability was slightly improved compared with that in WT and the deletion mutant. The half-life of the *mga* transcript as calculated by linear regression analyses was 0.57 min in WT, 1.15 min in $\Delta marS$, and 4.58 min in $\Delta marS::marS$. Thus, the effects on the Mga regulon in $\Delta marS$ were not caused by reduced *mga* mRNA stability in the *marS* deletion strain.

Down-regulation of MarS target gene transcription affects the proteome of GAS M49 591.

Given the differential expression of several Mga-controlled genes encoding surface proteins in $\Delta marS$, we set out to investigate the proteome of the *marS* deletion strain compared with WT and the complementation strain. Cytoplasm-depleted fractions were analysed by nano LC-mass spectrometry. The total number of proteins quantified by at least three and two peptides amounted to 885 and 1001, respectively, representing a high coverage of the proteome (Supplementary Data S1). Seventeen proteins were differentially regulated (a fold change above two) between the investigated strains (Table 2). For the majority of those, differential synthesis could be detected in the exponential (exp), transitional (tra), and stationary (stat) growth phases. Antiphagocytic M protein, fibronectin-binding protein, Fc-gamma receptor, and serum opacity factor, encoded by *emm49*, *sfbX49*, *Spy49_1672c*, and *sof*, respectively, were reduced in $\Delta marS$ samples compared with those in WT, whereas protein abundance was restored in the complementation strain (Table 2). Mga protein abundance was also reduced in the deletion strain in comparison to WT, but quantification was not meaningful in the cytosol-depleted samples that were used for the analyses. Mga contamination most likely resulted from an interaction with chromosomal DNA hampering complete removal from those samples. Thiol-activated cytolysin (*slo*) was reduced in $\Delta marS$ during exp and stat. In the complementation strain, the protein level was slightly increased in comparison to WT

Protein	Gene	Fold change (mean from three biological replicates)					
		WT/ $\Delta marS$			WT/ $\Delta marS::marS$		
		exp	tra	stat	exp	tra	stat
Protein abundance significantly reduced in $\Delta marS$							
Immunogenic secreted protein	<i>isp2</i>	3.1	2.4	5.3	2.0	1.3	1.7
Collagen-like surface protein A	<i>scfA</i>	n.d. ^a	6.6	16.2	n.d.	0.7	0.8
C5a peptidase	<i>scpA</i>	21.2 ^b	4.2	9.2	1.4 ^b	1.0	1.0
Antiphagocytic M protein	<i>emm49</i>	10.7	11.1	7.5 ^c	1.6	0.9	0.9
Fc-gamma receptor	Spy49_1672c	10.4	9.7	4.3	1.1	1.3	1.2
M protein trans-acting positive regulator	<i>mga</i>	117.2	62.5	45.2 ^c	2.2	1.2	1.1
Fibronectin-binding protein	<i>fbx49</i>	28.4	11.2	21.3	2.0	0.9	3.1
Serum opacity factor	<i>sof</i>	6.5 ^b	3.7	9.5	3.1	1.1	1.6
Putative secreted protein	Spy49_0015	1.6 ^b	2.6	1.3	1.5	2.0	0.8
Thiol-activated cytolysin	<i>slo</i>	3.1	1.1	3.2	1.1	0.4	0.6
Uncharacterized protein	Spy49_0343	n.d.	17.8 ^b	8.6 ^b	n.d.	1.0 ^b	0.6 ^b
Uncharacterized protein	Spy49_0412	n.d.	n.d.	8.7	n.d.	n.d.	0.8
Collagen-like surface protein B	<i>scfB</i>	4.7	5.4	5.3	1.1	1.0	0.9
Protein abundance significantly reduced in $\Delta marS$ and $\Delta marS::marS$							
Spi SpeB protease inhibitor	Spy49_1689c	n.d.	n.d.	2.3	n.d.	n.d.	6.9
Cysteine proteinase SpeB	<i>speB</i>	n.d.	2.4	5.2	n.d.	13.8	4.7
Protein abundance significantly increased in $\Delta marS::marS$							
Hyaluronan synthase	<i>hasA</i>	1.1	0.7	0.4	0.2	0.1	0.1
Putative UDP-glucose 6-dehydrogenase	<i>hasB</i>	1.2	1.5	1.2 ^b	0.1	0.3	0.5 ^b

Table 2. Differentially expressed proteins in the proteomes of GAS M49 591 WT, $\Delta marS$ and $\Delta marS::marS$. Detailed data are provided in Supplementary Data S1. ^an.d.: missing values for quantification due to growth phase-dependent low protein amounts. ^bMean from two biological replicates. ^cMean was calculated from two biological replicates due to an infinite fold change in the third biological experiment (protein was not detected in $\Delta marS$).

during tra and stat. Thus, down-regulation of the Mga-controlled gene transcription observed in $\Delta marS$ (Fig. 7A) resulted in a decreased synthesis of the corresponding gene products in the deletion mutant. Furthermore, the collagen-like surface proteins A and B and C5a peptidase were reduced in $\Delta marS$ samples in comparison to WT. The hyaluronic acid synthesis proteins HasA and HasB were increased in $\Delta marS::marS$, which is in accordance with the increased capsule production by this strain (Fig. 3A). Abundance of the cysteine proteinase SpeB was significantly reduced in both $\Delta marS$ and in $\Delta marS::marS$ in comparison to WT, indicating that these changes were not MarS-dependent. Taken together, of 13 proteins that were down-regulated in $\Delta marS$ compared with those in WT, 10 were known surface-associated or secreted molecules, and two were proteins of unknown function. Although the extracellular ratios of the secreted proteins may differ from the values measured in the cytoplasm-depleted fraction of the cell extracts, their general regulation should be reflected by the data. The protein abundance of the capsule synthesis proteins HasA and HasB was significantly increased in $\Delta marS::marS$ compared with those in WT.

Lack of MarS leads to a greater bacterial dissemination *in vivo*. To assess the influence of MarS on the virulence of GAS M49 591 *in vivo*, a mouse infection model was employed. Mice were infected i.p. with 8×10^7 colony forming units (CFUs) GAS M49 591 WT, $\Delta marS$, and $\Delta marS::marS$. All animals showed signs of severe bacterial infection and were sacrificed after 24 h. Bacteria were sampled from mouse liver, lung, kidney, and spleen for CFU determination. From the kidneys of infected mice, a significantly greater number of living $\Delta marS$ bacteria could be isolated compared with that in WT and the complementation strain (Fig. 8A). In the liver, significantly more $\Delta marS$ cells were detected than WT cells; in the spleen, the number of $\Delta marS::marS$ bacteria was significantly reduced in comparison to the parental and deletion strains (Fig. 8A). A slightly larger number of $\Delta marS$ was detected in the lungs of the infected mice compared with that of the other two strains, but the differences between the samples were not significant. Thus, in all organs tested, there was a greater number of viable bacteria in the deletion strain than in WT and the complementation strain.

Increased survival of $\Delta marS$ in the host kidney correlates to increased oxidative stress resistance. Reactive oxygen species (ROS)-related DNA damage was measured using a qPCR-based method³⁴. Therefore, total DNA from the kidney and spleen of infected mice, containing host DNA and bacterial DNA, and of PBS-treated controls, containing only host DNA, was isolated. DNA lesions were detected in the mitochondrial DNA (mtDNA) of the host and in the genomic DNA of bacteria using primers specific for the mitochondrial D-loop sequence and the bacterial *gyrA*, respectively. Infection with any of the three strains resulted in a high level of mtDNA damage in the kidney (≥ 30 lesions per 10 kb) (Fig. 8B). The differences between the mtDNA damage of the samples collected following infection with the different strains were not significant. In the spleen,

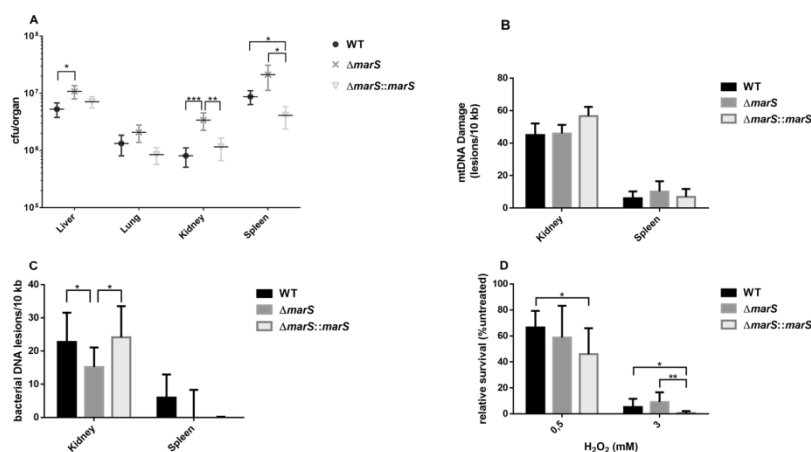


Figure 8. Deletion of *marS* leads to greater dissemination of GAS M49 591 in mice. **(A)** CFUs of $\Delta marS$ (dark grey) and $\Delta marS::marS$ (light grey) in comparison to WT (black) isolated from different organs 24 h after infection of BALB/c mice, $n = 15$ mice/group. **(B)** mtDNA damage of kidney and spleen tissue from infected mice, $n = 3$. **(C)** Bacterial DNA damage detected in kidney and spleen samples from infected mice, $n = 6$. **(D)** Survival of $\Delta marS$ (dark grey) and $\Delta marS::marS$ (light grey) and WT (black) following treatment with H_2O_2 as indicated; $n = 8$. The data are presented as the mean values \pm standard deviation. Statistical significance for was determined using the two-tailed Mann-Whitney U test. Differences between samples were expressed as “ns = not significant” ($P \geq 0.05$), marginally significant ($P < 0.05$)*, significant ($P < 0.01$)**, and highly significant ($P < 0.0001$)***.

which showed a higher bacterial load in this experiment (Fig. 8A), mtDNA damage was less severe than in the kidney (Fig. 8B). Again, no strain-specific differences in mtDNA damage could be detected. Corresponding to the mtDNA data, bacterial DNA isolated from the kidney showed a high level of damage. Bacterial DNA damage was significantly reduced in $\Delta marS$ in comparison to the parental and the complementation strains (Fig. 8C). In contrast, the overall bacterial DNA damage in samples isolated from the spleen was low. DNA from WT cells showed approximately 5 lesions/10 kb, but the difference in comparison to untreated bacteria was not significant (Fig. 8C). Survival of the different strains under conditions of oxidative stress was tested *in vitro* using H_2O_2 as a stressor. Under high oxidative stress conditions (3 mM H_2O_2), the *marS* deletion strain showed significantly increased survival compared with that of the complementation strain (Fig. 8D). These data correspond to the situation in the kidneys of infected mice (Fig. 8A,B and C). Taken together, high oxidative stress in the host kidney correlated with a lower bacterial load. Under these conditions, bacterial DNA damage was reduced in $\Delta marS$ compared with that in WT and survival of the deletion mutant was facilitated.

Discussion

In this study, we provide data regarding the role of the sRNA MarS in GAS M49 591 in the expression of virulence genes. GAS adheres to human tissue during colonization. Additionally, internalization by host cells has been discussed as a cause of recurrent disease, bacterial persistence in the host, and therapeutic failure of penicillin treatment^{35–38}. Deletion of *marS* in GAS M49 591 resulted in a reduced adherence to human keratinocytes and a greater susceptibility to phagocytosis. The M protein supports evasion of phagocytosis^{25,26,39,40} and is involved in adherence and internalization processes^{37,41,42}. Expression of *emm*, which encodes the antiphagocytic M protein, was dramatically reduced in $\Delta marS$, explaining the phagocytosis and the adherence phenotype of the deletion strain. Activation of *emm* expression is controlled by Mga. The *mga* mRNA, which was one of the MarS targets predicted by IntaRNA was also decreased in the deletion strain. In the case of a direct interaction of MarS with the predicted binding site located at the 5'-end of the *mga* transcript, translation may be diminished in the deletion strain. In turn, decreased protein levels of Mga would lead to hampered stimulation of *mga* transcription by Mga. The expression of *mga* is positively autoregulated⁴³. A small amount of *mga* transcript in $\Delta marS$ is consistent with the down-regulation of several genes that are known to belong to the Mga regulon³³, including *sclA* and *sof*. A low abundance of the collagen-like surface proteins A and B, and C5a peptidase was observed in the proteome of $\Delta marS$. Expression of the corresponding genes *sclA*, *sclB*, and *scpA* is known to be transcriptionally controlled by Mga^{44–46}. We conclude that an influence of MarS on *mga* expression leads to down-regulation of *mga* in the deletion strain and, consequently, a down-regulation of Mga-activated genes. Direct binding of MarS to the predicted *mga* mRNA binding site was supported by EMSAs. The *marS* gene is conserved throughout GAS, and the binding site in the 5' UTR of *mga* is conserved in several GAS *emm* types as determined by BLAST²³ analysis. Amongst others, these include *emm18*, *emm28*, *emm59*, and *emm83*, which are responsible for diseases as

diverse as acute rheumatic fever, puerperal sepsis, severe invasive disease, and skin tissue infections^{47–50}. Binding of sRNAs to their target mRNAs is a typical characteristic of trans-acting sRNAs in many bacteria. Recently, direct sRNA-mRNA binding has also been observed in GAS. The interaction of FasX with its targets mRNAs *prtF1* and *prtF2* and *cpa* could be observed *in vitro* by gel shift assays^{17,18}. FasX mediated regulation of pilus genes occurred in a serotype-specific manner¹⁶. Accordingly, target prediction in different GAS genomes in combination with *in vitro* binding studies might lead to the discovery of an *emm*-type specific target spectrum of MarS.

Depending on the GAS serotype, the infection model used, and the nature of the mutation, virulence of surface protein-deficient GAS strains in mice is affected differently. In a recent study, a commonly occurring single-nucleotide polymorphism (SNP) in GAS M59 increased expression of *mga* and 54 other genes, leading to significantly larger skin lesions in mice⁵¹. Decreased Mga activity or inactivation of *mga* or *emm*, respectively, led to attenuated virulence of GAS in mouse models for skin infection^{52–54}. While fibronectin binding promoted bacterial adherence, dissemination to the spleen of infected mice was less efficient in GAS expressing fibronectin-binding protein F1 in comparison to bacteria lacking this protein⁵⁵. Disruption of pilus assembly by sortase deletion rendered the GAS serotype M49 significantly more aggressive in a dermonecrotic mouse infection model⁵⁶. Taken together, the down-regulation of surface-bound virulence factors leads to hampered adherence. Under these circumstances, in systemic infection models, bacterial dissemination is promoted. In our model, deletion of *marS* led to down-regulation of several surface proteins, including the M protein and the fibronectin-binding proteins SfbX49 and Sof. Consequently, the ability to adhere to keratinocytes was diminished, while dissemination in a sepsis mouse model was increased.

One prerequisite for successful infection is the ability of the pathogen to withstand the oxidative stress conditions generated by the host at the site of infection. GAS employs a variety of resistance mechanisms towards ROS, including physical barriers, enzymatic reactions, and metal homeostasis⁵⁷. Bacterial DNA damage in $\Delta marS$ was decreased compared with that in WT under high oxidative stress conditions in the kidney, indicating that MarS influences the expression of genes involved in the oxidative stress response; however, the regulatory target remains unknown. In this context, a lack of MarS was advantageous for GAS M49 591-survival in the host.

In the proteomes of $\Delta marS$ and $\Delta marS::marS$, the abundance of the cysteine proteinase SpeB was significantly reduced compared with that in WT. SpeB production is regulated by the CovR/S two-component system and plays a specific role in invasive disease. Comparative genomics and transcriptomics revealed that invasive GAS M1 strains exhibit a SpeB switch caused by CovR/S mutations, leading to the increased expression of several virulence factor genes, including *ska*, *slo*, *sdal*, *sic*, and *scpA*, and to decreased SpeB abundance^{58,59}. SpeB production is also stimulated by Mga in GAS M49 591, but there is no direct binding of the *speB* promoter by Mga¹⁶. The down-regulation of SpeB in $\Delta marS$ could be caused by decreased levels of Mga in this strain. However, the phenotype was not complemented by ectopic *marS* expression from a plasmid, indicating a more complex situation.

One of the putative targets identified by the IntaRNA algorithm was *hasB*, encoding the UDP-glucose 6-dehydrogenase, which is part of the capsule synthesis operon in GAS. There were no significant differences in hyaluronic acid content between WT and $\Delta marS$, whereas $\Delta marS::marS$ produced significantly more capsule in comparison to the WT strain. Although the hyaluronic acid capsule is known to impact resilience to neutrophils^{25,26}, differential capsule production was not observed in the deletion mutant and did not lead to decreased survival in the phagocytosis assay. The capsule is also known to influence the adherence of GAS to human keratinocytes^{42,60}. In our model, $\Delta marS$ could not bind as efficiently as WT to HaCaT cells. $\Delta marS::marS$ was able to restore the WT phenotype, but the high hyaluronic acid content of the strain did not lead to significantly increased adherence. Therefore, hyaluronic acid does not seem to play a major role as an adhesin in this serotype. GAS M49 591 naturally produces small amounts of hyaluronic acid in comparison to other serotypes. Consequently, we observed a more pronounced regulatory effect of MarS on capsule production in GAS M18 MGAS8232.

Together, MarS modulates the expression of virulence factor genes belonging to the Mga regulon and influences hyaluronic acid production in GAS, thereby promoting virulence. While FasX is a negative regulator of pili and the fibronectin-binding proteins PrtF1 and PrtF2, it upregulates the expression of streptokinase, thereby functioning as a switch from colonization to dissemination^{17,18}. In contrast, MarS promotes adhesion by enhancing the expression of several extracellular matrix-binding surface proteins and stimulating capsule production while suppressing bacterial dissemination. We propose that MarS is involved in GAS colonization during the early stages of infection.

Methods

Bacterial strains and culture conditions. The GAS serotype M49 strain 591 was kindly provided by R. Lütticken (Aachen, Germany). The GAS serotype M18 strain MGAS8232 was obtained from the Centre of Epidemiology and Microbiology, National Institute of Public Health, Prague, Czech Republic. All GAS strains were cultured in chemically defined medium (CDM)⁶¹ or Todd-Hewitt broth (Thermo Fisher Scientific, Darmstadt, Germany) supplemented with 0.5% yeast extract (Thermo Fisher Scientific, Darmstadt, Germany) (THY), as indicated, at 37 °C with a 5% CO₂/20% O₂ atmosphere. *Escherichia coli* strain DH5 α (Gibco BRL, Eggenstein, Germany) was used as a host for the construction, proliferation, and storage of recombinant plasmids. All *E. coli* strains were cultured in Lennox L Broth Base (Thermo Fisher Scientific, Darmstadt, Germany). For selection, antibiotics were added at the appropriate concentrations.

Construction of recombinant GAS strains. For the construction of an isogenic *marS* deletion mutant of GAS M49 591 ($\Delta marS$) and GAS M18 MGAS8232 (GAS M18 MGAS8232 $\Delta marS$), *marS* was exchanged for a spectinomycin resistance cassette by homologous recombination⁶². To supply sequence to mediate homologous recombination, an upstream 800 bp flanking region 1 fragment and a downstream 931 bp flanking region 2 fragment were amplified by PCR using chromosomal DNA from the parental strain as a template. All primers

used for the generation of the respective fragments are listed in Supplementary Table S1. PCR products were sequentially cloned into the MCS of pUC18Erm1⁶³. Between the flanking regions, a spectinomycin resistance cassette from pFW5⁶² was cloned into the BamHI site. The resulting suicide plasmid was verified by classical Sanger sequencing (GATC Biotech AG, Konstanz, Germany) and was used to transform GAS strains M49 591 or M18 MGAS8232. Deletion of *marS* was confirmed by sequencing. Therefore, a PCR product of the genomic region was analysed by classical Sanger sequencing (GATC Biotech AG, Konstanz, Germany). Loss of MarS was determined by RT-qPCR. For construction of a complementation strain ($\Delta marS::marS$), a fragment including the endogenous promoter and terminator regions was amplified by PCR and cloned into the Sall/BamHI sites of the shuttle vector pAT19⁶⁴. The resulting vector was verified by sequencing and used for transformation of $\Delta marS$. The absence of spurious mutations in the recombinant strains was confirmed by MiSeq whole genome sequencing. The corresponding data were submitted to the European Nucleotide Archive (ENA/SRA) (Accession number: PRJEB18537).

Assays to assess the ability of the bacteria to survive in blood and plasma. The ability of the bacteria to survive in blood (short: blood survival assay) was assessed as described by Nakata *et al.*⁵⁶. Briefly, overnight cultures of the GAS parental strain and isogenic mutants were inoculated into fresh medium and grown to the exponential growth phase. The cultures were centrifuged, washed and suspended in phosphate-buffered saline (PBS). Next, 20 μ l of each respective cell suspension was used to inoculate 480 μ l heparinized human blood. Blood was obtained from at least three individual volunteers. The samples were incubated for 3 h at 37 °C under rotation. CFUs of the samples were determined following serial dilution and plating on THY agar plates and compared to the CFUs of the respective inoculate. The resulting multiplication factor (MF) was used to compare strains. The data were normalized by setting the MF of the WT to 100%. The ability of the bacteria to survive in plasma (short: plasma survival assay) was assessed accordingly using human plasma as the medium.

Quantitative phagocytosis assay. Human neutrophils were isolated from human blood using PolymorphPrepTM (PROGEN Biotechnik GmbH, Heidelberg) according to the instructions of the manufacturer. The neutrophils were suspended in RPMI 1640 (Invitrogen, Thermo Fisher Scientific, Darmstadt, Germany). Bacteria were grown overnight and washed with PBS. For opsonization 10⁷ CFU/ml were incubated for 20 min with 10% human serum at room temperature. The opsonized bacteria were incubated with 10⁷ human neutrophils/ml (1:1) and 5% serum for another 30 min at 37 °C. As a reference, a sample of the opsonized bacteria was incubated without neutrophils. To determine the survival rate, the samples were centrifuged and the pellets lysed in sterile distilled water. The counts of viable GAS were determined following serial dilution and plating on THY agar. To determine the proportion of extracellular bacteria, the samples were centrifuged for 5 min at 100 g for separation. The supernatant was collected, centrifuged at 13,000 g, and the bacterial pellet was dissolved in PBS.

Quantification of hyaluronic acid. The amount of cell-associated hyaluronic acid produced by GAS was determined by the release of capsule from cells in the exponential growth phase and subsequent measurement of the hyaluronic acid content using Stains-All (Sigma) as described previously³⁷. The absorbance at 640 nm was compared to a standard curve prepared with known concentrations of hyaluronic acid. The amount of hyaluronic acid in the samples was calculated in fg/CFU. The data are expressed relative to the content of hyaluronic acid in the respective WT strain.

Adherence and internalization assay. Bacterial adherence to and internalization into the human keratinocyte cell line HaCaT (DKFZ, Heidelberg, Germany) was quantified employing an infection assay⁶⁵. In brief, 24-well-plates were inoculated with 2.5×10^5 HaCaT cells per well in DMEM (Invitrogen, Thermo Fisher Scientific, Darmstadt, Germany) without antibiotics. Growth was allowed until confluence. Keratinocytes were washed with DMEM and infected separately with GAS strains of interest in DMEM at a multiplicity of infection (MOI) of 1:10. After 2 h incubation at 37 °C in a 5% CO₂ atmosphere, the keratinocytes were washed extensively with PBS. To detach the keratinocytes, trypsin/EDTA (Invitrogen, Thermo Fisher Scientific, Darmstadt, Germany) was added and the keratinocytes were lysed in sterile distilled water. CFU from GAS attached to and internalized into HaCaT keratinocytes were determined following serial dilution in PBS and plating on THY agar.

Electrophoretic mobility shift assay (EMSA). RNA:RNA EMSAs were performed as described by Danger *et al.*¹⁸. Briefly, RNA for RNA:RNA gel shift assays was prepared by *in vitro* transcription of the T7 promoter sequence containing PCR products using T7 polymerase. All primers used for the generation of the respective fragments are listed in Supplementary Table S1. Chromosomal DNA of GAS M49 591 served as the template for the *mga* 5' region and the *marS* fragments and pAT19_ *marS* 88-CC-89/88-GG-89 served as the template for the mismatch *marS* fragment. *In vitro* transcription reactions were performed using the MEGAscript kit (Thermo Fisher Scientific, Darmstadt, Germany) according to the instructions of the manufacturer. Template DNA was removed using TURBO DNase (Thermo Fisher Scientific, Darmstadt, Germany). The RNA was purified using the RNA Clean and Concentrator-25 kit (Zymo Research Europe, Freiburg, Germany). For probe labelling, *mga* mRNA was biotin-labelled using the Pierce RNA 3' end biotinylation kit (Thermo Fisher Scientific, Darmstadt, Germany). Probes were purified using the RNA Clean & Concentrator-5 kit (Zymo Research Europe, Freiburg, Germany). All RNAs were quantified using the Qubit 3.0 Fluorometer (Thermo Fisher Scientific, Darmstadt, Germany) and their quality was evaluated using the Agilent Bioanalyzer 2100 system. Labelled *mga* RNA (12 nM) was incubated in the presence or absence of MarS RNA (0, 10, 100, 1000 nM), mmmarS (1000 nM), unlabelled *mga* RNA (10, 100, 1000 nM) or unlabelled yeast tRNA (1000 nM). EMSA reactions (10 μ l) contained 1 μ l tRNA (10 μ g/ μ l stock) and 1 μ l of structure buffer (10 x stock; provided with the Lightshift RNA EMSA kit, Thermo Fisher Scientific, Darmstadt, Germany). Reactions were heated to 56 °C for 5 min before cooling to 37 °C for 30 min to allow refolding. REMSA loading buffer (Lightshift RNA EMSA kit, Thermo Fisher Scientific,

Darmstadt, Germany) was added to each sample. The samples were separated on a 5% TBE mini-gel in $0.5 \times$ TBE buffer, transferred by semi-dry blotting to a positively charged nylon membrane, and UV-crosslinked. The membrane was then blocked for one hour at RT (Odyssey Blocking Buffer, Li-Cor, diluted 1:3 in PBS), incubated with Streptavidin IRDye (Li-COR) at room temperature for 20 min in the dark, washed 3 x (PBST, 1% SDS), and the labeled RNA was detected using a Li-Cor Odyssey system. The membranes were rinsed and stored in PBS.

Transcript stability determination. GAS strains were grown to the transitional growth phase in THY (OD_{600} of 0.8) before the addition of rifampicin (to 1 mg/ml) to inhibit RNA synthesis. Following the addition of rifampicin, 10 ml samples were recovered after 0, 1, 2, 3, 5, 10, and 15 min, as indicated. Samples were pelleted by centrifugation and quickly frozen in liquid nitrogen. Total RNA was extracted as described below.

Reverse transcription followed by quantitative PCR (RT-qPCR). GAS strains were grown to the transitional growth phase in THY (OD_{600} of 0.8). Bacterial cells were either pelleted immediately and quickly frozen in liquid nitrogen or exposed to human blood for one hour prior to sample preparation. Total RNA from GAS strains was extracted according to the protocol supplied with the Direct-zol™ RNA MiniPrep Kit (Zymo Research, Irvine). After extraction, RNA was treated with acid phenol:chloroform:isoamyl alcohol (125:24:1), pH 4.5 (Thermo Fisher Scientific, Darmstadt, Germany), and TURBO™ DNase (Thermo Fisher Scientific, Darmstadt, Germany) according to the manufacturer's instructions. cDNA synthesis was performed using the Superscript first-strand synthesis system for RT-PCR (Invitrogen, Thermo Fisher Scientific, Darmstadt, Germany). Quantitative PCR amplification was performed with SYBR green (Thermo Fisher Scientific, Darmstadt, Germany) using the ViiA™ 7 Real-Time PCR System (Applied Biosystems, Darmstadt, Germany). The 5S rRNA gene and the DNA gyrase subunit A gene (*gyrA*) served as housekeeping genes. Relative expression was calculated employing the $2^{-\Delta\Delta Ct}$ method⁴⁶. All primers used for RT-qPCR are listed in Supplementary Table S1.

Northern blot analyses. Total RNA was isolated from GAS strains grown to the transitional growth phase in THY (OD_{600} of 0.8) as described above. RNA samples (10 µg) were loaded onto an 8% TBE-Urea polyacrylamide gel and separated by electrophoresis. Size standards (Ultra Low Range Ladder, Fermentas) were loaded on the same gel. RNA was electrophoretically transferred onto positively charged nylon membranes (Ambion) and UV cross-linked. Templates for the probes were generated by PCR with the same primers that were used for the PCR reaction in the RT-qPCR experiments. To the 5' end of the reverse primers was added the T7 promoter sequence (CTTAATACGACTCACTATAGGG) for *in vitro* transcription (MAXscript™ T7 Transcription Kit, Ambion). Probes were labelled with biotin prior to hybridization (Brightstar Psoralen-Biotin Labeling kit, Ambion). Membranes were hybridized overnight with a RNA probe complementary to MarS or 5S RNA, as indicated. A BrightStar BioDetect Kit (Ambion) was used for detection, and autoradiography films were exposed to the luminescent blots.

Extract preparation for proteome analyses. Bacteria were grown in THY and samples were collected at different time points during growth. Crude extracts were prepared in a precllys 24 homogenizer (peqLab Biotechnologie GmbH, Erlangen, Germany) and divided into cytoplasm-depleted and cytoplasmic fractions by centrifugation at 13000 g. Three biological replicates were performed.

Proteome analyses. Mass spectrometry was performed on a Synapt G2-S mass spectrometer coupled to a nanoAcquity UPLC system (Waters, Manchester, UK). Peptides of the tryptic digests were separated by reversed-phase UPLC and analysed in data-independent mode (HDMS²). Label-free protein quantification and expression analysis were performed using Progenesis Q1 for Proteomics (Nonlinear Dynamics, Newcastle upon Tyne, UK). A detailed description of the experimental procedures is provided as supporting information (Supplementary Methods S1).

Murine infection model. Naive, inbred, 8-week-old female BALB/c mice were purchased from Charles River Laboratories (Sulzfeld, Germany). Mice were inoculated intraperitoneally with 8×10^7 CFU of GAS strains, as indicated, in 0.2 ml PBS utilizing a BD Microlance 27 G 3/4" (Becton Dickinson GmbH, Heidelberg, Germany). Mock infection was performed with 0.2 ml PBS. As a vector control mice were infected with GAS M49 591 carrying pAT18/GFP. Twenty-four h post-infection, the mice were sacrificed using a ketamine/xylazine combination. Bacterial dissemination was investigated by determination of bacterial loads in different organs⁴⁷. All the experimental protocols were approved by a licensing committee as specified in the ethics statement.

Bacterial oxidative stress resistance. GAS strains were grown in THY to the early exponential growth phase. H_2O_2 (Roth, Karlsruhe, Germany) was added as indicated. Following incubation for 2 h at 37 °C, cells were transferred to ice, harvested, washed twice with PBS and plated on THY agar for CFU determination.

DNA damage detection. Total DNA from mouse tissues was isolated using the DNeasy Blood and Tissue Kit (Qiagen, Hilden, Germany) according to the manufacturer's instructions. DNA damage detection was performed as described elsewhere³⁴. In brief, DNA quantity and purity were determined by spectrophotometric analysis. DNA lesion rates were determined by sequence-specific qPCR of mouse mitochondrial DNA (mmtDNA) and bacterial DNA, respectively. Amplification of a long (mmtDNA: 618 bp, *gyrA*: 775 bp) and a short (mmtDNA: 87 bp, *gyrA*: 85 bp) fragment was performed relative to DNA isolated from untreated cells. The small amplicon served as an undamaged DNA reference and allowed for DNA concentration normalization. PCR was performed with SYBR green (Thermo Fisher Scientific, Darmstadt, Germany) using a Light Cycler® 480 Instrument (Roche Diagnostics, Mannheim, Germany). All primers used for qPCR are listed in Supplementary Table S1. DNA was isolated from at least four animals, and qPCR reactions were performed in triplicates.

Statistical Analyses. All experiments were performed at least three times or as indicated by the sample size (n). Statistical significance was determined for normalized data using the Wilcoxon signed-rank test. RNA stability tests were performed in three biological replicates; thus, the Student's t-test was used to calculate statistical significance. For all other experiments, the test used to determine statistical significance is indicated in the respective figure legend.

Ethics statement. The protocol for the collection of human blood for the blood survival assay was approved by the *Ethikkommission an der Medizinischen Fakultät der Universität Rostock* (ethics committee vote: A 2014-0131). The experiments were conducted in accordance with the ICH-GCP guidelines. Informed consent was obtained from all subjects. The protocol for the murine infection model was approved by the *Landesamt für Landwirtschaft, Lebensmittelsicherheit und Fischerei M-V* (Permit Number: 7221.3-1.1-090/12). Mice were sacrificed using a ketamine/xylazine combination. Animal experiments were performed in strict accordance with the German regulations of the Society for Laboratory Animal Science (GV-SOLAS) and the European Health Law of the Federation of Laboratory Animal Science Associations (FELASA).

Data availability. The whole genome sequencing datasets generated during the current study are available in the European Nucleotide Archive (ENA/SRA) repository (Accession number: PRJEB18537). The proteome data generated during this study are included in this published article (and its Supplementary Information files). All additional datasets generated during or analysed during the current study are available from the corresponding author upon reasonable request.

References

- Cunningham, M. W. Pathogenesis of group A streptococcal infections and their sequelae. *Adv. Exp. Med. Biol.* **609**, 29–42 (2008).
- Walker, M. J. *et al.* Disease manifestations and pathogenic mechanisms of group A Streptococcus. *Clin. Microbiol. Rev.* **27**(2), 264–301 (2014).
- Patenge, N., Fiedler, T. & Kreikemeyer, B. Common regulators of virulence in streptococci. *Curr. Top. Microbiol. Immunol.* **368**, 111–153 (2013).
- Storz, G., Vogel, J. & Wassarman, K. M. Regulation by small RNAs in bacteria: expanding frontiers. *Mol. Cell* **43**(6), 880–891 (2011).
- Podkaminski, D. & Vogel, J. Small RNAs promote mRNA stability to activate the synthesis of virulence factors. *Mol. Microbiol.* **78**(6), 1327–1331 (2010).
- Waters, L. S. & Storz, G. Regulatory RNAs in bacteria. *Cell* **136**(4), 615–628 (2009).
- Patenge, N., Pappesch, R., Khani, A. & Kreikemeyer, B. Genome-wide analyses of small non-coding RNAs in streptococci. *Front. Genet.* **6**, 189. <https://doi.org/10.3389/fgene.2015.00189> (2015).
- Li, Z., Sledjeski, D. D., Kreikemeyer, B., Podbielski, A. & Boyle, M. D. Identification of pel, a Streptococcus pyogenes locus that affects both surface and secreted proteins. *J. Bacteriol.* **181**(19), 6019–6027 (1999).
- Mangold, M. *et al.* Synthesis of group A streptococcal virulence factors is controlled by a regulatory RNA molecule. *Mol. Microbiol.* **53**(5), 1515–1527 (2004).
- Perez, N. *et al.* A genome-wide analysis of small regulatory RNAs in the human pathogen group A Streptococcus. *PLoS. One.* **4**(11), e7668. <https://doi.org/10.1371/journal.pone.0007668> (2009).
- Zhou, Y. *et al.* The sagA/pel locus does not regulate the expression of the M protein of the MIT1 lineage of group A Streptococcus. *Virulence.* **4**(8), 698–706 (2013).
- Roberts, S. A. & Scott, J. R. RivR and the small RNA RivX: the missing links between the CovR regulatory cascade and the Mga regulon. *Mol. Microbiol.* **66**(6), 1506–1522 (2007).
- Trevino, J., Liu, Z., Cao, T. N., Ramirez-Pena, E. & Sumbly, P. RivR is a negative regulator of virulence factor expression in group A Streptococcus. *Infect. Immun.* **81**(1), 364–372 (2013).
- Kreikemeyer, B., Boyle, M. D., Buttaro, B. A., Heinemann, M. & Podbielski, A. Group A streptococcal growth phase-associated virulence factor regulation by a novel operon (Fas) with homologies to two-component-type regulators requires a small RNA molecule. *Mol. Microbiol.* **39**(2), 392–406 (2001).
- Ramirez-Pena, E., Trevino, J., Liu, Z., Perez, N. & Sumbly, P. The group A Streptococcus small regulatory RNA FasX enhances streptokinase activity by increasing the stability of the ska mRNA transcript. *Mol. Microbiol.* **78**(6), 1332–1347 (2010).
- Liu, Z., Trevino, J., Ramirez-Pena, E. & Sumbly, P. The small regulatory RNA FasX controls pilus expression and adherence in the human bacterial pathogen group A Streptococcus. *Mol. Microbiol.* **86**(1), 140–154 (2012).
- Danger, J. L. *et al.* The small regulatory RNA FasX enhances group A Streptococcus virulence and inhibits pilus expression via serotype-specific targets. *Mol. Microbiol.* **96**(2), 249–262 (2015).
- Danger, J. L., Makthal, N., Kumaraswami, M. & Sumbly, P. The FasX Small Regulatory RNA Negatively Regulates the Expression of Two Fibronectin-Binding Proteins in Group A Streptococcus. *J. Bacteriol.* **197**(23), 3720–3730 (2015).
- Patenge, N. *et al.* Identification of novel growth phase- and media-dependent small non-coding RNAs in *Streptococcus pyogenes* M49 using intergenic tiling arrays. *BMC. Genomics* **13**(1), 550. <https://doi.org/10.1186/1471-2164-13-550> (2012).
- Weinberg, Z. *et al.* Comparative genomics reveals 104 candidate structured RNAs from bacteria, archaea, and their metagenomes. *Genome Biol.* **11**(3), R31. <https://doi.org/10.1186/gb-2010-11-3-r31> (2010).
- Tesorero, R. A. *et al.* Novel regulatory small RNAs in *Streptococcus pyogenes*. *PLoS. One.* **8**(6), e64021. <https://doi.org/10.1371/journal.pone.0064021> (2013).
- Cardineau, G. A. & Curtiss, R. III Nucleotide sequence of the *asd* gene of *Streptococcus* mutants. Identification of the promoter region and evidence for attenuator-like sequences preceding the structural gene. *J. Biol. Chem.* **262**(7), 3344–3353 (1987).
- Altschul, S. F., Gish, W., Miller, W., Myers, E. W. & Lipman, D. J. Basic local alignment search tool. *J. Mol. Biol.* **215**(3), 403–410 (1990).
- Cho, K. H., Wright, J., Svecionis, J. & Kim, J. H. The prince and the pauper: which one is real? The problem of secondary mutation during mutagenesis in *Streptococcus pyogenes*. *Virulence.* **4**(8), 664–665 (2013).
- Dale, J. B., Washburn, R. G., Marques, M. B. & Wessels, M. R. Hyaluronate capsule and surface M protein in resistance to opsonization of group A streptococci. *Infect. Immun.* **64**(5), 1495–1501 (1996).
- Foley, M. J. & Wood, W. B. Jr. Studies on the pathogenicity of group A streptococci. II. The antiphagocytic effects of the M protein and the capsular gel. *J. Exp. Med.* **110**, 617–628 (1959).
- Froude, J., Gibofsky, A., Buskirk, D. R., Khanna, A. & Zabriskie, J. B. Cross-reactivity between streptococcus and human tissue: a model of molecular mimicry and autoimmunity. *Curr. Top. Microbiol. Immunol.* **145**, 5–26 (1989).
- Crater, D. L. & Van, d. R. I. Hyaluronic acid synthesis operon (has) expression in group A streptococci. *J. Biol. Chem.* **270**(31), 18452–18458 (1995).

29. Dougherty, B. A. & Van, D. R. I. Molecular characterization of hasB from an operon required for hyaluronic acid synthesis in group A streptococci. Demonstration of UDP-glucose dehydrogenase activity. *J. Biol. Chem.* **268**(10), 7118–7124 (1993).
30. Busch, A., Richter, A. S. & Backofen, R. IntaRNA: efficient prediction of bacterial sRNA targets incorporating target site accessibility and seed regions. *Bioinformatics*. **24**(24), 2849–2856 (2008).
31. Wright, P. R. *et al.* CopraRNA and IntaRNA: predicting small RNA targets, networks and interaction domains. *Nucleic Acids Res.* **42**(Web Server issue), W119–W123 (2014).
32. Darty, K., Denise, A. & Ponty, Y. VARNA: Interactive drawing and editing of the RNA secondary structure. *Bioinformatics*. **25**(15), 1974–1975 (2009).
33. Hondorp, E. R. & McIver, K. S. The Mga virulence regulon: infection where the grass is greener. *Mol. Microbiol.* **66**(5), 1056–1065 (2007).
34. Rothfuss, O., Gasser, T. & Patenge, N. Analysis of differential DNA damage in the mitochondrial genome employing a semi-long run real-time PCR approach. *Nucleic Acids Res.* **38**(4), e24, <https://doi.org/10.1093/nar/gkp1082> (2010).
35. Ogawa, T. *et al.* Biofilm formation or internalization into epithelial cells enable *Streptococcus pyogenes* to evade antibiotic eradication in patients with pharyngitis. *Microb. Pathog.* **51**(1–2), 58–68 (2011).
36. Podbielski, A. & Kreikemeyer, B. Persistence of group A streptococci in eukaryotic cells—a safe place? *Lancet* **358**(9275), 3–4 (2001).
37. Schrage, H. M., Rheinwald, J. G. & Wessels, M. R. Hyaluronic acid capsule and the role of streptococcal entry into keratinocytes in invasive skin infection. *J. Clin. Invest* **98**(9), 1954–1958 (1996).
38. Sela, S., Neeman, R., Keller, N. & Barzilai, A. Relationship between asymptomatic carriage of *Streptococcus pyogenes* and the ability of the strains to adhere to and be internalised by cultured epithelial cells. *J. Med. Microbiol.* **49**(6), 499–502 (2000).
39. Horstmann, R. D., Sievertsen, H. J., Knobloch, J. & Fischetti, V. A. Antiphagocytic activity of streptococcal M protein: selective binding of complement control protein factor H. *Proc. Natl. Acad. Sci. USA* **85**(5), 1657–1661 (1988).
40. Staali, L., Morgelin, M., Björck, L. & Tapper, H. Streptococcus pyogenes expressing M and M-like surface proteins are phagocytosed but survive inside human neutrophils. *Cell Microbiol.* **5**(4), 253–265 (2003).
41. Courtney, H. S., Hasty, D. L. & Dale, J. B. Molecular mechanisms of adhesion, colonization, and invasion of group A streptococci. *Ann. Med.* **34**(2), 77–87 (2002).
42. Schrage, H. M., Alberti, S., Cywes, C., Dougherty, G. J. & Wessels, M. R. Hyaluronic acid capsule modulates M protein-mediated adherence and acts as a ligand for attachment of group A Streptococcus to CD44 on human keratinocytes. *J. Clin. Invest* **101**(8), 1708–1716 (1998).
43. McIver, K. S., Thurman, A. S. & Scott, J. R. Regulation of mga transcription in the group A streptococcus: specific binding of mga within its own promoter and evidence for a negative regulator. *J. Bacteriol.* **181**(17), 5373–5383 (1999).
44. Almengor, A. C. & McIver, K. S. Transcriptional activation of sclA by Mga requires a distal binding site in Streptococcus pyogenes. *J. Bacteriol.* **186**(23), 7847–7857 (2004).
45. Rasmussen, M. & Björck, L. Unique regulation of ScIB - a novel collagen-like surface protein of Streptococcus pyogenes. *Mol. Microbiol.* **40**(6), 1427–1438 (2001).
46. Ribardo, D. A. & McIver, K. S. Defining the Mga regulon: Comparative transcriptome analysis reveals both direct and indirect regulation by Mga in the group A streptococcus. *Mol. Microbiol.* **62**(2), 491–508 (2006).
47. Pittipaldi, N. *et al.* Full-genome dissection of an epidemic of severe invasive disease caused by a hypervirulent, recently emerged clone of group A Streptococcus. *Am. J. Pathol.* **180**(4), 1522–1534 (2012).
48. Green, N. M. *et al.* Genome sequence of a serotype M28 strain of group A streptococcus: potential new insights into puerperal sepsis and bacterial disease specificity. *J. Infect. Dis.* **192**(5), 760–770 (2005).
49. Smoot, J. C. *et al.* Genome sequence and comparative microarray analysis of serotype M18 group A Streptococcus strains associated with acute rheumatic fever outbreaks. *Proc. Natl. Acad. Sci. USA* **99**(7), 4668–4673 (2002).
50. Soriano, N. *et al.* Full-Length Genome Sequence of Type M/emm83 Group A Streptococcus pyogenes Strain STAB1101, Isolated from Clustered Cases in Brittany. *Genome Announc.* **3**(1), e01459–14, <https://doi.org/10.1128/genomeA.01459-14> (2015).
51. Sanson, M. *et al.* A naturally occurring single amino acid replacement in multiple gene regulator of group A Streptococcus significantly increases virulence. *Am. J. Pathol.* **185**(2), 462–471 (2015).
52. Luo, E., Lizano, S., Banik, S., Zhang, H. & Bessen, D. E. Role of Mga in group A streptococcal infection at the skin epithelium. *Microb. Pathog.* **45**(3), 217–224 (2008).
53. Boyle, M. D., Raeder, R., Flosdorff, A. & Podbielski, A. Role of emm and mrp genes in the virulence of group A streptococcal isolate 64/14 in a mouse model of skin infection. *J. Infect. Dis.* **177**(4), 991–997 (1998).
54. Hondorp, E. R. *et al.* PTS phosphorylation of Mga modulates regulon expression and virulence in the group A streptococcus. *Mol. Microbiol.* **88**(6), 1176–1193 (2013).
55. Nyberg, P. *et al.* Interactions with fibronectin attenuate the virulence of Streptococcus pyogenes. *EMBO J.* **23**(10), 2166–2174 (2004).
56. Nakata, M. *et al.* Mode of expression and functional characterization of FCT-3 pilus region-encoded proteins in Streptococcus pyogenes serotype M49. *Infect. Immun.* **77**(1), 32–44 (2009).
57. Henningham, A., Dohrmann, S., Nizet, V. & Cole, J. N. Mechanisms of group A Streptococcus resistance to reactive oxygen species. *FEMS Microbiol. Rev.* **39**(4), 488–508 (2015).
58. Fiebig, A. *et al.* Comparative genomics of Streptococcus pyogenes M1 isolates differing in virulence and propensity to cause systemic infection in mice. *Int. J. Med. Microbiol.* **305**(6), 532–543 (2015).
59. Sumbly, P., Whitney, A. R., Graviss, E. A., Deleo, F. R. & Musser, J. M. Genome-wide analysis of group A streptococci reveals a mutation that modulates global phenotype and disease specificity. *PLoS. Pathog.* **2**(1), e5, <https://doi.org/10.1371/journal.ppat.0020005> (2006).
60. Cywes, C. & Wessels, M. R. Group A Streptococcus tissue invasion by CD44-mediated cell signalling. *Nature* **414**(6864), 648–652 (2001).
61. van de Rijn, I. & Kessler, R. E. Growth characteristics of group A streptococci in a new chemically defined medium. *Infect. Immun.* **27**(2), 444–448 (1980).
62. Podbielski, A., Spellerberg, B., Woischnik, M., Pohl, B. & Luttkicken, R. Novel series of plasmid vectors for gene inactivation and expression analysis in group A streptococci (GAS). *Gene* **177**(1–2), 137–147 (1996).
63. Baev, D., England, R. & Kuramitsu, H. K. Stress-induced membrane association of the Streptococcus mutans GTP-binding protein, an essential G protein, and investigation of its physiological role by utilizing an antisense RNA strategy. *Infect. Immun.* **67**(9), 4510–4516 (1999).
64. Trieu-Cuot, P., Carlier, C., Poyart-Salmeron, C. & Courvalin, P. Shuttle vectors containing a multiple cloning site and a lacZ alpha gene for conjugal transfer of DNA from Escherichia coli to gram-positive bacteria. *Gene* **102**(1), 99–104 (1991).
65. Ozert, V., Rosenshine, I., Mosher, D. F., Fassler, R. & Hanski, E. Roles of integrins and fibronectin in the entry of Streptococcus pyogenes into cells via protein F1. *Mol. Microbiol.* **30**(3), 625–637 (1998).
66. Livak, K. J. & Schmittgen, T. D. Analysis of relative gene expression data using real-time quantitative PCR and the 2^{-ΔΔC_T} Method. *Methods* **25**(4), 402–408 (2001).
67. Oehmcke, S. *et al.* A Novel Role for Pro-Coagulant Microvesicles in the Early Host Defense against *Streptococcus pyogenes* 9(8) (2013).

Acknowledgements

We thank Brigitte Vollmar and the Core Facility "Zentrale Versuchstierhaltung" in the Rudolf-Zenker-Institut für Experimentelle Chirurgie, Universitätsmedizin Rostock, for laboratory animal care. The BMBF provided funding for Bernd Kreikemeyer in the framework of the ERA-Net PathoGenoMics 2 programme (FKZ 0315437B). The work of Nadja Patenge was supported by the University Medicine Rostock (Forun 889012). Sonja Oehmcke-Hecht was supported by a grant from the Deutsche Forschungsgemeinschaft (OE 547/2-1). Torsten Hain was supported by LOEWE Medical RNomics and the German Centre for Infection Research, Justus-Liebig University Giessen. The Synapt G2-S mass spectrometer was acquired with funds from "Europäischer Fonds für regionale Entwicklung" (EFRE), # 2007DE161PO003, awarded to the University Medicine Rostock.

Author Contributions

Conception and design for this study: N.P., R.P., P.W., S.M., and B.K. Acquisition, analysis, and interpretation of the data: R.P., P.W., S.M., J.N., A.W.-K., F.H., M.W., A.K., O.S., S.O.-H., T.H. and N.P. Drafting or revising the article: N.P., R.P., P.W., S.M., and B.K. All authors read and approved the final manuscript.

Additional Information

Supplementary information accompanies this paper at <https://doi.org/10.1038/s41598-017-12507-z>.

Competing Interests: The authors declare that they have no competing interests.

Publisher's note: Springer Nature remains neutral with regard to jurisdictional claims in published maps and institutional affiliations.



Open Access This article is licensed under a Creative Commons Attribution 4.0 International License, which permits use, sharing, adaptation, distribution and reproduction in any medium or format, as long as you give appropriate credit to the original author(s) and the source, provide a link to the Creative Commons license, and indicate if changes were made. The images or other third party material in this article are included in the article's Creative Commons license, unless indicated otherwise in a credit line to the material. If material is not included in the article's Creative Commons license and your intended use is not permitted by statutory regulation or exceeds the permitted use, you will need to obtain permission directly from the copyright holder. To view a copy of this license, visit <http://creativecommons.org/licenses/by/4.0/>.

© The Author(s) 2017

Inhibition of Growth and Gene Expression by PNA-peptide Conjugates in *Streptococcus pyogenes*

Nadja Patenge¹, Roberto Pappesch¹, Franziska Krawack¹, Claudia Walda¹, Mobarak Abu Mraheii², Anette Jacob^{3,4}, Torsten Hain² and Bernd Kreikemeyer¹

While *Streptococcus pyogenes* is consistently susceptible toward penicillin, therapeutic failure of penicillin treatment has been reported repeatedly and a considerable number of patients exhibit allergic reactions to this substance. At the same time, streptococcal resistance to alternative antibiotics, e.g., macrolides, has increased. Taken together, these facts demand the development of novel therapeutic strategies. In this study, *S. pyogenes* growth was inhibited by application of peptide-conjugated antisense-peptide nucleic acids (PNAs) specific for the essential gyrase A gene (*gyrA*). Thereby, HIV-1 Tat peptide-coupled PNAs were more efficient inhibitors of streptococcal growth as compared with (KFF)₃K-coupled PNAs. Peptide-anti-*gyrA* PNAs decreased the abundance of *gyrA* transcripts in *S. pyogenes*. Growth inhibition by antisense interference was enhanced by combination of peptide-coupled PNAs with protein-level inhibitors. Antimicrobial synergy could be detected with levofloxacin and novobiocin, targeting the gyrase enzyme, and with spectinomycin, impeding ribosomal function. The prospective application of carrier peptide-coupled antisense PNAs in *S. pyogenes* covers the use as an antimicrobial agent and the employment as a knock-down strategy for the investigation of virulence factor function.

Molecular Therapy—Nucleic Acids (2013) 2, e132; doi:10.1038/mtna.2013.62; published online 5 November 2013

Subject Category: Antisense oligonucleotides Peptide nucleic acids

Introduction

Streptococcus pyogenes (group A streptococci (GAS)) is an exclusively human pathogen, which causes a wide spectrum of infectious diseases ranging from mild superficial infections of the skin and the mucosal membranes to invasive diseases like necrotizing fasciitis (flesh-eating disease) or streptococcal toxic shock syndrome. Typically, superficial infections are associated with spontaneous recovery. However, if mild infections remain untreated, severe invasive infections or autoimmune sequelae can develop as a consequence.^{1,2} Therefore, antibiotic therapy is strongly indicated upon streptococcal infections. Currently, penicillin is the standard treatment of streptococcal pharyngitis. Reasons are the continuing susceptibility of GAS toward penicillin, its efficiency, safety, and the comparably low costs of penicillin treatment.^{3–5} However, penicillin-related treatment failure has been reported repeatedly in cases of streptococcal pharyngitis.^{6,7} Factors that have been discussed to be responsible for this phenomenon include the coexistence of β -lactamase-producing bacteria,⁸ biofilm formation by GAS,⁹ and internalization of GAS into epithelial host cells.^{10–12} Another problem poses the rising occurrence of macrolide resistance in GAS,^{13,14} which limits the use of macrolides to patients with significant penicillin allergies.¹⁵ Consequently, the development of novel therapeutic strategies remains an imperative.

Among the innovative therapeutic approaches, antisense molecules gain increasing importance. One advantage of antisense interference is the specific effect on target molecules. Another is the lack of already established bacterial resistance

mechanisms toward antisense agents. Peptide nucleic acids (PNAs) have been tested as antimicrobial agents in the past decade in a variety of bacterial species. Their chemical properties place PNAs between peptides and nucleic acids. Nucleobases, which are capable of sequence-specific base pairing, are present in PNAs. However, peptide bonds replace the nucleic acid-specific sugar-phosphate backbone.¹⁶ PNAs show a high stability in organic solutions as well as in water and their hybrid characteristics add to their stability in biological environments. So far, no nuclease or protease is known to be capable of hydrolyzing PNAs. Consequently, PNAs proved to be very stable in human serum and cellular extracts.¹⁷

PNA uptake is limited by the outer cell membrane in Gram-negative bacteria.¹⁸ Cell-penetrating peptides (CPPs) are naturally occurring or synthetic peptides containing positively charged residues that are able to enter eukaryotic cells and bacteria. They can be employed for the transduction of cargos into target cells.^{19,20} Transport of PNAs into Gram-negative bacteria could be facilitated by (KFF)₃K CPPs coupled to the PNA molecules.^{21–24} The mRNA of several essential genes has been targeted by PNA antisense interference to achieve inhibition of bacterial growth, including the gene for an RNA polymerase primary sigma factor (*rpoD*), the gene for the gyrase A subunit (*gyrA*), the gene coding for the anti-cycl carrier protein (*acpP*), and the *ompA* gene, coding for an outer membrane protein.^{24–26} In a different approach, bacterial protein biosynthesis has been inhibited by targeting with PNAs specific for the 16S or the 23S RNA.^{23,27}

In a limited number of studies, CPP-conjugated PNAs have been tested in Gram-positive bacteria. In general, the

¹Institute of Medical Microbiology, Virology and Hygiene, Rostock University Medical Center, Rostock, Germany; ²Institute of Medical Microbiology, Justus-Liebig-University, Giessen, Germany; ³Pepts4LS, Heidelberg, Germany; ⁴Functional Genome Analysis, Deutsches Krebsforschungszentrum, Heidelberg, Germany. Correspondence: Nadja Patenge, Institute of Medical Microbiology, Virology and Hygiene, Rostock University Medical Center, Schillingallee 70, 18057 Rostock, Germany. E-mail: Nadja.Patenge@med.uni-rostock.de

Keywords: antimicrobial; antisense; cell-penetrating peptides; HIV-1 peptide; PNA; *Streptococcus pyogenes*

Received 23 April 2013; accepted 29 August 2013; advance online publication 5 November 2013. doi:10.1038/mtna.2013.62



antisense effect was less pronounced in Gram-positive species than in *E. coli* and a higher PNA concentration was required to cause growth reduction.^{23,28}

Here, we aimed at inhibiting growth of GAS M49, which is a generalist known to be responsible for skin and throat infections, by antisense targeting of the essential gene *gyrA*. Its gene product represents the subunit A of the DNA topoisomerase gyrase, which is involved in replication and is thus required for bacterial growth. Growth reduction was achieved employing PNAs specific for *gyrA*, which were either coupled to (KFF)3K- or to Tat-peptides, respectively. Tat-conjugated anti-*gyrA* PNAs inhibited the growth of GAS M49 more efficiently than (KFF)3K-coupled anti-*gyrA* PNAs, while showing a lower unspecific CPP-related toxicity. Combination testing revealed antimicrobial synergy between antisense-PNAs and conventional antibiotics.

Results

GAS M49 growth reduction by carrier peptide-coupled anti-*gyrA* PNAs

Anti-*gyrA* PNAs were designed complementary to nucleotides covering the start codon of *gyrA* and three regions throughout the coding sequence of the gene (Table 1). We tested anti-*gyrA* PNAs with and without coupling to the synthetic (KFF)3K peptide, which had been used successfully before to support

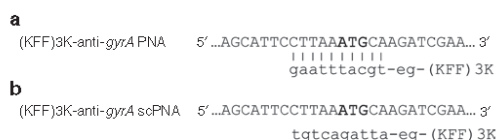


Figure 1 Design of antisense peptide nucleic acids (PNAs) specific for *gyrA* in GAS M49. Upper case: partial sequence of the gyrase A gene, start-codon marked in bold; lower case, respective PNA sequences, e.g., 8-amino-3,6-dioxaoctanoic acid. (a) (KFF)3K-coupled PNAs complementary to the start-codon region of *gyrA*. (b) (KFF)3K-coupled PNAs composed of the same bases as in A but in a randomized (scrambled) sequence. Scrambled PNAs show no complementarity to the target region.

PNA uptake in a variety of bacterial species. In Figure 1a, a schematic of (KFF)3K-coupled anti-*gyrA* PNAs complementary to the start region is shown as a representative example. First, the four different target sequences within *gyrA* were compared. PNAs lacking the (KFF)3K-carrier peptide did not influence bacterial growth at all (data not shown). Also, (KFF)3K-coupled PNAs complementary to *gyrA* nucleotides 91-105, 867-881, and 1925-1939, respectively, did not interfere with GAS M49 growth (Table 1). Exclusively, (KFF)3K-coupled PNAs complementary to the start codon region of the *gyrA* transcript (nucleotides -5 to 5) led to a concentration-dependent reduction of GAS M49 growth (Table 1; Figure 2a).

To control for specificity of the interaction, scrambled PNAs (scPNAs) were designed, which shared the same base composition with sequence-specific anti-*gyrA* PNAs but exhibited a randomized sequence (Figure 1b). Comparison with (KFF)3K-anti-*gyrA* scPNA revealed that growth reduction caused by treatment with (KFF)3K-anti-*gyrA* PNA was sequence specific (Figure 2b). No growth inhibition was achieved by addition of scPNA within a concentration range of 0.8–4.0 $\mu\text{mol/l}$. At PNA concentrations $\geq 5.6 \mu\text{mol/l}$, unspecific toxic effects of the scPNAs were observed (Figure 2b). Application of the (KFF)3K peptide alone also resulted in the reduction of bacterial growth at concentrations $\geq 5.6 \mu\text{mol/l}$ (data not shown). It is likely that growth inhibition upon application of high concentrations of (KFF)3K peptide-coupled PNAs is mediated at least in part by toxic effects of the leader peptide. The minimal inhibitory concentration (MIC) of (KFF)3K-anti-*gyrA* PNAs was 10 $\mu\text{mol/l}$. At this concentration, inhibition is caused by a combination of a sequence-specific action of the antisense molecule and an unspecific toxic effect of the leader peptide. Consequently, the following experiments were performed in the sub-MIC sequence-specific effective concentration range of (KFF)3K-anti-*gyrA* PNA. The observed effect upon treatment with (KFF)3K-anti-*gyrA* PNA was statistically relevant in the exponential (3 hours) as well as in the early stationary growth phase (6 hours) (Figure 2c–f). Dose dependency of GAS M49 growth inhibition became evident upon comparison of growth rates between samples (Supplementary Figure S1).

Table 1 Peptide nucleic acids (PNAs) and inhibitory concentrations

PNA	Target	Sequence	c ($\mu\text{mol/l}$)
anti- <i>gyrA</i> PNA	<i>gyrA</i> -5 to 5	Tgcatttaag	—
anti- <i>gyrA</i> scPNA		Attagactgt	—
(KFF)3K-anti- <i>gyrA</i> PNA	<i>gyrA</i> -5 to 5	(KFF)3K-eg ⁸ -tgcatttaag	1.6–4.0
(KFF)3K-anti- <i>gyrA</i> scPNA		(KFF)3K-eg ⁸ -attagactgt	≥ 5.6
(KFF)3K-anti- <i>gyrA</i> _91 PNA	<i>gyrA</i> 91 to 105	(KFF)3K-G-gcttgccagatgtg	—
(KFF)3K-anti- <i>gyrA</i> _867 PNA	<i>gyrA</i> 867 to 881	(KFF)3K-G-tgtgacgaatctag	—
(KFF)3K-anti- <i>gyrA</i> _1925 PNA	<i>gyrA</i> 1925 to 1939	(KFF)3K-G-aagaggagatcagc	—
(KFF)3K cell-penetrating peptides (CPP)		(KFF)3K	≥ 5.6
Tat-anti- <i>gyrA</i> PNA	<i>gyrA</i> -5 to 5	GRKKKRRQRRRYK-eg ⁸ -tgcatttaag	0.4–1.4
Tat-anti- <i>gyrA</i> scPNA		GRKKKRRQRRRYK-eg ⁸ -attagactgt	—
Tat CPP		GRKKKRRQRRRYK	≥ 20.0

⁸ethyleneglycol linker: 8-amino-3,6-dioxaoctanoic acid.

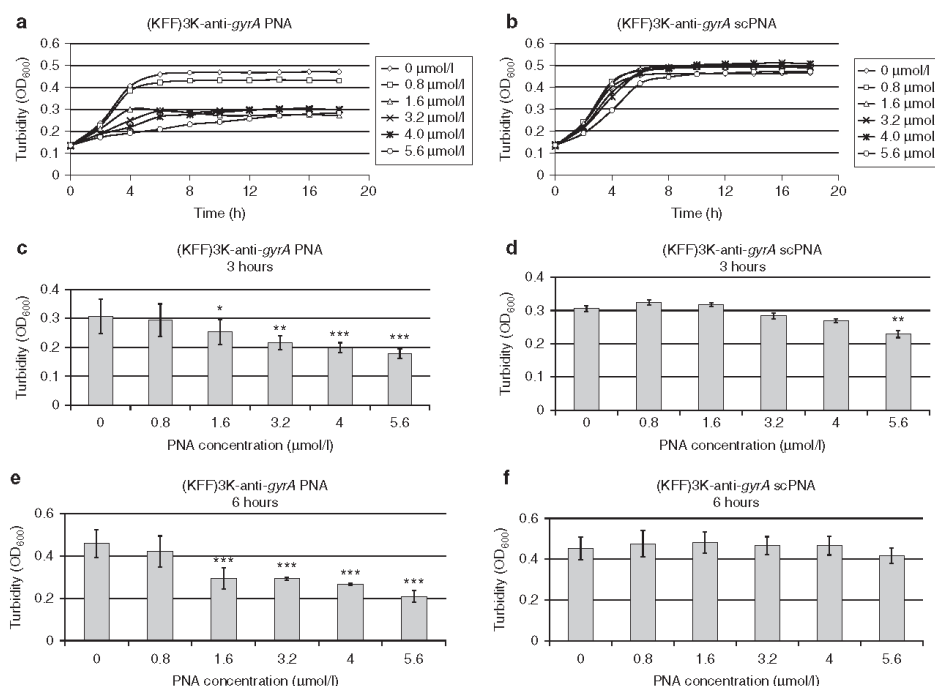


Figure 2 Effect of $(\text{KFF})_3\text{K}$ -coupled peptide nucleic acids (PNAs) on GAS M49 growth. (a) Concentration-dependent growth inhibition of GAS M49 by $(\text{KFF})_3\text{K}$ -anti-*gyrA* PNA. (b) No growth inhibition of GAS M49 by $(\text{KFF})_3\text{K}$ -anti-*gyrA* scPNA (0.8–4.0 $\mu\text{mol/l}$). At PNA concentrations ≥ 5.6 $\mu\text{mol/l}$, unspecific toxic effects of the scPNAs were observed. (c,d) Statistic evaluation of the growth inhibition effect of $(\text{KFF})_3\text{K}$ -anti-*gyrA* PNA (c) and $(\text{KFF})_3\text{K}$ -anti-*gyrA* scPNA (d) at 3 hours. Error bars represent the mean \pm SD, $n = 5$. (e,f): statistic evaluation of the growth inhibition effect of $(\text{KFF})_3\text{K}$ -anti-*gyrA* PNA (e) and $(\text{KFF})_3\text{K}$ -anti-*gyrA* scPNA (f) at 6 hours. Error bars represent the mean \pm SD, $n = 5$.

$(\text{KFF})_3\text{K}$ -anti-*gyrA* PNA effects the abundance of *gyrA* transcripts in GAS M49

We asked whether antisense binding of $(\text{KFF})_3\text{K}$ -anti-*gyrA* PNA to the *gyrA* mRNA was reflected by changes of the *gyrA* transcript level. The influence of the presence of sequence-specific PNAs on the amount of *gyrA* mRNA was tested by reverse transcription followed by quantitative reverse transcription polymerase chain reaction (Figure 3). Transcript abundance of the 5S RNA gene was used for normalization. The *gyrA* mRNA level in mock-treated GAS samples served as control. Upon treatment with 1.6 $\mu\text{mol/l}$ $(\text{KFF})_3\text{K}$ -anti-*gyrA* PNA, the amount of *gyrA* transcript was reduced to 50% of the amount detected in the untreated control sample. Addition of scPNA did not influence the relative *gyrA* mRNA level detected by quantitative reverse transcription polymerase chain reaction.

The HIV-1 Tat peptide supports the antimicrobial activity of anti-*gyrA* PNA more efficiently than the $(\text{KFF})_3\text{K}$ -carrier
In GAS M49, PNA uptake and PNA-mediated growth inhibition were not achieved when PNAs lacking a leader peptide were employed. Fusion of the CPP $(\text{KFF})_3\text{K}$ to *gyrA*-specific PNA enabled sequence-specific growth inhibition of GAS

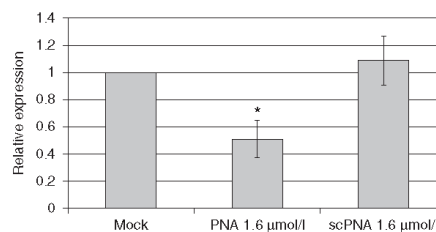


Figure 3 Effect of $(\text{KFF})_3\text{K}$ -anti-*gyrA* peptide nucleic acid (PNA) treatment on the abundance of *gyrA* transcripts. RNA was extracted from PNA-treated and scPNA-treated samples. The graph shows the relative *gyrA* expression compared to mock treated samples. Error bars represent the mean \pm SD, $n = 3$.

M49. The uptake efficiency of every given CPP varies between bacterial species. Similar to the cationic and hydrophobic $(\text{KFF})_3\text{K}$ peptide, the HIV-1 Tat protein-derived arginine-rich recombinant peptide YGRKKRRQRRR (Tat) translocates by destabilizing phospholipid bilayers and thereby induces transient pores in the respective membrane.²⁹ In contrast to $(\text{KFF})_3\text{K}$, Tat has not been used before for transduction into



bacteria. To test whether the Tat peptide could be employed as a leader peptide for the uptake of peptide oligonucleotides into GAS M49, it was coupled to *gyrA* antisense PNA. The effect of Tat-anti-*gyrA* PNA on growth of GAS M49 was compared with the growth inhibition mediated by Tat-anti-*gyrA* scPNA. Significant growth reduction in the presence of Tat-anti-*gyrA* PNA was observed in the concentration range of 0.4–1.4 $\mu\text{mol/l}$ (Figure 4a,c,d). Addition of higher concentrations of Tat-PNA anti-*gyrA* did not lead to a further increase of the observed effects (data not shown). Application of Tat-anti-*gyrA* scPNA did not lead to growth inhibition of GAS M49 (Figure 4b), indicating a sequence-specific inhibitory effect. Addition of Tat peptide alone did not lead to GAS M49 growth inhibition up to a concentration of 10 $\mu\text{mol/l}$ Tat peptide (data not shown). In comparison with anti-*gyrA* PNAs coupled to the (KFF)3K leader peptide, Tat-PNA anti-*gyrA* showed a much more efficient growth inhibition of GAS M49 (Table 1).

Antimicrobial synergy between peptide-coupled anti-*gyrA* PNAs and peptide-level antibiotics

The bacterial gyrase protein is a well-known target of antibiotics including aminocoumarins and quinolones. Given the fact that antisense-PNA treatment is reducing bacterial growth effectively but not completely, we wanted to test whether the combined application of peptide-coupled anti-*gyrA* PNAs with conventional antibiotics leads to synergistic effects. Gyrase peptide-targeting antibiotics were compared with the antibiotics targeting proteins unrelated to DNA replication. A widely used test for the determination of antimicrobial synergy between different inhibitors is the checkerboard assay.³⁰ Following this protocol, the MIC for each compound is determined independently. Following serial dilution of the individual inhibitors, each concentration of one agent is then combined with each concentration of the second agent. Bacterial growth is determined for the combinations after appropriate incubation of the samples. For analyses of the inhibitor interactions,

the fractional inhibitory concentration indices (FICI) are calculated.³¹ Checkerboard assay data have been interpreted variably, leading to ambiguous results.³² Furthermore, a linear dose dependency, which cannot be assumed for all antimicrobial substances, is a prerequisite for correct synergy determination using this method. Moreover, as pointed out before, at the MIC determined for (KFF)3K-anti-*gyrA* PNA, the sequence-specific effect of PNA was superimposed by toxic effects of the carrier peptide. For these reasons, the checkerboard assay was not feasible for combination testing of PNAs with antibiotics in GAS M49. To be able to work within the sequence-specific effective concentration range, spectrophotometric assessment of dose–response curves for antimicrobial combinations was employed.^{33–35}

As examples for antibiotics interfering with the same pathway as anti-*gyrA* PNAs, inhibitors of gyrase A (levofloxacin) and gyrase B (novobiocin) were chosen. These were compared with spectinomycin, which binds to the ribosomal 30S subunit and thereby inhibits a pathway distinct from DNA replication. In Figure 5a–c, the spectrophotometric recordings for the interaction of (KFF)3K-anti-*gyrA* PNAs with levofloxacin are shown as one representative example. Reduced growth of GAS M49 in the presence of levofloxacin (0.5–10 $\mu\text{g/ml}$) could be detected (Figure 5a). At a concentration of 0.5 $\mu\text{g/ml}$ levofloxacin, a slight growth repression was observed repeatedly. This concentration was chosen for combination testing. GAS M49 was incubated in the presence of 0.5 $\mu\text{g/ml}$ levofloxacin and 0.8–4.0 $\mu\text{mol/l}$ (KFF)3K-anti-*gyrA* PNAs, respectively. Upon addition of (KFF)3K-anti-*gyrA* PNAs to the culture, an increased inhibition of growth could be observed in comparison with samples containing levofloxacin alone (Figure 5b). Reduction of the growth constant $g = \ln(\text{OD}_{\text{tx}}/\text{OD}_{\text{t0}})/\text{tx}$ in the presence of one inhibitor or following application of a combination of the two agents served as a measure of interaction of the two effectors. For the combination of levofloxacin with (KFF)3K-anti-*gyrA* PNA, synergy was observed over the entire

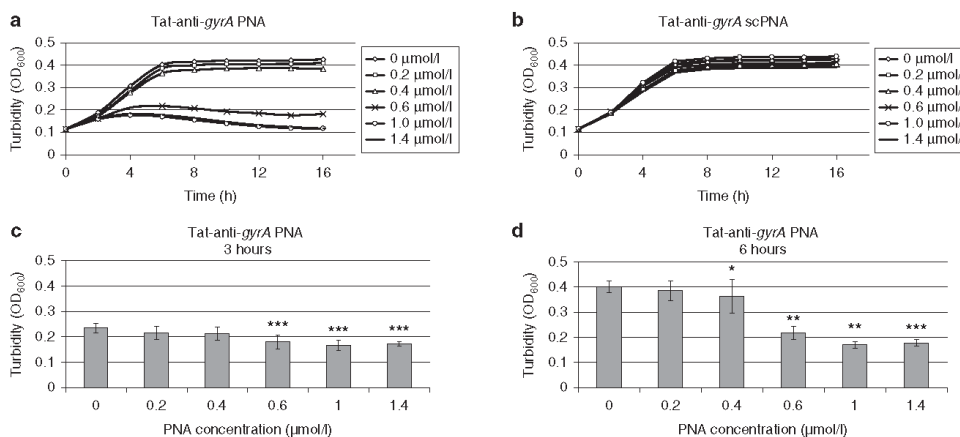


Figure 4 Effect of Tat-coupled peptide nucleic acids (PNAs) on GAS M49 growth. (a) Concentration-dependent growth inhibition of GAS M49 by Tat-anti-*gyrA* PNA. (b) No growth inhibition of GAS M49 by Tat-anti-*gyrA* scPNA. (c,d) statistical evaluation of the growth inhibition effect of Tat-anti-*gyrA* PNA at 3 (c) and at 6 hours (d). Error bars represent the mean \pm SD, $n = 6$.

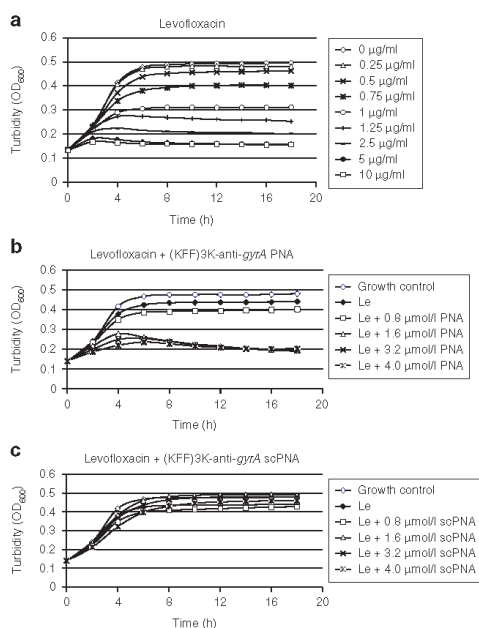


Figure 5 Combination testing of levofloxacin with (KFF)₃K-anti-gyrA peptide nucleic acid. (a) Dose-dependent growth inhibition of GAS M49 by levofloxacin. (b) Growth behavior of GAS M49 in the presence of 0.5 µg/ml levofloxacin and increasing concentrations of (KFF)₃K-anti-gyrA peptide nucleic acid (PNA) (0.8–4.0 µmol/l). (c) Growth behavior of GAS M49 in the presence of 0.5 µg/ml levofloxacin and increasing concentrations of (KFF)₃K-anti-gyrA scPNA (0.8–4.0 µmol/l).

PNA concentration range tested in this experiment (Table 2). (KFF)₃K-anti-gyrA scPNA did not enhance the effect of levofloxacin under these conditions (Figure 5b). The corresponding data for novobiocin and spectinomycin are presented in Supplementary Figures S2 and S3. Following treatment with novobiocin (0.2 µg/ml), synergy with (KFF)₃K-anti-gyrA PNA was detected only at 4.0 µmol/l PNA (Table 2). Incubation of 5 µg/ml spectinomycin in combination with (KFF)₃K-anti-gyrA PNA (0.8–4.0 µmol/l) led to synergistic effects at all PNA concentrations tested (Table 2). Again, no synergy was observed upon addition of (KFF)₃K-anti-gyrA scPNA (Supplementary Figures S2c and S3c).

Combination of Tat-anti-gyrA PNA with peptide antibiotics led to comparable results (Supplementary Figures S4–S6; Table 3). Upon combination of Tat-anti-gyrA PNA (0.2–1.2 µmol/l) with levofloxacin (0.5 µg/ml), a synergistic effect was observed at 0.4–0.8 and 1.2 µmol/l PNA (Table 3). Treatment with novobiocin (0.2 µg/ml) led to synergy with 0.4–0.8 µmol/l PNA (Table 3). Application of 5 µg/ml spectinomycin in combination with Tat-anti-gyrA PNA led to synergistic effects from 0.4 to 1.2 µmol/l PNA (Table 3). Tat-conjugated scPNA did not show interaction with the antibiotics tested (Supplementary Figures S4b, S5b, and S6b).

Table 2 Interpretation of the decreasing growth rate constant (6 hours) (KFF)₃K-anti-gyrA peptide nucleic acid (PNA)

c _{PNA} (µmol/l)	g _{PNA}	g _{antibiotic}	g ₀	g _{PNA+antibiotic}	(g _{PNA} × g _{antibiotic})/g ₀	Interpretation
0.5 µg/ml levofloxacin						
0	0.20	0.19	0.20	0.19	0.19	n.a. ^a
0.8	0.19	0.19	0.20	0.17	0.18	Synergy ^c
1.6	0.13	0.19	0.20	0.11	0.12	Synergy ^c
3.2	0.13	0.19	0.20	0.10	0.12	Synergy ^c
4.0	0.11	0.19	0.20	0.09	0.10	Synergy ^c
0.2 µg/ml novobiocin						
0	0.22	0.20	0.22	0.20	0.2	n.a. ^a
0.8	0.21	0.20	0.22	0.20	0.19	Autonomy ^b
1.6	0.11	0.20	0.22	0.10	0.10	Autonomy ^c
3.2	0.08	0.20	0.22	0.08	0.07	Autonomy ^c
4.0	0.08	0.20	0.22	0.03	0.07	Synergy ^c
5.0 µg/ml spectinomycin						
0	0.20	0.20	0.20	0.20	0.20	n.a. ^a
0.8	0.19	0.20	0.20	0.17	0.19	Synergy ^c
1.6	0.13	0.20	0.20	0.09	0.13	Synergy ^c
3.2	0.13	0.20	0.20	0.06	0.13	Synergy ^c
4.0	0.11	0.20	0.20	0.04	0.11	Synergy ^c

^anot applicable. ^bg_(A,B) = g_A or g_B. ^cg_(A,B) < g_A × g_B/g₀.

Both (KFF)₃K-anti-gyrA PNA and Tat-anti-gyrA PNA showed synergy with all three antibiotics tested in this study. The effect was independent of the pathway targeted by the antimicrobial substance. Combination of peptide-coupled anti-gyrA PNAs with antibiotics achieved a stronger overall growth inhibition than application of PNA alone.

Discussion

In the era of increasing drug resistance, it is more important than ever to assure timely development of innovative antimicrobial agents. Among antisense molecules, PNAs are particularly promising candidates due to their specific structural features. They are known for their strong pairing to DNA as well as to RNA and their pseudopeptide backbone confers stability while allowing molecular modifications, e.g., the conjugation of CPPs. The potency of antisense PNAs has been studied most thoroughly in *Escherichia coli*. Few reports are available about the effectivity of PNAs in Gram-positive pathogens. We set out to test whether PNA antisense targeting of a gene coding for an essential enzyme in GAS M49 will pose an impediment to its growth. We choose *gyrA*, because the gyrase enzyme represents a well-characterized target of antibiotics, including aminocoumarins and quinolones, and because *gyrA* has been successfully used before for PNA antisense-studies in other species.^{24,28}

We observed growth reduction in GAS M49 following the application of anti-gyrA PNAs. However, conjugation of anti-gyrA PNAs with CPPs was required for antimicrobial activity of the antisense-PNAs. This is in accordance with the previous studies. PNA uptake by the bacterial cell has repeatedly been described as a limiting factor in antimicrobial PNA action. To overcome this obstacle, a variety of


Table 3 Interpretation of the decreasing growth rate constant (6 hours) Tat-anti-*gyrA* peptide nucleic acid (PNA)

c_{PNA} ($\mu\text{mol/l}$)	g_{PNA}	$g_{\text{antibiotic}}$	g_0	$g_{\text{PNA, antibiotic}}$	$(g_{\text{PNA}} \times g_{\text{antibiotic}}) / g_0$	Interpretation
0.5 $\mu\text{g/ml}$ levofloxacin						
0	0.21	0.20	0.21	0.20	0.20	n.a. ^a
0.2	0.21	0.20	0.21	0.21	0.20	Autonomy ^b
0.4	0.20	0.20	0.21	0.18	0.19	Synergy ^c
0.6	0.15	0.20	0.21	0.11	0.14	Synergy ^c
0.8	0.12	0.20	0.21	0.10	0.11	Synergy ^c
1.0	0.09	0.20	0.21	0.09	0.09	Additivity ^d
1.2	0.08	0.20	0.21	0.07	0.08	Synergy ^c
0.2 $\mu\text{g/ml}$ novobiocin						
0	0.21	0.19	0.21	0.21	0.19	n.a. ^a
0.2	0.21	0.19	0.21	0.19	0.19	Autonomy ^b
0.4	0.20	0.19	0.21	0.17	0.18	Synergy ^c
0.6	0.16	0.19	0.21	0.12	0.14	Synergy ^c
0.8	0.14	0.19	0.21	0.12	0.13	Synergy ^c
1.0	0.11	0.19	0.21	0.11	0.10	Autonomy ^b
1.2	0.09	0.19	0.21	0.10	0.08	Autonomy ^b
5.0 $\mu\text{g/ml}$ spectinomycin						
0	0.22	0.22	0.22	0.22	0.22	n.a. ^a
0.2	0.22	0.22	0.22	0.22	0.22	Autonomy ^b
0.4	0.21	0.22	0.22	0.18	0.21	Synergy ^e
0.6	0.14	0.22	0.22	0.09	0.14	Synergy ^e
0.8	0.13	0.22	0.22	0.09	0.13	Synergy ^e
1.0	0.10	0.22	0.22	0.08	0.10	Synergy ^e
1.2	0.09	0.22	0.22	0.06	0.09	Synergy ^e

^anot applicable. ^b $g_{(\text{A,B})} = g_{\text{A}}$ or g_{B} . ^c $g_{(\text{A,B})} < g_{\text{A}} \times g_{\text{B}} / g_0$. ^d $g_{(\text{A,B})} = g_{\text{A}} \times g_{\text{B}} / g_0$. ^e $g_{(\text{A,B})} \leq g_{\text{A}}$ or g_{B} .

different strategies has been pursued in the past. The LPS layer-defective *E. coli*-mutant AS19³⁶ has been used frequently for PNA studies, because of its increased permeability. Another widely employed option is the conjugation of synthetic cationic peptides, which are able to penetrate the outer membrane of Gram-negative bacteria.²⁰ One well-studied example is the (KFF)₃K peptide, which has been used as a leader peptide to facilitate PNA uptake into *E. coli*.^{21,27} It has also been shown to support PNA function in other Gram-negative bacteria and in some Gram-positive species, e.g., *S. aureus*.^{22–24,28} We tested (KFF)₃K-PNA conjugates, which proved to be effective in GAS M49. While no activity of mere anti-*gyrA* PNAs could be observed, GAS M49 growth was inhibited in the presence of micromolar concentrations of (KFF)₃K-coupled anti-*gyrA* PNA. The (KFF)₃K-anti-*gyrA* PNA concentration range needed for a dose-dependent growth reduction in GAS M49 (1.6–4.0 $\mu\text{mol/l}$) was comparable with those reported from other species. In *S. aureus*, (KFF)₃K-anti-*gyrA* PNA showed a growth inhibitory effect at 2–10 $\mu\text{mol/l}$,²³ in *Klebsiella pneumoniae*, 10–40 $\mu\text{mol/l}$ (KFF)₃K-anti-*gyrA* PNA were needed for a dose-dependent inhibition.²⁴ Growth inhibition by (KFF)₃K-coupled antisense PNAs specific for *rpoD*, coding for the RNA polymerase primary sigma factor $\sigma 70$, required a PNA concentration of 12.5 $\mu\text{mol/l}$ in *S. aureus* and 40 $\mu\text{mol/l}$ in *K. pneumoniae*, respectively.^{25,38}

Even though involvement of antisense binding has been shown in the inhibition of gene expression by PNAs,³⁹ the exact mechanism is not known. The start codon region was found to be the most efficient target region to achieve inhibition of gene expression in *E. coli*, and impairment of translation initiation was considered to be a likely mechanism.⁴⁰ On the other hand, reduction of the corresponding mRNA has been observed, indicating mRNA degradation upon binding of complementary PNAs.^{24,25} In GAS M49, a decrease of *gyrA* mRNA abundance to 50% could be detected upon treatment with (KFF)₃K-anti-*gyrA* PNAs (Figure 3). Similar results have been obtained in *E. coli*, where application of (KFF)₃K-anti-*acpP*-PNAs caused a decrease of *acpP* mRNA abundance to about 60% of the untreated control.²⁶ Since ribosomal binding during translation acts as protective barrier against cleavage and thereby stabilizes mRNA,⁴¹ a hampered *gyrA* mRNA translation initiation due to PNA binding might be responsible for a moderate destabilization of the *gyrA* transcript in GAS M49.

The (KFF)₃K-anti-*gyrA* PNA concentration required for the implementation of growth inhibition in GAS M49 was much higher than reported from *E. coli* inhibition studies. The MIC in *E. coli* K12 varied between 2 and 6 $\mu\text{mol/l}$, depending on the target,⁴² whereas the apparent MIC observed for GAS M49 was about 10 $\mu\text{mol/l}$, which is an approximate value, because it is influenced by toxic effects of the (KFF)₃K leader. We speculated that import of PNAs into M49 could be improved by PNA coupling to a different CPP, preferentially to a peptide exhibiting lower toxicity. Besides the synthetic (KFF)₃K peptide, there are many naturally occurring CPPs known, which represent short sequences of amino acids that are capable of entering most mammalian cells.¹⁹ CPPs are often highly cationic and hydrophilic. Translocation of cargos across the cell membrane seems to involve destabilization of the membrane and formation of a pore by the cationic peptides.²⁹ The HIV-1 Tat protein contains a small region corresponding to residues ⁴⁷YGRKKRRQRR⁵⁷R, which is capable of membrane translocation by an apparently energy-independent mechanism.⁴³ This fragment of the basic protein domain was shown to exhibit no cytotoxicity in HeLa cells at concentrations up to 100 $\mu\text{mol/l}$.⁴⁴ However, translocation efficiency and toxicity have not been tested in bacteria, yet.

We used a synthetic HIV-1 Tat peptide derivative (Table 1) for conjugation to anti-*gyrA* PNA. Growth reduction of GAS M49 in a dose-dependent manner was achieved with 0.4–1.4 $\mu\text{mol/l}$ Tat-anti-*gyrA* PNA (Figure 4a–d). Thereby, Tat-conjugated anti-*gyrA* PNA showed an enhanced antimicrobial activity compared with PNA coupled to (KFF)₃K. Growth inhibition of GAS M49 was already detectable at Tat-PNA concentrations below 1 $\mu\text{mol/l}$. Upon application of the Tat-peptide alone, no toxicity was observed in GAS M49 cultures up to a concentration of 10 $\mu\text{mol/l}$ Tat-peptide. Improved antisense effects in combination with low general toxicity are very desirable properties. It has been speculated that treatment failure and recurrent infections are caused by the internalization of *S. pyogenes* into host cells.¹⁰ Antisense agents coupled to Tat, which allows import into host cells in order to target intracellular bacteria and at the same time exhibits low cytotoxicity, might help to circumvent these therapeutic obstacles. Recently, growth of *Brucella suis* in



infected macrophages was shown to be inhibited by 30 $\mu\text{mol/l}$ (KFF)₃K peptide-coupled PNAs.⁴⁵ Application of Tat-coupled PNAs might reduce the required PNA concentration for the targeting of intracellular bacteria.

In the near future, we plan to use Tat-conjugated antisense-PNAs in GAS for the directed knock down of putative virulence genes.⁴⁶ Experimental regulation of gene expression by antisense technology will help to study the function of virulence factors, including regulatory small RNAs, and will allow straight-forward screening for virulence specific phenotypes. Antisense-mediated downregulation of virulence-related streptococcal genes may provide also a therapeutic advantage. GAS with attenuated virulence could be targeted by the host immune system leading to a subsequent clearance of infection without the requirement of further antimicrobial treatment.

Combination of antimicrobial drugs is an interesting option for the improvement of therapy. The development of resistance to the respective drugs can be delayed or prevented by combinatorial administration. Another advantage is that the killing rate of bacteriostatic agents can be potentially increased in combination with a second drug. Moreover, in some cases, antimicrobial synergy can be observed upon combined treatment.^{30,47} Combination therapy may also be advantageous when resistance to a single agent develops rapidly.⁴⁸ Combined *in vitro* application of antisense PNAs and peptide-targeting antibiotics have been tested in *E. coli* and in *S. aureus*.⁴⁹ The authors described synergistic antimicrobial effects for combinations of drugs sharing the same genetic targets. By contrast, we found synergistic effects between peptide-coupled anti-*gyrA* PNA and three peptide level antibiotics, independent of the pathway targeted by the antibiotics (Tables 2 and 3). We speculate that during growth, inhibition of translation by ribosomal deficiency will interfere with DNA replication, because the required proteins are not replenished. Enhanced growth inhibition by (KFF)₃K-anti-*gyrA* PNAs as well as Tat-anti-*gyrA* PNAs upon coapplication with conventional antibiotics suggests that antisense PNAs are promising candidates for combination therapy.

Materials and Methods

PNA synthesis. PNAs and PNAs with carrier peptide conjugates were synthesized and purified by HPLC at the DKFZ (Heidelberg, Germany). All PNAs used in this work are listed in Table 1.

Bacterial strains and growth conditions. GAS serotype M49, strain 591, a clinical isolate from a skin infection, was kindly provided from R. Lütticken (Aachen, Germany). GAS M49 was cultured in Todd-Hewitt broth (Invitrogen, Life Technologies GmbH, Darmstadt, Germany) supplemented with 0.5% yeast extract (THY; Invitrogen) at 37 °C under a 5% CO₂ to 20% O₂ atmosphere.

Testing of bacterial growth. Overnight cultures of GAS M49 were diluted 1:20 in THY and allowed to grow to mid-exponential growth phase. Bacteria were diluted to $\sim 1 \times 10^7$ CFU/ml in THY. All inhibition experiments were performed in 96-well microtiter plates (Greiner Bio-One, Kremsmünster, Austria). PNAs of 20 μl diluted in H₂O to a final PNA concentration of

0.2–20 $\mu\text{mol/l}$, as indicated, were added per well. In experiments testing the effect of levofloxacin, novobiocin, or spectinomycin on the growth of GAS M49, 20 μl of the respective component diluted in the appropriate solvent to concentrations as indicated were added to each well. Bacterial suspension of 180 μl was added to a total volume of 200 μl /well. As a contamination control, 20 μl of H₂O was added to at least three wells on the same plate and 180 μl of THY was added. The microtiter plates were incubated at 37 °C, ambient air, in a temperature-controlled plate reader (SpectraMax M2; Molecular Devices, Sunnyvale, CA), which was set to shake the plate every 5 minutes before measuring absorption at 600nm. Viable cell counts were determined by plating appropriate dilutions on THY agar plates. The plates were incubated overnight at 37 °C under a 5% CO₂-20% O₂ atmosphere. CFUs were determined by visual inspection. At time point 0, the viable cell count corresponded to $1\text{--}3 \times 10^6$ CFU/well. Each sample was prepared in triplicate; each experiment has been performed in at least four independent biological replicates. Growth rates were determined in the exponential growth phase: $\mu = \log x_2 - \log x_1 / \log(e) \times (t_2 - t_1)$. $t_1 = 3$ hours; $t_2 = 3.5$ hours; $x_1 = \text{OD}_{600}$ at t_1 , $x_2 = \text{OD}_{600}$ at t_2 . The interaction of antimicrobial substances was determined in combination testing by calculation of the growth constant $g = \ln(\text{OD}t_x / \text{OD}t_0) / t_x$ in the presence of one inhibitor or following application of a combination of the two agents. Thereby, autonomy was defined as $g(A+B) = gA$ or gB and synergy as $g(A+B) < gA + gB/g0$.

RNA isolation. For RNA isolation, five wells were prepared for each experimental condition, treated as indicated, and pooled after 6 hours of incubation. Total bacterial RNA was then isolated using the FastRNAProBlue Kit from MP Biomedicals, Illkirch, France as outlined in the protocol provided by the manufacturer. The purified total RNA was extracted with acidic phenol and digested with DNaseI (Ambion, Life Technologies GmbH, Darmstadt, Germany) to remove remaining traces of chromosomal DNA. The RNA preparation was treated with 10U of DNaseI for 30 minutes at 37 °C. The enzyme was subsequently heat inactivated at 72 °C for 5 minutes.

Quantitative reverse transcription polymerase chain reaction. Fifty nanogram of acidic phenol-extracted and DNaseI-treated total RNA was reverse transcribed to generate cDNA using the First-Strand cDNA Synthesis Kit from Invitrogen following the protocol provided by the manufacturer. For reverse transcription, two reactions were performed using random hexamer primers provided by the kit. One reaction contained reverse transcriptase, a second control reaction was performed without enzyme to exclude product formation from residual genomic DNA templates in the following gene-specific polymerase chain reaction. All reactions were performed in triplicates. The real-time polymerase chain reaction amplification was performed with SYBR Green (Fermentas, Fisher Scientific-Germany GmbH, Schwerte, Germany) using an ABI PRISM 7000 Sequence Detection system (Applied Biosystems, Life Technologies GmbH, Darmstadt, Germany). The level of 5S RNA gene transcription was used for normalization.⁵⁰ Primers were designed based on the full genome sequence of *S. pyogenes* M49 strain NZ131 (NCBI accession number: NC011375). *gyrA*-specific primers:



5'-TGAGTGTCTATTGTGGCAAGAGC-3' and 5'-AGAGA-ATACGACGATGCACAGG-3'; 5S-specific primers: 5'-AGCGACTACCTTATCTCACAG-3' and 5'-GAGATACACCTGTACCCATG-3'. Primer efficiency was tested on genomic GAS M49 DNA before use in reverse transcription reactions. Relative gene expression was determined by the $\Delta\Delta\text{CT}$ method.⁵¹

Statistics. Statistical significance was determined using the two-tailed Mann-Whitney U test. Differences between samples were expressed as "not significant" ($P \geq 0.05$), marginally significant ($P < 0.05$)*, significant ($P < 0.01$)**, highly significant ($P < 0.001$ ***).

Supplementary material

Figure S1. Dose-dependent inhibition of the GAS M49 growth rate (μ) by (KFF)3K-anti-gyrA PNA.

Figure S2. Combination testing of novobiocin with (KFF)3K-anti-gyrA PNA.

Figure S3. Combination testing of spectinomycin with (KFF)3K-anti-gyrA PNA.

Figure S4. Combination testing of levofloxacin with Tat-anti-gyrA PNA.

Figure S5. Combination testing of novobiocin with Tat-anti-gyrA PNA.

Figure S6. Combination testing of spectinomycin with Tat-anti-gyrA PNA.

Acknowledgments. The work of N.P. and B.K. was supported by a BMBF grant in the framework of the ERA-Net PathoGenoMics 2 program (FKZ 0315437B). The work of M.M. and T.H. was supported by a BMBF grant ERA-NET PathoGenoMics program sncRNAomics project (62080061). An application has been filed for a patent relating to the small RNAs mentioned in this manuscript and their prospective inhibition by antisense PNAs. German Patent and Trade Mark Office (DPMA), official file number: 10 2012 104 814.2.

- Carapets, JR, Steer, AC, Mulholland, EK and Weber, M (2006). The global burden of group A streptococcal diseases. *Lancet Infect Dis* 5: 685–694.
- Cunningham, MW. (2006). Pathogenesis of group A streptococcal infections and their sequelae. *Adv Exp Med Biol* 609: 29–42.
- Bisno, AL, Gerber, MA, Gwaltney, JM Jr, Kaplan, EL and Schwartz, RH; Infectious Diseases Society of America (2002). Practice guidelines for the diagnosis and management of group A streptococcal pharyngitis. *Infectious Diseases Society of America. Clin Infect Dis* 35: 113–125.
- Dajani, A, Taubert, K, Ferrenti, P, Peter, G and Shulman, S (1995). Treatment of acute streptococcal pharyngitis and prevention of rheumatic fever: a statement for health professionals. Committee on Rheumatic Fever, Endocarditis, and Kawasaki Disease of the Council on Cardiovascular Disease in the Young, the American Heart Association. *Pediatrics* 96(4 Pt 1): 758–764.
- van Driel, ML, De Sutter, AI, Keber, N, Habraken, H and Christiaens, T (2010). Different antibiotic treatments for group A streptococcal pharyngitis. *Cochrane Database Syst Rev* CD009406.
- Kuhn, SM, Preiksaitis, J, Tyrrel, GJ, Jadavji, T, Church, D and Davies, HD (2001). Evaluation of potential factors contributing to microbiological treatment failure in *Streptococcus pyogenes* pharyngitis. *Can J Infect Dis* 12: 33–39.
- Macnis, MH, Hartman, N, Murray, B, Klein, RF, Roberts, RB, Kaplan, EL *et al.* (1998). Studies of the continuing susceptibility of group A streptococcal strains to penicillin during eight decades. *Pediatr Infect Dis J* 17: 377–381.
- Brook, I and Gober, AE (2006). Failure to eradicate streptococci and beta-lactamase producing bacteria. *Acta Paediatr* 97: 193–195.
- Baldassarri, L, Creli, R, Recchia, S, Imperi, M, Facinelli, B, Giovannetti, E *et al.* (2006). Therapeutic failures of antibiotics used to treat macrolide-susceptible

Streptococcus pyogenes infections may be due to biofilm formation. *J Clin Microbiol* 44: 2721–2727.

- Ogawa, T, Terao, Y, Okuni, H, Ninomiya, K, Sakata, H, Ikebe, K *et al.* (2011). Biofilm formation or internalization into epithelial cells enable *Streptococcus pyogenes* to evade antibiotic eradication in patients with pharyngitis. *Microb Pathog* 51: 58–68.
- Sela, S, Neeman, R, Keller, N and Barzilai, A (2000). Relationship between asymptomatic carriage of *Streptococcus pyogenes* and the ability of the strains to adhere to and be internalised by cultured epithelial cells. *J Med Microbiol* 49: 499–502.
- Podbielski, A and Kreikemeyer, B (2001). Persistence of group A streptococci in eukaryotic cells—a safe place? *Lancet* 358: 3–4.
- Michos, AG, Bakoula, CG, Braoudaki, M, Koutouzi, FI, Roma, ES, Pangalis, A *et al.* (2009). Macrolide resistance in *Streptococcus pyogenes*: prevalence, resistance determinants, and emm types. *Diagn Microbiol Infect Dis* 64: 295–299.
- Richter, SS, Heilmann, KP, Dohrn, CL, Beekmann, SE, Rhihi, F, Garcia-de-Lomas, J *et al.* (2006). Increasing telithromycin resistance among *Streptococcus pyogenes* in Europe. *J Antimicrob Chemother* 61: 603–611.
- Logan, UK, McAuley, JB and Shulman, ST (2012). Macrolide treatment failure in streptococcal pharyngitis resulting in acute rheumatic fever. *Pediatrics* 129: e798–e802.
- Nielsen, PE and Egholm, M (1999). An introduction to peptide nucleic acid. *Curr Issues Mol Biol* 1: 89–104.
- Demidov, VV, Potaman, VN, Frank-Kamenetskii, MD, Egholm, M, Buchard, O, Sönnichsen, SH *et al.* (1994). Stability of peptide nucleic acids in human serum and cellular extracts. *Biochem Pharmacol* 48: 1310–1313.
- Good, L, Sandberg, B, Larsson, O, Nielsen, PE and Wahlestedt, C (2000). Antisense PNA effects in *Escherichia coli* are limited by the outer-membrane LPS layer. *Microbiology (Reading, Engl)* 146 (Pt 10): 2665–2670.
- Gupta, B, Levchenko, TS and Torchilin, VP (2005). Intracellular delivery of large molecules and small particles by cell-penetrating proteins and peptides. *Adv Drug Deliv Rev* 57: 637–651.
- Vaara, M and Porro, M (1996). Group of peptides that act synergistically with hydrophobic antibiotics against gram-negative enteric bacteria. *Antimicrob Agents Chemother* 40: 1801–1805.
- Eriksson, M, Nielsen, PE and Good, L (2002). Cell permeabilization and uptake of antisense peptide-peptide nucleic acid (PNA) into *Escherichia coli*. *J Biol Chem* 277: 7144–7147.
- Ghosal, A and Nielsen, PE (2012). Potent antibacterial antisense peptide-peptide nucleic acid conjugates against *Pseudomonas aeruginosa*. *Nucleic Acid Ther* 22: 323–334.
- Halamoto, M, Nakai, K, Ohnishi, A and Imachi, H (2009). Sequence-specific bacterial growth inhibition by peptide nucleic acid targeted to the mRNA binding site of 16S rRNA. *Appl Microbiol Biotechnol* 84: 1161–1168.
- Kurupati, P, Tan, KS, Kumarasinghe, G and Poh, CL (2007). Inhibition of gene expression and growth by antisense peptide nucleic acids in a multiresistant beta-lactamase-producing *Klebsiella pneumoniae* strain. *Antimicrob Agents Chemother* 51: 805–811.
- Bai, H, You, Y, Yan, H, Meng, J, Xue, X, Hou, Z *et al.* (2012). Antisense inhibition of gene expression and growth in gram-negative bacteria by cell-penetrating peptide conjugates of peptide nucleic acids targeted to rpoD gene. *Biomaterials* 33: 659–667.
- Nikravesch, A, Drynselius, R, Fandani, OR, Goh, S, Sadeghzadeh, M, Behmanesh, M *et al.* (2007). Antisense PNA accumulates in *Escherichia coli* and mediates a long post-antibiotic effect. *Mol Ther* 15: 1537–1542.
- Xue-Wen, H, Jie, P, Xian-Yuan, A and Hong-Xiang, Z (2007). Inhibition of bacterial translation and growth by peptide nucleic acids targeted to domain II of 23S rRNA. *J Pept Sci* 13: 220–226.
- Nekhotova, N, Awasthi, SK, Nielsen, PE and Good, L (2004). Inhibition of *Staphylococcus aureus* gene expression and growth using antisense peptide nucleic acids. *Mol Ther* 10: 652–659.
- Heroe, HD, Garcia, AE, Litt, J, Kane, RS, Martin, P, Enrique, N *et al.* (2009). Arginine-rich peptides destabilize the plasma membrane, consistent with a pore formation translocation mechanism of cell-penetrating peptides. *Biophys J* 97: 1917–1925.
- Eliopoulos, G and Moellering, R (1996). *Antimicrobial combinations*. 4, 330–396. Williams & Wilkins: Baltimore, MD. *Antibiotics in Laboratory Medicine*, 4th edn, Lorian, V. Ref Type: Edited Book.
- den Hollander, JG, Mouton, JW and Verbrugh, HA (1998). Use of pharmacodynamic parameters to predict efficacy of combination therapy by using fractional inhibitory concentration kinetics. *Antimicrob Agents Chemother* 42: 744–746.
- Bonapace, CR, Bosso, JA, Friedrich, LV and White, RL (2002). Comparison of methods of interpretation of checkerboard synergy testing. *Diagn Microbiol Infect Dis* 44: 363–366.
- Geisler, N, Gatlinger, R, Graninger, W, Georgopoulos, A. (2003). Wirksamkeit von teicoplanin oder vancomycin in Kombination mit linezolid gegenüber methicillin-resistentem *Staphylococcus aureus* mittels spektrophotometrischer Trübungsmessung. *Antibiotika Monitor* 6.
- King, TC, Schlessinger, D and Krogstad, DJ (1981). The assessment of antimicrobial combinations. *Rev Infect Dis* 3: 627–633.
- King, TC and Krogstad, DJ (1983). Spectrophotometric assessment of dose-response curves for single antimicrobial agents and antimicrobial combinations. *J Infect Dis* 147: 758–764.
- Sekiguchi, M and Iida, S (1967). Mutants of *Escherichia coli* permeable to actinomycin. *Proc Natl Acad Sci USA* 58: 2315–2320.



37. Good, L, Awasthi, SK, Dryselius, R, Larsson, O and Nielsen, PE (2001). Bactericidal antisense effects of peptide-PNA conjugates. *Nat Biotechnol* 19: 360–364.
38. Bai, H, Sang, G, You, Y, Xue, X, Zhou, Y, Hou, Z *et al.* (2012). Targeting RNA polymerase primary *s70* as a therapeutic strategy against methicillin-resistant *Staphylococcus aureus* by antisense peptide nucleic acid. *PLoS ONE* 7: e28886.
39. Good, L and Nielsen, PE (1996). Antisense inhibition of gene expression in bacteria by PNA targeted to mRNA. *Nat Biotechnol* 16: 355–358.
40. Dryselius, R, Aswathi, SK, Rajarao, GK, Nielsen, PE and Good, L (2003). The translation start codon region is sensitive to antisense PNA inhibition in *Escherichia coli*. *Oligonucleotides* 13: 427–433.
41. Deana, A and Belasco, JG (2006). Lost in translation: the influence of ribosomes on bacterial mRNA decay. *Genes Dev* 19: 2526–2533.
42. Hatamoto, M, Ohashi, A and Imachi, H (2010). Peptide nucleic acids (PNAs) antisense effect to bacterial growth and their application potentiality in biotechnology. *Appl Microbiol Biotechnol* 86: 397–402.
43. Heroe, HD and Garcia, AE (2007). Molecular dynamics simulations suggest a mechanism for translocation of the HIV-1 TAT peptide across lipid membranes. *Proc Natl Acad Sci USA* 104: 20805–20810.
44. Vivès, E, Brodin, P and Lebleu, B (1997). A truncated HIV-1 Tat protein basic domain rapidly translocates through the plasma membrane and accumulates in the cell nucleus. *J Biol Chem* 272: 16010–16017.
45. Rajasekaran, P, Alexander, JC, Seleen, MN, Jain, N, Sriranganathan, N, Wattam, AR *et al.* (2013). Peptide nucleic acids inhibit growth of *Brucella suis* in pure culture and in infected murine macrophages. *Int J Antimicrob Agents* 41: 358–362.
46. Jarver, P, Langel, K, El-Andalousi, S and Langel, U (2007). Applications of cell-penetrating peptides in regulation of gene expression. *Biochem Soc Trans* 35(Pt 4): 770–774.
47. Amaral, L and Viveiros, M (2012). Why thionidazole in combination with antibiotics cures extensively drug-resistant *Mycobacterium tuberculosis* infections. *Int J Antimicrob Agents* 39: 376–380.
48. Eliopoulos, GM and Moellering, RC Jr (1982). Antibiotic synergism and antimicrobial combinations in clinical infections. *Rev Infect Dis* 4: 282–293.
49. Dryselius, R, Nekhotiaeva, N and Good, L (2005). Antimicrobial synergy between mRNA- and protein-level inhibitors. *J Antimicrob Chemother* 56: 97–103.
50. Patenge, N, Billion, A, Raasch, P, Normann, J, Wisniewska-Kucper, A, Reley, J *et al.* (2012). Identification of novel growth phase- and media-dependent small non-coding RNAs in *Streptococcus pyogenes* M49 using intergenic tiling arrays. *BMC Genomics* 13: 550.
51. Livak, KJ and Schmittgen, TD (2001). Analysis of relative gene expression data using real-time quantitative PCR and the 2^{-Delta Delta C(T)} Method. *Methods* 25: 402–406.



Molecular Therapy–Nucleic Acids is an open-access journal published by **Nature Publishing Group**. This work is licensed under a **Creative Commons Attribution-NonCommercial-NoDerivative Works 3.0 License**. To view a copy of this license, visit <http://creativecommons.org/licenses/by-nc-nd/3.0/>

Supplementary Information accompanies this paper on the Molecular Therapy–Nucleic Acids website (<http://www.nature.com/mtna>)

RESEARCH ARTICLE

Open Access

Identification of novel growth phase- and media-dependent small non-coding RNAs in *Streptococcus pyogenes* M49 using intergenic tiling arrays

Nadja Patenge¹, André Billion², Peter Raasch³, Jana Normann¹, Aleksandra Wisniewska-Kucper¹, Julia Reteý⁴, Valesca Boisguérin⁵, Thomas Hartsch⁴, Torsten Hain² and Bernd Kreikemeyer^{1*}

Abstract

Background: Small non-coding RNAs (sRNAs) have attracted attention as a new class of gene regulators in both eukaryotes and bacteria. Genome-wide screening methods have been successfully applied in Gram-negative bacteria to identify sRNA regulators. Many sRNAs are well characterized, including their target mRNAs and mode of action. In comparison, little is known about sRNAs in Gram-positive pathogens. In this study, we identified novel sRNAs in the exclusively human pathogen *Streptococcus pyogenes* M49 (Group A *Streptococcus*, GAS M49), employing a whole genome intergenic tiling array approach. GAS is an important pathogen that causes diseases ranging from mild superficial infections of the skin and mucous membranes of the naso-pharynx, to severe toxic and invasive diseases.

Results: We identified 55 putative sRNAs in GAS M49 that were expressed during growth. Of these, 42 were novel. Some of the newly-identified sRNAs belonged to one of the common non-coding RNA families described in the Rfam database. Comparison of the results of our screen with the outcome of two recently published bioinformatics tools showed a low level of overlap between putative sRNA genes. Previously, 40 potential sRNAs have been reported to be expressed in a GAS MIT1 serotype, as detected by a whole genome intergenic tiling array approach. Our screen detected 12 putative sRNA genes that were expressed in both strains. Twenty sRNA candidates appeared to be regulated in a medium-dependent fashion, while eight sRNA genes were regulated throughout growth in chemically defined medium. Expression of candidate genes was verified by reverse transcriptase-qPCR. For a subset of sRNAs, the transcriptional start was determined by 5' rapid amplification of cDNA ends-PCR (RACE-PCR) analysis.

Conclusions: In accord with the results of previous studies, we found little overlap between different screening methods, which underlines the fact that a comprehensive analysis of sRNAs expressed by a given organism requires the complementary use of different methods and the investigation of several environmental conditions. Despite a high conservation of sRNA genes within streptococci, the expression of sRNAs appears to be strain specific.

Keywords: *Streptococcus pyogenes*, Small noncoding RNAs, Virulence, Transcriptional regulation, Pathogenesis

* Correspondence: Bernd.Kreikemeyer@med.uni-rostock.de
¹Institute of Medical Microbiology and Hospital Hygiene, University of Rostock, Schillingallee 70, 18057, Rostock, Germany
 Full list of author information is available at the end of the article

Background

In recent years, the role of small non-coding RNAs (sRNAs) in regulation of bacterial gene expression has become more evident; however, the large number of sRNAs identified in different bacterial species was unexpected [1-3]. Even though sRNAs were conventionally regarded as inhibitory antisense regulators, a significant number of sRNAs that activate bacterial gene expression have been characterized [4]. Furthermore, regulatory mechanisms include both the stabilization and destabilization of target transcripts [5]. Bacterial sRNAs influence the expression of genes involved in processes as diverse as stress response, sugar metabolism, and surface composition [6-10]. With sRNAs representing a whole new level of post-transcriptional regulation, it is no surprise that these molecules play an important role in the tightly controlled expression of virulence factors in many pathogens [11,12].

We were interested in the regulatory sRNAome of *Streptococcus pyogenes* (group A streptococci, GAS), a common, exclusively human pathogen that causes a variety of diseases. GAS is responsible for mild superficial infections of the skin (impetigo contagiosa) and mucosal membranes (pharyngitis and tonsillitis). Additionally, there is a high global burden of severe GAS diseases such as post-streptococcal sequelae, and severe systemic (streptococcal toxic-shock-like syndrome) or invasive infections (necrotizing fasciitis), leading to over 500,000 deaths per year [13,14]. The controlled expression of virulence factors plays a role in GAS infection, persistence in the host, and development of invasive diseases, which makes the investigation of virulence factors and their regulation a research priority. GAS expresses a large number of virulence factor genes coding for a variety of proteins, including surface components, lytic enzymes, proteinases, cytotoxins, superantigens, and immunoprotective proteins, that are controlled at least partially by the 30 stand-alone transcriptional regulators and 13 two-component systems identified to date in GAS [15]. Virulence factor expression in GAS is highly responsive to environmental conditions and greatly depends on the growth phase.

Little is known, however, about the importance of sRNAs for virulence-related gene regulation in GAS. An overview of small RNAs in streptococci is nicely presented by Le Rhun and Charpentier [16]. Several individual sRNAs have been identified in GAS [17,18], with many more predicted by bioinformatic screens [12,19]. Previous analysis of sRNA expression in a GAS MIT1 serotype using an intergenic tiling array approach identified 40 potential sRNAs, with a very low predicted overlap with candidate genes [20]. The authors concluded that sRNA expression in GAS is serotype-dependent. The current work focused on sRNA expression in the skin isolate GAS M49. An intergenic tiling array identified 42 novel and 13 known sRNAs. Data from this

experiment were compared to the results of the former GAS MIT1 study, and to predictions of two recently published bioinformatics tools [19,21]. Additionally, we tested the regulation of sRNA expression in correlation to growth media and growth phase. We found very little overlap between the different screening methods, which underlines the importance of using several complementary methods, as well as several environmental conditions, to attain a comprehensive analysis of bacterial sRNAomes.

Results

Identification of sRNAs in the intergenic regions of GAS M49
Custom intergenic tiling arrays representing the genome of *S. pyogenes* NZ131 (NCBI accession number: NC_011375) were designed to detect the expression of potential sRNAs. A total of 17,823 50-mer probes with an overlap of 15 bp were synthesized to cover the intergenic regions, with 9,082 probes representing the positive strand and 8,741 probes covering the negative strand. Additionally, 174 probes were designed as control probes covering tRNA genes or genes coding for known sRNAs. For example, we probed for *fisX* [17], SR914400, and SR1754950 [20], all of which were detected in our experiments. Genedata Selector software was used to integrate genomes, tiling array probe sequences, sRNA predictions, and experimental data. Expression data were analysed in their genomic- and sequence-based contexts (Genedata AG).

Total RNA for the tiling array experiments was isolated from GAS M49 grown in chemically defined medium (CDM). Samples were taken from four biological replicates during both mid-log growth phase ($OD_{600} = 0.4-0.6$) and stationary growth phase ($OD_{600} = 1.2$). A signal intensity of >300 was set as a threshold. A positive signal required that a minimum of one probe specific for one strand showed an intensity above the threshold in at least three replicates. Intergenic regions featuring high intensities on both strands were manually removed following the analysis.

We identified a total of 55 putative sRNAs in GAS M49 that were expressed during growth in CDM, 42 of which were novel. Computational functional prediction revealed that a subset of the newly identified RNAs included molecules with similarities to one of the common non-coding RNA families included in the Rfam database [22]. The database covers functional categories of non-coding RNAs determined from multiple sequence alignments. Using the Rfam database, we predicted functions for 14 putative sRNAs. One of these RNAs was predicted to be the structural RNA of the bacterial signal recognition particle (SRP), and another was predicted to be the bacterial RNase P RNA. Further functional categories included three T-box leader elements, three CRISPR family members, one tmRNA, and one endoribonuclease, RNaseP_bact_b (Table 1). Table 1 contains a summary of the

Table 1 *S. pyogenes* M49 sRNAs, genomic location, Rfam predictions, and conservation across streptococcal genomes

No	ID	Left nucleotide	Right nucleotide	Size (nt)	Strand	Upstream adjacent gene	Downstream adjacent gene	Rfam and MOSES prediction	Previously published	Conservation
1	sRNASpy490131	141429	141478	49	-	ntpK	ntpE			a
2	sRNASpy490186c	194707	194791	84	+	Spy49_0186c	speG	SRP_bact	[37]	c
3	sRNASpy490206	216807 ^d	217021	215	+ ^e	fasA	mpA	MOSES2	fasX [i7]	b
4	sRNASpy490229	238850	238899	49	+	prgA	rpsL			b
5	sRNASpy490238	248530	248579	49	+	Spy49_0238	bacA			a
6	sRNASpy490241	251595	251644	49	+	rgpG	Spy49_0242			a
7	sRNASpy490305	318826	318910	84	+	Spy49_0305	Spy49_0306	23S-methyl		b
8	sRNASpy490306	319622	319776	154	+	Spy49_0306	Spy49_0307	FMN	RNA319780 [20]	b
9	sRNASpy490348	362857	362906	49	+	Spy49_0348	Spy49_0349c	MOSES6		a
10	sRNASpy490366c	373806	373855	49	+	Spy49_0366c	Spy49_0367c			-
11	sRNASpy490370	376843	376892	49	+	Spy49_0370	Spy49_0371			a
12	sRNASpy490380c	385431 ^d	385526	95	+ ^e	Spy49_0380c	mtsA			b
13	sRNASpy490388	393522	393571	49	+	rplA	pyrH			a
14	sRNASpy490434	431752	431836	84	+	Spy49_0434	thrS	T-box		b
15	sRNASpy490483c	476503 ^d	476600	97	+ ^e	Spy49_0483c	bgIG			b
16	sRNASpy490493	486133	486182	49	+	Spy49_0493	ptsK			a
17	sRNASpy490504	495351	495400	49	-	Spy49_0504	Spy49_0505c			a
18	sRNASpy490592	594852	594936	84	+	Spy49_0592	pheS			b
19	sRNASpy490727	733841	733890	49	-	Spy49_0727	Spy49_0728			a
20	sRNASpy490822	820820	820996 ^d	176	- ^e	Spy49_0822	Spy49_0823	CRISPR	RNA772970 [20]	c
21	sRNASpy490827	827456	827785	329	+	Spy49_0827	Spy49_0828	CRISPR MOSES14		a
22	sRNASpy490845c	846977	847061	84	+	trmE	rplJ	L10_leader		c
23	sRNASpy490948c	941583	941657 ^d	74	-	Spy49_0948c	guaA			a
24	sRNASpy490957c	950434	950518	84	- ^e	Spy49_0957c	Spy49_0958c		SR914400 [20]	b
25	sRNASpy491007c	1000709	1000828	119	+	pcrA	Spy49_1008	Glycine		b
26	sRNASpy491023c	1019382	1019746	364	+	Spy49_1023c	Spy49_1024	tmRNA	RNA983400 [20]	b
27	sRNASpy491061c	184794	184878	84	+	Spy49_1061c	Spy49_0176			c
28	sRNASpy491095c	1092894	1092943	49	-	ptsH	nrdH			c
29	sRNASpy491122c	1117169	1117218	49	-	sodM	holA			b
30	sRNASpy491163c	1156488	1156537	49	-	Spy49_1163c	clpE			a
31	sRNASpy491167c	1163270	1163319	49	-	ileS	divIVA	T-box		-
32	sRNASpy491206c	1201615	1201734	119	-	ccdA	Spy49_1207c	MOSES16	RNA1239700 [20]	a
33	sRNASpy491217c	1214010	1214059	49	-	Spy49_1217c	Spy49_1218c		SRI1251900 [20]	b
34	sRNASpy491243	1246370	1246419	49	+	Spy49_1243	Spy49_1244			a
35	sRNASpy491275c	1282084	1282413	329	-	Spy49_1275c	Spy49_1276c	RNaseP_bact b	RNA1320100 [20]	c
36	sRNASpy491311c	1321638	1321853 ^d	84	- ^e	glyQ	Spy49_1312c			b
37	sRNASpy491336c	1341554	1341603	49	+	rbfA	infB			b
38	sRNASpy491340c	1346300	1346349	49	-	nusA	Spy49_1341c			b
39	sRNASpy491354	1357803	1357852	49	-	manL	manM			b
40	sRNASpy491357	1360204	1360323	119	+	Spy49_1357	serS	T-box	RNA1439100 [20]	b
41	sRNASpy491409c	1413359	1413408	49	-	acpS	secA			a
42	sRNASpy491489c	1489011	1489060	49	+	Spy49_1489c	Spy49_1491c			b

Table 1 5. pyogenes M49 sRNAs, genomic location, Rfam predictions, and conservation across streptococcal genomes (Continued)

43	sRNASpy491555c	1528842	1528891	49	-	Spy49_1555c	Spy49_1556c			a
44	sRNASpy491560c	1533843	1533892	49	-	Spy49_1560c	pyrG			a
45	sRNASpy491561c	1535755	1535804	49	-	pyrG	rpoE			c
46	sRNASpy491562c	1536613	1536662	49	-	rpoE	tig			a
47	sRNASpy491591	1571896	1571945	49	-	lacR2	Spy49_1592	MOSES18	SR1604140 [20]	a
48	sRNASpy491596c	1574723	1574807	84	-	rplM 505	Spy49_1597c	L13_leader		c
49	sRNASpy491671c	1654859	1654908	49	-	emm49	Spy49_1672c			a
50	sRNASpy491707c	1693440	1693489	49	-	Spy49_1707c	Spy49_1708			a
51	sRNASpy491713	1698142	1698191	49	+	Spy49_1713	Spy49_1714c		SR1719800 [20]	a
52	sRNASpy491718c	1704471	1704525	54	-	ctsR	csp			a
53	sRNASpy491732c	1724321	1724370	49	+	Spy49_1732c	rpsB		SR1745900 [20]	b
54	sRNASpy491738	1733300	1733433 ^d	133	-	Spy49_1738	Spy49_1739c		SR1754950 [20]	b
55	sRNASpy491769c	1763496	1763545	49	+	his5	rpmF			b

Coordinates and gene designations of adjacent genes are relative to the *S. pyogenes* NZ131 genome (NCBI accession number: NC_011375).

^a *Streptococcus pyogenes*.

^b Beta-haemolytic streptococci.

^c Non-beta-haemolytic streptococci.

^d Transcriptional start site determined by 5' RACE.

^e Strand confirmed by gene specific RT-PCR.

information pertaining to all 55 candidate sRNAs, including the flanking genes, Rfam prediction, and conservation across other genomes. Five putative sRNA sequences overlapped with adjacent ORFs on the same strand. Functional studies will be necessary to clarify whether the corresponding sRNAs are transcribed independently. The overall GC content of all 55 sRNA candidate sequences was 38.3%. This correlates with the GC content of the whole NZ131 genome (38.0%). No specific strand prevalence and no clustering in specific genomic regions were observed for the regulatory sRNA genes. The replication-related gene orientation bias of the protein coding genes [23,24] was mirrored by the sRNA gene candidates. A circular depiction was created with the Artemis DNAPlotter tool [25] (Figure 1) to visualize the sRNA genes in the context of the NZ131 genome.

In a previous bioinformatic approach (MOSES), 20 probable candidates were predicted [19]. In our array analysis, expression of five of the predicted sRNAs was confirmed under the conditions studied (Table 1). Furthermore, we detected 12 streptococcal RNAs that were previously identified by Perez et al. [20] (Table 1). The phylogenetic conservation of the putative sRNAs was tested by BLAST analysis, and the taxonomic classification was presented following the nomenclature of Facklam [26]. The tiling array technique with overlapping probes did not allow us to detect an accurate start site for the respective sRNA genes. Thus, we described the nucleotides represented by the active probes as the preliminary start and end (Table 1).

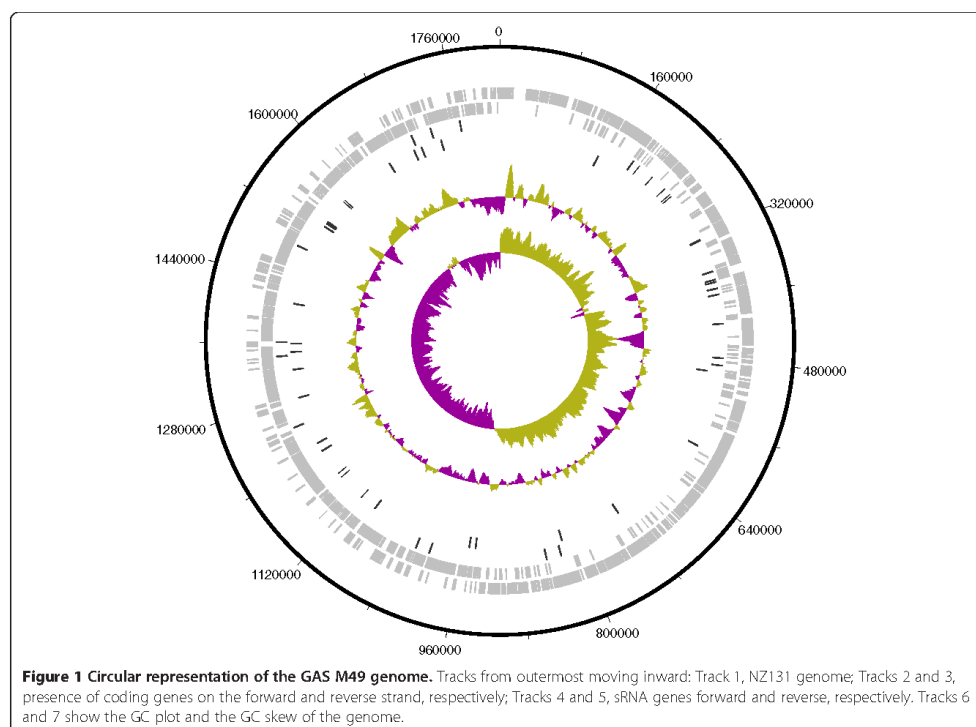
For a subset of six candidate sRNA genes, we determined the transcriptional start site (TSS) of the sRNA

molecules using the 5' rapid amplification of cDNA ends- (5' RACE) technology (Invitrogen). The TSS of the analysed sRNAs is shown in Table 1. 5' RACE was conducted for two known sRNA genes, *fasX* and sRNASpy490822 (CRISPR1), for one candidate predicted by MOSES (MOSES4), and for three novel sRNA candidates, sRNASpy490483c, sRNASpy491311c, and sRNASpy491738. The results of the 5' RACE analysis are shown in Figure 2. Promoter and terminator predictions for the respective sRNA candidate genes are also included.

Comparison of the sRNA expression data using different sRNA screens

The tiling array data were compared with the prediction results of two recently published bioinformatics tools, sRNAScanner [21] and MOSES [19]. As shown in Figure 3A, the overlap between the GAS M49 array data and the sRNA predictions performed with the sequence of the NZ131 genome was minimal. From 20 MOSES candidates, five were detected in the tiling array analysis, while from 137 sRNAScanner predictions, 11 showed a signal in the array. Eight putative sRNAs were selected by both programs. There was only one sRNA that was predicted by both algorithms and was also detected in the tiling array (Figure 3A). The general accuracy of the three independent screens was supported by the fact that this mutual candidate was the known streptococcal sRNA FASX [17].

We also compared our tiling array data with a previously published sRNA microarray study in GAS M1T1 [20]. The previous study identified 40 putative sRNAs.



Even though the sequences of the candidates were conserved across streptococcal genomes, serotype-specific variation of sRNA transcript abundance was observed in northern blot experiments. Screening of GAS MIT1 was conducted with cells grown in complex medium [20], whereas the expression experiments in this study were performed with GAS M49 grown in CDM. Consequently, we found only a limited overlap between the two microarray screens (Figure 3B). Twelve sRNA candidates were detected in both strains.

Analysis of common motifs in the GAS M49 sRNA population

To identify putative functional regions within the sRNA candidates, all sequences were screened for common features by motif-based sequence analysis using MEME SUITE [27]. The occurrence of shared sequence motifs in different sRNA species could be an indication of common structural properties with functional significance in this region. Seven motifs were identified with consensus sequences with p -values $< 1.0 \times 10^{-7}$, spanning 9–27 base pairs (Figure 4). Putative motif sequences were compared to members of the Rfam database families, and

were subjected to TOMTOM [28] motif analysis using the RegTransBase prokaryotic database. Candidates sRNASpy490592 and sRNASpy491336c shared a 14 bp consensus sequence with no apparent known function (motif 4, Figure 4). For all other identified motifs, a known function could be assigned to the respective candidates. The corresponding RNAs were either predicted to be RNAs with non-regulatory functions, e.g. RNaseP (motif 5, Figure 4), or more typically, to represent *cis*-regulatory RNA elements, e.g. FMN riboswitch or MET box (motif 6 and motif 7, Figure 4).

Regulated expression of sRNA genes in GAS M49

Regulation of sRNA gene expression in GAS M49 under different growth conditions was studied by intergenic tiling array analyses. Total RNA was isolated from bacteria grown in CDM, BHI, or THY. Samples were collected in the exponential and stationary phases. Transcript level changes were expressed as the \log_2 signal ratio between conditions, and are listed in Table 2. sRNA gene expression was considered significantly different when the \log_2 ratio of the signals was ≤ -1.58 or ≥ 1.58 . Twenty-four sRNA genes were regulated in a growth phase- and/or medium-

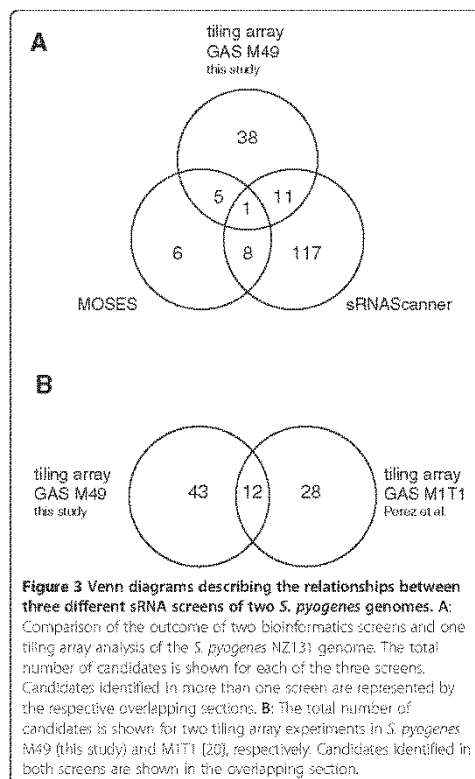


dependent fashion. During growth in CDM, five genes were up-regulated in the stationary growth phase compared to the exponential growth phase, whereas three genes were down-regulated. One of the down-regulated sRNA genes was *fasX*. This is in accord with previous results, where a reduction in *fasX* transcript abundance in the stationary growth phase was detected by northern blot analysis [17]. This observation was also confirmed by qRT-PCR analyses (Figure 5B). Comparison of sRNA gene expression during growth in THY with expression during growth in CDM revealed differential expression of 17 sRNA genes. Of these, 13 genes were down-regulated and four up-regulated in THY. Growth in BHI led to the detection of 12 media-dependent controlled sRNA genes. Nine genes were down-regulated and three were up-regulated during growth in BHI compared to growth in CDM. From the 20 sRNA genes that showed media-dependent regulation, seven were regulated in both THY and BHI, and showed the same direction of regulation compared to CDM. Twelve sRNA

genes were exclusively regulated in one of the two media, and only one gene was down-regulated in THY but up-regulated in BHI compared to CDM. These results are in accord with the fact that both media THY and BHI are complex media, as opposed to the synthetic medium CDM, which forces the bacteria to synthesize a number of components essential for growth. Thus, in CDM, changes in bacterial metabolism are necessary for successful growth and require adaption of the bacterial transcriptome, including the sRNAome.

Validation of sRNA expression by qRT-PCR and northern blot analyses

Expression of sRNA candidates by GAS M49 was tested by gene-specific reverse transcription followed by real-time PCR analysis. Experimental expression validation was performed for the RNAs FASX and sRNASpy490822 (CRISPR1), for the sRNA scan7, which was predicted using sRNAscanner [21], and for three more candidates



identified by tiling arrays in this study (sRNASpy490380c, sRNASpy490957c, and sRNASpy491311c). The expression of the candidates in GAS M49 was verified. Moreover, we confirmed the orientation of the sRNA genes by employing single gene-specific primers for the reverse transcription reaction. Three reactions were performed in parallel: one including the forward primer, one including the reverse primer, and one without any primers. Signals were only detected in samples containing the primer complementary to the coding strand of the respective gene (data not shown). We compared sRNA expression of GAS M49 cultured in CDM medium and THY broth throughout growth (Figure 5). 5S RNA was used as an internal control for normalization, and was expressed in comparable amounts under all conditions tested in this experiment. Expression of *fasX* was equivalent during growth in CDM and THY (Figure 5A). *FASX* was down-regulated in the stationary phase, an observation that confirmed the array data and previously published results from northern blot analyses [17]. We did not detect strong regulation during CRISPR1, sRNASpy490957c, or sRNASpy491311c during growth in

CDM (Figure 5B). In contrast, scan7 was highly up-regulated in the stationary phase (Figure 5B). The expression of sRNASpy490380c was much higher in THY compared to CDM (almost 100-fold, data not shown). During growth in CDM, no changes in the low level expression of sRNASpy490380c were observed (data not shown).

To further verify candidate gene expression, northern blot analysis of the same putative sRNA genes was performed (Figure 6). This method allows the determination of approximate transcript sizes. Probes specific for 5S RNA and *FASX* were included as controls. The apparent molecular weight of candidates CRISPR1, sRNASpy490380c, sRNASpy490483c, sRNASpy491311c, and scan7 corresponded to the length predicted by 5' RACE determination. The CRISPR transcript, tracrRNA, showed a band at the expected size of 176 nucleotides, as well as several smaller bands that were likely the result of RNA processing, as observed previously in GAS M1T1 [29] (Additional file 1A). For the putative sRNASpy490957c, transcript analysis by 5' RACE predicted a 161 nt full-length product, including the terminator region. However, the most prominent band detected by northern blot analysis migrated at approximately 80 nt. Low intensity bands were detected at approximately 90 nt and 160 nt (Additional file 1B), which might indicate post-transcriptional sRNA processing.

Discussion

Bacterial gene regulation by sRNAs has gained a lot of attention in recent years, because it plays an important role in many cellular processes, including response to environmental changes, growth, and pathogenesis. There is an intriguingly large diversity of regulatory mechanisms, including *cis*- and *trans*-acting sRNAs, untranslated regions, and riboswitches. Some sRNA molecules act as repressors of translation and destabilize mRNA transcripts, but others act by activating and stabilizing target mRNAs [30-32]. One of the best characterized sRNAs in GAS is *FASX*, which is involved in virulence-related gene regulation [17,33]. Knock-out mutants of *fasX* show a reduced expression of secreted virulence factors such as streptokinase and streptolysin S. The mechanism for streptokinase gene (*ska*) expression control is the stabilization of the *ska* transcript [33]. Lack of *FASX-ska*-mRNA-interaction in the *fasX* deletion mutant decreased transcript levels, and consequently decreased streptokinase protein abundance.

A second example of a regulatory RNA in GAS is the untranslated mRNA of the streptococcal pleiotropic effect locus (*pel*), which contains *sagA*, the structural gene for streptolysin S. This region was described as a positive regulator of important streptococcal virulence factors, including M-protein, Sic, and SpeB [34]. Strain specificity of PEL function is indicated by the fact that *emm* transcription was not affected in a *sagA*-deficient mutant with a M6 background [35]. Similar results have

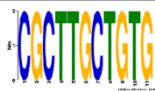
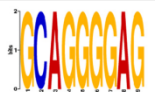
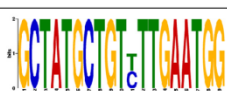

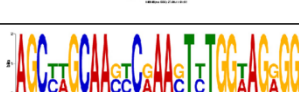

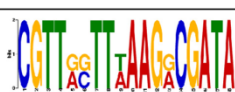
No	Motif	sRNA candidates	p-value	Function prediction
1		sRNASpy491167c sRNASpy491562c	8.45e-08 8.45e-08	T-box ^a
2		sRNASpy490845c sRNASpy490957c	8.85e-07 8.85e-07	L10_leader ^a
3		sRNASpy490822 sRNASpy490827	7.03e-12 2.68e-12	CRISPR ^a
4		sRNASpy490592 sRNASpy491336c	1.91e-09 4.99e-09	unknown function
5		sRNASpy491275c sRNASpy491732c	5.90e-15 2.68e-15	RNaseP bact_b ^a
6		sRNASpy490306 sRNASpy490504	1.91e-09 4.99e-09	FMN ^a
7		sRNASpy491217c sRNASpy491713	5.62e-11 3.85e-10	MET box ^b

Figure 4 Shared sequence motifs in sRNA candidates. ^aRfam, ^bTOMTOM.

been obtained in GAS M1 and M18 Tn916 *sagA* mutant strains [36]. Additionally, *pel* deletion mutant analysis of four MIT1 GAS isolates did not identify any regulatory function for the *pel* sRNA in this serotype [20].

Another, more recently described untranslated RNA with influence on streptococcal virulence is the 4.5S RNA, a component of the bacterial signal recognition particle (SRP) [37]. While the 4.5S RNA gene is not essential, mutation impairs bacterial growth, lowers virulence factor secretion, and reduces virulence in a mouse infection model.

Recently, several whole genome sRNA screens in Gram-positive bacteria, employing either tiling array or next generation sequencing approaches, revealed an unexpected number of potential sRNAs in several pathogenic species [38-42]. In this context, it is likely that GAS

expresses more sRNAs responsible for virulence gene expression control. One whole-genome intergenic tiling array screen of GAS MIT1 identified approximately 40 sRNAs that were expressed during the exponential growth phase in cells cultivated in THY complex medium [20]. The GAS M49 sRNAome in the present study was determined using cells grown in CDM. From 55 putative sRNAs in GAS M49, only 12 were detected previously in the GAS MIT1 screen (Figure 3B). This result is in accord with the concept that sRNA expression is serotype-dependent and regulated by environmental stimuli. Consequently, we detected media- and growth-phase-dependent sRNA gene regulation in the tiling array expression analysis, or by qRT-PCR of selected candidate genes. It would be interesting to monitor sRNA gene expression regulation under infection-relevant conditions.

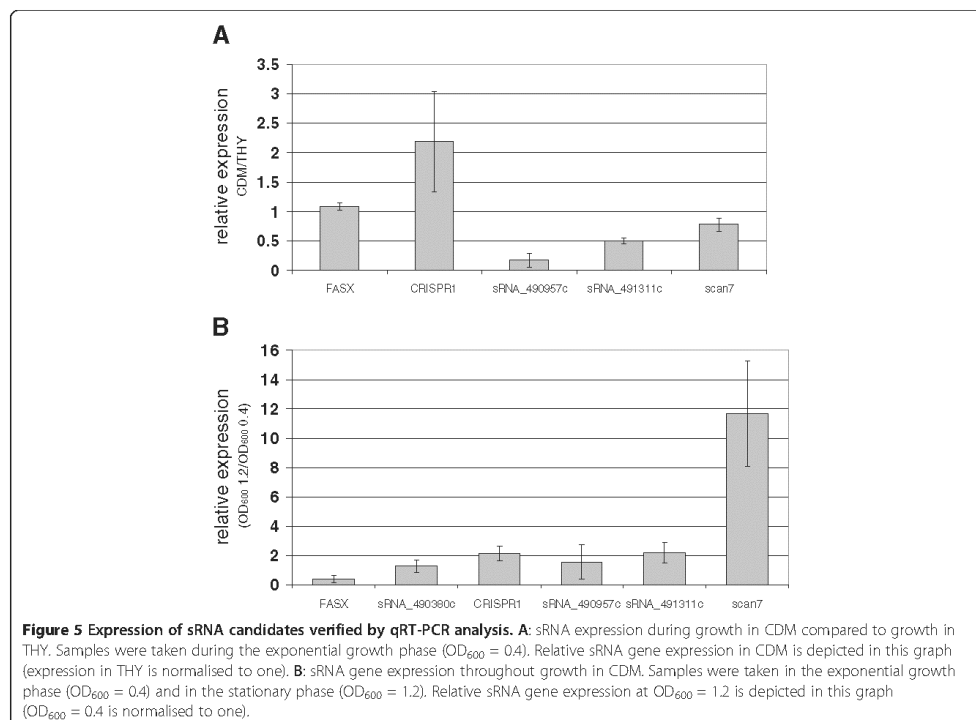
Table 2 Regulation of *S. pyogenes* M49 sRNA gene expression dependent on culture medium and growth phase

No	ID	THY vs CDM exponential growth phase	THY vs CDM stationary growth phase	BHI vs CDM exponential growth phase	BHI vs CDM stationary growth phase	Stationary vs exponential in CDM
1	sRNASpy490186c		-2,72			
2	sRNASpy490206	-1,78				-2,00
3	sRNASpy490238	3,33				
4	sRNASpy490305	-2,50	-3,03	-2,10	-3,59	
5	sRNASpy490306				1,72	
6	sRNASpy490348	3,42				
7	sRNASpy490370				-2,51	
8	sRNASpy490380c		-3,02	-2,28	-3,82	
9	sRNASpy490493	2,18				
10	sRNASpy490592					1,81
11	sRNASpy490827	-1,89				
12	sRNASpy490845c				-1,98	2,03
13	sRNASpy490957c		-2,67			
14	sRNASpy491007c		-1,73		-1,81	1,94
15	sRNASpy491023c	-1,84		1,92	3,54	
16	sRNASpy491206c	1,58			2,65	-2,41
17	sRNASpy491311c					-2,20
18	sRNASpy491561c	-1,99				
19	sRNASpy491596c		-1,60	-1,88		
20	sRNASpy491707c					1,68
21	sRNASpy491713					1,76
22	sRNASpy491718c			-1,71		
23	sRNASpy491732c		-2,38		-3,60	
24	sRNASpy491738		-3,40	-2,07	-4,30	

Clustered, regularly interspaced, short palindromic repeat (CRISPR) loci represent an adaptive RNA-based immune system that protects bacteria and archaea from horizontal transfer of phage and plasmid DNA [43]. Among the putative sRNA genes detected in GAS M49 by the tiling array approach, two sequences were categorised by the Rfam prediction program as CRISPR-related RNAs (Table 1). sRNASpy490822 and sRNASpy490827 are encoded by the system II (Nmni/CASS4 subtype) [44] CRISPR/Cas locus, which was characterized recently by differential RNA sequencing in GAS SF370 (M1 serotype) [29]. Our data suggest that this locus is also active in GAS M49. Expression of sRNASpy490822 was confirmed by RT-PCR on the opposite strand of the CRISPR-associated genes under all conditions tested in this study. This transcript corresponds to the *trans*-activating CRISPR RNA (tracrRNA), which is responsible for the maturation of CRISPR RNA in concert with RNase III and the CRISPR-associated Csn1 protein [29]. A third CRISPR-related RNA detected in our expression screen, sRNASpy491206c, is encoded in the system I-C (Dvulg/CASS subtype) [44]

CRISPR/Cas locus, which is also conserved in streptococcal genomes. In contrast to our array data, this locus appeared to be silent in GAS SF370, where no expression was detected in the differential RNA sequencing approach [29]. Even though the CRISPR loci are conserved throughout GAS genomes, the activity of different CRISPR subtypes appears to be serotype-specific.

In the early years of sRNA research, many bioinformatic prediction tools were developed. One of the most prominent programs was the SIPHT tool, which has been used for many bacterial species [45,46]. However, comparison of the prediction results with the actual *in vivo* expression of sRNAs often revealed very little overlap between the different screening methods [20,41,47]. The reasons for this discrepancy may be the limitations of the prediction programs as well as the fact that not all sRNAs are expressed under all conditions. The development of sRNA prediction software with improved properties is on-going. We compared our tiling array data with the prediction results of two recently published bioinformatics tools, sRNAScanner [21] and



MOSES [19]. As depicted in Figure 3A, the overlap between the tiling array expression data and the sRNA predictions was low. From the 20 most probable candidates of the MOSES analysis, 25% were expressed in GAS M49, whereas 8% of the predicted sRNAScanner predictions were found in the array analysis. Even the overlap between the two bioinformatics data sets was low. The only sRNA that was detected in all three screens was the previously characterized sRNA FASX [17]. These results strongly suggest that a comprehensive analysis of bacterial genomes requires the combination of mathematical predictions with the collection of expression data. In the long term, testing of different conditions, especially mimicking *in vivo* situations by employing infection models, might lead to an increased overlap of expression detection and bioinformatics analyses.

Conclusions

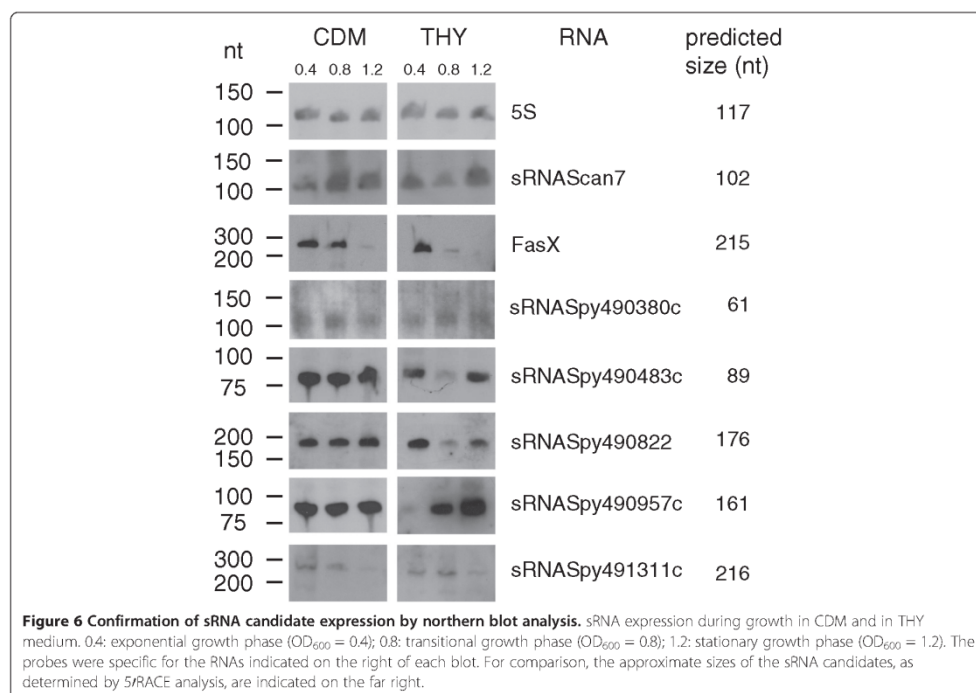
We present here the identification of 55 putative sRNAs in GAS M49 by an intergenic tiling array approach. The candidate sRNA genes were expressed during growth in CDM. Forty-two of the RNAs were novel, whereas 13 RNAs have been described previously. The sequences of

most of the candidates were conserved over streptococcal genomes. However, comparison of our GAS M49 sRNA expression data to another array analysis of a GAS M1 strain, and to two *in silico* screening methods, revealed little overlap between the different approaches. Thus, the investigation of several conditions and the combination of screening tools will be necessary to gain a comprehensive understanding of the abundance of sRNAs in GAS. The identification of novel differentially expressed sRNA genes will enhance our understanding of virulence related gene regulation in GAS. To account for specific expression patterns of putative sRNAs, infection relevant conditions combined with next generation RNA sequencing should be employed to investigate sRNA dependent regulatory networks in GAS.

Methods

Bacterial strains and culture conditions

GAS serotype M49 strain 591, a clinical isolate from a skin infection, was kindly provided by R. Lütticken (Aachen, Germany). The GAS strain was cultured in chemically defined medium (CDM) [48], Todd-Hewitt broth (Invitrogen) supplemented with 0.5% yeast extract



(THY; Invitrogen), or Brain-Heart-Infusion medium (BHI; Oxoid), as indicated, at 37°C under a 5% CO₂/20% O₂ atmosphere.

RNA isolation

Total bacterial RNA from cultures grown to exponential and stationary phase of growth was isolated using the FastRNAProBlue Kit from MP Biomedicals according to manufacturer's instructions. The purified total RNA was digested with DNaseI (Ambion) to remove remaining traces of chromosomal DNA. The RNA preparation was treated with 10 U of DNaseI for 30 min at 37°C. The enzyme was subsequently heat inactivated at 72°C for 5 min.

Enrichment of small RNAs

Five micrograms of total RNA were fractionated using the Ambion FlashPAGE Fractionator, Ambion FlashPAGE Precast Gels, and the Ambion FlashPAGE Buffer Kit, following manufacturer's instructions. To collect the fraction of RNA molecules <200 nucleotides in length, the protocol was modified by increasing the running time from 12 min to up to 45 min at 75 V.

Labelling

The small RNA fraction was ethanol-precipitated overnight at -20°C. The RNA was pelleted by centrifugation, dissolved in nuclease-free water, and labelled using the Ambion mirVana miRNA Labeling Kit following the manufacturer's instructions. In brief, this kit involves two main steps; the 3' amine-modified tailing reaction, and labelling with NHS-esters. Poly(A) Polymerase and a mixture of unmodified and amine-modified nucleotides were used to add a 20–50 nucleotide tail to the 3' end of each RNA molecule in the sample. The amine-modified RNA molecules were purified and coupled to amine-reactive labelled biotin moieties as NHS-esters.

Design and synthesis of microfluidic microarrays

We used a microfluidic biochip (Febit Biomed) consisting of eight independent reaction chambers, the arrays, enclosed in a cartridge for fully automated processing. Each array contains 15,625 features which are synthesized *in situ* inside the microchannels using the Geniom One technology (febit biomed) [49]. The 50mer probes were designed as a whole genome tiling array, covering the intergenic regions of the *S. pyogenes* NZ131 genome

(NCBI accession number: NC_011375). The forward and reverse oriented probes were synthesized in separate arrays. Thus, two arrays per sample were used.

Microarray hybridization and detection

All hybridization and detection steps were carried out using a Geniom RT Analyzer (febit biomed). Hybridizations were performed overnight (16 hours) at 42°C. Subsequently, biotin was detected with streptavidin-phycoerythrin (SAPE). A signal amplification step was added using biotinylated anti-streptavidin antibodies (Vector Laboratories) and a second incubation with SAPE (Invitrogen). Signal detection using the appropriate filter set (Cy3) of the Geniom device employed the auto-exposure function of the Geniom software. The data discussed in this publication have been deposited in the NCBI Gene Expression Omnibus [50] and are accessible through GEO Series accession number GSE31228 (<http://www.ncbi.nlm.nih.gov/geo/query/acc.cgi?acc=GSE31228>).

Microarray data analysis

Raw intensities were analysed and extracted using Geniom Wizard software (febit biomed) as a tab delimited text file. The data were then converted into a matrix, with rows corresponding to the features and columns corresponding to the different samples. Data analysis was performed using GeneSpring GX (version 11) software (Agilent Technologies). The array background was calculated as the median signal intensity of all "blank-control" features on the array. Data were background corrected and then normalized using quantile normalization [51]. Following normalization, a quality control step was performed that removed all data sets with a correlation coefficient less than 0.9 compared to the corresponding biological replicates. Of the original four biological replicate data sets representing cells grown in CDM, at least three were included in the analysis. The remaining probes of the biological replicates required intensity values greater than 300 on all three arrays. Regions that showed signals on probes of both strands were manually removed following the primary analysis. The statistical significance of the determined signals was tested by unpaired student's t-test with a false discovery rate of 5%. Resulting data were combined with gene information from the flanking coding regions. Terminators and promoters were predicted by TransTermHP [52] (http://transterm.cbcb.umd.edu/ft/Streptococcus_pyogenes_NZ131.ft) and BDGP Neural Network Promoter Prediction [53], and BProm (www.SoftBerry.com), respectively. To investigate sRNA gene regulation, two biological replicates of growth experiments conducted in THY or BHI were included. Following data normalization, three-fold signal intensity differences between various conditions were determined using the GeneSpring GX (version 11) software (Agilent Technologies). A motif search was

conducted using MEME Suite [27], followed by motif analyses using TOMTOM [28], (<http://meme.sdsc.edu/meme/intro.html>).

5' RACE

The transcriptional start sites of sRNA candidates were determined using 5' RACE (Invitrogen) following the manufacturer's instructions. Briefly, first strand cDNA was synthesized using gene-specific primers (Additional file 2). The original mRNA was enzymatically removed and the 3' end of the cDNA was tailed with dCTP by terminal deoxynucleotidyl transferase (TdT). PCR amplification was performed with nested, sequence-specific primers and an anchor primer provided by the 5' RACE system. Primers specific for the sRNA genes tested here are listed in Additional file 2. Following amplification, PCR products were cloned into a TOPO-TA vector (Invitrogen) and sequenced (GATC Biotech AG).

Quantitative reverse transcription PCR

Acidic phenol-extracted, DNaseI-treated total RNA was reverse transcribed to generate cDNA using the First-Strand cDNA Synthesis Kit from Invitrogen following the protocol provided by the manufacturer. For gene-specific reverse transcription (RT), three reactions were performed: two strand-specific reactions with either one forward or one reverse primer, and one control reaction without any primer. Primers were designed based on the full genome sequence of *S. pyogenes* M49 strain NZ131 (NCBI accession number: NC011375) and are listed in Additional file 3. Three independent RT experiments were performed and all subsequent PCR reactions were performed in triplicate. Primer efficiency was tested on genomic GAS M49 DNA prior to use in RT reactions. All cDNA products were amplified by PCR with two primers specific for the respective candidate sequences. Real time PCR amplification was performed with SYBR Green (Fermentas) using an ABI PRISM 7000 Sequence Detection system (Applied Biosystems). The level of 5S RNA gene transcription was used for normalization. Relative gene expression was determined by the $\Delta\Delta C_T$ method [54].

Northern blot analyses

Total RNA was isolated during exponential ($OD_{600} = 0.4$), transitional ($OD_{600} = 0.8$), and stationary ($OD_{600} = 1.2$) growth phases. RNA samples (10 μ g per growth phase) were loaded onto an 8% TBE-Urea polyacrylamide gel and separated by electrophoresis. Size standards (Ultra Low Range Ladder, Fermentas) were loaded on the same gel. RNA was electroblotted onto positively charged nylon membranes (Ambion), UV cross-linked, and probed overnight with a probe complementary to a candidate sRNA. Probes were generated by PCR with the same primers as

used for the PCR reaction in qRT-PCR experiments (listed in Additional file 3). Probes were labelled with biotin prior to hybridization (Brightstar psoralen-biotin labeling kit, Ambion). A BrightStar BioDetect Kit (Ambion) was used for detection, and autoradiography films were exposed to the luminescent blots.

Additional files

Additional file 1: A: northern blot analysis of CRISPR gene expression and transcript processing in GAS M49; B: northern blot analysis of sRNASpy490957c gene expression in GAS M49.

Additional file 2: Sequences of primers used for 5' RACE.

Additional file 3: Sequences of gene-specific primers employed for qRT-PCR.

Competing interests

We are currently applying for a patent relating to the small RNAs described in this manuscript. German Patent and Trade Mark Office (DPMA), official file number: 10 2012 104 814.2.

Authors' contributions

NP participated in the design of the study, carried out experiments, analysed the microarray data, and drafted the manuscript. JN and AWK carried out experiments. VB carried out the array probe hybridisation and participated in writing the manuscript. PR performed data analyses using the MOSES bioinformatics tool. AB and TH² participated in the design of the study and helped with data analysis and interpretation. JR and TH¹ helped with data integration, analysis and interpretation. BK conceived of the study, participated in its design and coordination, and participated in writing the manuscript. All authors read and approved the final manuscript.

Acknowledgements

The work of NP and BK was supported by a BMBF grant in the framework of the ERA-Net PathoGenoMics 2 program (FKZ 0315437B). The work of AB and TH² was supported by a BMBF grant ERA-NET Pathogenomics Network to the snCRNAomics project 62080061 to TH².

Author details

¹Institute of Medical Microbiology and Hospital Hygiene, University of Rostock, Schillingallee 70, 18057, Rostock, Germany. ²Institute of Medical Microbiology, Genome Research, Justus-Liebig-University, Frankfurter Strasse 107, 35392, Giessen, Germany. ³Systems Biology and Bioinformatics Group, University of Rostock, 18051, Rostock, Germany. ⁴Genedata AG, Margarethenstrasse 38, 4053, Basel, Switzerland. ⁵febit biomed GmbH, Im Neuenheimer Feld 519, 69120, Heidelberg, Germany.

Received: 4 July 2012 Accepted: 10 October 2012
Published: 13 October 2012

References

- Brantl S: Bacterial chromosome-encoded small regulatory RNAs. *Future Microbiol* 2009, **4**:85-103.
- Narberthus F, Vogel J: Regulatory RNAs in prokaryotes: here, there and everywhere. *Mol Microbiol* 2009, **74**:261-269.
- Waters LS, Storz G: Regulatory RNAs in bacteria. *Cell* 2009, **136**:615-628.
- Frohlich KS, Vogel J: Activation of gene expression by small RNA. *Curr Opin Microbiol* 2009, **12**:674-682.
- Podkaminski D, Vogel J: Small RNAs promote mRNA stability to activate the synthesis of virulence factors. *Mol Microbiol* 2010, **78**:1327-1331.
- Gorke B, Vogel J: Noncoding RNA control of the making and breaking of sugars. *Genes Dev* 2008, **22**:2914-2925.
- Heeb S, Valverde C, Gigot-Romney C, Haas D: Role of the stress sigma factor RpoS in GacA/RsmA-controlled secondary metabolism and resistance to oxidative stress in *Pseudomonas fluorescens* CHA0. *FEMS Microbiol Lett* 2005, **243**:251-258.
- Heldrich N, Chinnai A, Gerth U, Brantl S: The small untranslated RNA SR1 from the *Bacillus subtilis* genome is involved in the regulation of arginine catabolism. *Mol Microbiol* 2006, **62**:520-536.
- Gottesman S, McCullen CA, Guillier M, Vanderpool CK, Majdani M, Benhammou J, Thompson KM, FitzGerald PC, Sowa NA, FitzGerald DJ: Small RNA regulators and the bacterial response to stress. *Cold Spring Harb Symp Quant Biol* 2006, **71**:1-11.
- Vanderpool CK, Gottesman S: Noncoding RNAs at the membrane. *Nat Struct Mol Biol* 2005, **12**:285-286.
- Papenfuss K, Vogel J: Regulatory RNA in bacterial pathogens. *Cell Host Microbe* 2010, **8**:116-127.
- Livny J, Brenic A, Lory S, Waidor MK: Identification of 17 *Pseudomonas aeruginosa* sRNAs and prediction of sRNA-encoding genes in 10 diverse pathogens using the bioinformatic tool sRNAPredict2. *Nucleic Acids Res* 2006, **34**:3484-3493.
- Carapetis JR, Steer AC, Mulholland EK, Weber M: The global burden of group A streptococcal diseases. *Lancet Infect Dis* 2005, **5**:685-694.
- Cole JN, Barnett TC, Nizet V, Walker MI: Molecular insight into invasive group A streptococcal disease. *Nat Rev Microbiol* 2011, **9**:724-736.
- Fiedler T, Sugarsva V, Patenge N, Kreikemeyer B: Insights into *Streptococcus pyogenes* pathogenesis from transcriptome studies. *Future Microbiol* 2010, **5**:1675-1684.
- Le BA, Charpentier E: Small RNAs in streptococci. *BMC Biol* 2012, **9**:414-426.
- Kreikemeyer B, Boyle MD, Butzko BA, Heinemann M, Podbielski A: Group A streptococcal growth phase-associated virulence factor regulation by a novel operon (Fas) with homologies to two-component-type regulators requires a small RNA molecule. *Mol Microbiol* 2005, **39**:392-406.
- Roberts SA, Scott JR: RvR and the small RNA RvK: the missing links between the CovR regulatory cascade and the Mga regulon. *Mol Microbiol* 2007, **66**:1506-1522.
- Rasch P, Schmitz U, Patenge N, Vera J, Kreikemeyer B, Wolkenhauer O: Non-coding RNA detection methods combined to improve usability, reproducibility and precision. *BMC Bioinformatics* 2010, **11**:491.
- Perez N, Trevino J, Liu Z, Ho SC, Babitzke P, Sumbly P: A genome-wide analysis of small regulatory RNAs in the human pathogen group A *Streptococcus*. *PLoS One* 2009, **4**:e7668.
- Sidhar J, Sambaturu N, Sabarimathian R, Ou HY, Deng Z, Sekar K, Rafi ZA, Rajakumar K: sRNAscanner: a computational tool for intergenic small RNA detection in bacterial genomes. *PLoS One* 2010, **5**:e11970.
- Gardner PP, Dajub J, Tate JG, Nawrocki EP, Kolbe DL, Lindgreen S, Wilkinson AC, Finn RD, Griffiths-Jones S, Eddy SR, et al: Rfam: updates to the RNA families database. *Nucleic Acids Res* 2009, **37**:D136-D140.
- Tillier ER, Collins RA: The contributions of replication orientation, gene direction, and signal sequences to base-composition asymmetries in bacterial genomes. *J Mol Evol* 2000, **50**:249-257.
- Rocha EP: The replication-related organization of bacterial genomes. *Microbiology* 2004, **150**:1609-1627.
- Rutherford K, Parkhill J, Crook J, Horsnell T, Rice P, Rajandream MA, Barrell B: Artemis: sequence visualization and annotation. *Bioinformatics* 2000, **16**:944-945.
- Facklam R: What happened to the streptococci: overview of taxonomic and nomenclature changes. *Clin Microbiol Rev* 2002, **15**:615-630.
- Bailey TL, Boden M, Buske FA, Frith M, Grant CE, Clementi L, Ren J, Li WW, Noble WS: MEME SUITE: tools for motif discovery and searching. *Nucleic Acids Res* 2009, **37**:W202-W208.
- Gupta S, Stamatoyannopoulos JA, Bailey TL, Noble WS: Quantifying similarity between motifs. *Genome Biol* 2007, **8**:R24.
- Deltcheva E, Chylinski K, Sharma CM, Gonzales X, Chao Y, Pirzada ZA, Eckert MR, Vogel J, Charpentier E: CRISPR RNA maturation by trans-encoded small RNA and host factor RNase III. *Nature* 2011, **471**:602-607.
- Storz G, Vogel J, Wassarman KM: Regulation by small RNAs in bacteria: expanding frontiers. *Mol Cell* 2011, **43**:890-891.
- Thomason MK, Storz G: Bacterial antisense RNAs: how many are there, and what are they doing? *Annu Rev Genet* 2010, **44**:167-188.
- Gottesman S, Storz G: Bacterial small RNA regulators: versatile roles and rapidly evolving variations. *Cold Spring Harb Perspect Biol* 2011, **3**. doi:10.1101/cshperspect.a003798.
- Ramirez Pena E, Trevino J, Liu Z, Perez N, Sumbly P: The group A *Streptococcus* small regulatory RNA FasX enhances streptokinase activity

- by increasing the stability of the *ska* mRNA transcript. *Mol Microbiol* 2010, **78**:1332–1347.
34. Mangold M, Siller M, Roppenser B, Vlaminckx BJ, Penfound TA, Klein R, Novak R, Novick RP, Charpentier E: **Synthesis of group A streptococcal virulence factors is controlled by a regulatory RNA molecule.** *Mol Microbiol* 2004, **53**:1515–1527.
 35. Biswas I, Germon P, McDade K, Scott JR: **Generation and surface localization of intact M protein in *Streptococcus pyogenes* are dependent on *sagA*.** *Infect Immun* 2001, **69**:7029–7038.
 36. Betschel SD, Borgia SM, Barg NL, Low DE, De Azavedo JC: **Reduced virulence of group A streptococcal Tn916 mutants that do not produce streptolysin S.** *Infect Immun* 1998, **66**:1671–1679.
 37. Trevino J, Perez N, Sumbly P: **The 4.5S RNA component of the signal recognition particle is required for group A *Streptococcus* virulence.** *Microbiology* 2010, **156**:1342–1350.
 38. Beaume M, Hernandez D, Docquier M, Delucinge-Vivier C, Descombes P, Francois P: **Orientation and expression of methicillin-resistant *Staphylococcus aureus* small RNAs by direct multiplexed measurements using the nCounter NanoString technology.** *J Microbiol Methods* 2011, **84**:327–334.
 39. Chen Y, Indurthi DC, Jones SW, Papoutsakis ET: **Small RNAs in the genus *Clostridium*.** *MBio* 2011, **2**:e00340–10.
 40. Kumar R, Shah P, Swiatlo E, Burgess SC, Lawrence ML, Nanduri B: **Identification of novel non-coding small RNAs from *Streptococcus pneumoniae* TIGR4 using high-resolution genome tiling arrays.** *BMC Genomics* 2010, **11**:350.
 41. Mirahil MA, Billion A, Mohamed W, Mukherjee K, Kuenne C, Pischmarov J, Krawitz C, Retej J, Hartsch T, Chakraborty T, et al: **The intracellular sRNA transcriptome of *Listeria monocytogenes* during growth in macrophages.** *Nucleic Acids Res* 2011, **39**:4235–4248.
 42. Tsui HC, Mukherjee D, Ray VA, Sham LT, Feig AL, Winkler ME: **Identification and characterization of noncoding small RNAs in *Streptococcus pneumoniae* serotype 2 strain D39.** *J Bacteriol* 2010, **192**:264–279.
 43. Marraffini LA, Sontheimer EJ: **Self versus non-self discrimination during CRISPR RNA-directed immunity.** *Nature* 2010, **463**:568–571.
 44. Haft DH, Selengut J, Mongodin EF, Nelson KE: **A guild of 45 CRISPR-associated (Cas) protein families and multiple CRISPR/Cas subtypes exist in prokaryotic genomes.** *PLoS Comput Biol* 2005, **1**:e60.
 45. Livny J, Fogel MA, Davis BM, Waldor MK: **sRNAPredict: an integrative computational approach to identify sRNAs in bacterial genomes.** *Nucleic Acids Res* 2005, **33**:4096–4105.
 46. Livny J, Waldor MK: **Identification of small RNAs in diverse bacterial species.** *Curr Opin Microbiol* 2007, **10**:96–101.
 47. Arnvig KB, Young DB: **Identification of small RNAs in *Mycobacterium tuberculosis*.** *Mol Microbiol* 2009, **73**:397–408.
 48. van de Rijn I, Kessler RE: **Growth characteristics of group A streptococci in a new chemically defined medium.** *Infect Immun* 1980, **27**:444–448.
 49. Baum M, Bielaus S, Rittner N, Schmid K, Eggelbusch K, Dahms M, Schlauersbach A, Tahedl H, Beier M, Guimil R, et al: **Validation of a novel, fully integrated and flexible microarray benchtop facility for gene expression profiling.** *Nucleic Acids Res* 2003, **31**:e151.
 50. Edgar R, Domachev M, Lash AE: **Gene Expression Omnibus: NCBI gene expression and hybridization array data repository.** *Nucleic Acids Res* 2002, **30**:207–210.
 51. Bolstad BM, Irizarry RA, Astrand M, Speed TP: **A comparison of normalization methods for high density oligonucleotide array data based on variance and bias.** *Bioinformatics* 2003, **19**:185–193.
 52. Kingsford CL, Ayanbule K, Salzberg SL: **Rapid, accurate, computational discovery of Rho-independent transcription terminators illuminates their relationship to DNA uptake.** *Genome Biol* 2007, **8**:R22.
 53. Reese MG: **Application of a time-delay neural network to promoter annotation in the *Drosophila melanogaster* genome.** *Comput Chem* 2001, **26**:51–56.
 54. Livak KJ, Schmittgen TD: **Analysis of relative gene expression data using real-time quantitative PCR and the 2(-Delta Delta C(T)) Method.** *Methods* 2001, **25**:402–408.

doi:10.1186/1471-2164-13-550

Cite this article as: Patenge et al.: Identification of novel growth phase and media-dependent small non-coding RNAs in *Streptococcus pyogenes* M49 using intergenic tiling arrays. *BMC Genomics* 2012 **13**:550.

Submit your next manuscript to BioMed Central and take full advantage of:

- Convenient online submission
- Thorough peer review
- No space constraints or color figure charges
- Immediate publication on acceptance
- Inclusion in PubMed, CAS, Scopus and Google Scholar
- Research which is freely available for redistribution

Submit your manuscript at
www.biomedcentral.com/submit



METHODOLOGY ARTICLE

Open Access

Non-coding RNA detection methods combined to improve usability, reproducibility and precision

Peter Raasch¹, Ulf Schmitz¹, Nadja Patenge², Julio Vera¹, Bernd Kreikemeyer², Olaf Wolkenhauer^{1*}

Abstract

Background: Non-coding RNAs gain more attention as their diverse roles in many cellular processes are discovered. At the same time, the need for efficient computational prediction of ncRNAs increases with the pace of sequencing technology. Existing tools are based on various approaches and techniques, but none of them provides a reliable ncRNA detector yet. Consequently, a natural approach is to combine existing tools. Due to a lack of standard input and output formats combination and comparison of existing tools is difficult. Also, for genomic scans they often need to be incorporated in detection workflows using custom scripts, which decreases transparency and reproducibility.

Results: We developed a Java-based framework to integrate existing tools and methods for ncRNA detection. This framework enables users to construct transparent detection workflows and to combine and compare different methods efficiently. We demonstrate the effectiveness of combining detection methods in case studies with the small genomes of *Escherichia coli*, *Listeria monocytogenes* and *Streptococcus pyogenes*. With the combined method, we gained 10% to 20% precision for sensitivities from 30% to 80%. Further, we investigated *Streptococcus pyogenes* for novel ncRNAs. Using multiple methods—integrated by our framework—we determined four highly probable candidates. We verified all four candidates experimentally using RT-PCR.

Conclusions: We have created an extensible framework for practical, transparent and reproducible combination and comparison of ncRNA detection methods. We have proven the effectiveness of this approach in tests and by guiding experiments to find new ncRNAs. The software is freely available under the GNU General Public License (GPL), version 3 at <http://www.sbi.uni-rostock.de/moses> along with source code, screen shots, examples and tutorial material.

Background

Non-coding RNAs have drawn much attention in the last couple of years, after being neglected for a long time [1]. They are now known to play key roles in diverse cellular processes such as regulation of gene expression, splicing and directing chemical modifications [2,3]. Functional categorization of RNAs is not yet complete as new functions are discovered continuously [4,5].

Detection of non-coding RNA genes in genomic sequences is an urgent but unsolved problem in bioinformatics [6]. The accelerated pace of sequencing technology further increases the need for reliable identification of ncRNAs [7]. The main approaches to computational

prediction of ncRNAs are compositional analysis, secondary structure prediction, structural or sequence-based homology and the use of promoters and terminator signals. Numerous tools following one of these approaches or combinations thereof exist [6,8].

Compositional analysis can be a simple scan for local GC-content, an approach successful in AT-rich hyperthermophiles [9]. Considering more compositional features in a machine learning approach has also shown success [10]. Based on the fact that functional RNAs rely on a defined secondary structure, prediction of transcript minimum free energy is used as a means for detecting ncRNA genes [11]. Freyhult examined different quantities that can be used for this approach [12]. Sequence-based homology can be used for detection if reference genomes with appropriate evolutionary distances are available [13].

* Correspondence: olafwolkenhauer@uni-rostock.de

¹Systems Biology and Bioinformatics Group, University of Rostock, D-18057 Rostock, Germany

Full list of author information is available at the end of the article



Successful tools such as QRNA [14] and RNAz [15] combine secondary structure prediction with a homology approach relying on multiple alignments. The most comprehensive RNA family database RFAM [16] uses covariance models combining structural and sequence conservation to establish RNA families. The covariance model can be used to find new members of existing families, however, at the expense of computational effort. Dynalign [17] uses an approximation of Sankoff's Algorithm for structural alignment of two RNAs.

Xiao et al. used promoter and terminator prediction in intergenic regions aided by conservation and secondary structure analysis to predict ncRNAs [18].

To achieve better accuracy, some tools limit the scope to specific ncRNA families such as tRNA, miRNA and snoRNA [6].

However, none of the available tools for *general* ncRNA detection has reached a level of reliability comparable to protein-gene detection software. In contrast to ncRNA genes, protein genes exhibit codon-bias, open reading frames and strong sequence conservation, simplifying their detection. Since the diverse methods for ncRNA detection are complementary, a practical approach is to combine the available methods, as suggested by recent reviews [6,8,19,20]. Meyer et al. also remarked that many ncRNA detection methods rest on the assumption of a significant secondary structure, which may not always be necessary for a ncRNA to function [8]. Consequently, even the more successful methods, which rely on this assumption, need to be complemented with others to achieve more comprehensive predictions.

The combination of methods allows for precise predictions by using candidates that are predicted by several methods, or finding more candidates by using predictions from all methods. If the combination is done under a well designed framework, reproducibility, transparency and comparison of predictions are improved as well.

Previous efforts for the integration of data and algorithms in genomic research exist: RNAstructure integrated secondary structure prediction and structure based homology analysis but is not easily extended and not readily useable for genomic scans [21]. Tools such as sRNAfinder [22] combine several approaches to improve prediction results, but in a predefined way. The UCSC genome browser offers a huge amount of experimental data, pre-calculated predictions and analyses for a selected number of genomes [23]. Basic functions for comparative genomics are available, extended by an interface to Galaxy. Galaxy is a project that also aims to overcome custom and redundant scripting for bioinformatics tasks in genomic research, but does not yet offer specialized tools for ncRNA prediction [24]. TAVERNA is a powerful all-purpose framework, but its primary source of functionality "BioCatalogue" does not yet

contain essential ncRNA related tools such as RNAz and Dynalign [25]. LeARN is an extensible framework for annotating newly sequenced genomes, but it is more focused on processing trusted results from detection tools rather than improving predictions by the combination of analyses from different algorithms [26]. Consequently, there is a need for a framework that is easy to use and specialized for non-coding RNA detection. The main goals of our project are:

- **Combination:** Improving ncRNA detection by combining existing methods.
- **Comparison:** Easy comparison of the prediction performance of different methods must be possible.
- **Reproducibility:** application, combination and comparison of methods must be performed in a reproducible and transparent way.
- **Usability:** User experience should be improved by a GUI and visualization of all workflow steps and their respective results. No programming should be required to construct workflows, and to combine and compare methods.

Our software is aimed at three user groups: First, for bioinformaticians, the use and the combination of integrated tools must be simple. Second, developers of new algorithms for ncRNA detection must be provided with a ready-to-use environment and test bed. This removes the need to re-program solutions for tasks such as parsing files or visualization. Third, biologists must be able to re-use tested methods easily.

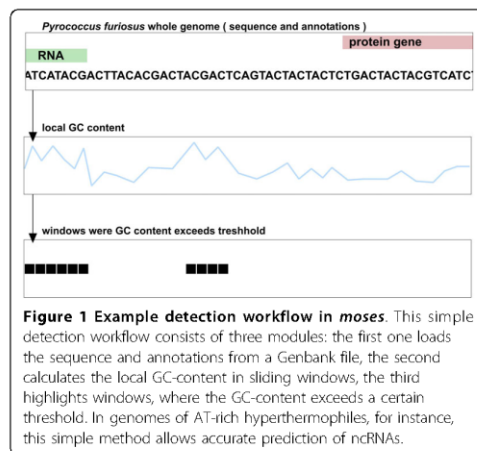
The implementation presented here supports compositional analysis, sequence-based homology (BLAST [27]), sequence and structural homology (RNAz [15] and Dynalign [17]) and secondary structure prediction (using RNAfold [28]). Our tool can easily be extended through an open architecture.

We will show how *moses* was designed to fulfill the given goals in the next section. In case studies we then demonstrate the effectiveness of combining methods: Precision or sensitivity are increased alternatively. Furthermore, our framework has been successfully applied to guide experiments in *Streptococcus pyogenes* to find new ncRNAs.

Methods

Key Idea

Our software *moses* (**modular sequence suite**) processes and combines the results of different methods to find regions in a genome that contain ncRNA gene candidates. To do so, the user constructs a workflow from modules. Figure 1 shows a simple example of such a workflow. It consists of three modules: the first one loads a sequence from a Genbank file [29], the second



calculates the GC-content using a sliding window for that sequence and finally a threshold filter module highlights regions of increased GC-content. In special cases such as *Pyrococcus furiosus*, increased GC-content is an accurate indication of a ncRNA gene [9]. After the threshold filter has been applied, for each window there is a prediction whether it contains a potential ncRNA gene or not. From this information a list of candidate locations can be constructed and used in experiments to verify the predictions. A more sophisticated detection workflow is shown in Figure 2. This workflow is also the one used for the case studies, described below.

An advantage of our modular approach is that it provides a good trade-off between flexibility and complexity: The user constructs workflows simply by chaining modules together and providing the parameters needed for its calculation. The output of every module can serve as the input for every other module. This allows for a free combination of modules while not requiring any programming skills.

The modules used to construct workflows can contain external tools, directly implemented analysis methods or helper functions. Each module represents one step in an analysis workflow. In the case of external tools, the module converts the input data, runs the tool, parses the output and converts it back into the *moses* format to ensure compatibility between all modules. Converting to one common data exchange format is more efficient than converting input and output between different tools, even though this is common practice in bioinformatics using custom scripts. The format we chose is a matrix of float values. Columns in the matrix correspond to nucleotide positions. Rows can hold different

kinds of information, for instance ncRNA probability scores from several detection methods.

This basic format is very simple and yet can hold all types of information needed for the purpose of ncRNA prediction. The modules can be written using a data structure that is familiar to most programmers.

The parameters needed to run a module are saved in human readable format in the corresponding *moses*-file along with IDs identifying the source modules. This creates a structure of dependent calculations that form a detection workflow. Individual modules of this workflow can be exchanged to modify and re-use the workflow. For example, the modules holding the analysed genome can be exchanged to perform an identical scan on a different species.

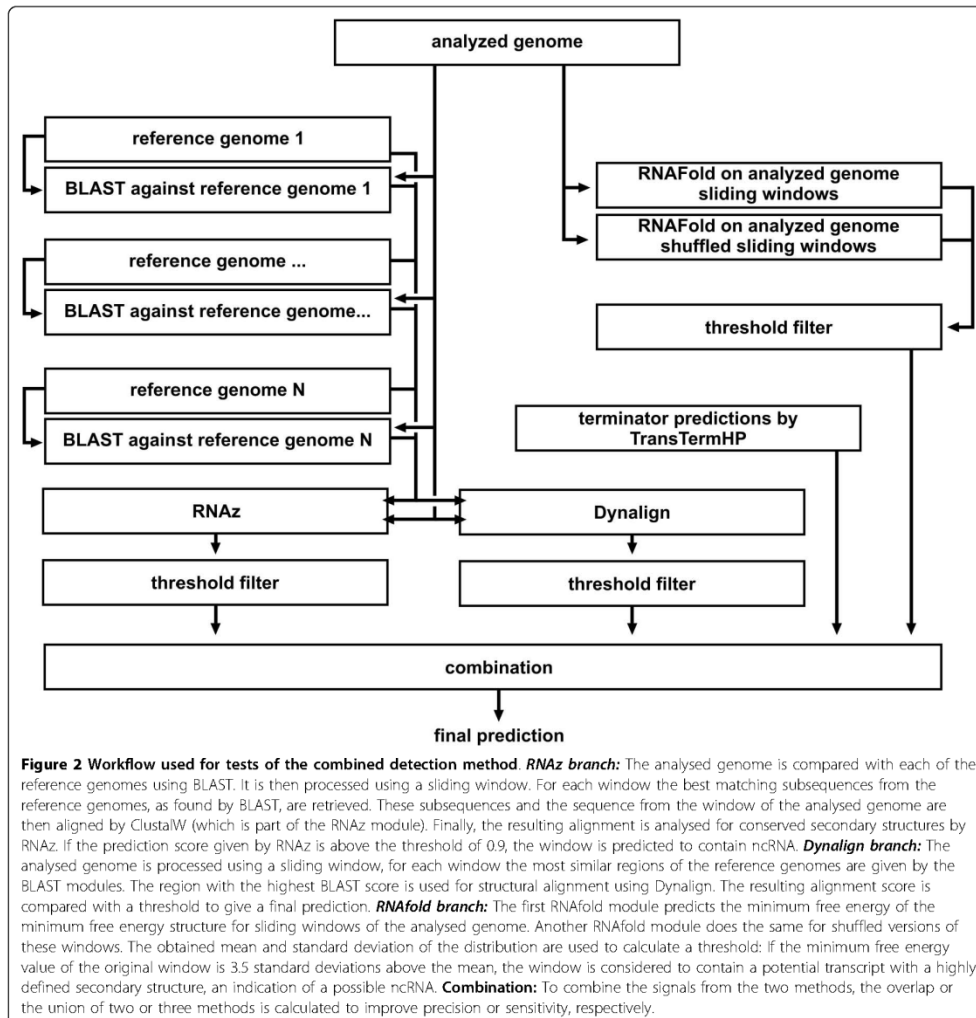
Main detection methods

The key modules *moses* provides are BLAST [27], word frequency analysis (typically used for GC-content analysis), RNAfold [28], RNAz [15] (using ClustalW [30] for alignments), Dynalign [17] and calculation of DNA properties, such as base stacking energy or bendability. BLAST can be used to compare two genomes, scan a genome for occurrences of a query sequence or locate conserved regions of a genome by BLASTing against a local database created with the BLAST helper tool formatDB. The RNAfold module uses a sliding window approach. For each sliding window the minimum free energy structure is predicted, and the corresponding minimum free energy value is stored at the centre position of the respective window. This results in a numerical profile aligned with the genome's base pairs.

The RNAz module scans a genome for ncRNA, requiring the output of several BLAST modules. Again, a sliding window approach is used. For each window, the most similar regions in reference genomes, as detected by BLAST, are used to construct a multiple alignment using ClustalW. This alignment is then analysed for ncRNA by RNAz. Finally the RNAz-score (called "RNA class probability") is stored at the window's centre position.

Similar to the RNAz module, the Dynalign module uses a sliding window and relies on BLAST modules to find the most similar regions in reference genomes for each window. A structural alignment of the analysed window and the region with the best BLAST-score is calculated using Dynalign. The output for each window is the alignment score.

The DNA properties module is similar to the RNAfold module, it calculates a numerical profile corresponding to a certain physical property of a DNA subsequence. The work of Abeel *et al.* shows that profiles of thermodynamic DNA properties can be used to



detect transcriptional signals. Those signals not pointing to known protein genes may be indications of ncRNA genes [31]. DNA base stacking energy, bendability or protein induced deformability are examples for such properties. To calculate a numerical profile we use the procedure given by Abeel *et al.* [31]: Each (overlapping) dinucleotide of a DNA sequence is converted into a number according to a conversion table. These values are then smoothed using a sliding

window, for each window the average is calculated and stored at the centre position of the window. Parameters for the properties were taken from EP3, a promoter detection tool developed by Abeel *et al.* [31]. The full list of available properties can be viewed on the tool's website (<http://bioinformatics.psb.ugent.be/webtools/ep3/?conversion>.)

Besides the key modules, predictions from RFAM can be incorporated by BLASTing against a RFAM dump.

To include terminator predictions, output from TransTermHP [32] can be loaded as well.

All available methods can also be applied to sub-regions of a sequence. This is useful, for instance, to exclude protein gene regions from analysis or limit the calculations to a region of interest. Furthermore, *moses* provides a number of arithmetic and logical function to process the result of any method.

These functions are also applied for combining the detection methods to arrive at more precise or more sensitive predictions. Usually, this involves trading precision for sensitivity or vice versa. A more precise combined prediction is achieved by considering only predictions made by more than one individual method. A more sensitive combined prediction is achieved by collecting the predictions from all individual methods. A more sophisticated combination is to use weighted scores of individual methods: Reliable methods can be weighed higher than relatively unreliable ones to get a combined result that is more precise yet retains much of the sensitivity of the individual methods.

The quality of any single or combined detection method can be analysed and compared using the built-in statistical evaluation, if data of known ncRNAs is available.

Graphical User Interface and Visualization

To make our software accessible to a wide range of users and to enhance usability, we provide a graphical user interface. Included features of the interface are:

- easy access to external tools as *moses* modules,
- constructing workflows with visualization of the modules' dependencies,
- multiple modes visualization of numerical profiles and for visual inspection, comparison and detection of correlations,
- browsing of genome annotations or calculated prediction signals,
- statistical assessment of each method, e.g., precision, sensitivity.

Integrated visualization of all intermediate results of a workflow helps finding mistakes, hypothesis generation and interpretation of results in the context of all available information.

Results & Discussion

Case Studies

To prove the effectiveness of combining detection methods, we used three methods, based on RNAz, Dynalign, RNAfold, and precalculated terminator predictions by TranstermHP on sets of known ncRNAs in *Escherichia coli*, *Listeria monocytogenes* and *Streptococcus pyogenes*. References for the known ncRNA sets are provided in Table 1. To give a reasonable estimation of the quality of the used methods we constructed test regions around known ncRNA extending 1500 bp up- and downstream around the known ncRNA. The flanking sequences serve as negative samples, the size was chosen to obtain a large number of negative samples while keeping the computational cost manageable. This results in regions composed of about 6% known ncRNA, 80% protein genes and 14% intergenic background, see Table 1. These compositions allow for the sampling of known positives as well as known negative regions in a realistic setting without the use of randomly generated negatives.

On this test region, we used the workflow shown in Figure 2. The complete workflow with parameters and all data calculated for the three genomes is available on the *moses* website (<http://www.sbi.uni-rostock.de/moses/data.html>). The workflow consists of four branches, one for each of the RNAz, RNAfold and Dynalign based methods and one for the terminator predictions by TranstermHP. The first three methods use a sliding window with window size 75 sliding 1 base pair at a time. We checked for the influence of the window size by also trying the sizes 51 and 101 with the RNAz and the RNAfold method, see Table 2 for a comparison. The tests suggest that each method has a different optimal window size. Since we want to combine methods we chose the same window size for all methods. We chose 75 bp because it seems to produce almost as good results as 101 bp but at lower computational costs. Data for these tests is also provided on the *moses* website.

The RNAz and the Dynalign branch both rely on BLAST modules that report for each window of the analysed sequence the most similar regions in four reference genomes. The reference regions are chosen to be the same size as the sliding windows. The reference genomes used are given in Table 3.

Table 1 Construction of the test regions for the case studies

	<i>Escherichia coli</i> str. K-12 substr. MG1655	<i>Listeria monocytogenes</i> EGD-e	<i>Streptococcus pyogenes</i> MGAS5005
regions size	222873 bp	284982 bp	212215 bp
known ncRNA	151 consisting of 11900 bp (5.3%) [29,35]	101 consisting of 19440 bp (6.8%) [36]	73 consisting of 14625 bp (6.9%) [34]
intergenic background	32754 bp (14.7%)	37317 bp (13.1%)	37067 bp (17.5%)
protein genes	180505 bp (81.0%)	231107 bp (81.1%)	163416 bp (77.0%)

Table 2 Influence of the window size in *Escherichia coli*

method	RNAz			RNAfold		
	51	75	101	51	75	101
precision	0.21923937	0.21484879	0.23922414	0.2338333	0.2634066	0.24783753
sensitivity	0.23058824	0.12596639	0.13058823	0.07991596	0.10773109	0.1107563

Test of the RNAfold method (Z-Score threshold 3.5) and the RNAz method (threshold 0) in *Escherichia coli* for different window sizes.

The RNAz module scans a genome for ncRNA using a sliding window. For each window, the most similar regions in the reference genomes, as detected by the BLAST modules, are alignment together with the analysed window using ClustalW. The resulting multiple alignment is then analysed by RNAz to give a so called "RNA class probability".

In the Dynalign method, only the reference region with the highest BLAST score is used for structural alignment using Dynalign.

The RNAfold method consists of two steps: First the minimum free energy value of the energetically optimal fold is calculated for each window. Second, the distribution of minimum free energy values for sequences of the nucleotide composition and length given by the analysed window is sampled. To this end RNAfold calculates the minimum free energy value for shuffled versions of the original window. The shuffling method by Altschul *et al.*

[33] is used to preserve not only the mono - but also the dinucleotide composition, because the secondary structure prediction is especially sensitive to the dinucleotide composition. For our tests we used 100 shuffled versions. Mean and standard deviation are obtained from the sampled distribution to estimate the significance of the actual minimum free energy value. The final output of the RNAfold method is the Z-score for each window. The Z-score is the difference of the value of the original window and the mean in standard deviations. The RNAfold module inverts the sign of the minimum free energy values for convenience. The RNAfold method and the RNAz method are closely related but RNAz does not use the Z-Score of the original sequence, it rather uses averages of the Z-Scores from all sequences in the alignment. Our results show that the pure Z-Score as used by Kavanaugh *et al.* [11] is useful for ncRNA prediction, however, the way RNAz approximates Z-Scores is orders of magnitudes faster and practically of the same accuracy.

For the integrated tools BLAST, ClustalW and RNAz default parameters are used. Graphical output of predicted structures is suppressed for RNAfold to save computation time. TranstermHP predictions for *Listeria monocytogenes* and *Streptococcus pyogenes* were downloaded from the TranstermHP website (<http://transterm.cbcb.umd.edu/>), predictions for *Escherichia coli* were performed using the downloaded program using default parameters.

The methods were combined by applying threshold filters to results of the RNAz, RNAfold and Dynalign method. The thresholds were 0.995, 4.5 and 550 respectively. For TranstermHP the confidence score threshold was 70, the default value used for the pre-calculated predictions from the TranstermHP website. Based on the parameter scans that were performed we selected values that gave intermediate precision and sensitivity for the individual methods.

After the thresholds have been applied in the centres of each window a "0" is stored if the value was below or equal to the threshold, "1" if above. The values for those three methods were added, additionally a "1" was added for each base pair of a predicted terminator.

The resulting sequence of integer values from 0-4 were then scanned using another sliding window. We tried different window sizes and 75 bp gave the best results (data available on the *moses* website). For each of those sliding windows the mean was calculated and

Table 3 Used Genomes

Species	Accession Number
Tested Genomes	
<i>Escherichia coli</i> str. K-12 substr. MG1655	NC_000913
<i>Listeria monocytogenes</i> EGD-e	NC_003210
<i>Streptococcus pyogenes</i> MGAS5005	NC_007297
Reference Genomes	
<i>Enterobacter</i> sp. 638	NC_009436
<i>Erwinia_tasmaniensis</i>	NC_010694
<i>Klebsiella pneumoniae</i> 342	NC_011283
<i>Salmonella enterica</i> subsp. <i>enterica</i> serovar <i>Enteritidis</i> str. P125109	NC_011294
<i>Listeria innocua</i> Clp11262	NC_003212
<i>Listeria welshimeri</i> serovar 6b str. SLCC5334	NC_008555
<i>Listeria seeligeri</i> serovar 1/2b str. SLCC3954	NC_013891
<i>Streptococcus agalactiae</i> 2603VR	NC_004116
<i>Streptococcus equi</i> subsp. <i>zooepidemicus</i> str. MGCS10565	NC_011134
<i>Streptococcus pyogenes</i> M1 GAS	NC_002737
<i>Streptococcus pyogenes</i> MGAS315	NC_004070
Genome for new predictions	
<i>Streptococcus pyogenes</i> NZ131	NC_011375
Genomes for BLAST sequence conservation analysis	see <i>moses</i> website

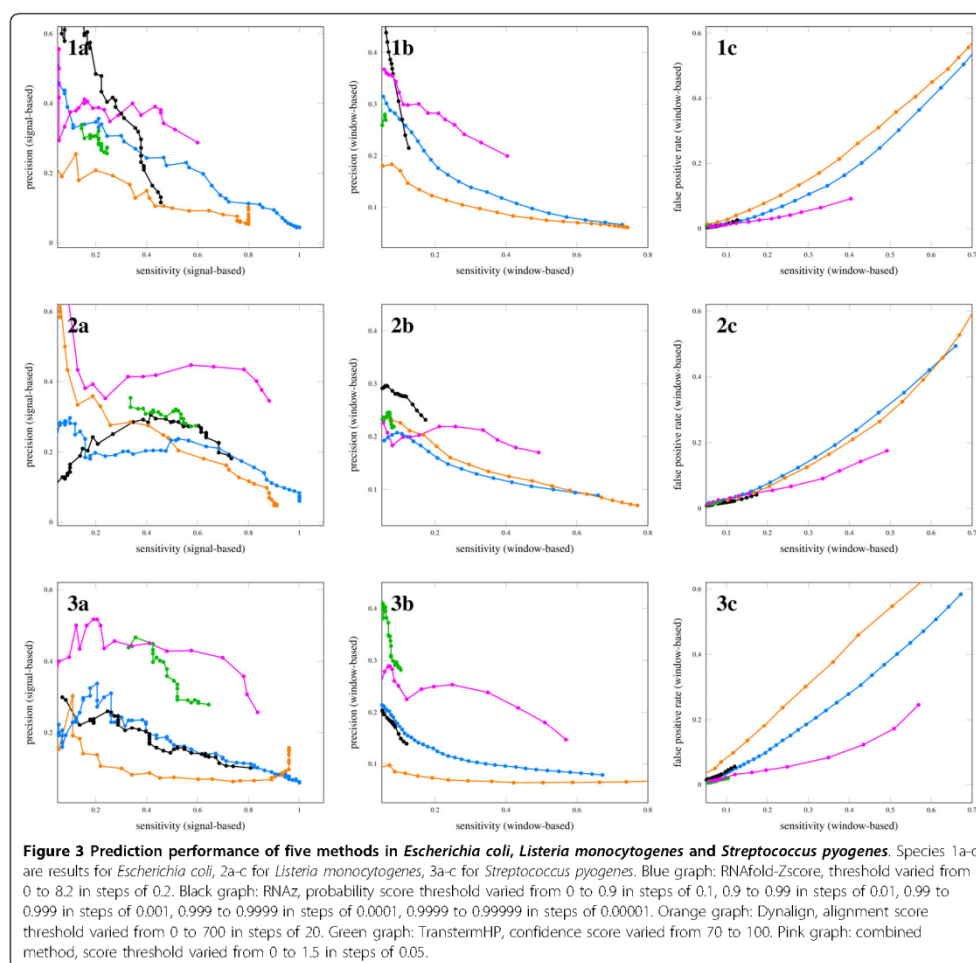
another threshold filter was applied. We used thresholds from 0-1.5 in steps of 0.05, resulting in predictions with sensitivity and precision given in Figure 3.

Sensitivity and precision were calculated using the usual definitions: Sensitivity is the ratio of true positive windows to all known ncRNA-containing windows. Precision is the ratio of true positive windows to the sum of true positive and false positive windows.

While window-based precision and sensitivity are good to compare different methods, they do not reflect the practical value of predictions that are to be used to guide experimental verification of candidates. In practice,

several windows next to each other that are predicted to contain ncRNA will be seen as one predicted locus or signal (for our purposes we want to neglect gaps). Those signals will then be used to guide experiments instead of each individual window.

Therefore, we define *signal precision* as the ratio of signals that overlap known ncRNA to all signals as an analogue to precision, and we define *signal sensitivity* as the ratio of known ncRNA that overlap a signal to all known ncRNA as analogue to sensitivity. The signal-based figures can be misleading if used alone, as too long signals will yield high signal precision and



signal sensitivity without being specific enough for experiments. In order to check the quality of the predictions, we also calculated the false positive rate defined as the ratio of false positive windows to all windows known to not contain ncRNA. Figure 3 shows the prediction quality of the four individual methods and the combined method for all species in terms of window-based and signal-based figures as well as the false positive rates.

The plots reveal that for a wide sensitivity range the combined method largely improves the “signal-precision” by 15% and the window-based precision by about 10% across the three tested species. The improvements are confirmed by the reduced false positive rate visible in Figure 3, subfigures 3a-c.

Our tests show that our software allows for a flexible and easy combination of ncRNA detection methods and that the combination improves detection results. Methods can easily be compared using the available statistics.

Prediction of novel ncRNAs

To show that *moses* can successfully guide experimental detection of ncRNA we present predictions for *Streptococcus pyogenes* NZ131, a human pathogen. We used four methods in a genomic scan to minimize false positives. As we have seen in the case studies, which were based on automated workflows, even the improved methods suffer from relatively high false positive rates. To arrive at a candidate list that had the most potential to be true ncRNA genes—in order to minimize unsuccessful experiments—we used manual inspection of multiple data sources instead.

All data calculated and the used parameters are available on the *moses* website.

The data sources were RNAfold secondary structure predictions, calculated DNA base stacking energy, BLAST-calculated conservation against related genomes and RNAz-predictions. The RNAfold module was used with window size 41, the DNA properties module with window size 81, step size 1 base pair in both cases. For RNAz the window size was 41 with step size 5 base pairs. The calculations were performed on the full genome sequence.

We examined the characteristic RNAfold and DNA base stacking energy profiles around known ncRNA genes to manually distinguish them from genomic background.

Also, isolated conserved spots were considered as clues for potential genes. Conservation was determined by BLASTing the NZ131 genome against all pyogenes serotypes in one module and against a selection of *Streptococcus* genomes in a second. Intergenic regions were examined for these four clues. Data used for the visual inspection is available on the *moses* website.

The procedure resulted in a list of 20 candidates. The features our selection of 20 candidates was based on, is listed in Table 4. We confirmed this list using the RNAz module with the same reference genomes as in the *Streptococcus pyogenes* test.

From the 20 candidates, four highly probable candidates were selected based on RNAz prediction and presence of a putative terminator, visible as a peak in the RNAfold profile. As the minimum free energy value calculated by RNAfold is a measure of the thermodynamic stability of RNA structures, such a peak can be an indicator of ncRNAs as well as of terminators. The locations of the putative terminators were used to aid placement of the downstream primer for the RT-PCR experiments, as a terminator gives an indication of where the 3' end of a possible ncRNA is located. RNAz predictions were used as the most probable centre of the potential transcript. An example of the information calculated in *moses* around the candidate regions is displayed in Figure 4. Corresponding screenshots of all four candidate regions and data used for primer design with genomic coordinates are given on the *moses* website.

The combination of multiple methods, possible in *moses*, has yielded highly probable candidates. RNAz or BLAST alone, for instance, would have given us hundreds of candidate loci to examine (data on the *moses* website).

Expression of the four highly probable candidates was verified by reverse transcription (RT) followed by PCR, see Figure 5. Reactions without addition of the RT enzyme served as negative controls. Reverse transcription of the EMM-gene was performed as a positive control, which is known to be expressed in this strain under the conditions tested in our experiments. Details of the experimental procedure, including the used primers, are available on the *moses* website and in Additional file 1. The candidates were named mopsRNA1-4 (*moses* predicted small RNA). Candidates 1 and 4 overlap with candidates reported as predictions by a previous bioinformatic search in the study of Perez et. al [34], labelled SR307231, SR759205 and SR758876.

Our predictions demonstrate that the integrated approach possible with *moses* is able to guide experimental detection of new ncRNAs. The RT-PCR experiments are not sufficient to rule out that the observations are related to neighbouring transcripts rather than true ncRNA. Accordingly, further experiments are in progress to confirm and characterize the four new candidate ncRNAs and their function in *Streptococcus pyogenes* physiology and virulence.

Limitations

The computationally more demanding algorithms RNAz-analysis and RNAfold secondary structure prediction with

Table 4 Criteria for visual inspection of intergenic regions in *Streptococcus pyogenes* NZ311

	start	1) BLAST vs <i>Streptococci</i>	2) BLAST vs <i>S. pyogenes</i>	3) DNA base stacking energy	4) RNAfold
1	202790	X		X	
2	216807	X		X	X
3	273446	X		X	X
4	308253		X	X	X
5	349593		X	X	X
6	362796		X		X
7	363720	X	X		X
8	407642		X	X	
9	506298	X	X		X
10	512500	X	X		X
11	554314	X		X	X
12	568980	X	X	X	
13	806825		X		X
14	827250	X	X		
15	949486	X			X
16	1201476		X		X
17	1487751	X	X	X	
18	1571435		X		X
19	1581266		X		
20	1704825	X		X	X

Criteria: 1) increased conservation shown by BLAST against selected *Streptococci* genomes (see the *moses* website for a List). 2) increased conservation shown by BLAST against all *Streptococcus pyogenes* substrains. 3) increased DNA base stacking energy profile or presence of two nearby peaks. 4) a peak in the RNAfold profile.

shuffled comparison sequences need approximately 120 hours for full prokaryotic genomes (assuming an average size of 4 MB) on standard workstation computers. Dynalign takes even longer because it performs full structural alignments.

Our tests were performed on a machine with Intel(R) Core(TM) 2 Duo CPU 2.66 GHz with 2 GB of RAM with the use of parallelization. The RNAfold method and then RNAz method both took three hours for 99.950 analysed windows (for an analysed genome, the number of base pairs minus the window size plus one equals the number of windows to analyse). The window size for both methods was 51. The windows step was one base pair to obtain maximum resolution. However, this is not to imply that we can predict the exact gene starts and ends. For the RNAfold method 100 shuffled windows were used and three reference genomes for the RNAz method. If the analysis is limited to the intergenic regions, the time is reduced depending on the percentage of coding regions of the genomes under examination (often, intergenic regions constitute 10% of prokaryotic genomes). Other ways to avoid too long calculations include choosing a larger step size and parallel calculations by dividing analysed genomes in smaller parts.

The methods used here are in principle not restricted to prokaryotes, but to the sheer size of the genome.

Conclusions

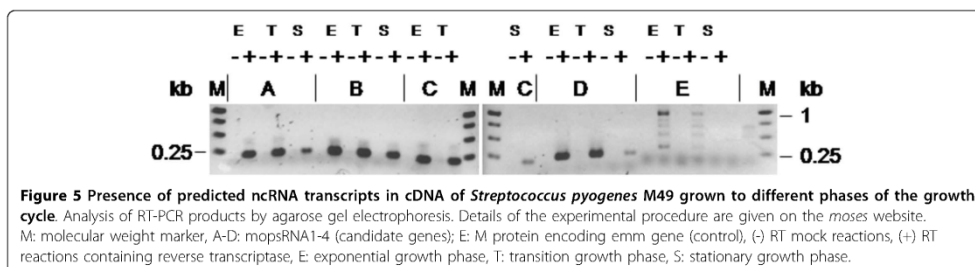
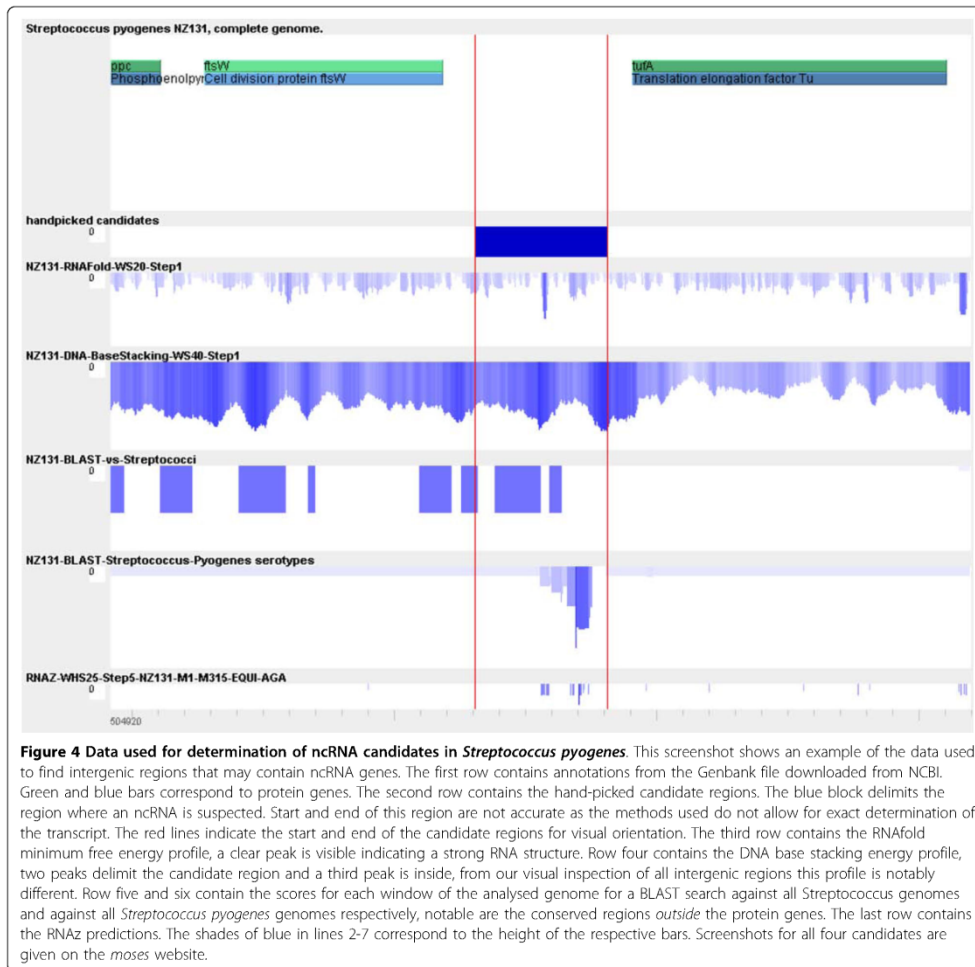
We developed a framework for reproducible, transparent and easy combination of existing ncRNA detection methods. Our contribution helps to satisfy the need for a combined approach as suggested by recent reviews [6,8,19,20]. The main improvements our framework provides are:

Improved ncRNA detection by combining existing methods

Wrapping existing tools and methods in *moses* modules that convert input and output formats to a common data interchange format makes combination possible. We have demonstrated the effectiveness of combining methods in tests on *Escherichia coli* and *Streptococcus pyogenes*. Further we predicted novel ncRNAs in *Streptococcus pyogenes* using multiple methods to yield highly probable candidates, thereby reducing unsuccessful experiments. Final confirmation and subsequent characterisation of the candidates is in progress.

Facilitated comparison of methods

The used methods can readily be compared using the integrated accuracy report. Statistical figures such as signal based and by-base-pair precision, sensitivity are readily at hand. This allows effective evaluation of existing methods



and the selection of appropriate methods, e.g., according to available reference genomes or given taxon.

Improved reproducibility, re-usability and transparency

Workflows are self-documented as all parameters and data dependencies are stored in the *moses* files. This means the workflows are transparent because no hidden conversions and no implied functions are performed, only the ones defined by the user. No custom scripts or custom in-house software is involved in studies carried out in *moses*. Furthermore, an existing workflow can be reused on different sequences, different data or altered parameters.

Improved Usability

We created a GUI and visualization for all intermediate steps of a workflow. This enables to detect flaws in a workflow and helps to interpret the results. The integrated environment supports hypothesis generation and brings data and results in context with all available information.

The method of constructing workflows in *moses* is easy as it requires no programming and no scripting. This makes it an attractive tool for bioinformaticians. Extending the framework with new algorithms is made easy through an open architecture with a plug-in mechanism. Programming effort is thus minimized and developers of new algorithms are provided with a ready-to-use platform. Biologists can easily reuse existing workflows.

Outlook

The next step in the development of our framework is the integration of further existing methods and algorithms. Combination of methods could be enhanced by including support for SVM training and classification. Possibly, in the course of adding more tools the scope could be expanded to not only find ncRNA genes but protein genes, promoters, terminators and transcription factor binding sites as well. The result would be a complete picture of a genome under one common framework.

A recent approach to detect regulatory regions is pattern recognition in profiles of physical properties of the DNA, see for instance [31]. As our framework offers different sources for such profiles, not only based on physical properties, it is a natural extension of our work to apply pattern detection to the profiles calculated by *moses*.

Additional material

Additional file 1: Experimental procedure for verification of four selected ncRNA candidates. Additional file 1 is a Microsoft Word document with a detailed description of the materials and methods employed for experimental verification of the final four ncRNA candidates.

Acknowledgements

The work of BK and NP was supported by a BMBF grant in the framework of the ERA-Net PathoGenoMics 2 program (FKZ 0315437B). The authors would like to thank Jana Normann for expert technical assistance and Alexander Raasch for helping with the Java implementation and preparation of figures. Ulf Liebal and Sarah Zaatreh helped proofreading the manuscript. The work of OW, JV, US and PR is funded by the University of Rostock. OW and US were also supported by the Deutsche Forschungsgemeinschaft (DFG), project WO 991/4-1 and by the German Federal Ministry for Education and Research (BMBF) as part of the SysMoll program. JV is supported by the BMBF FORSYS program. We thank the anonymous reviewers for their constructive comments.

Author details

¹Systems Biology and Bioinformatics Group, University of Rostock, D-18057 Rostock, Germany. ²Department of Medical Microbiology, Virology and Hygiene, University Hospital Rostock, Schillingallee 70, D-18055 Rostock, Germany.

Authors' contributions

PR and US designed the software framework. PR implemented the framework, performed the tests and predicted the new ncRNAs. BK and NP carried out the RT-PCR experiments to verify the predicted ncRNAs. OW participated in the design of the framework and helped to draft the manuscript. All authors read and approved the final manuscript.

Received: 10 May 2010 Accepted: 29 September 2010

Published: 29 September 2010

References

- Couzin J: Breakthrough of the year. Small RNAs make big splash. *Science* 2002, **298**:2296-2297.
- Storz G, Altuvia S, Wassarman KM: An abundance of RNA regulators. *Annu Rev Biochem* 2005, **74**:199-217.
- Eddy SR: Non-coding RNA genes and the modern RNA world. *Nat Rev Genet* 2001, **2**:919-929.
- Hannon GJ, Rivas FV, Murchison EP, Steitz JA: The expanding universe of noncoding RNAs. *Cold Spring Harb Symp Quant Biol* 2006, **71**:551-564.
- Mercer TR, Dinger ME, Mattick JS: Long non-coding RNAs: insights into functions. *Nat Rev Genet* 2009, **10**:155-159.
- Machado-Lima A, Portillo HAD, Durham AM: Computational methods in noncoding RNA research. *J Math Biol* 2008, **56**:15-49.
- Wold B, Myers RM: Sequence census methods for functional genomics. *Nat Meth* 2008, **5**:19-21.
- Meyer IM: A practical guide to the art of RNA gene prediction. *Brief Bioinform* 2007, **8**:396-414.
- Klein RJ, Misulovin Z, Eddy SR: Noncoding RNA genes identified in AT-rich hyperthermophiles. *Proc Natl Acad Sci USA* 2002, **99**:7542-7547.
- Carter RJ, Dubchak I, Holbrook SR: A computational approach to identify genes for functional RNAs in genomic sequences. *Nucleic Acids Res* 2001, **29**:3928-3938.
- Kavanaugh LA, Dietrich FS: Non-coding RNA prediction and verification in *Saccharomyces cerevisiae*. *PLoS Genet* 2009, **5**:e1000321.
- Freyhult E, Gardner PP, Moulton V: A comparison of RNA folding measures. *BMC Bioinformatics* 2005, **6**:241.
- Wassarman KM, Repollla F, Rosenow C, Storz G, Gottesman S: Identification of novel small RNAs using comparative genomics and microarrays. *Genes & Development* 2001, **15**:1637-1651.
- Rivas E, Eddy SR: Noncoding RNA gene detection using comparative sequence analysis. *BMC Bioinformatics* 2001, **2**:8.
- Washielt S, Hofacker IL, Stadler PF: Fast and reliable prediction of noncoding RNAs. *Proceedings of the National Academy of Sciences of the United States of America* 2005, **102**:2454-2459.
- Gardner PP, Daub J, Tate JG, Nawrocki EP, Kolbe DL, Lindgreen S, Wilkinson AC, Finn RD, Griffiths-Jones S, Eddy SR, Bateman A: Rfam: updates to the RNA families database. *Nucleic Acids Res* 2009, **37**:D136-D140.
- Mathews DH: Predicting a set of minimal free energy RNA secondary structures common to two sequences. *Bioinformatics* 2005, **21**:2246-2253.

18. Xiao B, Li W, Guo G, Li B, Liu Z, Jia K, Guo Y, Mao X, Zou Q: **Identification of small noncoding RNAs in *Helicobacter pylori* by a bioinformatics-based approach.** *Curr Microbiol* 2009, **58**:258-263.
19. Pichon C, Felden B: **Small RNA gene identification and mRNA target predictions in bacteria.** *Bioinformatics* 2008, **24**:2807-2813.
20. Solda G, Makunin I, Sezerman OU, Corradin A, Corti G, Guffanti A: **An Ariadne's thread to the identification and annotation of noncoding RNAs in eukaryotes.** *Brief Bioinform* 2009, **10**:475-489.
21. Mathews DH, Disney MD, Childs JL, Schroeder SJ, Zuker M, Turner DH: **Incorporating chemical modification constraints into a dynamic programming algorithm for prediction of RNA secondary structure.** *Proc Natl Acad Sci USA* 2004, **101**:7287-7292.
22. Tjaden B: **Prediction of small, noncoding RNAs in bacteria using heterogeneous data.** *J Math Biol* 2008, **56**:183-200.
23. Bina M: **The genome browser at UCSC for locating genes, and much more!** *Mol Biotechnol* 2008, **38**:269-275.
24. Giardine B, Riemer C, Hardison RC, Burhans R, Elnitski L, Shah P, Zhang Y, Blankenberg D, Albert I, Taylor J, Miller W, Kent WJ, Nekrutenko A: **Galaxy: a platform for interactive large-scale genome analysis.** *Genome Res* 2005, **15**:1451-1455.
25. Hull D, Wolstencroft K, Stevens R, Goble C, Pocock MR, Li P, Oinn T: **Taverna: a tool for building and running workflows of services.** *Nucleic Acids Res* 2006, **34**:W729-W732.
26. Noirot C, Gaspin C, Schiex T, Gouzy J: **LeARN: a platform for detecting, clustering and annotating non-coding RNAs.** *BMC Bioinformatics* 9:21-21.
27. Altschul SF, Gish W, Miller W, Myers EW, Lipman DJ: **Basic local alignment search tool.** *J Mol Biol* 1990, **215**:403-410.
28. Hofacker I, Fontana W, Stadler P, Bonhoeffer S, Tacker M, Schuster P: **Fast Folding and Comparison of RNA Secondary Structures.** *Monatsh Chem* 1994, **125**(188):167.
29. Benson DA, Karsch-Mizrachi I, Lipman DJ, Ostell J, Wheeler DL: **GenBank.** *Nucleic Acids Res* 2008, **36**:D25-D30.
30. Larkin MA, Blackshields G, Brown NP, Chenna R, McGettigan PA, McWilliam H, Valentin F, Wallace IM, Wilm A, Lopez R, Thompson JD, Gibson TJ, Higgins DG: **Clustal W and Clustal X version 2.0.** *Bioinformatics* 2007, **23**:2947-2948.
31. Abeel T, Saeys Y, Bonnet E, Rouz  P, Van de Peer Y: **Generic eukaryotic core promoter prediction using structural features of DNA.** *Genome Research* 2008, **18**:310-323.
32. Kingsford CL, Ayanbule K, Salzberg SL: **Rapid, accurate, computational discovery of Rho-independent transcription terminators illuminates their relationship to DNA uptake.** *Genome Biol* 2007, **8**:R22.
33. Altschul SF, Erickson BW: **Significance of nucleotide sequence alignments: a method for random sequence permutation that preserves dinucleotide and codon usage.** *Mol Biol Evol* 1985, **2**:526-538.
34. Perez N, Trevi o J, Liu Z, Ho SCM, Babitzke P, Sumbly P: **A Genome-Wide Analysis of Small Regulatory RNAs in the Human Pathogen Group A *Streptococcus*.** *PLoS ONE* 2009, **4**:e7668.
35. Wang C, Ding C, Meraz RF, Holbrook SR: **PSol: a positive sample only learning algorithm for finding non-coding RNA genes.** *Bioinformatics* 2006, **22**:2590-2596.
36. Toledo-Arana A, Dussurget O, Nikitas G, Sesto N, Guet-Revillet H, Balestrino D, Loh E, Gripenland J, Tiensuu T, Vaitkevicius K, Barthelemy M, Vergassola M, Nahori M, Soubigou G, Regnault B, Coppee J, Lecuit M, Johansson J, Cossart P: **The *Listeria* transcriptional landscape from saprophytism to virulence.** *Nature* 2009, **459**:950-956.

doi:10.1186/1471-2105-11-491

Cite this article as: Raasch *et al.*: Non-coding RNA detection methods combined to improve usability, reproducibility and precision. *BMC Bioinformatics* 2010 **11**:491.

Submit your next manuscript to BioMed Central and take full advantage of:

- Convenient online submission
- Thorough peer review
- No space constraints or color figure charges
- Immediate publication on acceptance
- Inclusion in PubMed, CAS, Scopus and Google Scholar
- Research which is freely available for redistribution

Submit your manuscript at
www.biomedcentral.com/submit



6.2 Vollständiges Publikationsverzeichnis

h-Index: 17

Begutachtete Originalarbeiten

1. Nakata, M., Sumitomo, T., **Patenge, N.**, Kreikemeyer, B. & Kawabata, S. 2019. Thermosensitive pilus production by FCT type 3 *Streptococcus pyogenes* controlled by Nra regulator translational efficiency. *Mol Microbiol.*, available from: PM:31633834
2. Barkowsky, G., Lemster, A.-L., Pappesch, R., Jacob, A., Krüger, S., Schröder, A., Kreikemeyer, B., & **Patenge, N.** 2019. Influence of different Cell-Penetrating Peptides on the antimicrobial efficiency of antisense PNAs in *Streptococcus pyogenes*. *Mol.Ther.Nucleic Acids*, 18, 444-454 available from: PM:31655262
3. Khani, A., Popp, N., Kreikemeyer, B., & **Patenge, N.** 2018. A Glycine Riboswitch in *Streptococcus pyogenes* Controls Expression of a Sodium:Alanine Symporter Family Protein Gene. *Front Microbiol.*, 9, 200 available from: PM:29527194
4. Pappesch, R., Warnke, P., Mikkat, S., Normann, J., Wisniewska-Kucper, A., Huschka, F., Wittmann, M., Khani, A., Schwengers, O., Oehmcke-Hecht, S., Hain, T., Kreikemeyer, B., & **Patenge, N.** 2017. The Regulatory Small RNA MarS Supports Virulence of *Streptococcus pyogenes*. *Sci.Rep.*, 7, (1) 12241 available from: PM:28947755
5. **Patenge, N.**, Pappesch, R., Krawack, F., Walda, C., Mraheil, M.A., Jacob, A., Hain, T., & Kreikemeyer, B. 2013. Inhibition of Growth and Gene Expression by PNA-peptide Conjugates in *Streptococcus pyogenes*. *Mol.Ther.Nucleic Acids*, 2, e132 available from: PM:24193033
6. **Patenge, N.**, Billion, A., Raasch, P., Normann, J., Wisniewska-Kucper, A., Retey, J., Boisguerin, V., Hartsch, T., Hain, T., & Kreikemeyer, B. 2012b. Identification of novel growth phase- and media-dependent small non-coding RNAs in *Streptococcus pyogenes* M49 using intergenic tiling arrays. *BMC.Genomics*, 13, 550 available from: PM:23062031
7. Siemens, N., Fiedler, T., Normann, J., Klein, J., Munch, R., **Patenge, N.**, & Kreikemeyer, B. 2012. Effects of the ERES pathogenicity region regulator Ralp3 on *Streptococcus*

- pyogenes* serotype M49 virulence factor expression. *J.Bacteriol.*, 194, (14) 3618-3626 available from: PM:22544273
8. **Patenge, N.**, Arndt, K., Eggert, T., Zietz, C., Kreikemeyer, B., Bader, R., Nebe, B., Stranak, V., Hippler, R., & Podbielski, A. 2012a. Evaluation of antimicrobial effects of novel implant materials by testing the prevention of biofilm formation using a simple small scale medium-throughput growth inhibition assay. *Biofouling.*, 28, (3) 267-277 available from: PM:22435853
 9. Siemens, N., **Patenge, N.**, Otto, J., Fiedler, T., & Kreikemeyer, B. 2011. *Streptococcus pyogenes* M49 plasminogen/plasmin binding facilitates keratinocyte invasion via integrin-integrin-linked kinase (ILK) pathways and protects from macrophage killing. *J.Biol.Chem.*, 286, (24) 21612-21622 available from: PM:21521694
 10. Bouman, L., Schlierf, A., Lutz, A.K., Shan, J., Deinlein, A., Kast, J., Galehdar, Z., Palmisano, V., **Patenge, N.**, Berg, D., Gasser, T., Augustin, R., Trumbach, D., Irrcher, I., Park, D.S., Wurst, W., Kilberg, M.S., Tatzelt, J., & Winklhofer, K.F. 2011. Parkin is transcriptionally regulated by ATF4: evidence for an interconnection between mitochondrial stress and ER stress. *Cell Death.Differ.*, 18, (5) 769-782 available from: PM:21113145
 11. Raasch, P., Schmitz, U., **Patenge, N.**, Vera, J., Kreikemeyer, B., & Wolkenhauer, O. 2010. Non-coding RNA detection methods combined to improve usability, reproducibility and precision. *BMC.Bioinformatics.*, 11, 491 available from: PM:20920260
 12. Carballo-Carbajal, I., Weber-Endress, S., Rovelli, G., Chan, D., Wolozin, B., Klein, C.L., **Patenge, N.**, Gasser, T., & Kahle, P.J. 2010. Leucine-rich repeat kinase 2 induces alpha-synuclein expression via the extracellular signal-regulated kinase pathway. *Cell Signal.*, 22, (5) 821-827 available from: PM:20074637
 13. Rothfuss, O., Gasser, T., & **Patenge, N.** 2010. Analysis of differential DNA damage in the mitochondrial genome employing a semi-long run real-time PCR approach. *Nucleic Acids Res.*, 38, (4) e24 available from: PM:19966269
 14. Rothfuss, O., Fischer, H., Hasegawa, T., Maisel, M., Leitner, P., Miesel, F., Sharma, M., Bornemann, A., Berg, D., Gasser, T., & **Patenge, N.** 2009. Parkin protects mitochondrial

- genome integrity and supports mitochondrial DNA repair. *Hum.Mol.Genet.*, 18, (20) 3832-3850 available from: PM:19617636
15. Hasegawa, T., Treis, A., **Patenge, N.**, Fiesel, F.C., Springer, W., & Kahle, P.J. 2008. Parkin protects against tyrosinase-mediated dopamine neurotoxicity by suppressing stress-activated protein kinase pathways. *J.Neurochem.*, 105, (5) 1700-1715 available from: PM:18248610
 16. Dachsel, J.C., Lucking, C.B., Deeg, S., Schultz, E., Lalowski, M., Casademunt, E., Corti, O., Hampe, C., **Patenge, N.**, Vaupel, K., Yamamoto, A., Dichgans, M., Brice, A., Wanker, E.E., Kahle, P.J., & Gasser, T. 2005. Parkin interacts with the proteasome subunit alpha4. *FEBS Lett.*, 579, (18) 3913-3919 available from: PM:15987638
 17. Zimprich, A., Biskup, S., Leitner, P., Lichtner, P., Farrer, M., Lincoln, S., Kachergus, J., Hulihan, M., Uitti, R.J., Calne, D.B., Stoessl, A.J., Pfeiffer, R.F., **Patenge, N.**, Carbajal, I.C., Vieregge, P., Asmus, F., Muller-Myhsok, B., Dickson, D.W., Meitinger, T., Strom, T.M., Wszolek, Z.K., & Gasser, T. 2004. Mutations in LRRK2 cause autosomal-dominant parkinsonism with pleomorphic pathology. *Neuron*, 44, (4) 601-607 available from: PM:15541309
 18. **Patenge, N.**, Elkin, S.K., & Oettinger, M.A. 2004. ATP-dependent remodeling by SWI/SNF and ISWI proteins stimulates V(D)J cleavage of 5 S arrays. *J.Biol.Chem.*, 279, (34) 35360-35367 available from: PM:15201272
 19. Mundy, C.L., **Patenge, N.**, Matthews, A.G., & Oettinger, M.A. 2002. Assembly of the RAG1/RAG2 synaptic complex. *Mol.Cell Biol.*, 22, (1) 69-77 available from: PM:11739723
 20. **Patenge, N.**, Berendes, A., Engelhardt, H., Schuster, S.C., & Oesterhelt, D. 2001. The fla gene cluster is involved in the biogenesis of flagella in *Halobacterium salinarum*. *Mol.Microbiol.*, 41, (3) 653-663 available from: PM:11532133
 21. **Patenge, N.**, Haase, A., Bolhuis, H., & Oesterhelt, D. 2000. The gene for a halophilic beta-galactosidase (bgaH) of *Haloferax alicantei* as a reporter gene for promoter analyses in *Halobacterium salinarum*. *Mol.Microbiol.*, 36, (1) 105-113 available from: PM:10760167

22. Padberg, F., Matsuda, M., Fenk, R., **Patenge, N.**, Kubuschok, B., Hohlfeld, R., Wekerle, H., & Spuler, S. 1999. Myasthenia gravis: selective enrichment of antiacetylcholine receptor antibody production in untransformed human B cell cultures. *Eur.J.Immunol.*, 29, (11) 3538-3548 available from: PM:10556808
23. **Patenge, N.** & Soppa, J. 1999. Extensive proteolysis inhibits high-level production of eukaryal G protein-coupled receptors in the archaeon *Haloferax volcanii*. *FEMS Microbiol.Lett.*, 171, (1) 27-35 available from: PM:9987838
24. Dervedde, J., Eitinger, T., **Patenge, N.**, & Friedrich, B. 1996. hyp gene products in *Alcaligenes eutrophus* are part of a hydrogenase-maturation system. *Eur.J.Biochem.*, 235, (1-2) 351-358 available from: PM:8631353

Übersichtsartikel mit Impact Faktor

1. **Patenge, N.**, Pappesch, R., Khani, A., & Kreikemeyer, B. 2015. Genome-wide analyses of small non-coding RNAs in streptococci. *Front Genet.*, 6, 189 available from: PM:26042151
2. **Patenge, N.**, Fiedler, T., & Kreikemeyer, B. 2013. Common regulators of virulence in streptococci. *Curr.Top.Microbiol.Immunol.*, 368, 111-153 available from: PM:23242855
3. Fiedler, T., Sugareva, V., **Patenge, N.**, & Kreikemeyer, B. 2010. Insights into *Streptococcus pyogenes* pathogenesis from transcriptome studies. *Future.Microbiol.*, 5, (11) 1675-1694 available from: PM:21133689

Buchbeiträge

1. **Patenge, N.** 2017. Quantification of DNA Damage and Repair in Mitochondrial, Nuclear, and Bacterial Genomes by Real-Time PCR. *Methods Mol.Biol.*, 1644, 159-166 available from: PM:28710762
2. Eitinger, T., L. Wolfram, J. Dervedde, I. Wolf, **N. Patenge** and B. Friedrich. 1997. Nickel metabolism in *Alcaligenes eutrophus*: Uptake by a Ni²⁺-specific permease and metal insertion into the hydrogenases. In *Deutsche Forschungsgemeinschaft, Bioinorganic Chemistry, Transition Metals in Biology and their Coordination Chemistry*. (Trautwein, A.X., Ed.), pp. 37-50, Wiley-VCH, Weinheim.

Vorträge auf Tagungen und auswärtigen Kolloquien

1. 2018, Workshop „RNA-Therapeutics“, Würzburg,
“Antisense-Peptidnukleinsäuren (PNAs)”
2. 2017, 1st International Conference on Respiratory Pathogens (ICoRP), Rostock,
“A glycine riboswitch controls expression of a sodium:alanine symporter family protein gene in *Streptococcus pyogenes* ”
3. 2017, Microbiology and Infection 2017 - 5th Joint Conference of the DGHM & VAAM, Würzburg,
“sRNAScanner66 influences the expression of pyrimidine metabolism genes in *Streptococcus pyogenes*”
4. 2017, Kickoff-Meeting, Exzellenzinitiative M.-V. KoInfekt, Insel Riems,
“Entwicklung neuartiger Anti-Infektiva auf Basis der Antisense-Peptidnukleinsäuren (PNAs)”
5. 2016, 3rd German Pneumococcal and Streptococcal Symposium, Braunschweig,
“A *Galleria mellonella* infection model for *Streptococcus pyogenes*”
6. 2015, Sensatory and Regulatory RNAs in Prokaryotes and CRISPR-Cas, Braunschweig,
“Virulence gene expression control by sRNAs in *Streptococcus pyogenes*”
7. 2014, NGS Workshop 2014, Dummerstorf,
“NGS in Molecular Bacteriology”
8. 2013, 65. Jahrestagung der Deutschen Gesellschaft für Hygiene und Mikrobiologie (DGHM), Rostock,
“Functional characterization of small non-coding RNAs in *Streptococcus pyogenes*”
9. 2012, The Joint Status Seminar 2012 of the ERA-NET PathoGenoMics, Tenerife, Canary Islands,
“Growth inhibition of *S. pyogenes* by antisense PNAs directed to essential genes”

7. Danksagung

Mein großer Dank gilt **Bernd Kreikemeyer**, der mich in der gesamten Zeit mit Rat und Tat unterstützt und ermutigt hat. Strategiebesprechungen, wissenschaftliches Feedback und die Bereitschaft, meine Texte zu lesen, bevor sie der Öffentlichkeit zugemutet wurden: all das hat die Qualität meiner Arbeit verbessert und die Freude an ihr vergrößert.

Andreas Podbielski bin ich dankbar, dass er uns alle mit großem Engagement unterstützt. Sein Rückhalt macht unsere Arbeit erst möglich.

Allen aktuellen und ehemaligen KollegInnen im IMIKRO möchte ich für die angenehme Arbeitsatmosphäre danken. Es gab immer Hilfe und Informationen, und niemals wurde ich allein gelassen.

Insbesondere möchte ich allen KollegInnen und Studierenden danken, die an den hier zusammengefassten Publikationen mitgearbeitet haben: **Jana Bull, Aleksandra Wisniewska-Kucper, Yvonne Humboldt, Roberto Pappesch, Afsaneh Khani, Gina Barkowsky, Franziska Huschka, Claudia Walda, Maja Wittmann, Nicole Popp, Anne Schröder, Anna-Lena Lemster, Selina Krüger, Philipp Warnke und Sonja Oehmcke-Hecht.**

Darüber hinaus bedanke ich mich bei unseren Kooperationspartnern, mit denen uns eine lange fruchtbare Zusammenarbeit verbindet: **Anette Jacob, Stefan Mikkat, Torsten Hain, Mraheil Mobarak, Olaf Wolkenhauer, Peter Raasch und André Billion.**

Tomas Fiedler möchte ich für den ausdauernden Gedankenaustausch zu Wissenschaft, Technik, Mensch und Esoterik danken, vor allem aber auch für seinen freundschaftlichen Rückhalt in allen Lebenslagen.

Robert danke ich für die Unterstützung in der Endphase dieser Arbeit. Danke für ein neues Leben voller neuer Pläne.

Bei meiner Familie und meinen Freunden möchte ich mich für die vielen Jahre der Liebe und Geborgenheit bedanken. Insbesondere danke ich **Kolya und Adrian**: Ihr seid großartig.

8. Selbstständigkeitserklärung

Ich erkläre hiermit an Eides statt, dass ich die vorliegende Arbeit mit dem Thema:

„Antisense-Regulation der Genexpression von *Streptococcus pyogenes* in Virulenz und Therapie“

selbstständig verfasst und keine anderen Hilfsmittel als die angegebenen benutzt habe. Die Stellen, die anderen Werken dem Wortlaut oder dem Sinn nach entnommen sind, habe ich in jedem einzelnen Fall durch Angabe der Quelle kenntlich gemacht.

Ich erkläre hiermit weiterhin, dass ich meine wissenschaftlichen Arbeiten nach den Prinzipien der guten wissenschaftlichen Praxis gemäß der gültigen „Regeln zur Sicherung guter wissenschaftlicher Praxis und zur Vermeidung wissenschaftlichen Fehlverhaltens“ an der Universität Rostock angefertigt habe.

Rostock, 10.12.2019

Nadja Patenge